

## CO<sub>2</sub> capture in oil refineries – an evaluation of different heat integration possibilities for heat supply to the post-combustion process

Daniella Johansson<sup>1,\*</sup>, Per-Åke Franck<sup>2</sup>, Thore Berntsson<sup>1</sup>

<sup>1</sup> Heat and Power Technology, Chalmers University of Technology, Gothenburg, Sweden

<sup>2</sup> CIT Industriell Energi AB, Gothenburg, Sweden

\* Corresponding author. Tel: +46 317723008 Fax: +46 317721152, E-mail: Daniella.johansson@chalmers.se

---

**Abstract:** This paper estimates the costs of CO<sub>2</sub> post-combustion capture for two refineries by comparing different alternatives for supplying the heat needed for the regeneration of the absorbent. The cost of capture ranges from 30 to 472 €/tCO<sub>2</sub> avoided, depending on technology choice for heat supply and energy penalty for the CO<sub>2</sub> separation. In this study, it is concluded that process integration leads to a reduction in avoidance costs. However, the avoidance cost depends greatly on which system perspective is considered, i.e. whether CO<sub>2</sub> emission changes outside the refinery are included or not.

**Keywords:** Carbon capture and storage, Post combustion, Oil refinery, Process integration

---

### 1. Introduction

The oil refining industry generates large amounts of CO<sub>2</sub> emissions. Today and in the future, harder regulations (e.g. the EU ETS system and the Renewable Energy Directive) both on CO<sub>2</sub> emissions from the refinery process and on the refinery products will give new incentives for the oil refining industry to act towards CO<sub>2</sub> mitigation measures. However, the process structure of a refinery implies that even a perfect, energy-efficient refinery will continue to emit significant amounts of CO<sub>2</sub>. Carbon Capture and Storage (CCS) is an alternative that can further reduce CO<sub>2</sub> emissions from the oil refining process. The interest in CCS has grown over the past years, among researchers as well as companies. Different capture technologies are possible: post-combustion, oxy-fuel combustion, chemical looping and pre-combustion. However, post-combustion is the most studied technology and is chosen in this paper as a promising technology since it does not require any extensive rebuilding of the existing refinery. Several previous studies have evaluated the costs for CCS at refineries [1-3], but none has been found that has investigated the costs with different heat supply options in combination with future energy market scenarios. Therefore, the aim of this paper is to examine how the avoidance costs for CO<sub>2</sub> in refineries are affected by different heat integration possibilities and future energy market scenarios.

In this paper, the CO<sub>2</sub> avoidance cost for post-combustion carbon capture, with monoethanolamine (MEA), is evaluated at two case refineries in the Skagerrak region. The oil refining industry is rather complex and therefore often offers opportunities for process integration which can facilitate substantial cost reductions for the heat supply. In this paper, possibilities to use excess heat from the main process to supply heat to the desorption unit, with or without the need of a heat pump, are evaluated as well as integration of a Natural Gas Combined Cycle (NGCC), a natural gas boiler and a biomass boiler. Also combinations of these alternatives are evaluated which is described in Section 2.1.

### 2. Studied systems and alternatives with related assumptions

The first case refinery is a hydroskimming refinery (Refinery no. 1) with a crude oil capacity of 6 Mt/y and ca. 0.5 Mt CO<sub>2</sub>. The second is a complex refinery (Refinery no.2) with a crude oil capacity of 11.4 Mt/y and ca. 1.9 Mt CO<sub>2</sub>. CO<sub>2</sub> emissions from the oil refining process originate from several sources. Only the largest CO<sub>2</sub> emission sources (89% of the total CO<sub>2</sub>

emissions) have been selected for capture, resulting in 2 sources (totally 0.45 Mt CO<sub>2</sub>/y) for Refinery no.1, and 4 sources (totally 1.7 Mt CO<sub>2</sub>/y) for Refinery no. 2.

In this analysis the desorption column in the CO<sub>2</sub> capture unit has a working temperature of 120°C. After capture, the CO<sub>2</sub> is compressed to a pressure of ca. 75 bar with an absorber efficiency of 0.85. In order to generate the absorbent (MEA), large quantities of energy are needed. There are uncertainties regarding the heat demand needed per CO<sub>2</sub> emission captured, and therefore, to handle this discrepancy, two levels of desorption heat demand in the desorption are used, 2800 kJ/kg CO<sub>2</sub> and 4700 kJ/kg CO<sub>2</sub>. The heat demand needed for desorption can be satisfied in different ways, and the alternatives used in this paper are described in more detail below. Key figures for the different alternatives are found in Table 1.

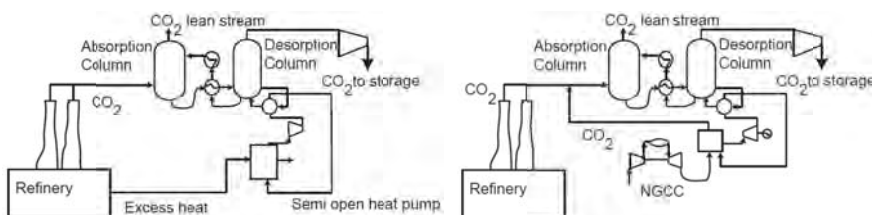
### 2.1. Process integration, utilization of excess heat (EH)

In this alternative the excess heat available above 129°C (EH) has been investigated in order to produce steam for the desorption unit. Two cases are used in Refinery no. 1. First, all excess heat is assumed to be available, presented as EH[1]&HP in Table 1. In the alternative with low heating demand (2800kJ/kgCO<sub>2</sub>) enough heat above 129°C is available. However, in the alternative with high heating demand (4700kJ/kg CO<sub>2</sub>) a heat pump must be used for supplying the additional heat needed. Second, due to contract regulations the amount of excess heat delivered to the current district heating network is assumed to be reserved. In this case only remaining excess heat is available for heat supply, and additional heat is supplied by a NGCC (EH[2]&NGCC), Biomass boiler (EH[2]&BB) or a Natural gas boiler (EH[2]&NB). Hence, the latter alternatives are a combination of excess heat above 129° (heat left after district heat delivery) and NGCC, BB and NB.

The prerequisites for Refinery no. 2 are different. The current district heat delivery is only a few percent of the excess heat, compared to over 50 percent for the first refinery. According to this fact, the alternative where the current level of district heat is reserved is not examined in Refinery no.2. On the other hand Refinery no.2 has the opportunity to increase the capacity of the current boilers. When evaluating Refinery no.2, the excess heat above 129°C is not enough to cover the whole heating demand for any of the levels of heating demands. Here, several alternatives to supply the additional energy needed are explored. First, a heat pump is used to supply the extra energy, presented as EH[1]&HP. Second, the capacity of the current steam boiler is increased (SP) and a biomass boiler, a natural gas boiler or a NGCC is used to supply the rest of the steam needed, presented as EH[3]&BB, EH[3]&NB and EH[3]&NGCC respectively. In both alternatives the available excess heat above 129°C has been used.

### 2.2. Heat pump (HP)

The heat pump uses heat available above 90°C at the refinery to produce LP steam (2.3 bar). The configuration is shown in Fig. 1. It is assumed that the temperature drop of available heat, related to the collection of heat from process streams, is 5°C. The heat pump is a semi-open cycle Mechanical Vapour Recompressor (MVR) using water vapour as working fluid [4].



Figs. 1 & 2. The design of the capture unit using a HP (Fig. 1) or a NGCC (Fig. 2) for heat supply.

### 2.3. Natural gas combined cycle (NGCC)

The NGCC alternative is designed so that the heat recovery steam generator (HRSG) produces enough HP steam (80 bar) to cover the demand of LP steam (2.3 bar) needed for capturing CO<sub>2</sub> generated from both the refinery process and the NGCC; see Fig. 2.

### 2.4. Biomass and natural gas boilers (BB and NB)

In the biomass boiler alternative, a boiler (with efficiency 0.9) is installed. The boiler produces HP steam (80 bar) that is expanded in a back-pressure steam turbine to produce LP steam (2.3 bar). The boiler capacity is adjusted to produce enough LP steam to cover the heat demand for CO<sub>2</sub> capture from both the current process and the biomass boiler; see Fig 3. The natural gas boiler follows the design of the biomass boiler, except from the efficiency (0.94).

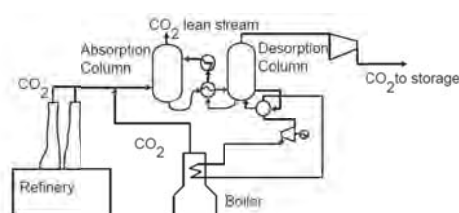


Fig. 3. The design of the capture unit using a biomass boiler or a natural gas boiler for heat supply.

Table .1 Key figures for the case refineries and the studied alternatives. Numbers within parentheses indicate figures for the high desorption heating demand (4700 kJ/kg CO<sub>2</sub>). Ref. indicates the current figures for the refinery. In the current refinery (ref.) excess heat used refers to district heat delivery.

| Refinery no.1                     | Ref. | EH[1]<br>&HP  | NGCC           | BB           | NB           | EH[2]&<br>NGCC | EH[2]<br>& BB | EH[2]<br>NB |
|-----------------------------------|------|---------------|----------------|--------------|--------------|----------------|---------------|-------------|
| Natural gas (MW)                  | 19   | 19 (19)       | 178 (458)      | 19 (19)      | 86 (153)     | 142 (397)      | 19 (19)       | 70 (134)    |
| Biomass (MW)                      | -    | -             | -              | 86 (195)     | -            | -              | 58 (195)      | -           |
| Excess heat used (MW)             | 120  | 37 (62)       | -              | -            | -            | 129            | 129           | 129         |
| CO <sub>2</sub> captured (t/h)    | 48   | 48            | 75 (123)       | 73 (114)     | 59 (71)      | 84 (113)       | 65 (105)      | 56 (67)     |
| Electricity import (MW)           | 21   | 29 (30)       | -39 (-157)     | 15 (-8)      | 16 (3)       | -21 (-132)     | 19(-3)        | 19 (6)      |
| Refinery no.2                     | Ref. | EH[1]<br>& HP | EH[3]&<br>NGCC | EH[3]<br>&BB | EH[3]<br>&NB | NGCC           | BB            | NB          |
| Natural gas (MW)                  | -    | -             | 118(843)       | 67 (67)      | 88 (304)     | 470(1420)      | 67(67)        | 236 (480)   |
| Biomass (MW)                      | -    | -             | -              | 28 (400)     | -            | -              | 218 (697)     | -           |
| ΔSP <sup>1</sup> (t/h)            | -    | -             | 80             | 80           | 80           | 80             | 80            | 80          |
| Excess heat used (MW)             | 27   | 136 (227)     | 82             | 82           | 82           | -              | -             | -           |
| CO <sub>2</sub> captured (tone/h) | 174  | 174 (174)     | 195(319)       | 194 (303)    | 189 (226)    | 255 (418)      | 250 (391)     | 215 (257)   |
| Electricity import (MW)           | 654  | 683 (704)     | 650(331)       | 668 (596)    | 668 (623)    | 637 (586)      | 631 (539)     | 638 (587)   |

<sup>1</sup> Increased capacity of the current boiler

### 3. Methodology

The main methodology in this work is to combine knowledge from process integration in the refinery industry with knowledge about the CCS technology (similar methodology is used in [5]). The methodology and data collection are described by the following steps:

- The potential for steam savings and usage of excess heat from the refinery process are investigated using Pinch analysis. A thorough description of the methodology can be found in several editions; one of the most recently updated is [6]. Heat exchanger cost calculations for collection of excess heat are taken from [7], and used also for calculations for collection of excess heat streams for heat pumping.  
The data regarding the CO<sub>2</sub> capture unit are taken from previous studies of the MEA absorption process [3, 5, 8, 9]. The cost for the capture plant (excluding costs for the energy plant) has originally been taken from studies by Tel-tek [8] and adjusted to fit the refineries studied by using cost information in [9].
- The SGT-800 is assumed to be representative for gas turbines and data are taken from [10]. The size of the gas turbine is scaled to fit the applications studied in this paper, and economic scaling is based on price levels for different NGCC sizes in [11].
- The heat pump is designed using the software IEA Annex 21[4]. Using the chemical engineering plant cost index from 2010, updated investment cost is provided by the software.
- Economic data for the biomass boiler case are taken from [12], including installation and engineering costs, and data for the natural gas boiler are taken from [5].
- To include costs for installation and engineering, the budget prices for all equipment are scaled using a factor 2 (in cases when this is not already included), which is a mean value from [11] and [13]. For the heat exchangers, however, a factor of 3.5 is used [7]. Data for economic calculations for the steam turbines are taken from [14].
- Finally, to evaluate the costs for the different cases, future energy market scenarios are used. The scenarios are based on an energy market model adapted for evaluation of long-term investments in the process industry; a thorough description is found in [15].

#### 3.1. Pinch analysis at the refineries

The pinch analysis only includes streams that are not already integrated (i.e. streams that are heated and cooled with utility, e.g. air). It shows that a significant amount of excess heat is available at Refinery no.1. Theoretical, 54 MW is available above 129°C, and 53 between 90° & 129°C. In the case when the current excess heat used for district heating delivery is inaccessible (EH[2]) the available excess heat is less: 9 MW above 129°C, and 15 MW between 90°C & 129°C. In Refinery no.2 the result shows a theoretically potential of 82 MW available excess heat above 129°C and 145 MW between 90°C & 129°C.

#### 3.2. Economic calculations

In order to evaluate the above-described alternatives, the cost of each avoided tonne of CO<sub>2</sub> emitted is calculated from both a company and a society point of view, in Eqs. (1-5).

$$C_{\text{avoided, company}} = \frac{C_{\text{annual}}}{CO_{2\_ \text{avoided, company}}} \quad \text{or} \quad C_{\text{avoided, society}} = \frac{C_{\text{annual}}}{CO_{2\_ \text{avoided, society}}} \quad [\text{€tonne CO}_2] \quad (1,2)$$

$$CO_{2 \text{ avoided, company}} = CO_{2 \text{ before capture}} - CO_{2 \text{ after capture}} \quad (3)$$

$$CO_{2 \text{ avoided, society}} = CO_{2 \text{ before capture}} - CO_{2 \text{ after capture}} + CO_{2 \text{ reduced by replacing electricity production}} \quad (4)$$

$$\text{Where: } C_{\text{annual}} = \Delta C_{\text{inv}} + \Delta C_{\text{running costs}} + \Delta E * p_e + \Delta F * p_f - \Delta n_{\text{biomass}} * p_{\text{CO}_2} \quad [\text{€/year}] \quad (5)$$

$\Delta C_{inv}$  = Annualised investment costs  
(including installation costs)

$\Delta C_{running\ costs}$  = Annual change in running  
costs except for energy (e.g.MEA costs)

$\Delta E$ = Annual change in electricity

$\Delta F$ = Annual change in fuel use

$\Delta n_{biomass}$  = Annual captured CO<sub>2</sub> from  
biomass (from BB)

$p_{CO_2}$  = Price of CO<sub>2</sub> permits

$p_f$  = Fuel price

$p_e$ = Electricity price

The avoided amount from a society point of view also includes the CO<sub>2</sub> emissions saved from replacing marginal electricity production, as shown in Fig. 4. In all calculations an annuity factor of 0.1 and operation time of 8000h are used. All costs are calculated in 2010 prices levels. In this paper, CO<sub>2</sub> emissions generated from biomass are evaluated as not included in the EU ETS system. However, since capturing CO<sub>2</sub> emissions from the biomass boiler leads to a reduction of CO<sub>2</sub>, and since alternative use of biomass – for example combustion for heat and power production – would otherwise release this CO<sub>2</sub>, revenues related to the price of the CO<sub>2</sub> emissions ( $p_{CO_2}$ ) are allocated to the captured CO<sub>2</sub> emissions from the biomass.

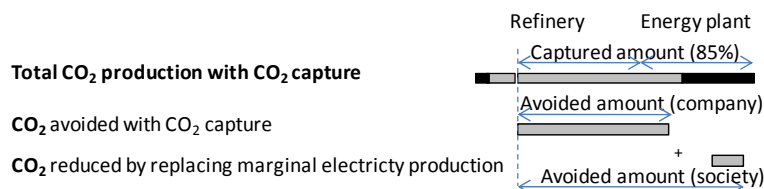


Fig. 4. Description of the avoided amount of CO<sub>2</sub>.

### 3.3. Future energy market scenario

The performance of the CO<sub>2</sub> capture investments is evaluated by using consistent energy market scenarios based on the tool ENPAC [15]. The scenario data are shown in Table 2.

Table 2. Energy market parameters for the different scenario

| Scenario  | 1    | 2    | 3    | 4    | 5    | 6    | 7    | 8         |
|---|------|------|------|------|------|------|------|-----------|
| Fossil fuel price                                 | Low  | Low  | Low  | Low  | High | High | High | High      |
| CO <sub>2</sub> -price [€/tCO <sub>2</sub> ]      | 15   | 27   | 45   | 85   | 15   | 27   | 45   | 85        |
| RES-E support <sup>1</sup> [€/MWh <sub>el</sub> ] | 20   | 20   | 20   | 20   | 20   | 20   | 20   | 20        |
| El price [€/MWh <sub>el</sub> ]                   | 56   | 66   | 81   | 87   | 62   | 72   | 87   | 95        |
| CO <sub>2</sub> from el [kg/MWh <sub>el</sub> ]   | 679  | 679  | 679  | 129  | 679  | 679  | 679  | 129       |
| Marginal technology for electricity production    | Coal | Coal, CCS |
| Price of biomass [€/MWh <sub>fuel</sub> ]         | 26   | 31   | 39   | 56   | 29   | 34   | 42   | 60        |
| Natural gas price [€/MWh <sub>fuel</sub> ]        | 33   | 33   | 33   | 33   | 51   | 51   | 51   | 51        |

<sup>1</sup>Premium paid to producers of renewable electricity from combustible renewable

By using a number of different scenarios that outline possible cornerstones of the future energy market, robust investments can be identified and the climate benefit can be evaluated. Since CO<sub>2</sub> capture is a technology under development and will most likely not be implemented before 2030, scenarios for 2030 are used. This case consists of eight scenarios which are a result of combining two levels of fossil fuel and four levels of CO<sub>2</sub> prices.

#### 4. Results

The results of the calculated avoidance costs are presented in Figs. 5 and 6, together with the price of the CO<sub>2</sub> emission certificates. The CO<sub>2</sub> price can be viewed as an estimate of the possible income from performing these measures at the refinery.

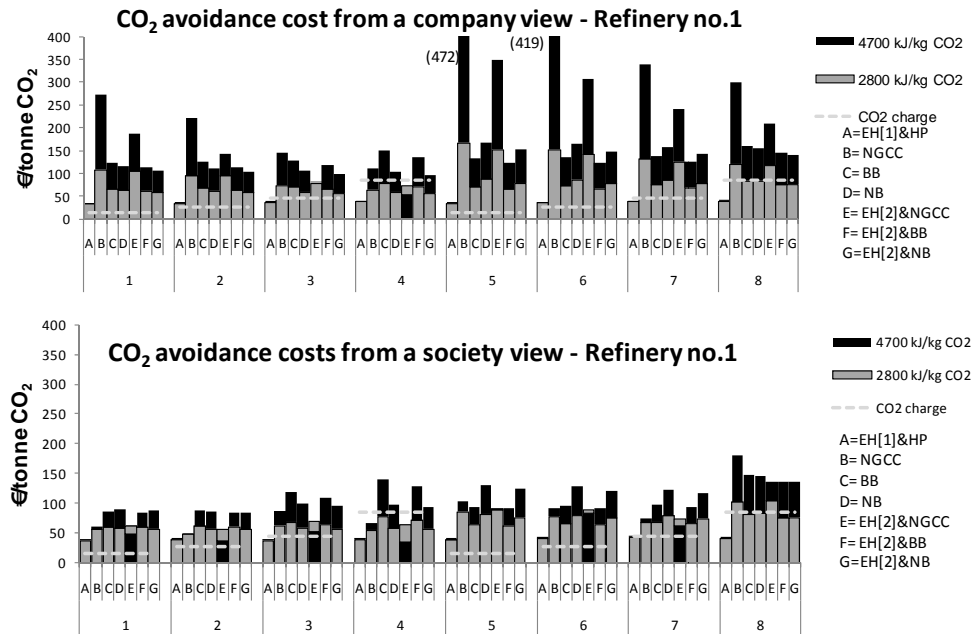


Fig. 5. The avoidance costs (from a company and a society view) for the different alternatives in Refinery no.1. Black bars lower than grey bars indicate that the high heating demand causes lower avoidance costs. Only one bar indicates that the avoidance costs for the two energy levels are similar.

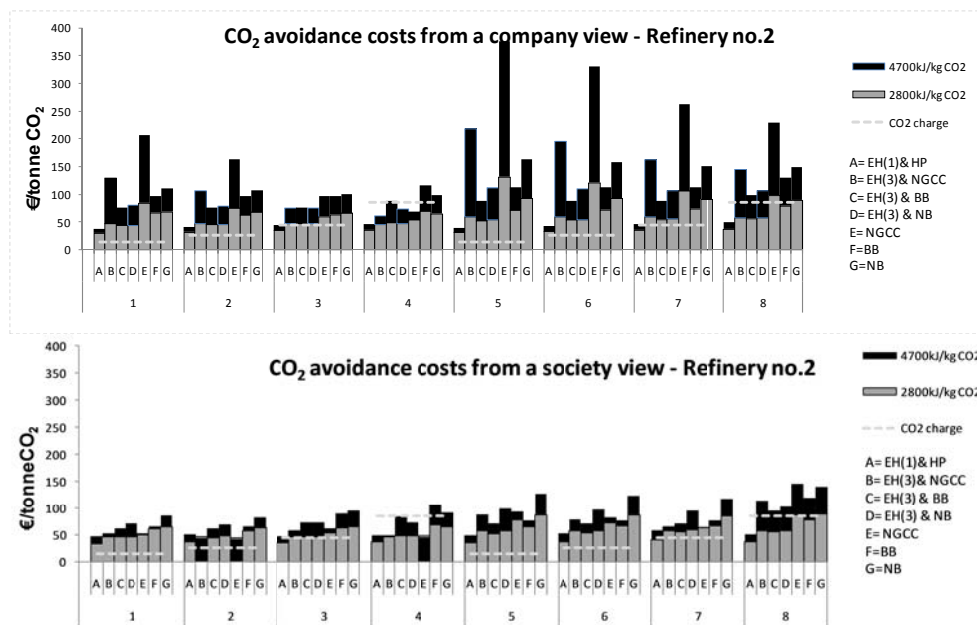


Fig. 6. The avoidance costs (from a company and a society view) for the different alternatives in Refinery no.2. Black bars lower than grey bars indicate that the high heating demand causes lower avoidance costs. Only one bar indicates that the avoidance costs for the two energy levels are similar.

The avoidance costs from a company view are for both refineries, in most scenarios, lowest for the alternatives using excess heat and heat pump. The avoidance costs for these

alternatives are also robust with respect to changes in scenario data, which is due to the relatively small amount of electricity used and the fact that no additional fuel is necessary. Figs. 5 and 6 show that only if the price of CO<sub>2</sub> emissions will become high (85 €/tCO<sub>2</sub>), and if excess heat is used to supply the heat demand, could investing in a capture unit be a robust and promising alternative. If the fossil fuel price is low at this level of CO<sub>2</sub> price, several more alternatives could be promising. Moreover, the results from Refinery no. 2 show lower avoidance costs for almost all alternatives compared to Refinery no.1. This can be explained by cheaper investment costs (in relative terms) and the fact that Refinery no. 2 has the opportunity to increase the capacity of current boiler.

When evaluating the costs from a society view, meaning that CO<sub>2</sub> changes outside the refinery are considered, most alternatives will have much lower avoidance costs compared to the results from a company view; see Figs. 5 and 6. The largest impact can be seen for the NGCC alternative. The large generation of electricity from the NGCC implies large CO<sub>2</sub> savings from marginal production of electricity, especially in Scenarios 1, 2, 5, 6 and 7 when marginal electricity producers are coal power plants without CCS. The benefits from including the reduction of CO<sub>2</sub> emissions from electricity production result in a lower avoidance cost for the high heating demand in almost all cases for the NGCC alternatives. The NGCC alternatives (in both refineries) with high heating demand (4700kJ/kg CO<sub>2</sub>) have the lowest avoidance costs.

## 5. Conclusions and discussion

The main conclusion from this study is that process integration of the capture process at the refinery, i.e. use of excess heat and heat pumping, can significantly reduce the avoidance costs for CO<sub>2</sub> capture at a refinery and be a robust and promising alternative at high CO<sub>2</sub> price levels. However, the avoidance cost depends greatly on which system perspective is considered, i.e. including CO<sub>2</sub> changes in marginal electricity production or not. The alternatives with NGCC could be competitive if high heating demand is needed in combination with a high CO<sub>2</sub> price and low fossil fuel prices (an unlikely combination).

Previous research by [1], [2] and [3] examining CO<sub>2</sub> capture at refineries reported capture costs in the range 50-120 €/tCO<sub>2</sub>. This study's estimates range between 30 and 472 €/tCO<sub>2</sub> avoided. However, the previous studies have all used natural gas CHP to supply the extra energy needed, and in this study that alternative ranges from 45 to 168 €/tCO<sub>2</sub> avoided. It should be noted that the estimated costs in other studies arise from different assumptions and the costs can be calculated per CO<sub>2</sub> captured or CO<sub>2</sub> avoided (as in this study and in [1] and [3]). First, different values for the desorption heat are used in the different studies: 2800 kJ/kg CO<sub>2</sub> in [3], 4700 kJ/kg CO<sub>2</sub> [2] and undefined in [1]. Second, the values for the different costs (e.g. investments and fuel) also arise from different assumptions. In this study, for example, fuel and electricity costs are calculated from future energy market scenarios. Moreover, in this study the transport costs are not included: however, studies by [16] indicate that the costs for transport and storage are around 15-25 €/t CO<sub>2</sub>.

Before CCS becomes a commercial technology, a lot can occur with the available excess heat levels and demands at a refinery. This is to be investigated in more detail in other studies. Finally, to improve the cost estimations of the post-combustion capture process, future work would also include a comparison of the avoidance costs for other absorbents, e.g. ammonia.

## Acknowledgement

This work has been carried out within the Energy Systems Programme, which is primarily financed by the Swedish Energy Agency, and within the project *CCS in the Skagerrak/Kattegat region*, which is an intraregional CCS project partly funded by the EU. The work has also been co-financed by Preem AB. Finally, the authors would also like to thank Preem AB for valuable inputs.

## References

- [1] MT. HO, GW. Allison, DE. Wiley, Comparison of MEA capture cost for low CO<sub>2</sub> emissions sources in Australia, *International Journal of Green Gas Control*.2011;5(1), pp. 49-60
- [2] Tel-Tek, CO<sub>2</sub> capture from industrial facilities, Tel-Tek, 2009, Tel-Tek Porsgrunn, Norway, 2009
- [3] J. Van Straelen, F. Geuzebroke, N. Goodchild, L. Mahony, CO<sub>2</sub> capture for refineries, a practical approach. *Energy Procedia*. 2009, pp.179-185
- [4] IEA Annex 21, Industrial heat pump screening program, IEA Heat Pump Centre c/o SP Technical Research Institute of Sweden, 1997
- [5] E. Hektor, Post-Combustion CO<sub>2</sub> Capture in Kraft Pulp and Paper Mills – Technical, Economic and System Aspects, PhD thesis, Chalmers University of Technology, Sweden, 2008
- [6] Kemp I, Pinch Analysis & Process Integration – A user guide on process integration for the efficient use of energy, 2nd ed., Butterworth-Heinemann, Oxford, UK, 2007
- [7] R. Sinnott, G. Towler, Chemical engineering design, 5th ed., Elsevier Ltd, 2009
- [8] Personal communication with Stefan Nyström and Christina Simonsson, Refinery Development, Preem AB, 2010-12-08
- [9] Sherif A, Integration of a Carbon Capture process in a chemical industry – Case study of a steam cracking plant, Master Thesis, Chalmers University of Technology, Gothenburg, Sweden, 2010
- [10] Siemens SGT-800 brochure, available online 2010-12-3:<http://www.energy.siemens.com>
- [11] Gas Turbine World Handbook, Performance Spec, 2007
- [12] E. Pihl, Integrating biomass in existing natural gas-fired power plants – a techno-economic assessment, Lic. Thesis, Chalmers University of Technology, Sweden, 2010
- [13] J. Strömberg, P.Å Franck, T. Berntsson, Learning from experiences with Gas-Turbine-Based CHP in Industry, CADDET Analyses Series No.9, 1993
- [14] E. Axelsson, Energy Export Opportunities from Kraft Pulp and Paper Mills and Resulting Reductions in Global CO<sub>2</sub> Emissions, PhD thesis, Chalmers University of Technology, Sweden, 2008
- [15] E. Axelsson, S. Harvey, Scenario assessing profitability and carbon balances of energy investments in industry, The AGS report: 2010: EU1, 2010
- [16] McKinsey & Company, Carbon Capture & Storage: Assessing the Economics, 2008

## BECCS in South Korea – An Analysis of Negative Emissions Potential for Bioenergy as a Mitigation Tool

Florian Kraxner<sup>1,\*</sup>, Kentaro Aoki<sup>1</sup>, Sylvain Leduc<sup>1</sup>, Georg Kindermann<sup>1</sup>, Jue Yang<sup>2</sup>,  
Yoshiki Yamagata<sup>2</sup>, Kwang Il Tak<sup>3</sup>, Michael Obersteiner<sup>1</sup>

<sup>1</sup> Forestry Program, International Institute for Applied Systems Analysis (IIASA), Laxenburg, Austria  
<sup>2</sup> Center for Global Environmental Research (CGER), National Institute for Environmental Studies (NIES),  
Tsukuba, Japan

<sup>3</sup> Forestry Department, Kookmin University, Seoul, Republic of Korea

\* Corresponding author. Tel: +43 2236 807 233, Fax: +43 2236 807 299, E-mail: kraxner@iiasa.ac.at

**Abstract:** The objective of this study is to analyze the in-situ BECCS capacity for green field bioenergy plants in South Korea. A technical assessment is used to support a policy discussion on the suitability of this mitigation tool. We first examined the technical potential of bioenergy production from domestic forest biomass. For this exercise, in a first step, the biophysical Global Forestry Model G4M was applied in order to estimate the biomass availability. In a second step, the biomass results from the forestry model were used as input data for an engineering model (BeWhere) for optimized scaling and locating of coupled heat and power plants (CHP). The obtained geographically explicit locations and capacities for forest-based bioenergy plants were then overlaid with a geological suitability map for carbon storage. From this, a theoretical potential for in-situ BECCS was derived. Results indicated that, given the abundant forest cover in South Korea, there is a substantial potential for bioenergy production which could contribute to substituting emissions from fossil fuels and to meeting the targets of the country's commitments under any climate change mitigation agreement. However, there seems to be only limited potential for direct in-situ carbon storage in South Korea.

**Keywords:** BECCS, Bioenergy, Carbon Capture and Storage, Biomass modeling, Energy policy

### 1. Introduction

An active debate in the scientific community is revolving around the possibility of using bioenergy in combination with carbon capture and storage (BECCS), which could remove CO<sub>2</sub> from the atmosphere in order to contribute substantially to achieving low levels of concentration. In the Fourth Assessment Report of the Intergovernmental Panel on Climate Change (IPCC), BECCS is considered "a potential rapid-response prevention strategy for abrupt climate change" and is consequently considered as one of the options to comply with the targets agreed in the Kyoto Protocol [1]. During the last decade it was demonstrated by e.g. [2-4] that terrestrial ecosystems when combined with the use of biomass energy can offer a permanent carbon sink by capturing carbon from biomass conversion facilities and permanently storing carbon in geological formations. However, compared to CCS (Carbon Capture and Storage) combined with conventional fossil fuel systems, very little information can be found in scientific literature so far for both the technical and potential application of BECCS. Moreover, apart from engineering papers presented at e.g. special BECCS conferences such as [5] on Europe, there is - according to our knowledge - to date no literature available that features geographic explicit BECCS applications, especially not for non-European countries.

Although the land base of Korea is small, as much as 64% of the country is forested. Due to a highly efficient and rapid national reforestation program in the 1970s, a majority of the forests in Korea has now reached age classes of 30 and 40 years, which require intensive care in terms of thinning and pruning. By-products from these silvicultural activities can generate a significant amount of raw material to produce e.g. wood pellets and wood chips. Korea

appears further to be an interesting study area for bioenergy, since the country's forestry regained importance both from an ecological as well as from an economical point of view only recently. While trying to build up a bioenergy sector for both energy security and contributing to reduce CO<sub>2</sub> emissions in order to comply with climate change mitigations efforts, sustainable forest management is seen as a key for mobilizing forest biomass for energetic use or direct carbon sequestration. Consequently, ambitious policies and plans for bioenergy production were introduced by the country's government (e.g. "Low Carbon – Green Growth" initiative by the National Energy Plan [6]). However, the lack of forestry infrastructure such as adequate forest roads - for important management activities like harvesting or replanting - causes still too high costs for biomass and related energy production [e.g. 7]. Moreover, this alternative energy sector is facing strong competition from e.g. lower cost fossil and nuclear energy sectors. Hence, being able to better quantify the sustainable bioenergy potential in these countries by identifying economically and biophysically optimized locations for new bioenergy plants and adding value to this information by selecting those locations with promising in-situ combination with CCS technology, policy makers in Korea would be able to develop and support improved and better targeted policies in the area of energy, climate and environment while being supportive to various co-benefits such as rural development, (re-) activation of sustainable forest management etc. The aim of the technical part of our manuscript was threefold. First, to help identifying - in a geographically explicit manner - the available biomass from forest for bioenergy production under sustainable management conditions in South Korea; second, to indicate the optimal size and location of green-field forest biomass-based bioenergy CHP (Coupled Heat and Power technology) plants; and third, to identify the amount and capacity of in-situ BECCS units in South Korea.

## **2. Method**

There are various systems for CCS, such as underground geological storage, ocean storage, mineral carbonation, or industrial use. In this study, we considered the CCS System (with post combustion capture technology) for the underground geological storage into a certain geological formation in the on-shore earth's subsurface. Additionally, we were especially aiming at direct "in-situ" storage. The storage happens in direct vicinity to the combustion units (CHP plants) in order to minimize transport costs and complications. Further we assumed that the total amount of CO<sub>2</sub> - emissions generated at a BECCS unit will be captured and stored in-situ. A technical assessment was used to support a policy discussion on the suitability of this mitigation tool. We first examined the technical potential of bioenergy production from domestic forest biomass. For this exercise, in a first step, the biophysical global forestry model G4M [8] was applied in order to estimate the biomass availability. In a second step, the biomass results from the forestry model were used as input data for the engineering model BeWhere [9] for optimized scaling and locating of CHP plants. The obtained geographically explicit locations and capacities for forest-based bioenergy plants were consequently overlaid with a geological suitability map for carbon storage. From this, a theoretical potential for "in-situ" BECCS was derived.

### **2.1. The Global Forest Model (G4M)**

The Global Forest Model (G4M) from IIASA was used to calculate the growing stock and the sustainable biomass extraction rate. G4M, as described by [8], has been developed in order to predict wood increment and stocking biomass in forests. As input parameter it uses yield power which is achieved through the net primary productivity (NPP) for a specific region. This NPP can be supplied by existing NPP-maps [e.g. 10] or – for higher accuracy – estimated with the help of driver information of soil, temperature and precipitation. The

model can be used like common yield tables to estimate the increment for a specific rotation time. It can further be used to estimate the increment– related optimal rotation time and to provide information on how much biomass can be harvested under a certain rotation time and how much biomass is stocking in the forest. G4M also supplies information on the harvesting losses like needles, leaves and branches which typically remain in the forests under sustainable management. Further, other economic parameters such as harvesting costs - depending on tree size and slope - can be calculated.

## **2.2. The BeWhere Model**

The BeWhere Model - a spatially explicit optimization model, depicting the supply chain of bioenergy industries - was used for the in-situ BECCS assessment [9]. The model, developed at IIASA, considers industries competing for wood resources. On the supply side, forest wood harvests, sawmill co-products (SCP) and wood imports serve as biomass resources for possible new bioenergy plants. Wood demand of pulp-and-paper mills, of existing bioenergy plants and of private households is considered on the demand side. The model assumes that the existing wood demand has to be fulfilled, allowing new plants to be built only if there is enough surplus of wood available. The model is spatially explicit and the transportation of wood from biomass supply to demand spots is considered either by truck, train or boat. The model selects optimal locations of green-field bioenergy plants by minimizing the costs of biomass supply, biomass transport and energy distribution. Full costs and emissions at the optimal locations were calculated such that we were able to indicate the BECCS potential for the country under investigation. Spatial distribution of forestry yields was estimated and provided by the G4M, as well as the harvesting costs (as a function of tree size depending on site quality and rotation time) and the slope steepness were provided by the same model.

## **3. Results**

There were 3 complementary main sets of results derived from this study and indicated at country level: 1) the sustainably available biomass potential for harvest together with the national heat demand as a main prerequisite for the installation of green-field CHP plants; 2) the geological suitability for CS (Carbon Storage); and 3) the identified locations for BECCS units together with their individual bioenergy production capacity as well as their carbon capture and storage capacity. All presented geographically explicit data sets were compiled at a 0.25-deg (degree grid cell) resolution (25 x 25 km). We used a conversion factor of 0.5 to estimate dry matter biomass (ton dry matter, tdm) from stem volume irrespective to the tree species. The defined forest harvesting scenarios were based on the amount of extracted biomass, while the baseline for harvesting was considered under a sustainable forest management regime, assuming that the average annual harvesting rate is substantially lower than the annual allowable cut. We further assumed that only stem biomass was extracted from the forest stands and that 100% of the extracted biomass was used for energy production. Following conversion factor for the national currency was applied for economic calculations of harvesting, transport and energy (heat) costs: 1 Korean Won = 0.000908987 USD (2008).

### **3.1. Biomass availability and energy demand**

For our analysis, we assigned a managed forest area of 4,852,330 ha (about 78 % of total South Korean forest area) for biomass extraction dedicated to energy production. This forest area was modeled as an aggregated forest cover map based on GLC 2000 [11], the Relative Human Influence concept for each terrestrial biome [12], a classification of pristine and non-pristine forest [13] and protected area [14]. We excluded the forest area where the Relative Human Influence was less than 50 % and where protected areas designated by IUCN

Categories I – VI were located. For the geographical distribution of the actual growing stock we calculated 555,363,300 m<sup>3</sup> (protected area excluded), which was achieved with the help of the global biomass map [15] which was harmonized with FAO statistics of 2005 [13], while the official national statistics of South Korea reported a total growing stock of 506,376,806 m<sup>3</sup> for 2005 [16]. Derived from Korean forest statistics in 2008, we limited the biomass extracted annually for energy production to 0.36 % of the total growing stock (sustainable forest management criteria), amounting 999,653 tdm/year (on average 1.62 tdm/ha-year) - see Fig. 1 for the spatial distribution. Further information for our economic optimization process with respect to costs (wood chip and stumpage price, harvesting and extraction costs) were derived from various Korean resources and adapted to local slope conditions for harvesting operations with different technologies.

In South Korea, the total heat energy consumption was 625,915 GJ/year in 2008 [6]. As input for the energy demand calculations, we geographically weighted the heat demand with the population for 2005 at 0.25 degree resolution and assumed that the average heat demand per person was 0.0127 GJ/person (Fig. 1). The average energy prices for Korea in 2008 were adapted from the national statistics.

The demand-supply optimization routines of the BeWhere model also consider transportation costs (truck, train, ship - derived from [17]), as well as the existing road and railway networks for South Korea which were taken from vmap0 [18], also considering different travel speeds.

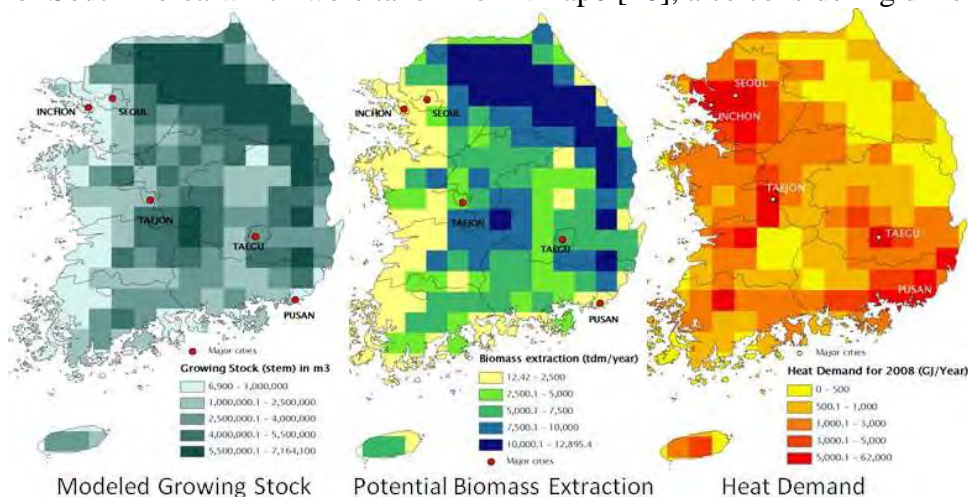


Fig. 1. Geographically explicit supply – demand situation for Korea. The map on the left hand side indicates the modeled spatial distribution of the growing Stock (m<sup>3</sup>) in Korean forests (biomass supply). The highest growing stock could be identified in the north-east and the center of Korea (dark pixels). The map in the center indicates the modeled potential biomass extraction rate (tdm/year) - under sustainable conditions - from Korean forests (biomass supply). Highest biomass extraction rates could be achieved also in the north-east and center of the country. The map on the right hand side indicates the modeled spatial distribution of the heat demand (GJ/year). Highest demand was identified around the large urbanized areas (e.g. Seoul) in the western and south-eastern part of the country.

### 3.2. Identification of geological suitability for C - storage

The geological CS facility can be installed only under specific conditions such as geological characteristics (e.g. tectonic activity, sediment type, geothermal and hydrodynamic regimes) and maturity of infrastructure to build CCS units. In general, sedimentary basins are the sites with the highest potential for geological CS. Suitable sites for geological CO<sub>2</sub> storage can be found on: 1) basins formed in mid-continent locations, 2) basins formed near the edge of stable continental plates, 3) basins behind mountains formed by plate collision such as European

basins immediately north of the Alps and Carpathians, 4) fold belts, and 5) some of the highs [e.g. 1]. Other geological formations such as shield areas (e.g. Scandinavia) or tectonically active areas (e.g. Japan) are less suitable for geological CO<sub>2</sub> storage. However, the suitability for geological CS depends to a great extent on their local conditions. We identified mostly basins as potentially suitable locations for geological in-situ CS in South Korea. The geological map shown in Fig. 2 was mainly based on the studies by [19] and [20]. The location for CO<sub>2</sub> injection can be different from the site of the bioenergy plants where CO<sub>2</sub> emissions occur. In the case of South Korea mainly the geological Gyeongsang Basin located in the south-east of the country could be identified to be potentially suitable for in-situ CS.



Fig. 2 Potential locations (Geologic Province) suitable for geological CO<sub>2</sub> storage in South Korea (on-shore only). Source: modified after [19] and [20].

### 3.3. Potential in-situ BECCS units identified for South Korea

To identify the optimal locations for green-field bioenergy plants, three different sizes of CHP plants are considered (5, 20, and 70 MW). We assumed that diversification with respect to plant size would on the one hand result in a better distribution of plants within the country, which increases usually also the co-benefits of bioenergy plants. On the other hand we expected to identify more bioenergy plants suitable for in-situ CS. Within each scenario (plant capacity) the aim was to meet the target for the maximum sustainable biomass extraction (about 1 M tdm/year).

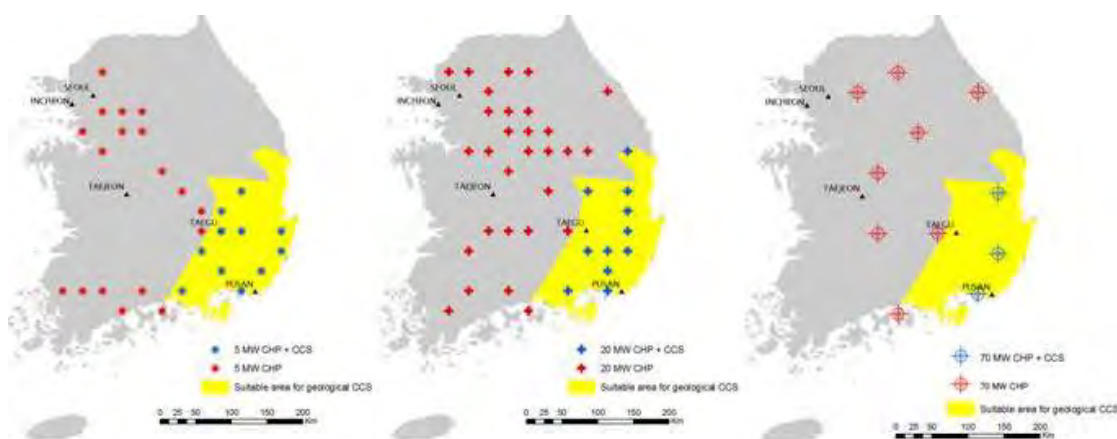


Fig. 3. Three different scenarios (from left to right 5; 20; 70 MW) for optimized green-field biomass plant locations in South Korea. The geographic explicit location of bioenergy plants without CCS is indicated in red color and the BECCS unit locations are indicated in blue color on light yellow background (geologically suitable formation for CS).

For this study we defined in-situ CS suitability such that the bioenergy plant needs to be located within a 0.5 degree grid cell (about 55 x 55 km) of the suitable geologic province in

order to directly inject CO<sub>2</sub> underneath a plant or at any place up to a maximum of 25 km radius distance (e.g. with the help of a short pipeline).

Based on these assumptions, Fig. 3 shows the optimized location in a geographically explicit manner by plant size. Table 1 indicates the optimized amount of green field bioenergy plants for Korea, listed by plants with and without in-situ CS suitability, divided into the different plant capacity categories.

Table 1. Energy produced, emissions substituted and CCS Capacity by forest biomass CHP plants with/without BECCS system under a sustainable forest biomass production regime.

| Plant size Technology                      | 5 MW<br>NO CCS | 20 MW<br>NO CCS | 70 MW<br>NO CCS | 5 MW<br>CCS    | 20 MW<br>CCS   | 70 MW<br>CCS   |
|--|----------------|-----------------|-----------------|----------------|----------------|----------------|
| Plant #                                    | 18             | 29              | 8               | 11             | 11             | 3              |
| Biomass used (tdm/year)                    | 117,000        | 716,300         | 712,400         | 71,500         | 271,700        | 267,150        |
| Heat produced (GJ/year)                    | 1,190,475      | 7,288,353       | 7,248,670       | 727,513        | 2,764,548      | 2,718,251      |
| El. produced (GJ/year)                     | 757,575        | 4,638,043       | 4,612,790       | 462,963        | 1,759,258      | 1,729,796      |
| Subst. emissions (tCO <sub>2</sub> /year)  | 215,516        | 627,050         | 625,036         | 131,704        | 237,847        | 234,389        |
| <b>CCS Capacity (tCO<sub>2</sub>/year)</b> | <b>0</b>       | <b>0</b>        | <b>0</b>        | <b>131,704</b> | <b>237,847</b> | <b>234,389</b> |

We could identify a maximum of 40 green-field bioenergy plants under the 20 MW-scenario of which 11 plants were located on geologically suitable ground in order to meet the criteria for BECCS units. Under the 5 MW scenario, 29 bioenergy plants were optimally distributed over the country, among which also 11 plants qualified as BECCS plants. Under the 70 MW scenario a total of 11 bioenergy plants were computed of which 3 met the criteria for BECCS units. In the best case (20 MW scenario), the “BECCS-effect” (emissions accounted as negative) could reach a potential capacity of some 238,000 tons of CO<sub>2</sub> to be directly stored permanently belowground per year and to be accounted as negative emissions.

#### 4. Discussion and Conclusions

Our BECCS exercise offers several new insights to the bioenergy sector in South Korea and provides crucial information for policy support and design. First of all, it is important to note that even under our rather conservative assumptions – especially with respect to sustainable biomass extraction - we still could theoretically produce some 10% of the present heat demand (being equivalent to a 20 times increment of the present bioenergy share for heat production in Korea [21]), and 1.3% of the total electricity produced in South Korea (15 times the present bioenergy share for electricity production [21]). These results indicate a substantial potential of bioenergy growth in South Korea – especially given the present policies and targets of the National Energy Plan to e.g. increase the bioenergy share in total energy production from 0.2% (2007) to 3.4% by 2030 [6].

Among the 3 different scenarios (plant capacities), the 20 MW scenario turned out to offer the best country-wide coverage with its 40 green-field bioenergy facilities, which consequently could provide direct and indirect co-benefits such as driving the green economy, i.e. providing job opportunities both at the facility and in the biomass production. Another major benefit of growth in the bioenergy sector would be the resulting investments in forest and forest management primarily by small-scale forest owners, e.g. in forest infrastructure. These benefits are based on the assumption that forest biomass would see a price increase, which justifies investments into forest infrastructure (to harvest the biomass more easily) which lowers harvesting costs and increases competitiveness.

Although the suitable geological formations for in-situ CS in South Korea are limited to about 1/5 of the country area (the Gyeongsang Basin), with the help of this study we could show that there is a theoretical potential for 3 (70 MW plants) to 11 (5 / 20 MW plants) green-field BECCS plants with in-situ CS. Based on our assumptions, the BECCS-effect might amount to 130,000 – 240,000 tons CO<sub>2</sub> per year in addition to a similar amount of substituted fossil fuel emissions. This means that about 3-4% of the total demand for heat energy in South Korea could be produced in BECCS plants with in-situ CS. As a consequence, 3-4% of the fossil fuel emissions could be substituted and additionally accounted as negative because they would be actively removed from the atmosphere by BECCS plants. This BECCS effect comes additionally to the biomass co-benefits discussed earlier and could be used as a key issue for future policy design and decision makers.

However, the BECCS effect - and with it a crucial lever for climate, environment and rural development policies - could certainly be substantially increased and strengthened. An important caveat to bear in mind is that with our study we only could point out the theoretical potential without considering the costs of the actual CCS process. If bioenergy plants with higher capacities would be applied, costs could be substantially decreased (scale effect or poly-production). Further, although the suitable geological formations for geological CCS appearing in South Korea are limited (e.g. earthquake and volcanic activity), there are wide off-shore prospective areas in this region (e.g. East Sea). Using further capacity for CS (non in-situ), basically all substituted emission from bioenergy production could additionally be stored and accounted as negative. The use of a (trans-national) CO<sub>2</sub>-pipeline could actually boost the BECCS effect and lower the costs, but further research needs to be done in this field. Also the joint use of off-shore CS together with e.g. Japan would substantially increase BECCS capacity, which requires similar research to be extended to South East Asia, potentially using a higher data resolution than 0.25-deg.

We conclude that policy targeted bioenergy-based re-activation of forest management in South Korea would evoke a real win-win-situation. First, bioenergy production and BECCS would directly contribute to meet ambitious climate change mitigation targets. Second, the forest ecosystem would benefit from sustainable management (including thinning etc.) e.g. in terms of improved forest health, stand stability and lower exposure to threatening hazards like wind throw or pests. Third, the forest owners - and with them the forest sector industry - would benefit from an increased value of the forest property, from better prized forest products, as well as from a higher quality of the grown timber and competitive harvesting conditions as a consequence of investment into forest infrastructure. And last not least, society would benefit through e.g. an improved protective function (from e.g. flooding, landslides, avalanches etc.) and an increased recreational value of the forest.

## **References**

- [1] IPCC, Special Report on Carbon Dioxide Capture and Storage. ISBN-13 978-0-521-86643-9. Cambridge University Press, 2005.
- [2] M. Obersteiner, C. Azar, P. Kauppi, K. Möllersten, J. Moreira, S. Nilsson, P. Read, K. Riahi, B. Schlamadinger, Y. Yamagata, J. Yan, J-P. van Ypersele, *Managing climate risk*, Science 294(5543), 2001, pp. 786–787.
- [3] F. Kraxner, S. Nilsson, M. Obersteiner, Negative emissions from BioEnergy use, carbon capture and sequestration (BECS)—the case of biomass production by sustainable forest management from semi-natural temperate forests, *Biomass and Bioenergy* 24, 2003, pp. 285–296.

- 
- [4] C. Azar, K. Lindgren, M. Obersteiner, K. Riahi, D.P. van Vuuren, K.M.G.J. den Elzen, K. Möllersten, E.D. Larson, The feasibility of low CO<sub>2</sub> concentration targets and the role of bioenergy with carbon capture and storage (BECCS). *Climatic Change* 100, 2010, pp. 195–202.
- [5] F. Kraxner, G. Kindermann, S. Leduc, K. Aoki, M. Obersteiner, Bioenergy Use for Negative Emissions – Potentials for Carbon Capture and Storage (BECCS) from a Global Forest Model Combined with Optimized Siting and Scaling of Bioenergy Plants in Europe. Paper presented at the First International Workshop on Biomass & Carbon Capture and Storage October 2010, University of Orléans, France, 2010.
- [6] Korea Energy Management Corporation, 2010, available at:  
[http://www.kemco.or.kr/new\\_eng/main/main.asp](http://www.kemco.or.kr/new_eng/main/main.asp)
- [7] F. Kraxner, J. Yang, Y. Yamagata, Attitudes towards forest, biomass and certification – A case study approach to integrate public opinion in Japan. *Bioresource Technology*, 100(17), 2009, pp. 4058–4061.
- [8] G. Kindermann, M. Obersteiner, B. Sohngen, J. Sathaye, K. Andrasko, E. Rametsteiner, B. Schlamadinger, S. Wunder, R. Beach, Global cost estimates of reducing carbon emissions through avoided deforestation, *PNAS* 105(30), 2008, pp. 10302-10307.
- [9] S. Leduc, E. Schmid, M. Obersteiner, K. Riahi, Methanol production by gasification using a geographically explicit model. *Biomass and Bioenergy*, 33(5), 2009, pp. 745-751.
- [10] S.W. Running, Terrestrial remote sensing science and algorithms planned for EOS/MODIS. *International Journal of Remote Sensing* 15, 1994, pp. 3587-3620.
- [11] JRC Global Land Cover 2000 version 1. Database. Joint Research Centre, European Commission, 2000, <http://bioval.jrc.ec.europa.eu/products/glc2000/products.php>
- [12] WCS-CIESIN, Last of the Wild Data Version 2, 2005 (LWP-2): Global Human Footprint data set (HF), 2005, <http://sedac.ciesin.columbia.edu/wildareas/downloads.jsp#infl>
- [13] FAO Global Forest Resources Assessment 2005. FAO Forestry Paper 147. Food and Agriculture Organization of the United Nations, Rome, 2005.
- [14] UNEP-WCMC, World Database on Protected Areas (WDPA), United Nations Environment Programme World Conservation Monitoring Centre, 2009.
- [15] G. Kindermann, I. McCallum, S. Fritz, M. Obersteiner, A global forest growing stock, biomass and carbon map based on FAO statistics. *Silva Fennica* 42(3), 2008, pp. 387-396.
- [16] Korea Forest Service, Statistical Yearbook of Forestry 2009. Korea Forest Service, Daejeon, 2009.
- [17] P. Börjesson, L. Gustavsson, Regional Production and Utilization of Biomass in Sweden. *Energy* 21, 1996, pp. 747-764.
- [18] National Imagery and Mapping Agency, World roads (VMAPO) Fairfax, VA: National Imagery and Mapping Agency, 1997
- [19] J.B. Bradshaw, T. Dance, Mapping geological storage prospectivity of CO<sub>2</sub> for the world sedimentary basins and regional source to sink matching, GHGT-7, September 5–9, 2004, Vancouver, Canada, v.I, pp. 583-592.
- [20] USGS, U.S. Geological Survey World Petroleum Assessment 2000 - Description and Results, DDS-60. United States Geological Survey, 2001.
- [21] IEA, International Energy Agency, Country Statistics, 2008, available at:  
<http://www.iea.org>

## What are the rules for biofuel carbon accounting?

Eric P Johnson<sup>1,\*</sup>

<sup>1</sup> Atlantic Consulting, Gattikon, Switzerland

\* Corresponding author. Tel: +41 44 772 1079, E-mail: [ejohnson@ecosite.co.uk](mailto:ejohnson@ecosite.co.uk)

---

**Abstract:** Most quantitative assessments of biomass fuels or biofuels assume that bioenergy is inherently carbon neutral, that biogenic emissions of carbon dioxide should be excluded from a carbon footprint. This ‘carbon neutral’ assumption makes an enormous difference in carbon accounts and in the policies that those accounts would suggest. For instance, if harvested logs burnt as fuel are considered carbon neutral, their carbon footprint is far lower than that of natural gas. However, if the logs’ biogenic carbon emissions are counted, then their carbon footprint is much higher than gas’s. Moreover, this can lead to absurd conclusions. If carbon neutrality is presumed, it makes no difference to a carbon footprint if a forest is standing or if it has been chopped down for fuel wood. Since the mid-1990s, some researchers have contradicted the ‘carbon neutral’ assumption, and their view that biogenic emissions should be counted has begun to attract significant attention of policy makers. This paper reviews the history and current state of biogenic-carbon accounting rules, including the ISO/CEN rules being developed under the EU Renewable Energy Directive. Without taking sides, it will define the debate for researchers and policy-makers, reflect on its significance and suggest possible means of resolution.

**Keywords:** *biofuels, carbon accounting, carbon neutral*

---

### 1. Introduction: The premise of carbon neutral

In the fields of life-cycle assessment and carbon footprinting, biofuels traditionally have been considered as inherently carbon neutral: biogenic emissions of carbon dioxide are excluded from the inventory or footprint. Two landmark studies in the field, (Argonne Labs GREET) and (Joint Research Centre of the EU Commission, EUCAR et al. 2008) take this position as given, and many other studies follow their leads.

More recently, however, some researchers have begun to question this approach. Probably the best-known are (Searchinger, Hamburg et al. 2009), but the issue had already been raised by others, namely (Rabl, Benoist et al. 2007) and (Johnson 2009). More recently (Manomet Center for Conservation Sciences 2010) published a large report that questioned the ‘carbon-neutral-assumption’. The International Energy Agency’s (IEA) Bioenergy Task 38 group, ‘Greenhouse Gas Balances of Biomass and Bioenergy Systems’, has also raised questions<sup>1</sup>, particularly from (Berntsen and Peters 2010) and (Cowie 2010).

Some regulators appear to be taking these questions seriously. The (Manomet Center for Conservation Sciences 2010) report was commissioned by and adopted by the US Commonwealth of Massachusetts with respect to its regulation of biomass-fueled power plants. Presumably Task 38 is being taken seriously by IEA member governments, and at the United Nations level, the idea of that REDD (Reducing Emissions from Deforestation and Forest Degradation) is generally desirable seems to be undisputed.

Furthermore, the issue has come into the domain of standards organizations. Technical Committee 383 at CEN is working on norms in this area, as is ISO Project Committee 248 (of which the author is a member).

---

<sup>1</sup> See a March 2010 conference record at <http://ieabioenergy-task38.org/workshops/brussels2010/>

And what is the question? Primarily it is this: should biofuels be considered inherently carbon neutral? The first-generation position was yes (although it was more an assumption than an answer to a question); the emerging position is at minimum not an automatic yes, but a definitive second-generation answer is yet to be determined fully.

The importance of this question, in environmental terms, is very high. Biofuels are clearly the main solution proposed by governments to the twin problems of climate change and energy security. Non-bio, non-fossil energies – such as solar, tidal and wind – are and will for the medium term be marginal contributors, whereas biofuels are aimed at taking, for instance, a 20% share of the EU energy mix by 2020. If these biofuels turn out to be, relative to conventional fossil fuels, carbon negative rather than positive, then their subsidies will not only have cost billions<sup>2</sup>, they will also have worsened rather than mitigated global warming!

This paper is meant to elaborate the issue from the perspective of carbon footprinting. After a brief statement of method, it presents results, i.e. characterization of the ‘carbon neutral’ question from six different methodological perspectives. It concludes with findings and suggestions for further study.

## **2. Method**

The author has reviewed the literature as well as the political and the standards documentation, and then refracted these in the light of carbon-footprint methods.

## **3. Results: how the ‘carbon neutral’ question can be categorised**

Using the method of carbon footprinting or life-cycle assessment, the question of biofuel carbon neutrality can be characterized in six ways, which are described in the following six subsections.

### **3.1. Boundary of the system**

In impact analyses such as life-cycle assessment or carbon footprinting, for a full life-cycle the ideal boundary is ‘cradle-to-grave’, i.e. from the environment to the environment. As the ISO standard for life cycle assessment (ISO 2006, section 5.2.3) expresses it: “Ideally, the product system should be modelled in such a manner that inputs and outputs at its boundary are elementary flows.” In other words, the life-cycle boundary begins and ends with human intervention. Purely natural processes – biogenic as opposed to anthropogenic – are not included.

Growing of crops, say as feedstock for fuel, is of course an anthropogenic activity. Fields of rapeseed, soybeans or wheat do not spring up on their own. The carbon released in creating and maintaining such fields (so-called ‘land-use change’ emissions), as well as the carbon emitting in cropping them, is included in current assessments; however, the carbon taken in during a growing season is netted out against the carbon emitted in combustion. And this seems consistent with the boundary definition above.

But what about a natural forest? If human activity was not needed to create it, why should its carbon emitted in combustion – clearly a human activity – be netted against carbon taken from the atmosphere to create the trees? This seems inconsistent with the human/nature

---

<sup>2</sup> OECD countries’ annual subsidy of biofuels in 2007 was estimated at about \$15 billion.

boundary applied to other assessments. To be consistent, human harvesting of natural forests should not be netted against their biogenic creation. (Plantations are a different matter; they are created by humans.) This would be consistent with how harvest of other natural resources – say, oil or limestone – is treated in LCA and footprints. Harvest of these is not netted against their creation.

### **3.2. Temporal definition of the system**

In common usage, the terms biofuels and renewables are actually misnomers. Surely conventional oil and gas, which are derived from long-dead plants and animals – are biofuels? And solar power, as astrophysicists tell us, is not renewable. The sun does not recycle its hydrogen, and in some millions of years will burn itself out. These observations are more than just amusing. They point out the temporal boundaries placed implicitly on LCAs and carbon footprints. To be careful in carbon accounting, analyses should recognize such temporal boundaries explicitly.

Also, researchers should consider the theoretical basis for granting carbon credits to biofuels, yet not doing so to fossil-biofuels. At present this appears to be done out of intuition – not out of thought-through reasoning. The reasoning should be developed, or the practice should be ended.

People often justify ‘carbon neutrality’ of biofuels by saying: ‘the tree will grow back’. If it grows back in 10 minutes, fine. But what if it grows back in 10 years, or 100 years? Surely there is an inflection point (and it could be calculated) as to when the grow-back timing changes from favourable to unfavourable.

### **3.3. Shadow/alternative/counterfactual scenarios**

If we had not grown a crop to be used as fuel, what would have happened to the carbon balance then?

This idea of a ‘shadow’ or alternative scenario, sometimes called ‘the counterfactual’, is not present in most studies of biofuels. In a 2008 survey of over 100 publications by 56 researchers about solid biomass fuels (Johnson 2009), not one of them postulated a shadow scenario. After extensive work on liquid biofuels over the past eight years, the author is aware of only two researchers who have applied it in this area: (Joint Research Centre of the EU Commission, EUCAR et al. 2006) and (Heinen and Johnson 2008).

Broader research by (Manomet Center for Conservation Sciences 2010) and IEA Task 38 suggest that shadow scenarios should be standard, not the exception. Moreover, the idea of REDD (Reducing Emissions from Deforestation and Forest Degradation) in the UNFCCC and the idea of ‘additionality’ in the Clean Development Mechanism (CDM) and elsewhere, both suggest that counterfactuals should be customary.

### **3.4. Allocation**

There are two open issues here. One is allocating carbon burden to crop components by weight. This has led to the dubious practice of assigning the majority of a grain footprint to the straw that is grown along with the grain. Dubious yes, but it has been applied in numerous studies for the German government, only a few years ago, that the government then promoted.

The other is the allocation of CO<sub>2</sub> capture, i.e. the removal of carbon dioxide from the atmosphere by photosynthesis. Why is the captured CO<sub>2</sub> always allocated to a biofuel? Why

cannot a fossil fuel take that carbon credit? Or should the credit be shared proportionately between the two? The answers here are not immediately obvious, but even more obvious is that the questions appear not to be asked in most studies – and yet they should be.

### **3.5. Marginal/consequential modelling**

Simply put, current practice presumes that every additional unit of biogenic CO<sub>2</sub> emitted is recycled to the biosphere via photosynthesis – from the earth to the earth. By contrast, every additional unit of fossil CO<sub>2</sub> emitted stays in the atmosphere, creating more heat.

Yet as pointed out in the allocation discussion, this cannot make sense: carbon dioxide is carbon dioxide. Also, the ability of the biosphere to capture carbon can and does change, depending particularly on forest conditions and water-saturation levels. Once again, the answers here are not immediately obvious, but the questions should be addressed.

### **3.6. Additionality and subtractionality**

The idea of additionality may be useful in creating accurate accounts of forest carbon. If a forest is planted on previously non-forested land, with the express intent of using the harvested trees as biofuel, then this might properly be considered as carbon neutral. Indeed, it probably is carbon negative: although carbon is being harvested, on a net basis, more carbon might be returned to the soil and the vegetation above.

Likewise, what about ‘subtractionality’? If trees are being harvested for fuel that otherwise would have remained standing, their carbon surely should be removed from the forest’s carbon stock, and debited against the footprint. The case for this has been made by (Rabl, Benoist et al. 2007), (Johnson 2009) and (Searchinger, Hamburg et al. 2009), but the term subtractionality – you first heard it here.

## **4. Discussion and conclusions**

This paper has raised more questions than it has answered – and that is its intent. Without addressing these questions, carbon accounting will continue to be wildly inaccurate. And ‘wildly’ is no overstatement: the current discussion in CEN and ISO<sup>3</sup> of biofuel standards demonstrates how divergent current opinion is on these issues.

Getting more convergent opinion is important, and not just for the reputation of LCA and carbon footprint analysts, who often are cursed with the epithet of ‘you can get any answer you want’. More convergence will be critical to investors, policy makers and the general public. If we really believe that reducing carbon emissions is critical to our future, the questions raised in this paper are worth serious exploration.

To conclude, there might be a simple principle to guide further research: *efficiency is the key*. The source of carbon is surely less important than the efficiency by which it is used. Moreover, efficiency also drives economics; efficient fuels generate the most consumer demand. Efficiency can and should guide the evaluation of future fuels, and the rules of carbon accounting should be constructed to promote this.

Put another way, the key to reducing atmospheric concentrations of carbon is to put less carbon up there in the first place and to keep more of it down here on the ground. We should

---

<sup>3</sup> The author is a delegate and part of the ongoing discussions.

be more worried about how much net carbon is being emitted, and less worried about which kind of carbon, i.e. biogenic or fossil, is being emitted. If we use this simple concept as our guide, I think we will make much greater progress toward solving this great problem.

## References

- [1] Argonne Labs GREET, Greenhouse Gases, Regulated Emissions, and Energy Use in Transportation, Version 1.8c.
- [2] Joint Research Centre of the EU Commission, EUCAR, et al. (2008). Well-to-Wheels analysis of future automotive fuels and powertrains in the European context.
- [3] Searchinger, T. D., S. P. Hamburg, et al. (2009). "Fixing a critical climate accounting error." *Science* 326 (23 October 2009): 527-528.
- [4] Rabl, A., A. Benoist, et al. (2007). "How to Account for CO<sub>2</sub> Emissions from Biomass in an LCA." *International Journal of LCA* 12(5): 281.
- [5] Johnson, E. (2009). "Goodbye to carbon neutral: getting biomass footprints right. ." *Environmental Impact Assessment Review*.
- [6] Manomet Center for Conservation Sciences (2010). *Massachusetts Biomass Sustainability and Carbon Policy Study: Report to the Commonwealth of Massachusetts Department of Energy Resources*. Brunswick, Maine.
- [7] Berntsen, T. and G. P. Peters (2010). CO<sub>2</sub> perturbation and associated global warming potentials following emissions from biofuel based on wood. *Greenhouse gas emissions from bioenergy systems: impacts of timing, issues of responsibility Brussels*.
- [8] Cowie, A. (2010). *Is bioenergy really carbon neutral? Greenhouse gas emissions from bioenergy systems: impacts of timing, issues of responsibility Brussels*.
- [9] ISO (2006). *ISO 14040: Environmental management — Life cycle assessment — Principles and framework*.
- [10] Heinen, R. and E. Johnson (2008). "Carbon footprints of biofuels & petrofuels." *Industrial Biotechnology* 4(3): 257-261.

## Coupling mass transfer with mineral reactions to investigate CO<sub>2</sub> sequestration in saline aquifers with non-equilibrium thermodynamics

Yuanhui Ji<sup>1,\*</sup>, Xiaoyan Ji<sup>1</sup>, Xiaohua Lu<sup>2</sup>, Yongming Tu<sup>3,4</sup>

<sup>1</sup> Division of Energy Engineering, Luleå University of Technology, 971 87 Luleå, Sweden

<sup>2</sup> State Key Laboratory of Materials-Oriented Chemical Engineering, Nanjing University of Technology, 210009, Nanjing, P. R. China

<sup>3</sup> Key Laboratory of Concrete and Prestressed Concrete Structures of Ministry of Education, Southeast University, 210096, Nanjing, P. R. China

<sup>4</sup> Division of Structural Design and Bridges, Royal Institute of Technology (KTH), 10044 Stockholm, Sweden

\* Corresponding author. Tel: +46 920491271, Fax: +46 920491074, E-mail: yuanhui.ji@ltu.se

**Abstract:** The coupling behaviors of mass transfer of aqueous CO<sub>2</sub> with mineral reactions of aqueous CO<sub>2</sub> with rock anorthite are investigated by chemical potential gradient and concentration gradient models, respectively. SAFT1-RPM is used to calculate the fugacity of CO<sub>2</sub> in brine. The effective diffusion coefficients of CO<sub>2</sub> are obtained based on the experimental kinetic data reported in literature. The calculation results by the two models and for two cases (mass transfer only and coupling mass transfer with mineral reaction) are compared. The results show that there are considerable discrepancies for the concentration distribution with distance by the concentration gradient and chemical potential gradient models, which implies the importance of consideration of the non-ideality. And the concentrations of aqueous CO<sub>2</sub> at different distances by the concentration gradient model are higher and further than that by the chemical potential gradient model. The mineral reaction plays a considerable role for the CO<sub>2</sub> geological sequestration when the time scale reaches 10 years for the anorthite case.

**Keywords:** CO<sub>2</sub> geological sequestration, Non-equilibrium thermodynamics, Chemical potential gradient, Mass transfer, Geochemical reaction

### 1. Introduction

Geological sequestration of anthropogenic CO<sub>2</sub> is a promising carbon mitigation strategy<sup>[1, 2]</sup>, which includes the injection of CO<sub>2</sub> into deep saline aquifers, depleted oil and gas reservoirs, and deep coal seams<sup>[2, 3]</sup>, and the storage in deep saline aquifers seems to have the largest potential capacity<sup>[3, 4, 5]</sup>. The four main CO<sub>2</sub> sequestration mechanisms in deep saline aquifers proposed are solubility trapping; capillary trapping; hydrodynamic trapping and mineral trapping<sup>[1, 2]</sup>. In order to study the long-term behaviors of CO<sub>2</sub> in formations, and to estimate the possible CO<sub>2</sub> leakage risk, it is necessary to investigate the dissolution of CO<sub>2</sub> in brine, the mass transfer of dissolved CO<sub>2</sub> and the coupling behaviors of mass transfer with the mineral reactions of aqueous CO<sub>2</sub> with rocks over a wide range of spatial and temporal scales<sup>[1, 3, 6-8]</sup>.

Phase equilibria of CO<sub>2</sub> in water and brines have been widely studied<sup>[9-12]</sup>. The molecular-based statistical associating fluid theory (SAFT) equation of state (EOS) is a promising model for systems up to high pressures, which represents the density and phase equilibrium for CO<sub>2</sub>-H<sub>2</sub>O from 285 to 473 K and up to 600 bar, and for CO<sub>2</sub>-H<sub>2</sub>O-NaCl from 298 to 373 K and up to 200 bar<sup>[10, 13]</sup>. For the kinetics research, numerous investigations on the mass transfer of CO<sub>2</sub> in high-pressure water or brines have been conducted to simulate CO<sub>2</sub> geological or ocean disposal processes<sup>[5, 14-16]</sup>. Yang and Gu<sup>[5]</sup> studied CO<sub>2</sub> dissolution in brine at elevated pressures experimentally and described the mass transfer of CO<sub>2</sub> in brine using Fick's Second Law with an effective diffusion coefficient considering the effect of convection, which are two orders of magnitude larger than the molecular diffusivity of CO<sub>2</sub> in water<sup>[5]</sup>, and it implies that the density-driven natural convection greatly accelerates the mass transfer of CO<sub>2</sub> in brines. Generally, mass transfer flux is described with concentration gradient as the driving

force. However, in real systems, Fick's law must be amended to account for nonideal behavior. So the driving force for solute fluxes is not the concentration gradient, but the chemical potential gradient<sup>[17, 18]</sup>. Our previous work<sup>[19, 20]</sup> also reveals that it is necessary to consider the non-ideality of the complicated systems. Therefore, on the basis of the work by Yang and Gu<sup>[5]</sup>, the mass transfer of CO<sub>2</sub> in brines is investigated by chemical potential gradient model<sup>[21]</sup> based on derivation of  $\partial a_i / \partial t$  ( $a_i$  is the activity of species  $i$ ). The calculated results show the importance of the consideration of the non-ideality. Moreover, path-of-reaction and kinetic modeling of CO<sub>2</sub>-brine-mineral reactions in deep saline aquifers have been conducted<sup>[9, 22-25]</sup>. The nonisothermal reactive transport code TOUGHREACT<sup>[26, 27]</sup> were developed which introduced reactive chemistry into the multi-phase fluid and heat flow code TOUGH2<sup>[28]</sup>.

In this paper, the coupling behaviors of the mass transfer of aqueous CO<sub>2</sub> with the typical mineral reactions of aqueous CO<sub>2</sub> with rocks will be investigated and analyzed by chemical potential gradient and concentration gradient models, respectively.

## 2. Thermodynamic model

The fugacities of the aqueous CO<sub>2</sub> are calculated using SAFT1-RPM EOS<sup>[13]</sup> and the details are described in literature<sup>[13]</sup>.

## 3. Kinetics modeling

### 3.1. Model description

#### 3.1.1. Mass transfer

##### Concentration gradient model

The flux generalized to three dimensions is described as<sup>[18, 29]</sup>

$$J_i = -D_C \nabla C_i \quad (1)$$

where,  $J_i$  is molar flux of species  $i$ ;  $D_C$  is the effective diffusion coefficients in concentration gradient model;  $C_i$  is the molar concentration of species  $i$ .

##### Chemical potential gradient model

As described in above text, in real systems, chemical potential gradient is the driving force for solute fluxes<sup>[17, 18]</sup>, and the flux generalized to three dimensions is described as<sup>[18, 29]</sup>

$$J_i = - (D_\mu C_i / RT) \nabla \mu_i \quad (2)$$

where,  $J_i$  is molar flux of species  $i$ ;  $D_\mu$  is the effective diffusion coefficients in chemical potential gradient model;  $\mu_i$  is the chemical potential of species  $i$  and described by Eq. (3)<sup>[30]</sup>.

$$\mu_i = \mu_i^0 + RT \ln(f_i / f_i^0) = \mu_i^0 + RT \ln a_i \quad (3)$$

where,  $\mu_i^0$ ,  $a_i$ ,  $f_i$  and  $f_i^0$  are the standard chemical potential, activity, fugacity and standard fugacity of component  $i$ , respectively. At a certain T and P, both  $\mu_i^0$  and  $f_i^0$  are constants. In this paper, one-dimensional case is studied, and the convective molar flux by the bulk motion of the fluid is not added in Eqs. (1) and (2), but an effective diffusion coefficient considering the effect of convection is used. Combining Eq. (2) with Eq. (3), Eq. (4) can be obtained.

$$J_i = - \frac{D_\mu C_i}{RT} \nabla (RT \ln f_i) = -D_\mu C_i \nabla \ln f_i \quad (4)$$

### Diffusion coefficient determination

The effective diffusion coefficient is obtained based on the experimental kinetic data in Test 4 reported by Yang and Gu<sup>[5]</sup>. At the temperature and different pressures of Test 4, the quantitative relations of fugacities of aqueous CO<sub>2</sub> with their concentrations are determined from fitting according to the calculation results by SAFT1-RPM EOS<sup>[13]</sup> with a function form as  $f_{CO_2(aq)} = a + b \cdot C_{CO_2(aq)}$  in which a and b are parameters at a certain temperature and pressure. The aqueous CO<sub>2</sub> concentrations at the interface are calculated with SAFT1-RPM<sup>[13]</sup> by assuming instantaneous saturation of CO<sub>2</sub><sup>[21]</sup>. In the work of Ref. [5], the CO<sub>2</sub> dissolution was performed in a PvT cell with a cross-sectional area  $A$  ( $7.9273 \times 10^{-4} \text{ m}^2$ ) and brine phase height  $H$  (0.0442 m), the CO<sub>2</sub> pressures  $P_t$  at different time  $t$  were recorded. The number of moles of dissolved CO<sub>2</sub> ( $n_t$ ) are determined from the gaseous pressure at different time  $t$  and the initial experimental conditions. Based on the mass balance, Eq. (5) can be obtained.

$$\int_0^x C_{CO_2(aq)} A dx = n_t \quad (5)$$

where  $C_{CO_2(aq)}$  ( $\text{mol} \cdot \text{m}^{-3}$ ) is the concentration of aqueous CO<sub>2</sub> in brines, and  $A$  ( $\text{m}^2$ ) is the contact area of gaseous CO<sub>2</sub> with brine and is assumed to be the cross-sectional area of the cell, and  $x$  (m) is the mass transfer distance. In the work of Yang and Gu<sup>[5]</sup>, only the experimental kinetics data after 180s were used to analyze the mass-transfer process of CO<sub>2</sub> in the brine. In this paper, we also take the flux  $J$  and  $n_t$  after 180s.

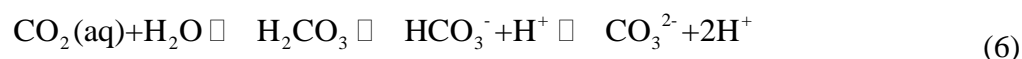
According to the flux  $J$  and  $n_t$  at different pressures in Test 4<sup>[5]</sup> and combining Eqs. (1) with (5), the effective diffusion coefficient at respective pressures in the one-dimensional concentration gradient model can be determined directly. While for the effective diffusion coefficient in the chemical potential gradient model, a simple but effective method, direct search method, can be used, in which the initial value and step length of the effective diffusion coefficient are assumed as  $1.0 \times 10^{-9} \text{ m}^2 \cdot \text{s}^{-1}$ , while the maximum value is  $1.0 \times 10^{-6} \text{ m}^2 \cdot \text{s}^{-1}$ . The minimum, maximum values and step length of the distance  $x$  are assumed as  $1.00 \times 10^{-6}$ ,  $H$  and  $5.00 \times 10^{-4} \text{ m}$ . Then according to the flux  $J$  and  $n_t$  at different pressures in Test 4<sup>[5]</sup> and combining Eqs. (4) and (5), the effective diffusion coefficient at respective pressures can be determined by the numerical simulation calculation.

### 3.1.2. Mineral reaction rate

#### Mineral reaction

Mineral trapping is the fixing of CO<sub>2</sub> in carbonate minerals due to a series of geochemical reactions<sup>[9, 31]</sup>. It is reported that the most promising reactions for mineral trapping involve the minerals which provide divalent cations (Ca<sup>2+</sup>, Mg<sup>2+</sup>, Fe<sup>2+</sup>) for precipitation of carbonate<sup>[9, 31]</sup>. One of the most common sedimentary-mineral sources of divalent cations is anorthite and is studied as a case in this paper. The mineral trapping takes place due to the following reactions as demonstrated by the example of anorthite dissolution:

Dissolution of CO<sub>2</sub> acidifies formation water through the following reaction<sup>[31]</sup>.



Aqueous CO<sub>2</sub> dissociates in water and produces carbonic acid, bicarbonate and carbonate ions, the acid attacks anorthite, leaching Ca<sup>2+</sup> and neutralizing the acid through Reaction (7)<sup>[9, 31]</sup>.



The divalent cations precipitates as calcium carbonate through Reactions (8) and (9)<sup>[9, 31]</sup>.



In this work, Eq. (7) and the following net reaction are considered to study the mineral reaction rate.



#### Mineral reaction rate

According to nonequilibrium thermodynamics, the chemical reaction rate of a single reaction is described as Eq. (11)<sup>[32]</sup>,

$$\text{Rate} = R_f (1 - e^{-A/RT}) \quad (11)$$

where,  $R_f$  is the forward rate of the reaction,  $A$  is the affinity and is described as the negative of the molar Gibbs free energy change of reaction,  $R$  is the gas constant,  $T$  is the temperature. Based on Eq. (11), the general rate equation for geochemical reaction kinetics is<sup>[22, 24]</sup>:

$$\text{Rate} = (1/V) \cdot \frac{dn_i}{dt} = (1/V) \cdot K \cdot A_{\text{min}} \cdot \exp(-E_a / RT) \cdot [1 - \frac{Q}{K_{\text{eq}}}] \quad (12)$$

where,  $V$  is the volume of brines,  $K$  is the rate constant,  $A_{\text{min}}$  is the reactive surface area,  $E_a$  is the activation energy,  $Q$  is the activity product and is described through Eq. (13), and  $K_{\text{eq}}$  is the equilibrium constant.

$$Q = \frac{[\text{H}^+]}{[\text{Ca}^{2+}] \cdot f_{\text{CO}_2(\text{aq})}} \quad (13)$$

In Eq. (13),  $[\text{H}^+]$  and  $[\text{Ca}^{2+}]$  are the molar concentrations of  $\text{H}^+$  and  $\text{Ca}^{2+}$  ions, respectively.

#### Mineral reaction rate parameters

Anorthite is chosen for a case study. The volume of brines is assumed as 1 m<sup>3</sup> (approximately equals to 1 kg). The rate constant, activation energy and specific reactive surface area of the rocks used are taken from literature<sup>[23]</sup> and shown in Table 1. The water:rock ratio is fixed at 1 kg water per 15 kg of rock<sup>[24]</sup>. The gas constant is taken as 8.3145 J·mol<sup>-1</sup>·K<sup>-1</sup>. The effect of temperature on the mineral reaction rate is neglected and the temperature is taken as 298.15K. In the calculation of  $Q$ ,  $[\text{H}^+]$  and  $[\text{Ca}^{2+}]$  are taken from the pH value and composition of Rose Run brines<sup>[22]</sup>. The fugacities of aqueous CO<sub>2</sub> are determined by SAFT1-RPM EOS<sup>[13]</sup>. According to the equilibrium constants of the following Eqs. (14) and (15), the equilibrium constant of Eq. (10) can be obtained as shown in Eq. (16).



Table 1. The mineral considered and its reaction rate constant ( $K$ ), activation energy ( $E_a$ ) and specific reactive surface area<sup>[23]</sup>.

| Mineral   | $K$ (mol·m <sup>-2</sup> ·s <sup>-1</sup> ) | $E_a$ (J·mol <sup>-1</sup> ) | Specific reactive surface area (m <sup>2</sup> ·g <sup>-1</sup> ) |
|-----------|---|------------------------------|---|
| Anorthite | $7.6 \times 10^{-10}$                       | $1.78 \times 10^4$           | $1.00 \times 10^{-3}$   |

### 3.1.3. Model of coupling mass transfer with mineral reaction

The model of coupling mass transfer with mineral reaction can be derived from the equation of continuity for species  $i$  in a multicomponent reacting mixture as shown in Eq. (17)<sup>[29]</sup>.

$$\frac{\partial C_i}{\partial t} = -(\nabla \cdot J_i) - r_i \quad (17)$$

where,  $r_i$  is the consumption rate of  $i$  by reaction. According to the different flux forms of Eqs. (1) and (4) and the reaction rate form of Eq. (12), the concentration gradient and chemical potential gradient models of coupling mass transfer with mineral reaction can be obtained.

### 3.2. Initial and boundary conditions

The initial condition is given by Eq. (18)

$$C_i(x,t)|_{t=0} = \begin{cases} C_{i0} & (x=0) \\ 0 & (x>0) \end{cases} \quad (18)$$

where,  $C_{i0}$  is the aqueous CO<sub>2</sub> saturated concentration. The left boundary conditions are the interface concentrations of aqueous CO<sub>2</sub> calculated with SAFT1-RPM<sup>[13]</sup> by assuming instantaneous saturation of CO<sub>2</sub><sup>[21]</sup>. The right boundary condition is

$$\frac{\partial C_i(x,t)}{\partial x} \Big|_{x=x_R} = 0 \quad (t > 0) \quad (19)$$

where,  $x_R$  represents the distance between the right boundary and the interface.

### 3.3. Numerical solution

The partial differential equations are solved numerically using the built-in “pdepe” in the MATLAB program, which solves initial-boundary value problems for systems of parabolic and elliptic partial differential equations. The diffusion coefficient is taken the value calculated in this paper at 7.5322 MPa and the other experimental conditions of Test 4<sup>[5]</sup>.

## 4. Results and Discussions

### 4.1. Effective diffusion coefficient

The effective diffusion coefficients at different pressures and other experimental conditions of Test 4<sup>[5]</sup> are calculated and shown in Fig. 1. Fig. 1 shows that the effective diffusion coefficients by both concentration gradient and chemical potential gradient models are close to each other and decrease with increasing pressure. Moreover, the effective diffusion coefficients calculated in this paper are close to that in our previous work by the chemical potential gradient model based on the derivation of  $\partial a_i / \partial t$ <sup>[21]</sup>.

#### 4.2. Concentration distribution by concentration and chemical potential gradient models

The concentration distribution of aqueous CO<sub>2</sub> with distance at 10 and 20 years through the concentration gradient and chemical potential gradient models coupling mass transfer with mineral reaction is shown in Fig. 2. From Fig. 2, there are considerable discrepancies for the concentration distribution with distance by the two models, which implies the importance of the consideration of non-ideality. The concentrations of aqueous CO<sub>2</sub> by the concentration gradient model are higher and further than that by the chemical potential gradient.

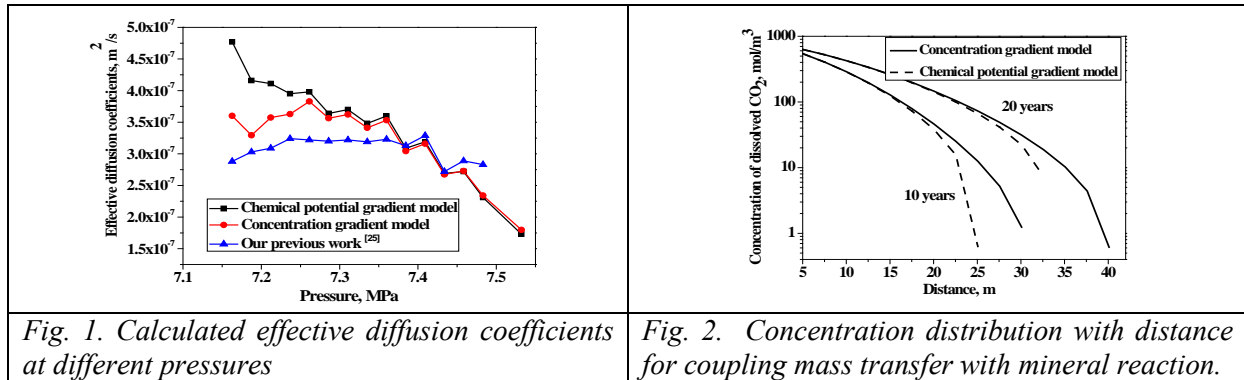


Fig. 1. Calculated effective diffusion coefficients at different pressures

Fig. 2. Concentration distribution with distance for coupling mass transfer with mineral reaction.

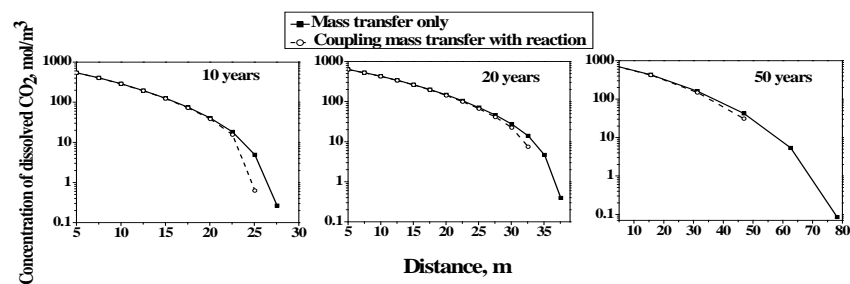


Fig. 3. Calculated concentration distribution with distance at different time scales in which two different cases are considered (1) mass transfer only; (2) coupling mass transfer with mineral reaction.

#### 4.3. Concentration distribution by chemical potential gradient model for two cases: mass transfer only and coupling mass transfer with mineral reaction.

The concentration distribution of aqueous CO<sub>2</sub> with distance at 10, 20, 50 years by the chemical potential gradient model for two cases (mass transfer only and coupling mass transfer with mineral reaction) is shown in Fig. 3. From Fig. 3, for the anorthite case, it is observed that the mineral reaction plays a considerable role for the geological sequestration when the time scale reaches 10 years. Moreover, our results show that the mineral reaction does not bring obvious effect on the concentration distribution of aqueous CO<sub>2</sub> for time scale less than 10 years, and when the time scale is 1000 years, the aqueous CO<sub>2</sub> by the mass transfer can be completely reacted by the model rock anorthite due to the neglect of the effects of hydrodynamics and gravity. In future work, more types of rocks and the effects of hydrodynamics and gravity should be considered.

### 5. Conclusions

In this paper, the coupling behaviors of the mass transfer of aqueous CO<sub>2</sub> with the mineral reactions of aqueous CO<sub>2</sub> with model rock anorthite are investigated by chemical potential gradient and concentration gradient models, respectively. The effective diffusion coefficients of CO<sub>2</sub> are obtained based on the experimental kinetic data reported in literature. The results

show that there are considerable discrepancies for the concentration distribution with distance by the concentration gradient and chemical potential gradient models, which implies the importance of the consideration of the non-ideality. And the concentrations of aqueous CO<sub>2</sub> at different distances by the concentration gradient model are higher and further than that by the chemical potential gradient. The mineral reaction plays a considerable role for the geological sequestration when the time scale reaches 10 years for the anorthite case.

### Acknowledgment

The authors thank Luleå University of Technology, the Swedish Research Council, the National Basic Research Program of China (2009CB226103), the National Natural Science Foundation of China (50808039) and the Natural Science Foundation of Jiangsu Province, China (BK2009138) for the financial supports.

### References

- [1] D. P. Schrag, Preparing to capture carbon, *Science* 315, 2007, pp. 812-813.
- [2] A. Firoozabadi, P. Cheng, Prospects for subsurface CO<sub>2</sub> sequestration, *AIChE J.* 56, 2010, pp. 1398-1405.
- [3] R. G. Jr. Bruant, A. J. Guswa, et al. Safe storage of CO<sub>2</sub> in deep saline aquifers, *Environ. Sci. Technol.* 36(11), 2002, pp. 240A-245A.
- [4] S. Bachu, J. J. Adams, Sequestration of CO<sub>2</sub> in geological media in response to climate change: capacity of deep saline aquifers to sequester CO<sub>2</sub> in solution, *Energy Convers. Manage.* 44, 2003, pp. 3151-3175.
- [5] C. Yang, Y. Gu, Accelerated mass transfer of CO<sub>2</sub> in reservoir brine due to density-driven natural convection at high pressures and elevated temperatures, *Ind. Eng. Chem. Res.* 45, 2006, pp. 2430-2436.
- [6] S. M. V. Gilfillan, B. S. Lollar, et al. Solubility trapping in formation water as dominant CO<sub>2</sub> sink in natural gas fields, *Nature* 458, 2009, pp. 614 -618.
- [7] D. W. Keith, J. A. Giardina, et al. Regulating the underground injection of CO<sub>2</sub>, *Environ. Sci. Technol.* 39, 2005, pp. 499A-505A.
- [8] C. M. Oldenburg, Transport in geologic CO<sub>2</sub> storage systems, *Transp. Porous Med.* 82, 2010, pp. 1-2.
- [9] B. Zerai, CO<sub>2</sub> sequestration in saline aquifer: geochemical modeling, reactive transport simulation and single-phase flow experiment. Doctoral Dissertation, January, 2006.
- [10] Y. H. Ji, X. Y. Ji, et al. Progress in the study on the phase equilibria of the CO<sub>2</sub>-H<sub>2</sub>O and CO<sub>2</sub>-H<sub>2</sub>O-NaCl systems. *Chin. J. Chem. Eng.*, 15(3), 2007, pp. 439-448.
- [11] N. A. Darwish, N. Hilal, A simple model for the prediction of CO<sub>2</sub> solubility in H<sub>2</sub>O-NaCl system at geological sequestration conditions, *Desalination* 260, 2010, pp. 114-118.
- [12] N. N. Akinfiyev, L. W. Diamond, Thermodynamic model of aqueous CO<sub>2</sub>-H<sub>2</sub>O-NaCl solutions from 22 to 100 degrees C and from 0.1 to 100 MPa, *Fluid Phase Equilibria* 295, 2010, pp. 104-124.
- [13] X. Y. Ji, S. P. Tan, et al. SAFT1-RPM approximation extended to phase equilibria and densities of CO<sub>2</sub>-H<sub>2</sub>O and CO<sub>2</sub>-H<sub>2</sub>O-NaCl systems. *Ind. Eng. Chem. Res.* 44, 2005, pp. 8419-8427.
- [14] B. Arendt, D. Dittmar, R. Eggers, Interaction of interfacial convection and mass transfer effects in the system CO<sub>2</sub>-water, *Int. J. Heat Mass Transfer* 47, 2004, pp. 3649-3657.

- [15] R. Farajzadeh, H. Salimi, et al. Numerical simulation of density-driven natural convection in porous media with application for CO<sub>2</sub> injection projects, *Int. J. Heat Mass Transfer* 50, 2007, pp. 5054-5064.
- [16] R. Farajzadeh, P. L. J. Zitha, J. Bruining, Enhanced mass transfer of CO<sub>2</sub> into water: experiment and modeling, *Ind. Eng. Chem. Res.* 48, 2009, pp. 6423-6431.
- [17] N. Kocherginsky, Y. K. Zhang, Role of standard chemical potential in transport through anisotropic media and asymmetrical membranes, *J. Phys. Chem. B* 107, 2003, pp. 7830-7837.
- [18] G. A. Truskey, F. Yuan, D. F. Katz., *Transport phenomena in biological systems*. Prentice Hall, 2009.
- [19] C. Liu, Y. Ji, et al. Thermodynamic analysis for synthesis of advanced materials. *Molecular Thermodynamics of Complex Systems, Struct Bond* 131, 2009, pp. 193-270.
- [20] Y. H. Ji, X. Y. Ji, et al. Modelling of mass transfer coupling with crystallization kinetics in microscale, *Chem. Eng. Sci.* 65(9), 2010, pp. 2649-2655.
- [21] Y. H. Ji, X. Y. Ji, X. H. Lu, Modeling mass transfer of CO<sub>2</sub> in brine at high pressures by chemical potential gradient, *Fluid Phase Equilibria* 2010 submitted.
- [22] B. Zerai, B. Z. Saylor, G. Matisoff, Computer simulation of CO<sub>2</sub> trapped through mineral precipitation in the Rose Run Sandstone, Ohio, *Applied Geochemistry* 21, 2006, pp. 223-240.
- [23] F. Gherardi, T. Xu, K. Pruess, Numerical modeling of self-limiting and self-enhancing caprock alteration induced by CO<sub>2</sub> storage in a depleted gas reservoir, *Chemical Geology* 244, 2007, pp. 103-129.
- [24] R. T. Wilkin, D. C. Digiulio, Geochemical impacts to groundwater from geologic carbon sequestration: controls on pH and inorganic carbon concentrations from reaction path and kinetic modeling, *Environ. Sci. Technol.* 44, 2010, pp. 4821-4827.
- [25] T. Xu, Y. K. Kharaka, et al. Reactive transport modeling to study changes in water chemistry induced by CO<sub>2</sub> injection at the Frio-I Brine Pilot, *Chemical Geology* 271, 2010, pp. 153-164.
- [26] T. Xu, K. Pruess, Modeling multiphase non-isothermal fluid flow and reactive geochemical transport in variably saturated fractured rocks: 1. Methodology. *Am. J. Sci.* 301, 2001, pp. 16-33.
- [27] T. Xu, E. L. Sonnenthal, et al. TOURGHREACT: a simulation program for non-isothermal multiphase reactive geochemical transport in variably saturated geologic media. *Comp. Geosci.* 32, 2006, pp. 145-165.
- [28] T. Xu, J. A. Apps, K. Pruess, Numerical simulation to study mineral trapping for CO<sub>2</sub> disposal in deep aquifers. *Appl. Geochem.* 19, 2004, pp. 917 – 936.
- [29] R. B. Bird, W. E. Stewart, et al. *Transport Phenomena*, John Wiley & Sons, Inc., 2006.
- [30] J.M. Prausnitz, R.N. Lichtenthaler, E.G. de Azevedo, *Molecular Thermodynamics of Fluid-phase Equilibria*. Third edition, NJ, Prentice Hall PTR, 1999.
- [31] J. M. Matter, P. B. Kelemen, Permanent storage of carbon dioxide in geological reservoirs by mineral carbonation, *Nature Geoscience* 2, 2009, pp. 837 – 841.
- [32] D. Kondepudi, I. Prigogine, *Modern Thermodynamics: From Heat Engines to Dissipative Structures*. John Wiley & Sons, Chichester, 1998.

## Clean Coal Utilization Based on Underground Coal Gasification Integrated Solid Oxide Fuel Cells and Carbon dioxide Sequestration

Prabu V\*, Jayanti S

Indian Institute of Technology Madras, Chennai, India

\* Corresponding author. Tel: +4422575152 E-mail: vprabu1979@yahoo.co.in

**Abstract:** Underground coal gasification (UCG) is a clean coal technology which converts coal into a combustible gas *in situ* without mining and without bringing up the ash contained in the coal. Thus, the attendant problems of coal washing, ash handling and disposal can be avoided. The combustible gas mixture, consisting primarily of hydrogen, methane, carbon monoxide--all of which are fuels for an solid oxide fuel cell (SOFC) system-- and carbon dioxide, can be fed to a battery of SOFC after gas cleaning to remove hydrogen sulphide and other impurities. A large portion, typically 50%, of the chemical energy contained in the product gas can be converted into electrical energy by the SOFC. The exhaust gases from the SOFC are typically at a temperature of the order of 600 to 800 deg C. Heat energy from these will be extracted to produce steam, part of which will be used for UCG and the rest will be sent for SOFC internal reforming and shifting reactions. The exhaust gases, consisting primarily of carbon dioxide and steam, will be finally fed through a condenser and will then be sent for compression and sequestration. Thus, the overall system envisaged makes use of oxygen-fed UCG and SOFC to generate electrical energy and an exhaust gas consisting primarily of carbon dioxide and the easily condensable steam which enables CO<sub>2</sub> sequestration. The overall integrated system can be divided into five units namely underground coal gasification, UCG product gas purification, electrical power generation from SOFC, heat recovery system and carbon sequestration unit. An energy analysis with heat integration of all the systems for a nominal 500 MWt will be discussed.

**Keywords:** Underground coal gasification, Solid oxide fuel cell, Carbon sequestration, Heat integration.

### Nomenclature

|   |  |
|---|--|
| $W_{ele}$ electrical work.....kJ              | $\eta$ efficiency.....                             |
| $F$ Faraday's constant.....C                  | $f$ flow rate ..... mol·s <sup>-1</sup>            |
| $K$ equilibrium reaction constant.....        | $c_p$ specific heat..... kJ/kg K                   |
| $p$ partial pressure.....bar                  | $E$ Nernst potential..... V                        |
| $T$ mean temperature.....K                    | $E_o$ Ideal potential at standard condition..... V |
| $R$ universal gas constant ..... kJ/kmol K    | $j$ electron number.....                           |
| $H$ enthalpy .....kJ                          | $U_f$ fuel utilization factor.....                 |
| $N_{H_2}$ moles of hydrogen converted.....mol | $HV$ Heating value.....kJ/mol                      |
| $\Delta H_R$ Heat of reaction.....kJ/mol      | $Q$ excess heat.....kW                             |

### 1. Introduction

Coal is the major fossil fuel in the world and 70% of electricity produced in India comes from coal. Coal is expected to be the mainstay of electricity generation in India for the next several decades. However, coal utilization is fraught with environmental problems. Given that Indian coal typically has large ash content, its mining, washing, and final utilization in pulverized coal boilers leads to significant land, water and air pollution. The ash collected from the stacks also poses a disposal problem. On top of these, there is increased awareness of the need to reduce CO<sub>2</sub> emissions into the atmosphere. Hence it is necessary to develop suitable technologies for coal conversion efficiently without environmental pollution.

Underground coal gasification (UCG) is a clean coal technology with *in situ* gasification having no mining problem, no ash disposal, offering economical exploitation of low grade coal. It is a clean coal technology which enables exploitation of coal reserves in an

environmental friendly manner. A large amount of work has been reported in the 1970s and 80s on UCG [1-5] and there has been renewed interest in UCG as showed by a number of publications in the last decade [6-10]. These studies have focused on coal gasification per se and not much on CO<sub>2</sub> sequestration. In the present paper, we describe a process by which UCG can be coupled to a solid oxide fuel cell (SOFC) system to develop an integrated power plant which makes use of the fuel gas from the UCG, generates electricity from it and leaves an exhaust gas consisting of 85% CO<sub>2</sub> which can therefore be readily sequestered. The layout of the proposed plant is described in Section 2 and a thermodynamic analysis of the system is discussed in Section 3.

## **2. Description of the coupled UCG-SOFC system**

A schematic diagram of the integrated UCG-SOFC system is shown in Figure 1. The product gas from the UCG system typically has some particulate matter and impurities in the form of tar, sulphur and its compounds. These are removed as the gas passes through a cyclone separator, a gas filter unit and a tar removal unit. The hot gas from the cyclone separator exchanges heat with the clean gas coming from the tar removal system in a gas-to-gas heat exchanger. The clean fuel gas is further heated (by the hot anode side exhaust of the solid oxide fuel cell (SOFC) unit) and is mixed with steam and is fed to the anode side of the SOFC unit. The unused portion of hydrogen and carbon mono oxide (85% fuel utilization efficiency is assumed in the SOFC) is then fed to a combustor to completely convert the remaining fuel into CO<sub>2</sub> and steam. These gases are fed to a condenser in which most of the steam is removed and the remaining gas, consisting mostly of CO<sub>2</sub> is sent to the CO<sub>2</sub> sequestration unit. The thermal energy in the exhaust gas of the combustor is used to generate steam in the condenser unit which is used for fuel reforming in the SOFC as well as for coal gasification in the UCG gasifier. Further, the thermal energy of the hot air from the cathode code is also used to preheat the air that is supplied to the cathode so as to maintain the SOFC temperature at the design condition. In order to eliminate nitrogen from the system (so as to facilitate CO<sub>2</sub> sequestration), an air separation unit is used to supply oxygen in required quantity to the combustor (this is especially needed to maintain stable combustion as the anode gas from the SOFC contains only a small percentage of fuel, namely, H<sub>2</sub> and CO, the rest being CO<sub>2</sub> and steam) as well as that required for gasification in the UCG gasifier unit. The flow paths of the various streams are shown in Figure 1.

The above coupling of the UCG with an SOFC enables proper thermal integration of the various units to produce electrical energy directly from the product gas of the UCG. Moreover, the combination of UCG and SOFC is such that the integration can be done in such a way that all the CO<sub>2</sub> that is produced in the fuel utilization can be captured in a relatively straightforward manner without the need for an external CO<sub>2</sub> absorption unit as is required in normal combustion of the UCG gas. One disadvantage however is the need to clean the UCG gas to remove tar and sulphur products so that it can be used in an SOFC. The technology for the required gas cleaning already exists; the calculations described in the next section show that the gas cleaning can also be done without a significant energy penalty resulting in a combined system with a significantly higher overall thermal efficiency and little environmental pollution.

## **3. Thermodynamic model and analysis**

The overall integrated plant consist of five units, namely, underground coal gasification, UCG product gas purification, electrical power generation from SOFC, heat recovery systems and carbon sequestration unit. An energy balance on these units has been carried out to determine

the overall utilization of energy. The UCG system is considered to be operating at atmospheric pressure and the bituminous grade coal in underground undergoes partial oxidation and gasification in presence of pure oxygen to produce calorific value synthesis gas. The electrical efficiency of SOFC fuel cell is found out based on the shifting, reforming and electrochemical reaction with reaction kinetics.

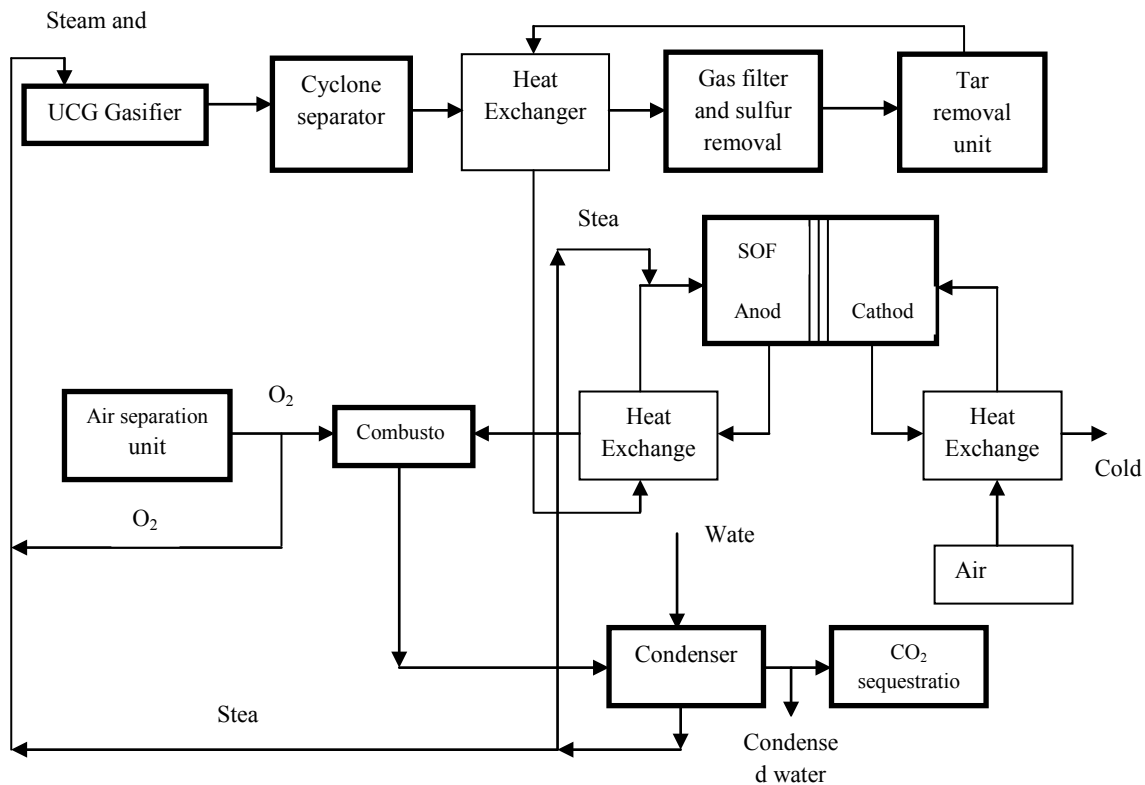


Fig.1. Schematic of the integrated underground coal gasification with solid oxide fuel cell

### 3.1. UCG Plant

A 500 MW of product gas generated from UCG and the flow rate of input and output stream of gases and its molar composition has taken from Lawrence Livermore national laboratory (LLNL) literature [11] and used for the basis of theoretical calculation. Table 1 represents the product gas molar composition and total product gas flow rate from UCG of 2600 mol/s.

Table 1. Product gas composition from UCG plant

| Species         | Mole fraction | Product gas flow rate[mol/s] |
|-----------------|---------------|------------------------------|
| N <sub>2</sub>  | 0.018         | 47.36                        |
| CO              | 0.11          | 289.47                       |
| CO <sub>2</sub> | 0.44          | 1157.89                      |
| H <sub>2</sub>  | 0.37          | 973.68                       |
| CH <sub>4</sub> | 0.05          | 131.58                       |

Heat of combustion of product gas (HV) = 190 kJ/mol

Product gas flow rate from UCG to SOFC ( $f_p$ ) = 2631.58 mol/s

Total injection flow rate of steam and oxygen = 2255.63 mol/s

Injection mole fraction of oxygen = 0.47

The UCG gasifier operating temperature is assumed to about 800°C in oxyfuel mode. Pure oxygen from air separation unit and steam generated from condenser unit are injected into

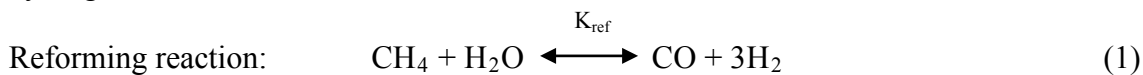
injection hole and the gasified products at 650°C are collected from the production hole of UCG.

### 3.2. UCG product gas purification system

In UCG system, volatile matter liberated during combustion, gasification and pyrolysis zone will move along the cavity and make contact with the fresh coal. This would result in product gas enriched with tar content since there is no further thermal cracking [12]. The issue of removal of mercury, arsenic and other trace metals is not addressed here as not much is known about their formation and presence in the UCG gas. In order to utilize these product gases in SOFC for power generation, it is necessary to remove the tar and sulfur content impurities. Cyclone separator and ceramic filters are used to remove the particulate matter and alkali compounds from product gases before the tar removal. A wet electrostatic precipitator is used for tar condensation and removal. The purified gas stream is cooled to about 50° C and the enthalpy is again gained from the inlet gas stream of purification system and fed into the SOFC.

### 3.3. SOFC fuel cell system

The purified hot gas stream from with steam is introduced at the anode side of the SOFC. To avoid the carbon deposition in SOFC, a steam to carbon ratio of 2:1 is assumed [13]. Excess oxygen of 400% in air is supplied at the cathode side to recover the generated heat energy. The operating temperature of SOFC is assumed to be 700°C. The temperature of exit stream from anode and cathode side is same as the operating temperature of SOFC. In IRSOFC (Internal reforming SOFC), only hydrogen is assumed to undergo oxidation for electric power generation. Carbon monoxide, methane undergoes reforming and water gas shifting reactions [Eq. (1)] with steam and produces hydrogen. High operating temperature of SOFC is suitable for reforming and shifting reaction which converts the CO and other hydrocarbons to hydrogen. A fuel utilization factor of 0.85 is assumed for the fuel cell.



$$K_{\text{ref}} = [\text{CO}][\text{H}_2]^3/[\text{CH}_4][\text{H}_2\text{O}] \quad (2)$$

$$K_{\text{shf}} = [\text{H}_2][\text{CO}_2]/[\text{CO}][\text{H}_2\text{O}] \quad (3)$$

where  $K_{\text{ref}}$  and  $K_{\text{shf}}$  are the equilibrium constants for reforming and shifting reaction respectively. The equilibrium constants are calculated using the temperature dependent polynomial expressions [14]. The equilibrium gas composition can be determined using Eq. (2 & 3).

### 3.4. Estimation of Overall Thermal Energy Conversion Efficiency

The overall thermal energy conversion efficiency ( $\eta$ ) of the coupled UCG-SOFC process can be estimated from the thermal energy content in the UCG gas and the electrical power output from the SOFC system. The latter is estimated as follows. The cell e.m.f,  $E$ , of the SOFC is calculated for the particular concentrations of hydrogen, oxygen and steam produced ( $p_{\text{H}_2}$ ,  $p_{\text{O}_2}$ ,  $p_{\text{H}_2\text{O}}$ ) used in the cell using the Nernst equation [15]:

$$E = E_0 + (RT/jF) \ln[(p_{\text{H}_2} \cdot p_{\text{O}_2}^{1/2})/p_{\text{H}_2\text{O}}] \quad (4)$$

where  $E_0$  is the ideal potential at standard condition,  $j$  is the electron number.

The electrical power output from the SOFC is then calculated as

$$W_{\text{ele}} = EN_{\text{H}_2} jF \quad (5)$$

where  $N_{\text{H}_2}$  is the number of moles of hydrogen, and  $F$  is the Faraday's constant.

The overall thermal energy conversion efficiency can now be calculated by dividing the electrical power output by the thermal energy flow rate in the UCG gas:

$$\eta = W_{\text{ele}} / (f_p \times HV) \quad (6)$$

where  $f_p$  is product gas flow rate from UCG in mol/s and  $HV$  is the heating value of the product gas from UCG.

### 3.5. Estimation of the air inlet temperature for the SOFC

Energy balance can be made over the SOFC fuel cell system to calculate the air inlet temperature to the cathode side [Fig.2]. Eq. (7) gives the excess energy generated in the fuel cell is taken up by the incoming air and gas stream to maintain a constant operating temperature in the cell.

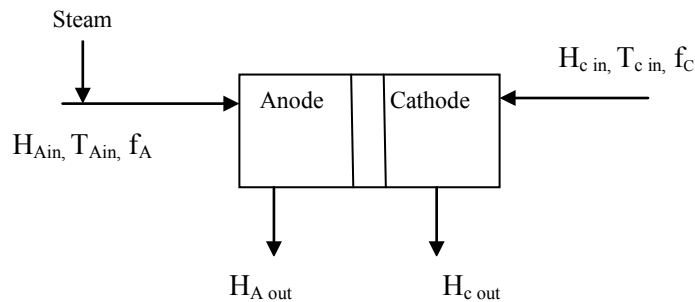


Fig.2. Schematic diagram of SOFC Model

$$\Delta H_R = W_{\text{ele}} + Q \quad (7)$$

where  $\Delta H_R$  is the heat of reaction (kJ/mol),  $Q$  is the excess energy generated in the fuel cell.

$$Q = f_A \int_{T_{\text{Ain}}}^{T_{\text{sofc}}} C_p dT + f_C (H_{\text{SOFC}} - H_{\text{C in}}) \quad (8)$$

where  $f_A$  and  $f_C$  are the input flow rates of anode side gas stream and cathode side air stream respectively.

From Eq. (8), the air inlet temperature to cathode side of the fuel cell is calculated.

### 3.6. Heat recovery system

The outlet gas from anode and cathode of SOFC at high temperature of 700°C are utilized for the heat recovery system. The inlet gas streams of cathode and anode are heated using heat exchangers by their respective outlet gas streams. The trace quantity of unconverted gas from SOFC can be burnt in a combustor with oxygen and the hot gas from combustor has sent to the condenser. A fresh steam is generated from condenser which is then supplied to the SOFC

cathode inlet and UCG injection hole. The two heat exchangers at the inlet of SOFC system of cathode and anode and the combustor and the condenser for fresh steam generation will constitute the heat recovery system of the integrated system.

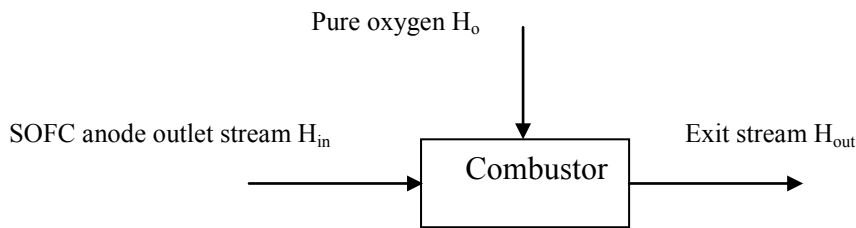


Fig.3. Schematic diagram of combustor model.

Complete combustion of remaining hydrogen, carbon monoxide and trace amount of methane are assumed in the combustor. Pure oxygen of 150% in excess of stoichiometric requirement for complete combustion is supplied to the combustor. The temperature of the exit stream from combustor (Fig.3) can be calculated from the enthalpy balance [Eq. (9)] over combustor.

$$H_{in} + H_o = H_{out} \quad (9)$$

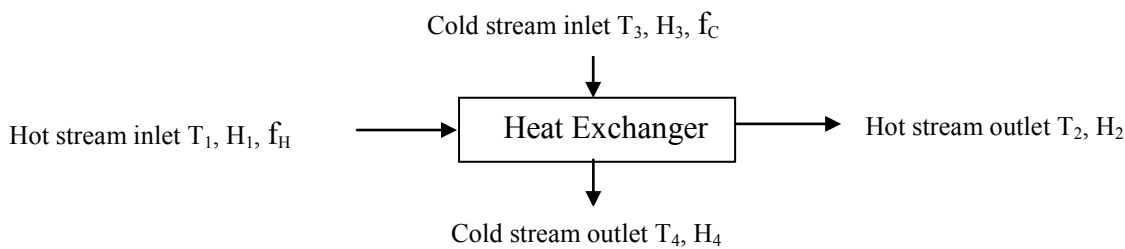


Fig.4. Schematic diagram of Heat Exchanger model

Fig.4 represents the schematic diagram of heat exchanger model. The cold stream outlet temperature can be calculated from the enthalpy balance equation [Eq. (10)].

$$f_H (H_1 - H_2) = f_C \int_{T_3}^{T_4} C_p dT \quad (10)$$

where  $f_H$  and  $f_C$  are the flow rates of hot and cold streams respectively.

#### 4. Results and Discussion

An overall energy balance is made for the entire thermodynamic model for the integrated system of UCG and SOFC. The steam generated from condenser at 600°C is sent to the UCG and SOFC with approximately equal proportion.

The hot product gas from the UCG plant enters the purification system at 650°C and cooled in a heat exchanger to 200°C and then it enters into the filter. Small particulate matters and condensed alkali compounds are filtered through the gas filter. Particulate free gases are then entered into the wet electrostatic precipitator to remove the tar which is enriched in the product gases. The tar free product gas are coming out from the wet ESP at about 50°C are heated to about 525°C using the exit gas stream of UCG. In order to raise the temperature of

the product gas at about 650°C to meet the SOFC operating temperature, the purified gas is heated again with the outlet gas stream of SOFC at anode side.

Table 2. SOFC inlet and outlet gas stream composition.

| Species          | Inlet stream mole percent | Outlet stream mole percent |
|------------------|---------------------------|----------------------------|
| N <sub>2</sub>   | 1.28                      | 1.19                       |
| CO <sub>2</sub>  | 31.25                     | 38.15                      |
| CO               | 7.81                      | 1.64                       |
| CH <sub>4</sub>  | 3.55                      | 0.000044                   |
| H <sub>2</sub>   | 26.28                     | 6.52                       |
| H <sub>2</sub> O | 29.83                     | 52.5                       |

Table 2 represents the SOFC inlet and outlet gas composition of cathode side. In outlet gas stream, only a trace amount of methane is present and constitutes 50 mole % of steam. The electrochemical work done by the SOFC can be calculated using the Nernst equation as 312.53MW. Electrical efficiency of the SOFC cell is found as 62.5%.

The unconsumed fuel from SOFC is burnt in the combustor with pure oxygen to extract more energy and the outlet gas is purely a composition of steam and carbon dioxide. The combustion of unconsumed fuel from SOFC in the combustor can be carried out using excess oxygen.

Table 3. Combustor inlet and outlet gas stream composition

| Species          | Inlet stream mole percent | Outlet stream mole percent |
|------------------|---------------------------|----------------------------|
| N <sub>2</sub>   | 1.08                      | 1.125                      |
| CO <sub>2</sub>  | 34.62                     | 37.49                      |
| CO               | 1.49                      | 0                          |
| CH <sub>4</sub>  | 0.00004                   | 0                          |
| H <sub>2</sub>   | 5.91                      | 0                          |
| H <sub>2</sub> O | 47.64                     | 55.62                      |
| O <sub>2</sub>   | 9.25                      | 5.77                       |

Table 3 shows the combustor outlet gas composition. Combustor outlet stream contains 37% of CO<sub>2</sub> and 55% of steam which is then sent to the condenser to extract the heat energy. All the steam can be condensed and the pure CO<sub>2</sub> is separated and sent to sequestration unit.

## 5. Conclusion

A fully integrated UCG-SOFC system is proposed to provide clean electrical energy from underground coal. The combination of UCG and SOFC is such that thermal as well as system integration of the two units can be carried out readily. A first-cut energy analysis, without including the cost of the air separation unit and the cost of compression of the CO<sub>2</sub> for the purposes of, say, underground sequestration, gives an overall thermal efficiency of above 60%. The combined system also utilizes fossil fuel in a clean manner without any particulate or gaseous emissions, thus providing a clean source of energy from conventional sources.

## References

- [1] W.R.Aiman, W.T.Fisher, Lawrence Livermore National Laboratory Insitu coal gasification Program Quarterly Progress Report. January through March 1978, UCRL 50026-78-1
- [2] C.B.Thorsness, J R Creighton. Review of underground coal gasification field experiments at HOE creek. Report No.UCRL-87662-Rev.1. U.S.DOE. Livermore, CA: Lawrence Livermore National Laboratory; 1983
- [3] P.N.Thompson, Gasifying coal underground. Endeavour 1978;2: 93 -97
- [4] A.M.Winslow, Numerical Model of coal gasification in a packed bed. Symposium on combustion (international) 1977:16:503 – 513.
- [5] C B Thorsness, E A Grens, A Sherwood, A one dimensional Model for Insitu coal gasification. Report No.UCRL-52523, U.S.DOE.Livermore, CA: Lawrence Livermore National Laboratory; 1978.
- [6] M.S.Blinderman, D.N.Saulov, A.Y.Klimenko. Forward and reverse combustion linking in underground coal Gasification. Energy 2008; 33: 446-454.
- [7] L Yang, J Liang, L Yu, Clean coal technology – Study on the pilot project experiment of underground coal gasification. Energy 2003;28:1445 – 1460
- [8] L Yang, X Zhang, S Liu, W. Zhang, Field test of large-scale hydrogen manufacturing from underground coal gasification. International journal of Hydrogen Energy 2008; 33:1275 – 1285.
- [9] G.Perkins, V.Sahajwalla. A Mathematical Model for the chemical reaction of a semi-infinite block of coal in underground coal Gasification. Energy and fuels 2005;19:1679 – 1692
- [10] S.Daggupati, N.Ramesh. R.N.Manadapati, S.M.Mahajani, A.Ganesh, D.K Mathur, R.K Sharma, P.Aghalayam, Laboratory studies on combustion cavity growth in lignite coal blocks in the context of underground coal Gasification. Energy 2010;35: 2374-2386.
- [11] W.R.Aiman, M L Donohue, LLL insitu coal gasification project, Quarterly progress Report, Lawrence Livermore laboratory, Report No. UCRL 50026 -79 -3, 1979.
- [12] T.Kivisaari, P Bjornbom, C Sylwan, B Jacquinet, D Jansen, A Groot, The feasibility of a coal gasifier combined with a high temperature fuel cell, Chemical Engineering Journal 100, 2004, pp 167 -180.
- [13]A.O.Omosun, A.Bauen, N.P.Brandon, C.S.Adijman, D.Hart, Modelling system efficiencies and costs of two biomass-fuelled SOFC systems, Journal of power sources 131, 2004, pp 96 – 106.
- [14] S.Ghosh, S.De, Thermodynamic performance study of an integrated fuel cell combined Cycle- an energy analysis, Journal of Power and Energy 217, 2002, pp 137 -147.
- [15] S.Ghosh, S.De, Energy analysis of a cogeneration using coal gasification and solid oxide fuel cell, Energy 31, 2006, pp 345 – 363.

## Climate Change and Water Resources for Energy Generation in Tanzania

Z. J .U. Malley<sup>1\*</sup>

<sup>1</sup>Agricultural Research Institute-Uyole P.O. Box 400, Mbeya, Tanzania

\*Corresponding author's Tel: +255252510363, Fax: +255252510065, Email: [zjmalley@yahoo.co.uk](mailto:zjmalley@yahoo.co.uk)

---

**Abstract:** Tanzania is one of the low income countries, which heavily depends on hydro-power for electric energy supply to the national grid. Impacts of climate change patterns on water resources supply to dams for hydro-energy generation is now evident. In turn, this has impacted national socio-economic development in numerous ways. The objective of this work was to analyze the link of climate change to water shortages for hydro-power generation in the Mtera reservoir, which supply 50% of the hydro-power to the national grid. Literature survey, records collection and analyses and observations were research tools used. The study revealed that, 64% of increasing variability in rainfall over years in the watersheds described declining water levels in Mtera dam. This strong relationship means that climate change is main driver of water shortages for hydro-power generation. This suggests a need for national adaptation strategies to water supply shortages. Improvements in the present hydro-power sources for water recycling and/or development of micro-dams for storage of excess water need exploration. Rain-water harvesting and recycling seems important adaptation strategies to changing hydrological patterns for water supply to the hydro-energy plants in Tanzania.

**Keywords:** *Electric energy supply, Hydro-energy plants, Increasing rainfall variability, National grid, Water supply*

---

### 1. Introduction

Climate change and variability are now becoming one of the significant development challenges due to shift in the average patterns of weather. Environmental change, manifested by climate change and variability, is no longer a mythical discourse; the scientific consensus is not only that, human activities have contributed to it significantly, but that the change is far more rapid and dangerous than thought earlier (IPCC, 2007). While climate change results from activities all over the globe, with rather unevenly spread contributions to it, it may lead to very different impacts in different countries, depending on local, regional environmental conditions and on differences in vulnerability to climate change (UNEP/Earthscan, 2002). The Millennium Ecosystem Assessment (2005) shows that, in all ecosystems of the world, the climate changes impacts are rapidly increasing, such as, on water resources, environmental services and other livelihoods capital assets for sustainable human development. In the World Summit on Sustainable Development (WSSD) held from August 26-4 September 2002 in Johannesburg, South Africa, the UN Secretary General outlined priority areas for sustainable development as water and sanitation, energy, health, agriculture and biodiversity protection and ecosystems management (WSSD, 2002).

Climate change impact on water resource supply significantly affects all aspects of sustainable socio-economic development of a country or a society, where energy sector is heavily dependent on hydropower. Current contribution of hydro-power in Tanzania to national grid is 52% and the rest is from thermal sources (Karekezi et al. 2009). There has been a concern over water supply for energy generation in Mtera reservoir. This concern is manifested at national level a decade ago by the government declaration in March 2001 that, the Great Ruaha River should return to its year-round flow characteristics by 2010. The concern comes from power shortages in early-

1990s, attributed to low water flows into the Mtera/Kidatu hydropower system from the Great Ruaha River (Lankford *et al.*, 2004; Yawson, *et al.*, 2003). The hydrological change in the Usangu-Mtera ecosystem has attracted number of investigations into causes of this problem, which include: Sustainable Management of the Usangu Wetlands and its Catchments (SMUWC) from 1998-2002 (Lankford *et al.*, 2004); investigation into cause of the failure of the Mtera-Kidatu Reservoir system (Yawson *et al.*, 2003); a study of the effects of land degradation in the uplands on land use changes in the plains (Mwalukasa, 2002); a study of the socio-economic root cause of the loss of biodiversity in the Ruaha Catchment Area (Sosovele and Ngwale, 2002). These studies agree that, there is hydrological flow change in Mtera reservoir, but there is no consistent consensus on cause of hydrological change. These studies did not attempted to directly link change in rainfall variability with water supply from Mtera reservoir. This work focuses on the hydrological flow change and how it links to changes in rainfall variability. Therefore, this paper explores the trends in variability of the Mtera reservoir mean water levels and watershed rainfall amounts and discusses linkages to energy generation for the national grid and socio-economic development. Furthermore, it recommends opportunities for harnessing in the national adaptations strategies to climate influenced hydrological flows changes.

## **2. Methodology**

The study area is Usangu-Mtera ecosystem, which covers, south-western Tanzania's highlands watershed catchments to the Mtera reservoir, which is used to conserve water for hydro-electricity generation in Kidatu, downstream. Data collection tools from the area were survey of literature, key informants interviews, informal appraisals, questionnaire interviews and biophysical records collections and analysis.

The literature was searched from the Internet, published and grey materials of the relevant regional, national and area studies. Then a critical analysis of information gathered through literature surveys was undertaken. Key informants interviews were held with Rufiji Basin Water Office (RBWO) and the Tanzania Electricity Company (TANESCO). Informal village appraisals were conducted in six villages, which were Ikoga and Sololwambo in lower part, Yala and Matebete middle part, and Mhwela and Mabadaga in upper part of the Usangu central plain. Informal interviews were supplemented with participatory village resources mapping and on the ground observations through transect walks.

Household questionnaire interviews were held in April to December 2004, involving 266 households in six above villages. Interviews assessed climate change perceptions and its link to water problems at local level. Verification of this perceptions, were done through collection and analysis of biophysical records on rainfall and water levels in the Mtera reservoir over 22-years (1982-2003). A 22-years measurements data of Mtera reservoir water levels collected from TANESCO and rainfall data from the Agricultural Research Institute meteorological station located in the Uyole-Uporoto uplands watershed, typical of the south-western watersheds.

Analysis of the total annual rainfall amounts were summation of monthly precipitations. Monthly sum of each rainfall year starts in October of the preceding year and ends in September of the following year. The relationship was tested and linkage established between rainfall variability and water supply shortage experienced by analyses of the collected information. Quantitative data were analysed using the Statistical Package for Social Science (SPSS).

### 3. Results

#### 3.1 Climate change Indicators

Local people experience strongly attested links of climate changes with respect to water resources, rainfall amount and duration, temperature, land resources degradation and land use change in the Usangu-Mtera ecosystem (SMUWC, 2002; Malley *et al*, 2007). Interview of 266 household, in area of study, about 82.6% of respondents, reiterated that rainfall amount has decreased, and a similar number (83%), reported shortened duration of rainfall in Usangu-Mtera ecosystem. These perceptions are supported by analysis of rainfall trends (Table 1).

Analysis revealed that annual rainfall amounts in the south-western watershed, is declining, though not statistically significant ( $p= 0.05$ ). However, a high variability pattern of rainfall amount from year to year is evident. More frequencies of below average annual rainfall amounts were conspicuously notable, from late 1980s to 2003, which indicate increased frequency of drier-years than normal in about last 22 years.

#### 3.2 Water supply for energy generation in Mtera

The Mtera reservoir mean annual water levels trend, over 22-years, depicts closely similar pattern to the annual rainfall amounts trend in the south-western highlands watersheds (Table 1). More frequencies of low mean annual water levels were observed from the late 1980s to 2003. This similarity in the pattern, attest a possible linkage between the annual hydrological droughts in the reservoir to the rainfall amount and pattern change in the south-western highlands watersheds.

*Table 1 Trends in rainfall, water levels and their relationships in Usangu-Mtera ecosystem*

| Environmental variable                                  | Direction           | Method of analysis     | Extent (%) | Sign. |
|---|---------------------|------------------------|------------|-------|
| <b>Trends</b>   |                     |                        |            |       |
| Rainfall quantity                                       | Declining           | PRA                    | -          |       |
|   |                     | Respondents perception | 82.6       | ***   |
|   |                     | Regression over years  | 6.8        | Ns    |
| Rainfall variability                                    | Increasing          | PRA                    | -          |       |
|   |                     | Respondents perception | 83         | ***   |
| Patterns of mean annual water levels in Mtera reservoir | Declining           | Regression over years  | 5.8        | Ns    |
| Mean annual water level variability                     | Increasing          | Regressions over years | 10.2       | Ns    |
| Rainfall variability vs water levels                    | Positive and strong | Regression             | 64.2       | ***   |

Ns = not significant, \* significant at  $P \leq 0.05$ ; \*\* significant at  $P \leq 0.01$ , \*\*\* Significant at  $P \leq 0.001$

Source: Own analyses of field data (2004)

#### 3.3 Climate change indicators and Mtera reservoir water supply

Regression analysis of variations in the amounts of rainfall, significantly ( $p < 0.001$ ) accounted for 64.2% of the variations in mean annual water levels in Mtera reservoir (Table1). This suggests that, the lower the annual rainfall amount in the upper catchments the lower the mean annual

water supply from the Mtera reservoir. It implies that, increasing variability in the annual rainfall amounts is a cause of increasing variability in the mean annual water supply in the Mtera reservoir for electricity generation. These direct close relationship, gives new evidence, that there is a strong causal relationship between the perceived changes in climate indicators with the changes in the hydrology of the Usangu-Mtera eco-system.

#### 4. Discussions

Lankford *et al.*, (2004), showed that SMUWC investigation found that hydrological change in the Great Ruaha River is linked to dry season abstraction for irrigation activities and environmental losses, but not to climate change. Mwalukasa (2002) showed that, there is significant degradation of the land cover in the plain and upland of the Chimala River catchments, and there is increase in land use for irrigated agriculture in the plain. According to Yawson *et al.*, (2003), the failure of the Mtera/Kidatu system is due to unaccounted spillage from Mtera reservoir, caused by inefficient management of the system. These investigations did not attempt to analyse linkage of climate indicators with water supply from Mtera reservoir. Sosovele and Ngwale, (2002) and Malley *et al.*, (2007) analysed rainfall trends from different stations which indicated that climate change might have played a significant role in the experienced water supply shortages. These studies supported the anecdotal evidence that, climate change plays a greater role in the observed hydrological flow change. The results of present findings, which established direct relationships between water supply change and rainfall variability further supports findings of Sosovele and Ngwale (2002) and Malley *et al.* (2007) and the anecdotal evidence.

According to Karl *et al.*, (1995), increase in frequency of drought or rainfall variability is linked to climate change, which is also characterised with events of short severe storms. According to U.S. National Drought Monitor (2006), hydrological drought is manifested by shortfalls in surface and sub-surface water supply, which can be detected through decline in water levels in rivers, reservoirs, lakes and aquifers. Frequency and severity of hydrological drought is discernible at a watershed or river basin scale (Wilhite and Glantz, 1985). Mbwambo (2010) reported decline in number of flowing rivers from 79 to 39 now in Kilombero basin in Morogoro, Tanzania, due to climate change. In the Usangu-Mtera ecosystem, work of Sosovele and Ngwale (2002) reported that, rivers from upper watersheds of Uporoto and Mbeya mountains, which flow into the Usangu plain, and then to the Great Ruaha River only Chimala and Mbarali still have flows, however, amount of flowing water has declined substantially. These observations are supported by SMUWC (2002) measurements of flows in the rivers, which show that dry season flows of rivers have declined. Dried and silted up perennial rivers and streams were encountered during the course of this study, in the middle and lower villages of the Usangu plain. The SMUWC (2002), indicated that the western wetlands area (about 900 km<sup>2</sup>), experienced reduced seasonal flooding in recent years, and it seem it no longer qualifies as a wetland, only remaining indicators of its past wetlands status is vegetation and soils. Kashaigili (2005) results show that, the eastern wetland perennial swamp size has shrunk by almost 70% between 1984 and 2000. According to Yawson *et al.* (2003), in 1991 and 1992, water levels in the Mtera-Kidatu reservoir system, went very low to its dead levels. This is attested by the increasing frequency of below average mean annual water levels in Mtera reservoir. Presence of these indicators in the watersheds, fans and wetlands ecosystems in Usangu, and in the Mtera reservoir, explain the link of climate change-to-water supply problem from Mtera reservoirs for hydropower generation.

#### **4.1 Impact of climate change on energy generation and socio-economic development**

According to Libiszewski (1992), socio-economic impacts of environmental change may include: (1) decrease economic production, (2) general economic decline, (3) population displacements, and (4) disruption of institutions and the social relations. In the Usangu-Mtera ecosystem, similar socio-economic impacts, linked to hydrological change are evident. To abate, water shortage problem for energy generation, pastoral communities were forcefully displaced from their livelihood resources, water sources and dry season grazing land (Edwin, *The East African*, April 9-15, 2007). This forceful displacement of pastoral people has resulted into disruptions of their social institutions and soured their relations with the state, which mean a disruption of social capital, important in development process.

Climate change impact on water supply, results into reduced hydro-power production, which causes increase in outages and load shedding. In Tanzania, in dry year of 1997, the Mtera dam water went down, due to drought causing 17% drop in hydropower generation (Karekezi *et al*, 2009). In the period, 1990-2008, the water supply problem from the Mtera reservoir led to electric power shortage, which in turn affected the national grid, because the Mtera-Kidatu system generates about 50% of the power to national grid (WWF, 2002). The electric generation failures caused the nation wide power rationing, which impacted the industrial economic production, either, through increased costs of production of goods, or through reduced level of production, due to unavailability of power during certain periods of operations. Energy shortage affected economic production, raises the costs of electricity and thus goods and socio-economic service provisions from trade, health, education and domestic sectors, which in turn affect the welfare and livelihoods of the people in different ways. The emergency response, to reduce the impacts of the national power crisis, by hiring and/or investing into expensive alternative power sources, greatly constrained the government budget for the socio-economic development activities, and has forced the nation to a debt burden (Simbeye, *The East African*, July 12-18, 2004). Furthermore, in 2006, according to analysis of Kerekezi *et al* (2009), Tanzania incurred a loss of about 1% of its GDP earnings due to drought related load shedding exercise.

#### **4.2 Conclusion and Recommendations**

##### **4.2.1 Conclusion**

Climate change and variability is evident from increasing frequency of annual rainfall amounts variability in the upper catchments of south-western highlands of the Usangu-Mtera ecosystem. Increasing frequency of hydrological drought as manifested by mean annual water supply from Mtera reservoir for energy generation has strong relationship with increasing rainfall amount variability.

##### **4.2.2 Recommendations**

- Micro-dams for rainwater harvesting to adapt to years of extreme rainfall variability would help conserve water to support the main dam if constructed on the upper side of the Mtera reservoir along the Great Ruaha River to harvest excess water and store it, when the reservoir capacity approaches its maximum (698.5m.a.s.l). The stored water would be the source for recharge of the reservoir, when its water level approaches the critical minimum level (690m.a.s.l). The restriction at Nyaluhanga is another opportunity need to be explored for storage

of water in the western wetlands, and then slowly released over time to recharge eastern wetlands and hence the Great Ruaha River.

- An investment into alternative energy sources is a commendable strategy. The use of coal in electricity generation appears available and potentially cheap alternative in Tanzania. However, in the long term, the coal burning is one of the highest emitters of a greenhouse gas, the carbon dioxide, which significantly contribute to the environmental changes, which would be environmentally un-friendly investment. This means heavy investment to this source, would seem to compromise the environmental sustainability efforts in a long-term, therefore a modest investment in coal energy plants as an emergency backups during the hydropower shortage is recommended.
- The hydro-power remains the known clean and cheapest sources of electric energy for sustainable economic development. This implies that, more careful considerations should be on improvement and maintenance of the present hydro-power sources and new ones identified and developed. The design should incorporate multiple and efficient re-use of water through recycling system as an important aspect of water management, which should be considered in planning and designs of new development in hydro-power generation plants.

### **Acknowledgements**

The data was collected by the financial support of the International Foundation for Science (IFS) in Sweden and the United Nations University Institute of Advanced Studies (UNU/IAS) in Japan. The Ministry of Agriculture and Food Security in Tanzania made its research facilities available for the work and administered the funds at the Agricultural Research Institute-Uyole (ARI-Uyole). I wish to thank and appreciate the assistance of the Mbarali District council, the TANESCO, Regional Water Engineer-Mbeya and the Directorate of Meteorological services, Tanzania for availing the information needed to undertake the reported analysis in this work.

### **References**

- [1] IPCC, Climate Change 2007: The Physical Science Basis: Summary for Policy Makers, Paris: IPCC, WMO, 2007.
- [2] UNEP/Earthscan, United Nations Environmental Program/ Earths can. Global Environmental Outlook 3. London: Earthscan, 2002.
- [3] Millennium Ecosystem Assessment (MA), International scientific assessment: ecosystem changes and human well-being. [www.millenniumassessment.org](http://www.millenniumassessment.org), 2005.
- [4] World Summit on Sustainable Development (WSSD), A framework for Action on Agriculture. Johannesburg: WEHAB Working Group, 2002
- [5] S. Karekezi, J. Kimani, O. Onguru, Climate Change and Energy Security in East Africa. Energy Environment and Development Network for Africa (AFREPREN/FWD), 2009 46 pp.

- [6] B. Lankford, B. Koppen, T. Franks, and H. Mahoo, Entrenched views or insufficient science? Contested causes and solutions of water allocation, insights from the Great Ruaha River Basin, Tanzania. *Agricultural Water Management* 2004, pp 135-153.
- [7] D.K. Yawson, J.J. Kashaigili, J. Kachroo, and F.W. Mtaló, Modelling the Mtera-Kidatu reservoir system to improve integrated water resources management. *International Conference on Hydropower*. (Arusha: Hydro Africa), 2003.
- [8] SMUWC, Baseline 2001. <http://www.usangu.org/baseline2001/part1-5.shtml>, 2001.
- [9] E.H. Mwalukasa, Effects of Land Degradations in the Uplands on Land Use Changes in the Plains: The Case Study of Chimala River Catchment in the Usangu Plains. MSc. Dissertation. Sokoine University of Agriculture, 2002.
- [10] H. Sosovele, and J.J. Ngwale, Socio-economic Root Cause of the Loss of Biodiversity in the Ruaha Catchment Area. (Dar-es-salaam: WWF-Tanzania), 2002.
- [11] Z.J.U. Malley, M. Taeb, T. Matsumoto, T. and H. Takeya, Environmental change and vulnerability in Usangu plain, South-western Tanzania: Implications for Sustainable Development. *The International Journal of Sustainable Development and World Ecology*, 2007, pp 145-159.
- [12] T.R. Karl, R.W. Knight, and N. Plummer, Trends in High Frequency of Climatic Variability in the Twentieth Century. *Nature*, 1995, pp 217-220.
- [13] U.S. National Drought Monitor, <http://www.drought.unl.edu/dm/monitor.html>, 2006.
- [14] D.A. Wilhite, and M.H. Glantz, Understanding the drought phenomenon: the role of definitions. *Water International* 1985, pp 111-120.
- [15] J. Mbwambo, Kilombero: Kutoka mito 79 hadi 39 ya sasa, kulikoni? (Kilombero: From 79 rivers to 39 now, what need be done?), *Raia Mwema Issue No 161*, November 24-30, 2010, pp 12-13.
- [16] J. J. Kashaigili, Integrated Hydrological Modelling of Wetlands for Environmental Management: The Case of the Usangu Wetlands in the Great Ruaha Catchment. RIPARWIN Seminar Presentation, Mbeya Peak Hotel: Mbeya, 2005.
- [17] S. Libiszewski, What is an environmental conflict? (ENCOP Occasional papers: Center for Security Studies, ETH Zurich/Swiss Peace Foundation Zurich/ Berne 1992-1995), 1992.
- [18] W. Edwin, Thousands of cattle dying as Dar relocates herders from the Wetlands, *The East African*, 2007, April 9-15.
- [20] F. Simbeye, Songas to Replace Imported Furnace Oil. *The East African*, July 12-18, 2004.
- [21] World Wide Fund (WWF), African Rivers Initiative: Concept Paper. Living Water Programme. Iringa, WWF, 2002.

## Optimal hydraulic structures profiles under uncertain seepage head

Raj Mohan Singh<sup>1,\*</sup>

*1 Motilal Nehru National Institute of Technology, Allahabad-211004, India*

*\* Corresponding author. Tel: +91-532-2271322(O); Fax: +91-532-2545341 E-mail: rajm@mnnit.ac.in;  
[rajm.mnnit@gmail.com](mailto:rajm.mnnit@gmail.com)*

---

**Abstract:** Most of the hydraulic structures are founded on permeable foundation. There is, however, no procedure to fix the basic barrage parameters, which are depth of sheet piles/cutoffs and the length and thickness of floor, in a cost-effective manner. Changes in hydrological and climatic factors may alter the design seepage head of the hydraulic structures. The variation in seepage head affects the downstream sheet pile depth, overall length of impervious floor, and thickness of impervious floor. The exit gradient, which is considered the most appropriate criterion to ensure safety against piping on permeable foundations, exhibits non linear variation in floor length with variation in depth of downstream sheet pile. These facts complicate the problem and increase the non linearity of the problem. However, an optimization problem may be formulated to obtain the optimum structural dimensions that minimize the cost as well as satisfy the exit gradient criteria. The optimization problem for determining an optimal section for the weirs or barrages normally consists of minimizing the construction cost, earth work, cost of sheet piling, length of impervious floor etc. The subsurface seepage flow is embedded as constraint in the optimization formulation. Uncertainty in design, and hence cost from uncertain seepage head are quantified using fuzzy numbers. Results show that an uncertainty of 15 percent in seepage will result in 22 percent of uncertainty in design represented by overall design cost. The limited evaluation show potential applicability of the proposed method.

**Keywords:** *Nonlinear Optimization Formulation, Genetic Algorithm, Hydraulic Structures, Barrage Design, Fuzzy Numbers, Uncertainty Characterization.*

---

### 1. Introduction

Hydraulic structures such as weirs and barrages are costly water resources projects. A safe and optimal design of hydraulic structures is always being a challenge to water resource researchers. The hydraulic structure such as barrages on alluvial soils is subjected to subsurface seepage. The seepage head causing the seepage vary with variation in flows. Design of hydraulic structures should also insure safety against seepage induced failure of the hydraulic structures.

The variation in seepage head affects the downstream sheet pile depth, overall length of impervious floor, and thickness of impervious floor. The exit gradient, which is considered the most appropriate criterion to ensure safety against seepage induced piping (Khosla, et al., 1936; Asawa, 2005) on permeable foundations, exhibits non linear variation in floor length with variation in depth of down stream sheet pile. These facts complicate the problem and increase the non linearity of the problem. However, an optimization problem may be formulated to obtain the optimum structural dimensions that minimize the cost as well as satisfy the safe exit gradient criteria.

The optimization problem for determining an optimal section for the weirs or barrages consists of minimizing the construction cost, earth work, cost of sheet piling, and length of impervious floor (Garg et al., 2002; Singh, 2007). Earlier work (Garg et al., 2002) discussed the optimal design of barrage profile for single deterministic value of seepage head. This study first solve the of nonlinear optimization formulation problem (NLOP) using genetic algorithm (GA) which gives optimal dimensions of the barrage profile that minimizes unit cost of concrete work, and earthwork and searches the barrage dimension satisfying the exit gradient criteria. The work is then extended to characterize uncertainty in design due to

uncertainty in measured value of seepage head, an important hydrogeologic parameter. Uncertainty in design, and hence cost from uncertain head value are quantified using fuzzy numbers

## 2. Subsurface flow

The general seepage equation under a barrage profile may be written as:

$$\frac{\partial^2 h}{\partial x^2} + \frac{\partial^2 h}{\partial y^2} + \frac{\partial^2 h}{\partial z^2} = 0 \quad (1)$$

This is well known Laplace equation for seepage of water through porous media. This equation implicitly assumes that (i) the soil is homogeneous and isotropic; (ii) the voids are completely filled with water; (iii) no consolidation or expansion of soil takes place; and (iv) flow is steady and obeys Darcy's law.

For 2-dimensional flow, the seepage equation (1) may be written as:

$$\frac{\partial^2 h}{\partial x^2} + \frac{\partial^2 h}{\partial y^2} = 0 \quad (2)$$

The need to provide adequate resistance to seepage flow represented by equation (1) both under and around a hydraulic structure may be an important determinant of its geometry (Skutch, 1997). The boundary between hydraulic structural surface and foundation soil represents a potential plane of failure.

Stability under a given hydraulic head could in theory be achieved by an almost limitless combination of vertical and horizontal contact surfaces below the structure provided that the total length of the resultant seepage path were adequately long for that head (Skutch, 1997; Leliavsky, 1979). In practical terms, the designer must decide on an appropriate balance between the length of the horizontal and vertical elements. Present work utilized Khosla's Method of independent variables (Asawa, 2005) to simulate the subsurface behavior in the optimization formulation. Method of independent variables is based on Schwarz-Christoffel transformation to solve the Laplace equation (1) which represents seepage through the subsurface media under a hydraulic structure. A composite structure is split up into a number of simple standard forms each of which has a known solution. The uplift pressures at key points corresponding to each elementary form are calculated on the assumption that each form exists independently. Finally, corrections are to be applied for thickness of floor, and interference effects of piles on each others.

## 3. Optimal design methodology

$$\text{Minimize } C(L, d_1, d_d) = c_1(f_1) + c_2(f_2) + c_3(f_3) + c_4(f_4) + c_5(f_5) \quad (4)$$

$$\text{Subject to } SEG \geq \frac{H}{d_d \pi \sqrt{\lambda}} \quad (5)$$

$$L^l \leq L \leq L^u \quad (6)$$

$$d_1^l \leq d_1 \leq d_1^u \quad (7)$$

$$d_d^l \leq d_d \leq d_d^u \quad (8)$$

$$L, d_1, d_d \geq 0 \quad (9)$$

where  $C(L, d_1, d_d)$  is objective function represents total cost of barrage per unit width (Rs/m), and is function of floor length ( $L$ ), upstream sheet pile depth ( $d_1$ ) and downstream sheet pile depth ( $d_d$ );  $f_1$  is total volume of concrete in the floor per unit width for a given barrage profile and  $c_1$  is cost of concrete floor (Rs/m<sup>3</sup>);  $f_2$  is the depth of upstream sheet pile below the concrete floor and  $c_2$  is the cost of upstream sheet pile including driving (Rs/m<sup>2</sup>);  $f_3$  is the depth of downstream sheet pile below the concrete floor and  $c_3$  is the cost of downstream sheet pile including driving (Rs/m<sup>2</sup>);  $f_4$  is the volume of soil excavated per unit width for laying concrete floor and  $c_4$  is cost of excavation including dewatering (Rs/m<sup>3</sup>);  $f_5$  is the volume of soil required in filling per unit width and  $c_5$  is cost of earth filling (Rs/m<sup>3</sup>); SEG is safe exit gradient for a given soil formation on which the hydraulic structure is constructed and is function of downstream depth and the length of the floor;  $\lambda = \frac{1}{2}[1 + \sqrt{1 + \alpha^2}]$ ;  $\alpha = \frac{L}{d_d}$ ;  $L$  is total length of the floor;  $H$  is the seepage head;  $d_1$  is the upstream sheet pile depth;  $d_2$  is downstream sheet pile depth;  $L^l, d_1^l$ , and  $d_d^l$  is lower bound on  $L, d_1$  and  $d_d$  respectively;  $L^u, d_1^u, d_d^u$  are upper bound on  $L, d_1$  and  $d_d$  respectively. The constraint equation (5) may be written as follows after substituting the value of  $\lambda$  :

$$L - d_d \left( \left\{ 2 \left( \frac{H}{d_2 \pi (SGE)} \right)^2 - 1 \right\}^2 - 1 \right)^{1/2} \geq 0 \quad (10)$$

In the optimization formulation, for a give barrage profile and seepage head  $H$ ,  $f_1$  is computed by estimating thickness at different key locations of the floor using Khosla's method of independent variables and hence nonlinear function of length of floor ( $L$ ), upstream sheet pile depth ( $d_1$ ) and downstream sheet pile depth ( $d_2$ ). Similarly  $f_4$ , and  $f_5$  is nonlinear. The constraint represented by equation (10) is also nonlinear function of length of the floor and downstream sheet pile depth ( $d_2$ ). Thus both objective function and constraint are nonlinear; make the problem in the category of nonlinear optimization program (NLOP) formulation, which are inherently complex. Characterization of functional parameters is available in literature (Singh, 2007; Garg et al., 2002).

### 3.1. Characterizing model functional parameters

For a given geometry of a barrage and seepage head  $H$ , the optimization model functional parameters  $f_1, f_2, f_3, f_4$  and  $f_5$  are characterized for the barrage profile shown in Fig. 1.

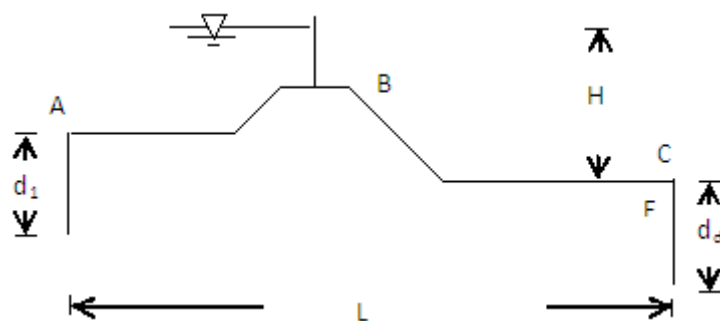


Fig. 1. Schematic of barrage parameters utilized in performance evaluation

Intermediate sheet-piles are not effective in reducing the uplift pressures and only add to the cost of in reducing the uplift pressures and only add to the cost of the barrage (Garg et al., 2002). In present work, no intermediate sheet piles are considered.

### 3.2. Optimization procedure using genetic algorithm

GA was originally proposed by Holland (Holland, 1975) and further developed by Goldberg (Goldberg, 1989). It is based on the principles of genetics and natural selection. GA's are applicable to a variety of optimization problems that are not well suited for standard optimization algorithms, including problems in which the objective function is discontinuous, non-differentiable, stochastic, or highly nonlinear (Haestad 2003). The GA search starts from a population of many points, rather than starting from just one point. This parallelism means that the search will not become trapped on local optima (Singh and Datta, 2006).

The optimization model represented by equations (4)-(10) and the functional parameters embedded in the optimization model are solved using Genetic Algorithm on MATLAB platform. The basic steps employed in solution are available in Singh, 2007. Table 1 shows physical parameters obtained by conventional methods for Fig. 2.

Table 1. Physical parameters values of barrage profile

| Physical parameters | Values (meters) |
|---------------------|-----------------|
| *L                  | 105.37          |
| H                   | 7.12            |
| *d <sub>1</sub>     | 5.45            |
| *d <sub>2</sub>     | 5.9             |

\* Decision variables to be optimized

## 4. Uncertainty characterization in the optimization model

Real-world problems, especially those that involve natural systems, such as soil and water, are complex and composed of many non-deterministic components having non-linear coupling. In dealing with such systems, one has to face a high degree of uncertainty and tolerate imprecision. There is a high degree of local soil variability, and imprecision in the determination of soil parameters and hydrological parameters like seepage head. Statistical techniques have been traditionally used to deal with parametric variation in model inputs, but these require substantial hydrogeologic explorations data for estimates of probability distributions. In the presence of limited, inaccurate or imprecise information, simulation with fuzzy numbers represents an alternative tool to handle parametric uncertainty. Fuzzy sets offer an alternate and simple way to address uncertainties even for limited exploration data sets. In the present work, the optimal design is first obtained assuming a deterministic value of hydrogeologic parameter, safe exit gradient, in optimization model. Uncertainty in safe exit gradient is then characterized using fuzzy numbers. The fuzzified NLOF is then solved using GA.

Uncertainty in general comes in two forms: aleatory (stochastic, random natural variability or noncognitive) and epistemic (cognitive or subjective) (Hofer et al., 2002). Recently, Srinivasan et al. (2007) identified these uncertainties in hydrogeological applications. Aleatory uncertainty refers to uncertainty that cannot be reduced by more exhaustive

measurements or by a better model. Epistemic uncertainty, on the other hand, refers to uncertainty that can be reduced (Ross et al., 2009).

One of the milestones in the evolution of these new uncertainty theories is the seminal paper by Lofti A. Zadeh (1965). He proposed a new mathematical tool in his paper and called this new mathematical tool “fuzzy sets.” He proposed the concept of fuzzy algorithms in 1968 (Zadeh, 1968), and together with Bellman, proposed a new approach for decision-making in fuzzy environments in 1970 (Bellman & Zadeh, 1970). Fuzzy set theory has been recently applied in various fields for uncertainty quantification (Cho et al., 2002; Hanss, 2002; Kentel & Aral, 2004; Mauris et al., 2001).

The transformation method presented by Hanss, (2002) uses a fuzzy alpha-cut (FAC) approach based on interval arithmetic. The uncertain response reconstructed from a set of deterministic responses, combining the extrema of each interval in every possible way unlike the FAC technique where only a particular level of membership ( $\alpha$ -level) values (Hanss & Willner, 1999) for uncertain parameters are used for simulation.

Fuzzy modeling of uncertainty for hydrogeologic parameters such as exit gradient and seepage head is based on Zadeh’s extension principle (Zadeh, 1968) and transformation method (TM) (Hanss, 2002). In present study only seepage head is considered to be imprecise. Input seepage head as imprecise parameter, is represented by fuzzy numbers. The resulting output i.e. minimum cost obtained by the optimization model is also fuzzy numbers characterized by their membership functions. The reduced TM (Hanss, 2002) is used in the present study. The measure of uncertainty used is the ratio of the 0.1-level support to the value of which the membership function is equal to 1 (Abebe et al., 2000).

## 5. Results and discussion

Earlier (mid 19th century), weirs and barrages have been designed and constructed in India on the basis of experience using the technology available at that period of time. Some of them were based on Bligh’s creep theory, which proved to be unsafe and uneconomical. Comparison of the parameters of these structures with the proposed approach is, thus, not justified. Therefore, a typical barrage profile, a spillway portion of a barrage, is chosen for illustrating the proposed approach as shown in Fig. 2. The barrage profile shown in Fig. 2 and parameters values given Table 1 is solved employing the methodology presented in this work. The optimized values of parameters for a deterministic seepage head value of 7.12m are shown in Table 2. During the process of optimization, the process of going into new generation continues until the fitness of the population converged i.e. average fitness of population almost matches with the best fitness. This criterion proves the solution to be optimized. The optimized values of parameters for a deterministic seepage head value of 7.12m are shown in Table 2.

Table 2. Optimized parameters for safe exit gradient equal to 1/8 and minimum thickness of floor as 1m

| Physical parameters | Values |
|---------------------|--------|
| L                   | 61     |
| d <sub>1</sub>      | 3.1    |
| d <sub>2</sub>      | 9.2    |

It also resulted in a smaller floor length and overall lower cost. It has shown a savings in the barrage cost ranging from 16.73 percent.

For characterization of uncertainty, seepage head is assumed to vary from 6.0m to 8.19m with central value of 7.12m i.e. almost 15 percent in triangular fuzzy numbers representation. The result of variation in cost is corresponding different degree of membership for seepage head shown in Fig.2. The measure of uncertainty is found to be 22 percent. Since, left and right spread from central value of exit gradient is almost 15 percent, it can be concluded that uncertainty in seepage head reflects comparatively more uncertainty) more than 15 percent) in cost.

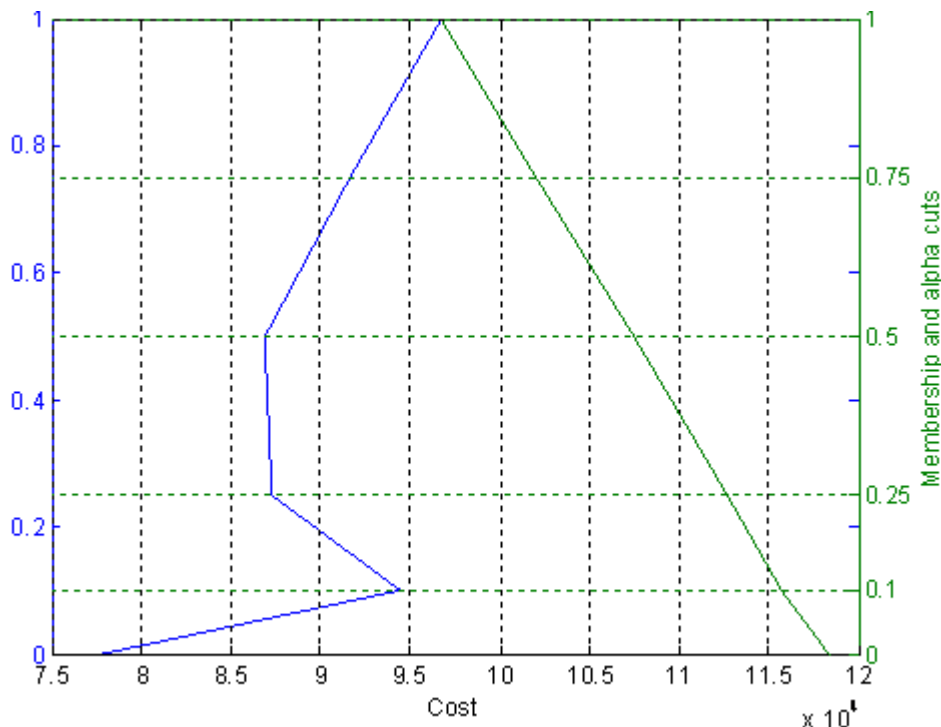


Fig.2. Costs variations corresponding to different  $\alpha$ -cuts of seepage head

## 6. Conclusions

The present work also demonstrates the fuzzy based framework for uncertainty characterization in optimal cost for imprecise hydrologic parameter such as seepage head. The uncertainty in cost is found not to be directly proportional to uncertainty in seepage head. The GA based optimization approach is equally valid for optimal design of other major hydraulic structures.

## References

- [1] Khosla, A. N., Bose, N. K., and Taylor, E. M., Design of weirs on permeable foundations. *CBIP Publication No. 12*, Central Board of Irrigation and Power, New Delhi, 1936, Reprint 1981.
- [2] Asawa, G.L. Irrigation and water resources engineering, New Age International (P) Limited Publishers, New Delhi. 2005.
- [3] Garg, N.K., Bhagat, S.K., and Asthana, B.N., Optimal barrage design based on subsurface flow considerations. *Journal of Irrigation and Drainage Engineering*, Vol. 128, No. 4, 2002, 253-263.

- [4] Singh, R.M., Optimal design of barrages using genetic algorithm. Proceedings of National Conference on Hydraulics & Water Resources (Hydro-2007) at SVNIT, Surat, 2007, 623-631.
- [5] Skutch, J., Minor irrigation design DROP - Design manual hydraulic analysis and design of energy-dissipating structures. *TDR Project R 5830*, Report OD/TN 86, 1997.
- [6] Leliavsky, S., Irrigation engineering: canals and barrages. Oxford and IBH, New Delhi, 1979.
- [7] Holland, J. H., Adaptation in natural and artificial systems. University of Michigan Press, Ann Arbor, MI, 1975.
- [8] Goldberg, D. E., *Genetic algorithms in search, optimization and machine learning*. Kluwer Academic Publishers, Boston, MA, 1989.
- [9] Haestad, M., Walski, T. M., Chase, D. V., Savic, D. A., Grayman, W., Beckwith, S., and Koelle, E., *Advanced water distribution modeling and management*. Haestad Press, Waterbury, CT, 2003, 673-67.
- [10] Singh, R. M., and Datta, B. 2006. Identification of unknown groundwater pollution sources using genetic algorithm based linked simulation optimization approach. *Journal of Hydrologic Engineering*, ASCE, Vol. 11, No.2, 101-109.
- [11] Hofer, E., Kloos, M., Krzykacz-Hausmann, B., Peschke, J. and Woltereck, M., An approximate epistemic uncertainty analysis approach in the presence of epistemic and aleatory uncertainties. *Reliab. Eng. Syst. Safety*, 77(3), 2002, 229– 238.
- [12] Srinivasan, G., Tartakovsky, D. M., Robinson, B. A., and Aceves, A. B., Quantification of uncertainty in geochemical reactions. *Water Resour. Res.* 43, 2007, W12415.
- [13] Ross, J.L., Ozbek, M.M. and Pinder, G.F., Aleatoric and epistemic uncertainty in groundwater flow and transport simulation. *Water Resour. Res.*, 45, 2009, W00B15.
- [14] Zadeh, L., Fuzzy sets. *Information and Control*, 8, 1965, 338– 353.
- [15] Zadeh, L. A., Fuzzy algorithms. *Information and Control* 12, 1968, 94-102.
- [16] Bellman, R.E., Zadeh, L.A., Decision-making in a fuzzy environment. *Management Science*, 17, 1970, 141-164.
- [17] Cho, H.N., Choi, H.-H., Kim, Y.B., A risk assessment methodology for incorporating uncertainties using fuzzy concepts. *Reliability Engineering and System Safety* 78, 2002, 173-183.
- [18] Kentel, E., Aral, M.M., Probabilistic-fuzzy health risk modeling. *Stochastic Environmental Research and Risk Assessment (SERRA)* 18, 2004, 324-338.
- [19] Mauris, G., Lasserre, V., Foulloy, L., A fuzzy approach for the expression of uncertainty in measurement. *Measurement*, 29, 2001, 165-177.
- [20] Hanss, M., Willner, K., On using fuzzy arithmetic to solve problems with uncertain model parameters. In Proc. of the Euromech 405 Colloquium, Valenciennes, France, 1999, 85-92.
- [21] Abebe, A.J., Guinot, V., Solomatine, D.P., Fuzzy alpha-cut vs. Monte Carlo techniques in assessing uncertainty in model parameters. 4th Int. Conf. Hydroinformatics, Iowa, USA, 2000.

## The impact of the March 10, 2009 dust storm on meteorological parameters in central Saudi Arabia

Abdullrahman H. Maghrabi

National Centre For Mathematics and Physics, King Abdulaziz City For Science and Technology, Riyadh , Saudi Arabia

\* Corresponding author. Tel: +966-501051884, Fax: +966-14813521, E-mail. amaghrabi@kacst.edu.sa

**Abstract:** Dust particles play an important role in air quality and environmental health. They affect both solar and terrestrial radiation by scattering and absorption and are therefore considered to be a significant climate-forcing factor. Dust storms are natural hazards that affect daily life for an interval ranging from a few hours to a few days, and they are a very frequent phenomenon in Saudi Arabia, especially in the pre-monsoon season. On 10th March 2009 a widespread and severe dust storm event that lasted several hours struck Riyadh (24.9 1° N, 46.41° E, 764 m) and represented one of the most intense dust storms experienced in Saudi Arabia in the last two decades. In this study, the effect of this dust storm on meteorological parameters was investigated. These parameters are relative humidity, air temperature, visibility and atmospheric pressure. Around noon local time on the event day, with the arrival of the dust plume, there were dramatic changes in weather conditions. Air temperature dropped by about 6 °C, relative humidity increased dramatically reaching a value of 33 %. The visibility deteriorated dramatically to a value of 1 m. These results also, show that the effect of this storm was associated with an increase in both atmospheric pressure and relative humidity as well as a reduction in temperature and visibility for the two days following the storm in comparison with conditions before the storm. The impact of several other dust storms on meteorological parameters during the year of 2009 were investigated and compared to the March 10th storm. It was found that this storm had a greater effect on the meteorological variables than the other storms.

**Keywords:** Dust Storm, Riyadh, Temperature, Solar Radiation

### 1. Introduction

Atmospheric aerosols are linked to the climate system and to the hydrologic cycle. Depending on their composition, atmospheric aerosols can absorb solar radiation in the atmosphere, producing further cooling of the surface and warming the atmosphere. Dust particles affect both solar and terrestrial radiation and are thus considered a significant climate-forcing factor and an important parameter in radiation budget studies [1]. The net effect of atmospheric aerosols is to cool the planet by reflecting incoming solar radiation. One of the major problems associated with dust storms is the considerable reduction of visibility that limits various activities, increases traffic accidents, and may increase the occurrence of vertigo in aircraft pilots [2]. Other environmental impacts include reduced soil fertility at the source area, damage to crops, a reduction of solar radiation, and, consequently, a reduction in the efficiency of solar devices, damage to telecommunications and mechanical systems, dirt, and air pollution. In addition, aerosols have a significant impact on human health. Goudie[3] recently provided an up-to-date and comprehensive review on dust storms and their significance for many fields.

The frequency of dust-storm occurrence in Saudi Arabia is at a maximum during the pre-monsoon (March–May) season, when dust aerosols are transported by south-westerly winds from the arid and semi-arid regions around the Arabian Sea.

In Saudi Arabia, dust storms are considered among the most severe environmental problems. Several investigators have studied desert dust in Saudi Arabia [4]. Most of the previous studies have used either surface or satellite observations to characterise the large-scale dust loading of the atmosphere over the Arabian Peninsula. However, almost nothing has been

done to study the effect of these dust storms on meteorological parameters and solar and infrared radiation in this region.

On the 10th of March 2009, a dramatic windstorm moved over Riyadh that was accompanied by a strong dust storm. This short-lived but intense dust storm caused a widespread, heavy dust load, greatly affected visibility and air quality, and caused a total airport shutdown as well as damage to buildings, vehicles, power poles and trees throughout the city of Riyadh. This storm was massive enough to be seen clearly from outer space and is considered to be one of the heaviest recorded dust storms in the last two decades. The outbreak of the dust storm was associated with a cold frontal passage that coincided with the propagation of a pre-existing synoptic-scale upper tropospheric jet stream over the northern and central parts of Saudi Arabia.

An investigation of the impact of this storm on solar and infrared radiation will be presented in another paper. This paper studies the impact of this severe storm on meteorological parameters and shows the variability of these parameters due to the storm.

## **2. Experimental Site and data:**

The study area of Riyadh lies in the central region of the Arabian Peninsula at 24° 43 'N; 46° 40'E, 764 m a.s.l. Riyadh is the capital of Saudi Arabia and its largest city; its population is 4500000 according to the 2005 census. It is a purely urbanised area and is one of the most polluted areas in the Kingdom because it is surrounded by industrial areas and traffic arterials, with the natural environment of the Empty-Quarter Desert lying beyond. The arid conditions prevailing at this site are responsible for large seasonal temperature differences, providing cool winters and very hot summers. The area experiences extremely low humidity, particularly in the summer. The climate of the region exhibits four dominant seasons each year: winter (December–February), pre-monsoon (March–May), monsoon (June–August), and post-monsoon (September–November). The pre-monsoon season, during which the present case study was conducted, is characterised by frequent dust storms and long dry spells.

Standard meteorological observations such as air temperature, relative humidity, and cloud information were used in the current study. These data were obtained using Riyadh Airport records provided by the Presidency of Meteorology and Environment.

## **3. Results and Discussion**

### **3.1. Event Description**

For the purpose of clarification the discussion of results will include the behaviour of the considered variables two days before and two days after the storm along with the event day. These will be referred as pre-event, post-event and the event day respectively.

The hourly values of four meteorological variables; relative humidity (RH), temperature (T), visibility (vis), and atmospheric pressure (P) for March 8-12, 2009, are plotted in Figure 1. As shown in Figure 1a, both T and RH reveal a diurnal cycle throughout, displaying a trend opposite to what one would expect. Visibility was in the 8-10 km range on the 8<sup>th</sup> and 9<sup>th</sup> of March and on the morning of the 10<sup>th</sup>, which is the normal maximum visibility found in Riyadh at this time of the year. The atmospheric pressure shown in Figure 1b shows a less clear diurnal cycle with some variability from one hour to the next on each day. Through most of the period from the morning of the 8th of March until the morning on the 10<sup>th</sup>, wind

directions were consistently southerly. Wind speeds increased during this period from ~10 m/s on the 8<sup>th</sup> to ~20 m/s on the 9<sup>th</sup>.

On the day of the event, before the arrival of the storm, the weather was stable; T was ~28 °C, P was 939.8 hPa, RH was 10%, and the local wind was relatively light towards the south. Around noon local time, with the arrival of the dust plume, there were dramatic changes in weather conditions. The wind swung to a northerly direction and wind speed rapidly increased to a maximum of 30 ms<sup>-1</sup>.

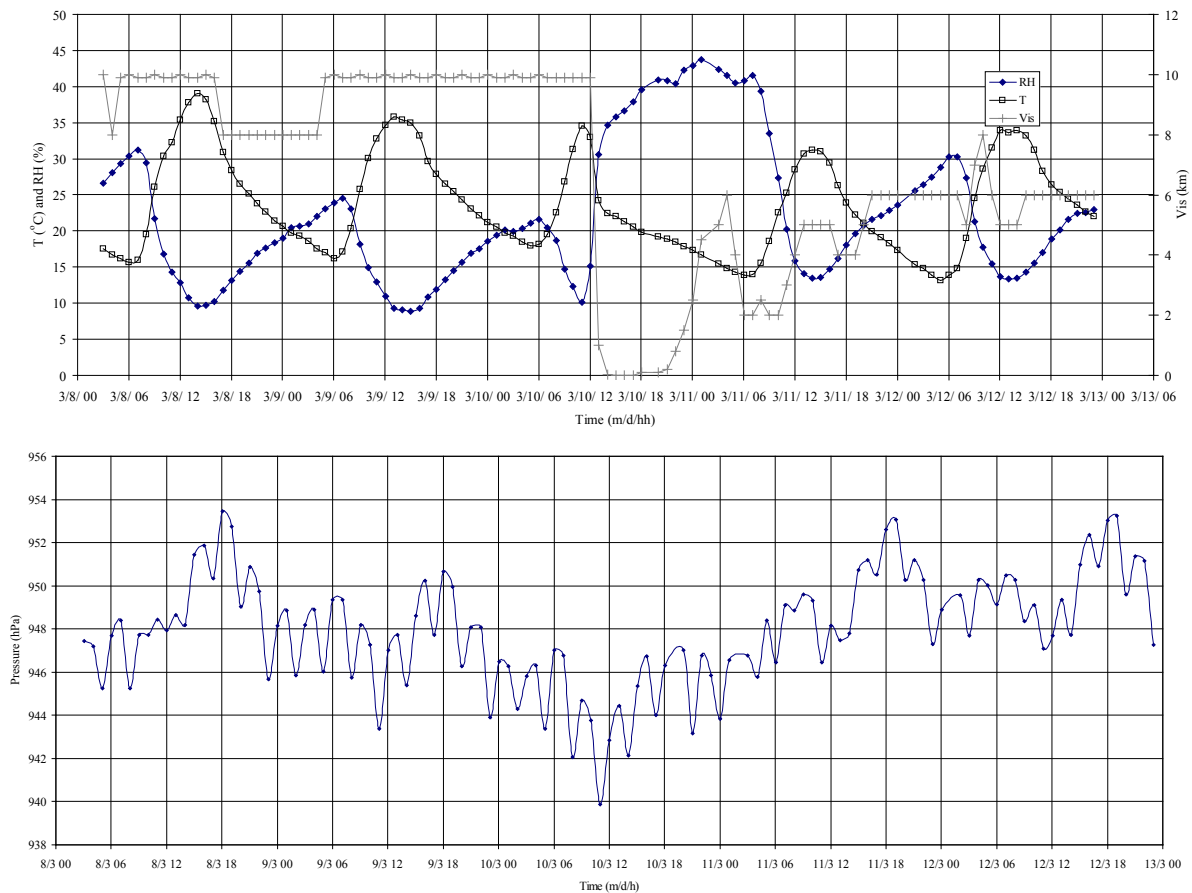


Fig. 1. Day-to-day variations of meteorological parameters (a) relative humidity ,air temperature, and visibility ;and(b) atmospheric pressure for the period from March 8th to March 12th 2009.

Because of the wind change and dust storm, T dropped by about 6 °C within an hour to reach 22 °C. The temperature continued to decrease until it reached the daily minimum of about 14 °C at 07:00 a.m. on the 11th. The air temperature then resumed its normal daily cycle, although temperatures remained cool on the 11th with a maximum of only 23 °C. It is likely that this reduction in the daytime temperature was caused by the reduced heating near the surface resulting from shortwave energy extinction by the additional aerosol loads arriving with the storm on the 10th. Relative humidity, on the other hand, increased dramatically with the arrival of the dust storm, reaching a maximum of 44 % at 01:00 on the 11th. The change in relative humidity is partly due to the cooler air temperatures but is also likely due to the moisture brought to the region by the storm. The visibility deteriorated dramatically with the arrival of the dust storm and then remained around 1 m for the 3 hours following the event. It then increased to 6 km by 03:00 on the 11th. After another decrease to ~ 2 km in the early

hours of the morning, it rose to between 5 km and 6 km and stayed around this mark for the rest of the period considered.

Several investigations on the dust storms in the Arabian Gulf and adjacent Gulf countries [5] and other places around the world [6] have reported similar variations and characteristic changes in meteorology.

### 3.2. Comparisons with other events

Table 1 shows a list of seven storm events during 2009. It summarises the change of the four meteorological parameters during these events. These changes represent the difference between the measured value immediately before the event and the maximum and minimum values reached immediately due to the event. In the last column, the time of maximum change occurs after the arrival of the storm is provided. Three of these events occurred in the pre-monsoon season, two in spring, one in summer and one in winter. In the last row of the table, the changes in the meteorological parameters for the 10<sup>th</sup> of March are summarised. Apart from the 18/9 event, the ranges of the changes in both atmospheric pressure and air temperature are confined between 2-4 hPa and 2-3 °C, respectively. The drop in the visibility varies between a minimum of 4 to a maximum of 8 km. The maximum changes in the relative humidity occurred on 4/6 and 18/9, followed by that on 20/5. For the events on 19/3 and 6/10, the RH dropped by -7 and -5 respectively. This drop may be due to the characteristics of the dry air mass that brought the storm to the study region. The 4/6 event is considered the strongest of the seven events. For this event, two hours after the storm, RH and atmospheric pressure increased by 10% and 3 hPa; temperature and visibility dropped by 3°C and 8 km, respectively. Comparisons between the 10<sup>th</sup> of March event and the seven other storm events showed, with the exception of the atmospheric pressure, that the changes in the meteorological variables are higher for the 10<sup>th</sup> March. In addition, although the two hours after the event on the 10<sup>th</sup> are considered to be relatively short, dramatic changes occurred during this time.

*Table 1 shows the difference between the meteorological variables before the storm and after the storm for the storm event in 2009. The last column is the time when maximum change occurred after the arrival of the storm*

| DAY/MONTH   | $\Delta$ VIS ( KM) | $\Delta$ T (°C) | $\Delta$ P (HPA) | $\Delta$ RH (%) | TIME OF MAX. (HOURS) |
|-------------|--------------------|-----------------|------------------|-----------------|----------------------|
| 20/5        | 4                  | 2               | 3                | 9               | 2                    |
| 28/5        | 7                  | 3               | 2                | 7               | 3                    |
| 4/6         | 8                  | 3               | 3                | 10              | 2                    |
| 19/3        | 8                  | 3               | 2                | -7              | 2                    |
| 6/10        | 5                  | 2               | 4                | -5              | 2                    |
| 28/2        | 6                  | 2               | 3                | 9               | 3                    |
| 18/9        | 5                  | 4               | 5                | 10              | 2                    |
| <b>10/3</b> | <b>9.9</b>         | <b>6</b>        | <b>4</b>         | <b>25</b>       | <b>2</b>             |

The effect of different aerosol loads on both the spectral and broadband solar radiation components have been investigated extensively both experimentally and theoretically by several researchers. It has been found that the aerosols may reduce the solar radiation by as much as 50% [7]. Additionally, it was found that dust storms severely affect meteorological variables. Their impact on these variables is different and becomes severe in some cases,

such as the one presented in this paper. Moreover, because several models have been developed to predict the solar radiation components (e.g., global and diffuse), it is important to consider the impact of such transient and severe events and study their effects to produce the appropriate predictability.

#### 4. Conclusion

On 10 March 2009, a severe and extensive dust storm event struck Riyadh and lasted for several hours. The impact of this event on ground-based measurements of meteorological parameters was investigated. These parameters are relative humidity, air temperature, visibility and atmospheric pressure. The analysis for the behaviour of the considered variables two days before and two days after the storm along with the event day were conducted and presented.

The investigations show significant changes in all of the measured parameters as a result of this event. Around noon local time on the event day, with the arrival of the dust plume, there were dramatic changes in weather conditions. Air temperature dropped by about 6 °C, relative humidity increased dramatically reaching a value of 33 %. The visibility deteriorated dramatically to a value of 1 m. These results also, show that the effect of this storm was associated with an increase in both atmospheric pressure and relative humidity as well as a reduction in temperature and visibility for the two days following the storm in comparison with conditions before the storm. Comparisons between this storm event and seven other reported events that occurred in the same year showed that this event was the most extreme and the most severe.

#### References

- [1] A. Jayaraman, Lubin, D., Ramachndran, S., Ramanathan, V., Woodbridge, E., Collins W. and Zalupuri, K. S.. Direct observation of aerosol radiative forcing over the tropical Indian Ocean during the Jan.- Feb. 1996 pre-INDOEX cruise. *J. Geophys. Res.* 1998, 103,13827–13836.
- [2] H. Kutiel, and Furman, H.,. Dust storms in the Middle East: Sources of origin and their temporal characteristics. *Indoor and Built Environment*, 2003, 12(6),419-426
- [3] A.S., Goudie, Dust storms: Recent developments. *Journal of Environmental Management*, 2009,90,89-94.
- [4] B. H. Alharbi, and Moied, K. 2005. R iyadh air quality report (1999-2004), King Abdulaziz City for Science and Technology, No. 279-25-ER.
- [5] D. L. McNaughton, Possible connection between anomalous anticyclones and sandstorms. *Weather*, 1987, 42 (1),8-13.
- [6] P. M., Pauley, Baker, N. L. and Barker, E. H., An Observational Study of the “Interstate 5” Dust Storm Case; *Bulletin of the American Meteorological Society*, 1996, 77 ( 4), 693-720.
- [7] K.V.S., Badarinath, Kharol, S.K., , Kaskaoutis, D.G., and Kambezidis , H.D. 2007. Case study of a dust storm over Hyderabad area, India: Its impact on solar radiation using satellite data and ground measurements; *Science of the Total Environment* 384 :316–332.

## The medium to long-term role of renewable energy sources in climate change mitigation in Portugal

Sofia Simões<sup>1,\*</sup>, Júlia Seixas<sup>1</sup>, Patrícia Fortes<sup>1</sup>, Luís Dias<sup>1</sup>, João Gouveia<sup>1</sup>, Bárbara Maurício<sup>1</sup>

<sup>1</sup> CENSE, Departamento de Ciências e Engenharia do Ambiente, Faculdade de Ciências e Tecnologia, Universidade Nova de Lisboa, Caparica, Portugal

\* Corresponding author. Tel: +351 212948354, Fax: +351 212948354, E-mail: sgcs@fct.unl.pt

---

**Abstract:** Portuguese policy-makers have adopted ambitious targets for RES promotion until 2020, but there are no national targets for the medium to long-term (2050) and it is not clear to what extent which RES can contribute to CC mitigation. This paper aims to assess the contribution of RES for the CC mitigation in Portugal until 2050, under cost-effectiveness criteria. The TIMES\_PT linear optimization bottom-up technology model was used to generate six scenarios to 2050 combining GHG emission caps, levels of socio-economic growth and share of RES electricity. In order to meet the 2050 energy demand, the share of RES in primary energy consumption increases 4 to 6 times from 2005 and in final energy grows from 15% in 2005 to 56-59% in 2050. RES were found to be cost-effective even without a GHG cap. Regarding CC mitigation the high RES shares in final energy correspond to less 49-74% GHG emissions in 2050 compared to a baseline without cap. The role of renewable electricity is determinant to mitigate CC especially due to hydro and onshore wind. Other important deployments of RES technologies are solar water heating and heat pumps in buildings, biomass use for process heat in industry and biodiesel in transport.

**Keywords:** Climate change mitigation, Renewable energy, Energy modeling, Portugal.

---

### 1. Introduction

Renewable energy sources (RES) play a key-role in climate change (CC) mitigation. Moreover, RES have added benefits of reducing external energy dependency and fostering economic development. Acknowledging this, Portugal has been pointed worldwide as a success case for RES deployment (IEA, 2009, NYT, 2010). National CC & energy policy-makers have adopted ambitious targets for RES promotion until 2020. The National Energy Strategy for 2020 (Cabinet Resolution n. ° 29/2010 of April 15) defines the following main objectives: i) reduce the external energy dependency to 74% (it was 87% in 2008); ii) ensure compliance of commitments within EU climate change policies, allowing that in 2020 60% of generated electricity is renewable based (RES-E) and 31% of final energy consumption is from RES (respectively 50% RES-E in September 2010 and 20% in 2005), and iii) achieving a reduction of 20% final energy consumption in the terms of the Energy-Climate policy package. The Portuguese National Action Plan (PNAER) within the Directive 2009/28/EC sets even more ambitious policies & measures (P&M) that will allow reaching 70% RES-E in 2020 and 10% biofuels in transport (update on PNAER by the Decree-Law n° 117/2010 of October 25). Other P&M are in place to promote RES heating and cooling and end-use energy efficiency, namely through the National Energy Efficiency Action Plan (RCM 80/2008).

Although there is high policy focus on medium-term RES promotion (2020) there are no national targets for the medium to long-term (2050). Likewise there are no quantitative estimates on avoided GHG emissions due to RES promotion, both in medium and long-term. Furthermore, there is no information on which RES (e.g. solar or waves) and which RES technologies (e.g. PV panels or biomass boilers) are the most cost-effective for Portugal. This is highly relevant to support national policy making, particularly regarding the design of incentives to promote the most cost-effective RES. This paper aims to assess the contribution of RES for the reduction of GHG emissions in Portugal until 2050 looking into detail into which technologies are most cost-effective.

## 2. Methodology

To assess the role of RES in CC mitigation in Portugal up to 2050, we used the TIMES\_PT model to generate six scenarios combining different assumptions as presented in Table 1.

Table 1. GHG and RES scenarios for Portugal up to 2050

| Scenario | GHG cap             | Economic Growth <sup>a)</sup> | Minimum fossil electricity |
|----------|---------------------|-------------------------------|----------------------------|
| C        | None                | Conservative                  | 30% of total electricity   |
| F        | None                | Fenix                         | 30% of total electricity   |
| -50C     | -50% in 2050 / 1990 | Conservative                  | 30% of total electricity   |
| -50F     | -50% in 2050 / 1990 | Fenix                         | 30% of total electricity   |
| Cefre    | None                | Conservative                  | None                       |
| Fefre    | None                | Fenix                         | None                       |

<sup>a)</sup> Two socio-economic scenarios were developed for Portugal as briefly outlined below.

To assess RES contribution to CC mitigation, we consider a **GHG<sup>1</sup> emission cap** in the -50C and -50F scenarios starting from 2015 with +27% of the 1990 (the Kyoto target for 2010-2012 extended to 2015) and linearly more stringent until -50% of 1990 for combustion and productive processes GHG emissions in 2050. (A trend line was then generated from the 2015 to the 2050 cap to obtain intermediate emission caps for every 5 years. The -50% cap is quite severe as it roughly leads to per capita emissions of 2.04 t CO<sub>2</sub>e in 2050 whereas in 2008 Portugal had 7.4 t CO<sub>2</sub>e. The per capita EU 15 average in 2008 was 10.1 tCO<sub>2</sub>e according to EEA data.

Regarding **economic growth and demand for energy services**, two contrasting socio-economic scenarios were used: Conservative and Fenix. The Conservative scenario follows the current economic and demographic trends (1% GDP annual growth rate and population decrease); whereas the Fenix scenario has more optimistic economic and population evolution forecasts (2 to 2.26% GDP annual growth rates and more 12% inhabitants in 2050 compared to 2005). These scenarios were used to generate two demand projections for materials and energy services such as residential lighting or cement which are inputs of the TIMES\_PT model. More information on the demand projections and can be found on Seixas *et al.* (2009).

Finally, in four of the six studied scenarios (C, F, -50C and -50F) we assumed a conservative requirement to assure the reliability of the power system translated as a **minimum of 30% of total generated electricity is produced by centralized fossil plants** from 2015 to 2050. In the Cefre and Fefre scenarios we removed this constraint and the system is free to adopt as much RES-E as needed according to cost-effectiveness criteria. Such approach could be associated with ensuring security of supply via expanded transmission capacity and increased electricity trade. In this paper however, we do not deal with electricity trade. We assumed that the net electricity imports are nil from 2025 onwards following the Portuguese transmission system operator expectations. If assumed otherwise the entire configuration of the electricity system would alter depending on how much electricity could be exported. However, at the moment there are absolutely no expectations on amounts of electricity traded after 2025 and any scenarios would be highly uncertain and out of the scope of this paper. Thus we have focused instead on the cost-effective assessment of maximum potential of national renewable

<sup>1</sup> This paper solely refers to energy related GHG emissions, i.e. from fuel combustion activities, fugitive emissions from oil, natural gas and other sources and from major industrial processes. These were approximately 81% of 2005 national emissions.

resources for the national CC mitigation considering nil electricity imports after 2025.

All these assumptions were inputted into the linear optimization bottom-up technology TIMES\_PT<sup>2</sup> model which represents the Portuguese energy system from 2005 to 2050. The TIMES\_PT is an implementation of the TIMES family of models developed by ETSAP of IEA which has been implemented at global, regional or national level (ETSAP, 2008), namely for the whole of UE (Pan European Times model from the NEEDS project) or for the countries Spain (Labriet, *et al.*, 2010), Belgium (Proost, *et al.*, 2009) or Germany (Blesl, *et al.*, 2007), among other EU countries. It considers both the supply and demand sides and disaggregates the energy demand sectors. The model is supported by a detailed database, which includes the technical and economical characteristics of the existing and future energy technologies and present and future sources of primary energy supply and their maximum technical and economic potentials (e.g. maximum available biomass or area for solar panels). TIMES\_PT finds the optimum combination of energy supply and demand technologies to satisfy the demand with the lowest possible total costs. More information on the details of the model can be found in Simões *et al.* (2008) and more details on the technology and primary energy assumptions in Seixas *et al.* (2009). The learning curves for RES-E solar and wave technologies are from the IEA (IEA, 2010, IEA, 2008) which were validated by national stakeholders. Wind RES-E technologies learning curves were supplied by national experts of the National Energy and Geology Research Institute (LNEG, 2010).

Other exogenous assumptions are very briefly outlined: 1) 8% discount rate for centralized electricity generation, buses and trains; 12% for commercial, industry, decentralized electricity generation, CHP and freight transport; and 17.5% for residential, cars and motorcycles. 2) maximum of 5000 Gg CO<sub>2</sub> carbon capture and storage potential were assumed as available since there is no data at the moment available for Portugal. More information on CCS cost data can be found at Simões *et al.* (2008); 3) no nuclear due to current policies and the purpose of this work focusing the role of RES; 4) new coal power plants without CCS not allowed due to climate policy; 5) RES targets, subsidies or feed-in tariffs not considered; 6) cost of oil barrel of 100 USD\$<sub>2008</sub> for the year 2020, 115 in 2030 and 145 in 2050.

### 3. Results

#### 3.1. RES in primary energy consumption

In order to meet the 2050 energy demand, the share of RES in primary energy consumption can increase to two to three times the 2005 values in the scenarios without GHG emission cap (Figure 1) which shows the cost-effectiveness of RES. To meet the CO<sub>2</sub> caps (-50C and -50F) RES can further increase to 4 to 6 times the 2005 values. The most competitive RES in all scenarios are wind and hydro which achieve its maximum potential in 2050. Solar, national biomass and, to a lesser scale, geothermal are also competitive but only if a GHG cap is in place. Removing the 30% fossil electricity requirement does not lead to significant changes in RES in 2020. However, in 2050 the higher RES-E share leads to higher consumption of solar especially in the Fefre scenario, where it achieves its maximum potential.

The increase in RES allows decreasing the external energy dependency from 87% in 2008 to 70-77% in 2020 and to 58-72% in 2050. The lowest values are not obtained due to the GHG

---

<sup>2</sup> The Portuguese model development was undertaken within the EU FP7 research project NEEDS ([www.needs-project.org](http://www.needs-project.org)). The NEEDS RS2a research team is responsible for the model structure. The authors are responsible for some structural changes, the base-year and new technologies information and for calibration and validation of the national model.

cap but instead due to 100% RES-E. If a backup of 30% fossil electricity is removed imports of natural gas for centralized CCGT plants can be reduced already in 2020. In any case, in 2050 a new energy import paradigm appears; instead of being dependent on imported fossil fuels the energy system will import biomass, particularly biofuels for transports.

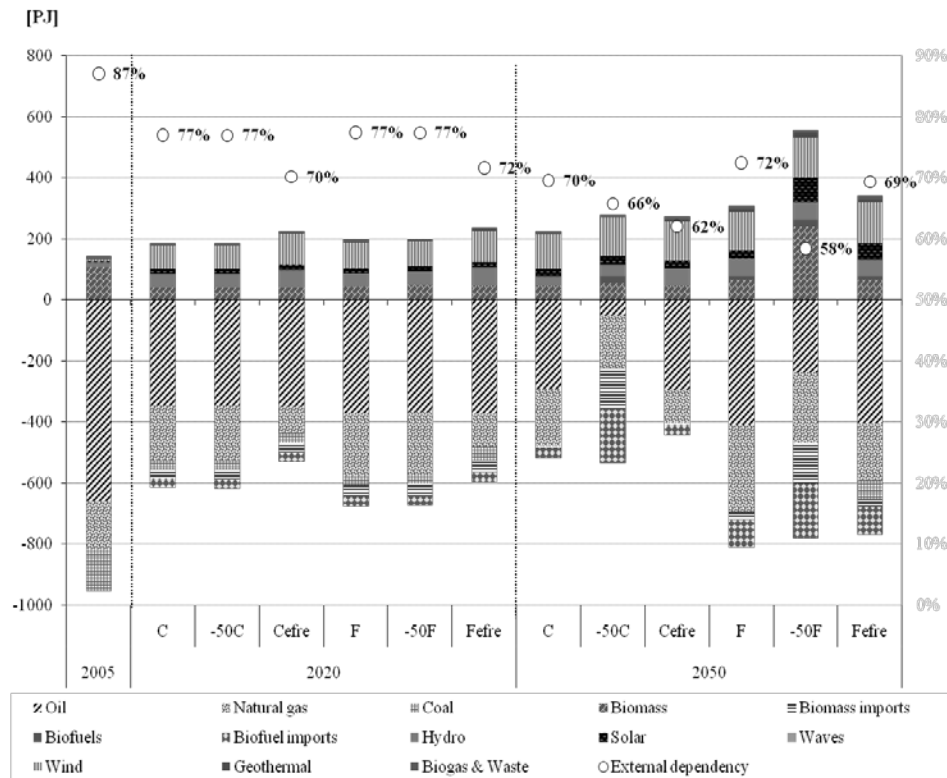


Fig. 1. Primary energy consumption in the studied scenarios, % of external energy dependency and % of RES (in the top rectangle). The lower values for 2020 are due to increase of refinery exports, decommissioning of a major coal power plant and slow recovery from 2010-2015 economic crisis.

### 3.2. RES in electricity generation

Until 2020 the electricity sector profile will be similar to 2009 since it will rely in recent investments both on RES (wind and hydro) and on new gas CCGT. Globally, approximately 58% of total electricity in 2020 is RES-E, in all scenarios with minimum 30% fossil electricity. In 2050 the GHG cap has a significant effect in RES-E technologies profile only in the -50F scenario since there is a higher overall demand for electricity (107.16 TWh, in comparison with 84.03 TWh in F). In -50C wind and hydro are sufficient to meet the demand. The system will firstly use all available hydro and onshore wind resources and in -50F this is followed by centralised PV, biomass and biogas CHP, and both geothermal steam turbines and hot dry rock systems. These technologies are practically negligible in 2050 in C, F, and -50C as the demand for RES-E is not high enough also due to the requirement for minimum 30% electricity from centralised fossil fuel. Without this requirement, in Cefire and Fefire, already in 2020 at least 78% of electricity will be RES-E and hydro and wind potentials will be achieved (9.7 and 6.5 GW, respectively). In 2050 74-89% electricity is RES and in Fefire large PV plants achieve the maximum potential (9.33 GW) and appears 0.50 GW of wind offshore. Both in 2020 and 2050 the gas CCGT plants will not work due to higher fuel and O&M costs.

In Cefire and Fefire there is a lower demand for electricity than in the other scenarios due to the higher contribution of efficient equipments and appliances in buildings, district heating in

commercial and biomass and insulation in the residential. This means that the 30% fossil electricity requirement hampers energy efficiency and RES use in final energy.

### 3.3. RES in final energy consumption

Concerning final energy consumption (FEC) in 2020, no significant changes in the energy profile are expected, even with the cap, although RES share increases from 15% of total FEC in 2005 to 30-35%. In the long term (2050) it is clear that the increase in electricity is a major strategy to mitigate CC as there are endogenous energy resources used to generate RES-E, especially wind and hydro, as mentioned before. In 2050, the FEC in the F scenario is almost 70% higher than in the C leading to new technologies to meet the cap, such as H2 for transports. The share of RES in FEC in 2050 varies from 31-36% in scenarios without the GHG cap to 56-59% with the cap (Table 2). The RES share grows more due to the GHG cap in the transports (both in C and F) and industry (only in the -50F scenario) sectors.

Table 2. RES contribution in final energy consumption for the six scenarios

| Sector/Scenario<br>[PJ]    | 2005      | 2050      |           |           |           |           |           |
|----------------------------|-----------|-----------|-----------|-----------|-----------|-----------|-----------|
|                            |           | C         | -50C      | Cefre     | F         | -50F      | Fefre     |
| RES Electricity            | 32        | 159       | 188       | 203       | 221       | 300       | 252       |
| RES Heat & cold            | 96        | 69        | 68        | 69        | 91        | 206       | 93        |
| Residential                | 50        | 34        | 32        | 34        | 39        | 38        | 39        |
| Commercial                 | 0         | 11        | 8         | 10        | 14        | 13        | 13        |
| Industry                   | 45        | 25        | 27        | 25        | 39        | 155       | 41        |
| RES in Transport           | 0         | 36        | 245       | 36        | 98        | 200       | 98        |
| Final Renewable Energy (a) | 128       | 263       | 501       | 307       | 410       | 707       | 442       |
| Total Final Energy (b)     | 826       | 863       | 846       | 860       | 1225      | 1253      | 1224      |
| <b>% Renewables (a/b)</b>  | <b>15</b> | <b>31</b> | <b>59</b> | <b>36</b> | <b>33</b> | <b>56</b> | <b>36</b> |

Other relevant uses of RES are solar for water and space heating in buildings, which in all scenarios, regardless of GHG cap and RES-E restrictions; achieve its maximum potential already in 2020. In 2050 with the GHG cap, solar panels are also cost-effective to generate heat for industry and the potential is also achieved. The role of biomass is reduced in buildings as electricity, solar thermal and heat pumps become more appealing. On the other hand, biomass will become more cost-effective in CHP to generate heat for industry. In transports the share of biofuels is expected to increase above 10% in 2020 in all scenarios and in 2050 up to 60-40% due to the GHG cap. Other impacts of the GHG cap in 2050 in the transport sector are to create room and need for electric vehicles and for H2 freight trucks.

## 4. Discussion

We found that RES technologies are highly cost-effective in the Portuguese energy system even without any CO2 cap (36-38% of PEC and 31-33% of FEC in 2050). If an ambitious CC mitigation cap is in place, the contribution of RES is even higher to 65-72% of PEC and 59-56% of FEC in 2050. If the layout of the power sector does not require centralised fossil plants, for example by ensuring security of supply via expanded transmission capacity, RES contribute with 41-44% of PEC and 36% of FEC in 2050. So, a cap on GHG emissions has a larger impact in RES contribution than a reconfiguration of the power system. Although RES play a fundamental role in CC mitigation in Portugal it should be noted that it is not possible to reduce external energy dependency below 77% in 2020 and below 50% in 2050. Further reductions are only possible with stronger efforts on energy efficiency, which were not in the

scope of this paper.

Regarding RES technologies, hydro and wind power can achieve the maximum technical and economic potential in Portugal in the medium run (2020) and contribute significantly to generated electricity. To some extent, this already occurs as in 2009 wind and hydro ensured 34% of total generated electricity. Until 2050 they can generate 60-80% of total electricity, respectively if a GHG cap is in place or if no fossil electricity backups are required. On the other hand, electricity generation technologies from solar are still in an early-phase and need extra incentives to become competitive before 2050. Nonetheless, policy support to solar technologies should be considered from a R&D perspective anticipating future technology costs reductions since Portugal already has know-how in this area and some national companies manufacture components. Electricity generation from waves and offshore wind technologies are competitive from 2035 onwards only if Portugal adopts an aggressive GHG cap or no centralised fossil backup is needed. In these conditions and considering the existing national R&D capacities and wind parts supply chain, these two technology groups should be considered by policy makers as a priority.

Besides RES electricity, solar (both for water and space heating) is highly competitive already in the medium term (2020) even without any GHG emission cap. Heat pumps are also extremely competitive but only if a cap is in place. On the other hand electric vehicles are only cost-effective in 2050 if a cap is in place and the technology evolves to supply long-distance mobility as existing cars do. Otherwise, biofuels are a cheaper alternative.

Finally, the results presented have the following main caveats: 1) learning curve for energy technologies with high uncertainty, especially for the least mature technologies; 2) high uncertainty of profile of electricity trade within the Iberian electricity market; 3) high uncertainty on the availability of endogenous and imported biomass and biofuels. Moreover, the TIMES\_PT is a partial equilibrium model and thus does not model economic interactions outside the energy sector and does not consider in detail demand curves and non-rational aspects that condition investment in new technologies. All of these caveats reflect real life uncertainties which policy makers have to deal with especially when thinking of long-term policies. An approach to try to handle uncertainty is to perform sensitivity analysis which the authors did for the RES electricity technologies learning curve (solar, wind offshore and waves) and for available biofuels and biomass. For electricity trade this was not done due to lack of any indication of plausible scenarios and involved amount of work considering the scope of the paper, as mentioned in section 2. It was found that assumptions on the technology learning rate affect the share of the different RES-E technologies in the energy system but the total share of RES-E is not altered. Variations on the amounts and prices of available biomass significantly affect RES potential for CC mitigation in Portugal, as biomass and biofuels are preferable to RES-E in the industry and transport sectors, since they are more cost-effective. However, it is not in the scope of this paper to discuss and assess uncertainty in detail and thus it is not possible here to present and discuss in detail the performed sensitivity analysis, but only to draw attention to the limitations of the results, which serve to illustrate that in Portugal RES are very effective for CC mitigation goals.

## **5. Conclusions**

This paper's objective is to assess the contribution of RES for CC mitigation in Portugal until 2050 looking into detail into which technologies are most cost-effective. We have found that the RES share in final energy consumption can increase from 15% in 2005 to 31-33% in 2050 in a baseline scenario without an emission cap. This illustrates that RES are cost-effective

regardless of the goal of CC mitigation, especially in the electricity generation sector (mostly hydropower and wind onshore technologies). To meet the GHG cap of -50% in 2050 this share can further increase to 56-59% of total final energy consumption. This represents a growth of more than 200% of 2005 values. Although the increase of energy efficiency is an alternative cost-effective strategy to CC mitigation, the GDP energy intensity in 2050 is only less 32-40% of 2005 values. This seems to suggest that RES can contribute more significantly to the emission targets than energy efficiency improvements.

Regarding GHG emission reduction, a 49-74% emission reduction is achieved in 2050 for the -50% cap compared to the baseline. Electricity generation is the most relevant sector for abatement. This sector can be responsible for up to 98% of all abatement in 2050 if the constraint of a minimum of 30% total generated electricity is produced by centralized fossil plants is not present. In this situation all electricity will be renewable. In the scenarios where this minimum fossil electricity is required the electricity sector is not completely renewable and the transport sector is the most important sector for total GHG abatement (up to 57% of total GHG emission reduction in 2050 compared to baseline). In both sectors RES are the main reason for emission abatement, both hydropower and onshore wind technologies, followed to a lesser extent by solar PV and geothermal electricity generation technologies, and biofuels for individual cars and freight trucks.

## References

- [1] IEA. Energy Policies of IEA Countries – Portugal 2009 Review. OECD / International Energy Agency. Paris, France, 2010, pp. 131-146.
- [2] J. Seixas, S. Simões, P. Fortes, L. Dias, J. Gouveia, B. Alves, B. Maurício, [New Energy Technologies: Road Map Portugal 2050, D3: Competitiveness Assessment of New Energy Technologies], Novas Tecnologias Energéticas: Road Map Portugal 2050, D3: Análise da Competitividade das Novas Tecnologias Energéticas, Portuguese Innovation Fund for Renewable Energy of the Ministry of Economy, 2010, pp. 1-88.
- [3] NYT. Portugal Gives Itself a Clean-Energy Makeover, The New York Times, August 10<sup>th</sup>, 2010, pp. A1. Available at: [[http://www.nytimes.com/2010/08/10/science/earth/10portugal.html?\\_r=2&ref=global-home](http://www.nytimes.com/2010/08/10/science/earth/10portugal.html?_r=2&ref=global-home)]
- [4] ETSAP – International Energy Agency Implementing Agreement for a Programme of Energy Technology Systems Analysis, Global Energy Systems and Common Analysis Final Report of Annex X (2005-2008), Ed. G. Goldstein, G. Tosato, ETSAP, 2008, pp. 21 - 77.
- [5] S. Simões, J. Cleto, P. Fortes, J. Seixas, G. Huppel, Cost of energy and environmental policy in Portuguese CO<sub>2</sub> abatement - scenario analysis to 2020. Energy Policy, 2008, Vol. 36, Issue 9, pp. 3598 - 3611.
- [6] M. Labriet, H. Cabal, Y. Lechon, G. Giannakidis, A. Kanudia, The implementation of the EU renewable directive in Spain. Strategies and challenges. Energy Policy, 2010, Vol. 38, Issue 5, pp. 2272 - 2281.
- [7] S. Proost, E. Delhaye, W. Nijs, D. van Regemorter, Will a radical transport pricing reform jeopardize the ambitious EU climate change objectives? Energy Policy, 2009, Vol. 37, Issue 10, pp. 3863 - 3871.
- [8] M. Blesl, A. Das, U. Fahl, U. Remme, Role of energy efficiency standards in reducing CO<sub>2</sub> emissions in Germany: An assessment with TIMES. Energy Policy, 2007, Vol. 35,

Issue 2, pp. 772 - 785.

- [9] IEA, Technology Roadmap – Solar Photovoltaic Energy, OECD/International Energy Agency. Paris, France, 2010, pp. 7 – 9.
- [10] IEA, Technology Roadmap – Concentrating Solar Power, OECD/International Energy Agency. Paris, France, 2010, pp. 27 - 28.
- [11] IEA, Energy Technology Perspectives, OECD/International Energy Agency. Paris, France, 2008, pp. 400.
- [12] LNEG, 2010. Personnel communication from Eng. Ana Estanqueiro from LNEG Unit of Solar, Wind and Ocean Energy. June 16, 2010.

## Diversified analysis of renewable energy contribution for energy supply in Asian regions

Genku Kayo<sup>1,\*</sup>, Takashi Ikegami<sup>2</sup>, Tomoki Ehara<sup>3</sup>, Kazuyo Oyamada<sup>3</sup>,  
Shuichi Ashina<sup>1</sup>, Junichi Fujino<sup>1</sup>

<sup>1</sup> National Institute for Environmental Studies (NIES), Ibaraki, Japan

<sup>2</sup> Institute of Industrial Science (IIS), Tokyo, Japan

<sup>3</sup> Mizuho Information and Research Institute (MHIR), Tokyo, Japan

\* Corresponding author. Tel: +81-29-850-2019, Fax: +81-29-850-2422, E-mail: kayo.genku@nies.go.jp

---

**Abstract:** Renewable energy is one of the key drivers for reducing CO<sub>2</sub> emissions in the future. In order to support effective policy-making relating to renewable energy, estimation of available potentials mixed with all energy resources including fossil fuels is needed. However, previous research has sometimes focused on only one particular approach. Therefore, a diversified analysis of potential renewable energy contributions to energy supply in Asian regions was carried out in this paper. In order to estimate physical potential, a grid cell approach using geographical information system (GIS) data was adopted. Once the physical and technical potential had been estimated, the economic potential was then calculated. Socio-economic potential was analyzed using energy outlook data collected and reviewed from various publications in order to assess trends in energy demand and supply. The results indicate that almost all Asian countries will continue to develop and that the demand for energy will grow. With the aspect from potential amount, renewable energy supply is effective even though fossil fuels will continue to dominate totally energy mixes for the foreseeable future. In renewable energy supply, potential of solar is dominated and bears on wide implication compared with that of wind and biomass. To ensure the best possible results, further research should be carried out on the optimal schedule for the multi-phased introduction of renewable energy in long-term policy.

**Keywords:** Solar energy potential, Wind energy potential, Biomass energy potential, Asian region

---

### 1. Introduction

Renewable energy is one of the key drivers for reducing CO<sub>2</sub> emissions in the future. The third annual report (TAR) compiled by the IPCC expresses the relative potential of several phases of renewable energy in terms of physical, technological, socio-economic, economic and market potentials. In order to support effective policy-making relating to renewable energy, estimation of available potentials mixed with all energy resources including fossil fuels is needed. However, previous researches have sometimes focused on only one particular resource, for instance, solar energy (Hofman et al., 2002), wind energy (Grubb and Meyer, 1993) and biomass energy (Berndes et al., 2003). In this paper, diversified analysis of renewable energy contributions was carried out considering energy mix with fossil fuels and trends of energy demand. Renewable energy potentials were estimated in ten Asian regions. These regions included Japan (JPN), China (CHN), India (IND), Indonesia (IDN), Korea (KOR), Thailand (THA), Malaysia (MYS), Viet Nam (VNM), the Philippines (PHL) and Singapore (SGP).

#### 1.1. Renewable energies

In this paper, three renewable energy sources were selected for investigation: solar, wind and biomass energy. It is expected that technologies to make use of these energy sources will be introduced into Asian countries in order to create a decentralized energy generation and supply system. Solar energy is included in this paper only in terms of the electricity generation provided by photovoltaic (PV) cells.

## 1.2. Definition

According to TAR (IPCC, 2001a), renewable energy can be described in terms of the following “potentials”. The physical potential of a renewable energy source is the amount of that resource theoretically available in the area in question, and which can be considered suitable for production. This includes any constraints imposed by land use considerations or local site characteristics such as elevation and slope. The technical potential of a renewable energy source is the part of physical potential remaining after all losses due to conversion from the extractable primary energy source to secondary energy carriers or other forms of energy (electricity, fuel etc.) are taken into account. The socio-economic potential of a renewable energy source is the actual capacity for renewable energy use, taking into consideration the distribution of energy mixes and the growth of primary energy demand. The economic potential of a renewable energy source is the technical potential, based on the estimated production cost of a secondary form of energy which is competitive with a specified, locally relevant alternative. A flexible way to represent the economic potential is, therefore, in the form of energy production potential, expressed as a function of the production cost.

## 2. Methodology

### 2.1. Estimation of physical and technological potential

#### 2.1.1. Data collection

In order to estimate physical potential, a grid cell approach using geographical information system (GIS) data was adopted. The physical potentials were estimated on a global basis using previously collected data such as insolation and wind speed measurements, land cover, elevation and wilderness area data. After calculation of the optimal inclination angle for solar PV cells in each grid cell, the total amounts of generation were estimated per cell and aggregated on a country-by-country basis. Table 1 shows the GIS data list that was used in this estimation process. (All the data used has been published on websites and made available for simulation purposes [5, 6, 7, 8, 9, 10, 11]).

Table 1. Data sources

| Category   | Data source   | Original data provider  |
|------------|---|---|
| Land cover | MODIS/Terra Land Cover Type Yearly L3 Global 1km, Land Cover Type 1 (IGBP), 2005  | NASA Land Processes Distributed Active Archive Center         |
| Elevation  | The Global Land One-km Base Elevation (GLOBE) Data, 1999  | National Geophysical Data Center                              |
| Bathymetry | GEBCO One Minute Grid Version 2.00, 2006  | General Bathymetric Chart of the Oceans                       |
| Wilderness | World Wilderness Areas, 1993  | UNEP/GRID   |
| Insolation | Surface Meteorology and Solar Energy Release 6.0 Data Set; Monthly averaged insolation incident on a horizontal surface, 2008 | NASA Langley Research Center, Atmospheric Science Data Center |
| Wind Speed | Surface Meteorology and Solar Energy Release 5.0 Data Set; Monthly averaged wind speed at 50m above the surface, 2005         |   |

### 2.1.2. Solar energy potential

Monthly and hourly solar energy potential in 3-by-3 arc-minute grid cells was calculated from averaged insolation data, averaged wind speed data, land cover type data, and so on. Compared with the previous method used (Bert. J. M. de Vries, 2007), extra parameters were included in the form of solar elevation angle, solar azimuth angle, land surface slope and elevation angle. In addition, the optimum inclination angle of each solar PV cell was calculated per grid cell and this information was also taken into account. The inclusion of these factors allowed a more accurate estimation to be made of the solar energy potential. The available area was determined using a suitability fraction, as shown in Table 2. For technical reasons, the area studied was limited to less than 5000m elevation and less than 60% slope. Solar energy potential,  $EPS$  [kWh/yr], was calculated using Eq. (1).

$$EPS_g = \sum_{M,T} I_{g,M,T} \cdot A_g \cdot \frac{e}{100} \quad (1)$$

where  $I$  is the insolation intensity at the optimum inclination angle of solar PV [ $\text{kW}/\text{m}^2$ ],  $A$  is the PV cell area [ $\text{m}^2$ ], and  $e$  is the PV module efficiency (=13%). The subscripts  $g$ ,  $M$  and  $T$  stand for the grid cell, month and time, respectively.

### 2.1.3. Wind energy potential

The wind turbine was assumed to be 80m high with a capacity of 2MW and rotors 90m in diameter. The available area was determined using a suitability fraction, as shown in Table 2, and restricted to less than 2000m elevation and less than 60% slope. Since the reference wind measurements provided by the surface meteorology dataset (NASA, 2005) were for a height of 50m, averaged wind speed was adjusted to a height of 80m, equal to that of the wind turbine. When the wind energy potential,  $EPW$  [kWh/yr], was calculated the probability distribution of wind speed  $v$  [m/s], the wind power correction factor  $k$ , and the availability rate  $j$  [%] were also taken into account, as shown in Eq. (2).

$$EPW_g = \sum_{v,LC} P(v) \cdot R(v) \cdot 8760 \cdot j \cdot k_{LC} \cdot (1-l) \cdot Nw_{g,LC} \quad (2)$$

where  $l$  is the loss rate,  $LC$  is the land cover,  $P(v)$  [kW] is the output of the wind turbine when the wind speed is  $v$  [m/s], and  $R(v)$  refers to the appearance probability distribution of the wind speed  $v$  [m/s]. Table 2 shows the parameter values for each type of land cover. Seventeen land cover categories were consolidated into four land use patterns. The suitability fraction values were one of the effective factors used in this estimation method. Therefore, in future, adequate suitability fractions should be estimated and modified by comparison with other, more precise calculations.

Table 2. Parameter values for each type of land cover

| Land cover  | Suitability Fraction [%] |      | Power Correction Factor [%] |
|---|--------------------------|------|-----------------------------|
|   | Solar                    | Wind |                             |
| All Forest, Closed Shrublands, Woody Savannas, Permanent Wetlands, Snow and Ice, Water Bodies | 0                        | 0    | 90                          |
| Urban and Built-Up Areas  | 1                        | 0    | 90                          |
| Croplands, Natural Vegetation Mosaic  | 0                        | 30   | 90                          |
| Open Shrublands, Savannas, Grasslands, Barren or Sparsely Vegetated Areas                     | 1                        | 50   | 95                          |

#### 2.1.4. Biomass energy potential

In the biomass energy potential calculation, twelve different resources (provided by the FAO statistical report, FAOSTAT, FAO, 2001) were taken into account. These resources included industrial round wood residues, pulp used for paper, sawn wood, mill residues, paper scrap, timber scrap, crop residues, sugarcane residues, bagasse, dung, kitchen refuse, and human feces. Each resource was assigned a different residual rate - defined as the fraction of the total amount available in production and able to be used for production purposes. Statistical data were, therefore, prepared in terms of volume or weight. The residual volumes were then converted to calorific values for calculation purposes.

#### 2.1.5. Renewable energy potential grades

Renewable energy potentials were calculated and classified into three grades. When physical potentials were calculated, each grid cell was classified in terms of its renewable resource advantage. Grade I had some specific advantage in terms of its use as a renewable energy source, while grade III had some specific disadvantage associated with its use, due to location or climatic conditions. In the case of solar energy, the grade was determined by the insolation intensity received by each solar PV module [ $\text{kWh/m}^2/\text{yr}$ ]. In the case of wind energy, the grade was determined by the utility operation rate,  $UC$  [%], defined by the percentage of annual electricity [ $\text{TWh/yr}$ ] generated by full load operation throughout the year. The classified grades are shown in Table3 and 4.

### 2.2. Socio-economic potential estimation

Many institutes have published reports presenting statistical data or perspectives concerning the future of the Asian region, and this information is essential in order to estimate the contribution of renewable energies. However, because the Asian region is growing so rapidly and so dramatically, it is difficult to accurately construct future scenarios. Some reports published by international institutes (IPCC, 2001; IEA, 2009; EUROPEAN COMMISSION, 2006; ADB, 2009; Greenpeace, 2008; Shell, 2008; Energy Research Institute, 2009; OECD, 2008 and so on) present various possible energy outlooks for future scenarios. Consequently, in this study, data relating to energy outlook were collected and reviewed in order to estimate expected trends in energy demand, supply and energy share in each country. After collecting data on the relevant parameters, maximum and minimum values were selected and a range of growth rates were established.

### 2.3. Economic potential estimation

After the calculations for physical and technical potential were completed, the production cost in each grid cell,  $g$ , was determined for each energy generation system. The production costs of solar energy,  $CS$  [ $\text{USD/kWh}$ ], and wind energy,  $CW$  [ $\text{USD/kWh}$ ], were calculated using Eq. (3) and Eq. (4).

$$CS_g = \frac{r}{1 - (1+r)^{-LS}} \cdot \frac{(1+OM) \cdot INVS \cdot A_g}{EPS_g} \quad (3)$$

$$CW_g = \frac{r}{1 - (1+r)^{-LW}} \cdot \frac{(1+OM) \cdot INVW \cdot A_g}{EPW_g} \quad (4)$$

where  $OM$  is the operation and maintenance cost expressed as a fraction of the investment cost,  $r$  is the discount rate, and  $LS$  or  $LW$  is the durable period.  $EPS$  and  $EPW$  are the energy potentials calculated using Eq. (1) or Eq. (2).  $INVS$  and  $INVW$  represent the cost of the system. In the case of solar energy,  $INVS$  was set at 780 [ $\text{USD/m}^2$ ], which assumes 6 [ $\text{USD/Wp}$ ]

included per PV module and BOS.  $A$  represents the area of the PV cell [m<sup>2</sup>]. On the other hand, in the case of wind power,  $INVW$  was set at 760 [USD/kW], and  $A$  represents the construction area in each grid cell.

### 3. Results

#### 3.1. Physical and technical potentials

##### 3.1.1. Potential grades

Table 3 and 4 show the calculated results for physical and technical potential, broken down by grade. Comparing the three renewable energies studied shows that the solar energy potential is the largest, especially in grade II. China, India and Indonesia have some potential in grade I, reflecting good insolation conditions. However, regions such as Japan, China, Indonesia, Korea and Malaysia have more potential in grade III, overall, than in grade II. Wind energy potential is not as large as that of solar energy. Only China possesses significant potential in grade I. However, in the case of biomass energy, both China and India possess large potentials because of their large population and large plantation area. This physical potential analysis confirms that some countries have suitable renewable energy resources.

Table 3. Physical and technical potential, by grade (Solar Energy and Wind Energy)

| Country code | Solar Energy Potential [TWh/yr]          |  |                                       |        | Wind Energy Potential [TWh/yr] |              |             |       |
|--------------|--|--|---------------------------------------|--------|--------------------------------|--------------|-------------|-------|
|              | Grade I                                  | Grade II                                 | Grade III                             | Total  | Grade I                        | Grade II     | Grade III   | Total |
|              | 2200-2600<br>[kWh/m <sup>2</sup> /y<br>] | 1800-2200<br>[kWh/m <sup>2</sup> /y<br>] | 0-1800<br>[kWh/m <sup>2</sup> /y<br>] |        | 40-100<br>[%]                  | 30-40<br>[%] | 0-30<br>[%] |       |
| JPN          | 0  | 465                                      | 39,692                                | 40,157 | 0                              | 38           | 26          | 64    |
| CHN          | 434                                      | 32,845                                   | 45,610                                | 78,889 | 337                            | 1,925        | 3,318       | 5,580 |
| IND          | 4,255                                    | 46,136                                   | 169                                   | 50,560 | 0                              | 177          | 721         | 898   |
| IDN          | 5  | 1,625                                    | 3,699                                 | 5,329  | 0                              | 0            | 45          | 45    |
| KOR          | 0  | 3,759                                    | 6,604                                 | 10,363 | 0                              | 0            | 17          | 17    |
| THA          | 0  | 10,322                                   | 881                                   | 11,203 | 0                              | 0            | 38          | 38    |
| MYS          | 0  | 1,243                                    | 2,361                                 | 3,604  | 0                              | 0            | 5           | 5     |
| VNM          | 0  | 1,278                                    | 535                                   | 1,813  | 0                              | 3            | 60          | 63    |
| PHL          | 0  | 1,304                                    | 9                                     | 1,313  | 0                              | 0            | 42          | 42    |
| SGP          | 0  | 1,180                                    | 776                                   | 1,956  | 0                              | 4            | 88          | 92    |

Table 4. Physical and technical potential, by grade (Biomass Energy)

| Country code | Biomass Energy Potential [TWh/yr] |          |           |       |
|--------------|-----------------------------------|----------|-----------|-------|
|              | Grade I                           | Grade II | Grade III | Total |
| JPN          | 109                               | 15       | 15        | 139   |
| CHN          | 735                               | 51       | 51        | 837   |
| IND          | 577                               | 8        | 8         | 593   |
| IDN          | 121                               | 7        | 7         | 135   |
| KOR          | 25                                | 3        | 3         | 31    |
| THA          | 79                                | 1        | 1         | 80    |
| MYS          | 47                                | 1        | 1         | 48    |
| VNM          | 19                                | 5        | 5         | 29    |
| PHL          | 39                                | 1        | 1         | 40    |
| SGP          | 1                                 | 0        | 0         | 1     |

### 3.2. Socio-economic potentials

#### 3.2.1. Review of expected energy demand in Asia

Fig. 1 shows expected total primary energy demand throughout Asia, as reported by IPCC (SRES2001, IPCC, 2001b). The curved lines indicate the forecasts simulated by several different models. The predicted maximum value in 2050 is approximately 3.84 times larger than the minimum value in 2050. The calculated results for physical and technical potentials are represented by the horizontal dashed lines in Fig. 1. The solar energy potentials, alone, can be seen to be large enough to meet the primary energy demand in all future scenarios. Wind energy potentials can also be seen to constitute an effective energy source. On the other hand, the biomass energy calculation shows that it is not large enough to constitute a major energy supply resource.

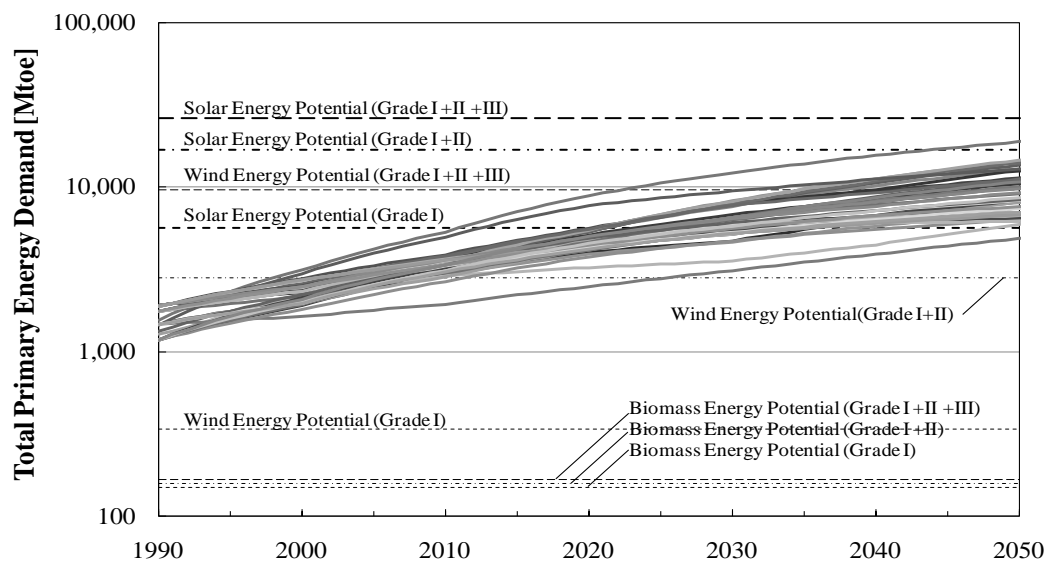


Fig. 1. Total primary energy forecast in published reports, and renewable energy potential

#### 3.2.2. Renewable energy contributions in each region

Fig. 2 shows the outlook for primary energy supplies, fossil fuel supplies and renewable energies in three Asian regions: Japan, China and India. Each graph includes the maximum and minimum trends derived from the various reports collected and reviewed as part of this study. It can be seen that the renewable energy share is extremely small, overall. Fig. 2 also shows the calculation results obtained for physical and technical potentials (bold dashed lines). In the case of Japan and India, the solar energy potential (alone) exceeds the maximum predicted primary energy demand. On the other hand, China's energy growth is more rapid and larger than that of other Asian countries. Therefore, the renewable energy potential of China is not large enough to meet all of China's expected primary energy demand in the predicted maximum growth scenario. Renewable energy supply is effective even though fossil fuels will continue to dominate totally energy mixes for the foreseeable future.

### 3.3. Economic potentials

Fig. 3 shows the potential cost curve for three Asian regions: Japan, China and India. The horizontal axis (logarithmic scale) indicates the market potential. In the case of Japan, grade III solar energy shows most potential but has a high introduction cost. In contrast, the introduction cost of biomass energy is very low but the expected potential is small. In order to increase its share of renewable energy, Japan should, therefore, focus mainly on the installation of solar energy generation systems. In the case of China, the most potential is for grade II solar energy. The cost of grade III wind energy is more than 0.9USD/kWh higher

than other renewable resources. In India, grade I solar energy shows the most potential. Grade III wind energy also has a high cost, even in China and India. Consequently, solar energy should receive first priority for introduction and wind energy should be second. The potential for biomass energy is not as large, but its cost intensity is lower than either wind or solar power. Therefore, the immediate introduction of biomass energy systems could be an effective strategy in some Asian regions.

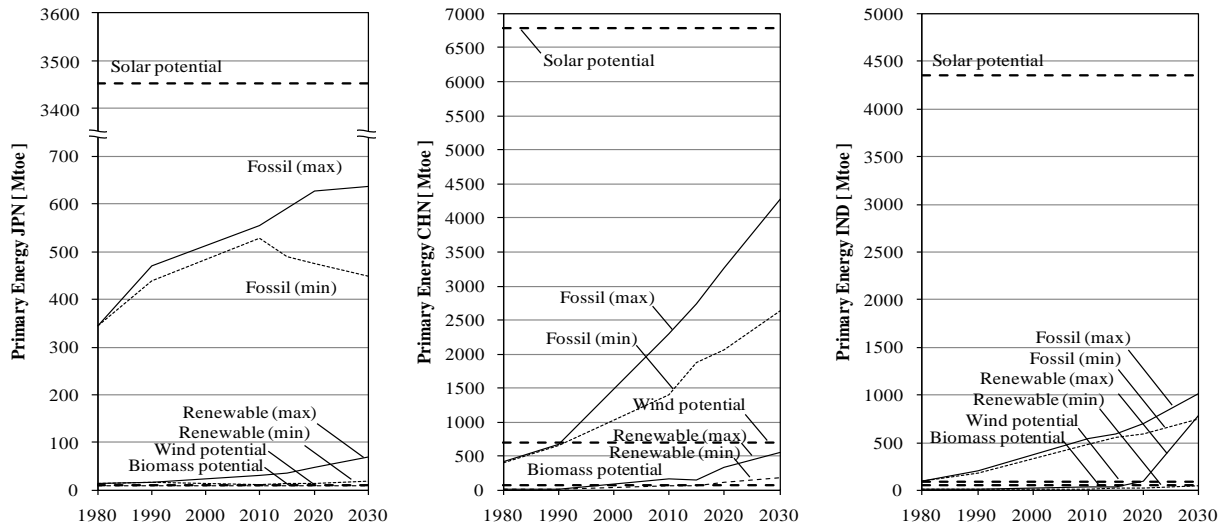


Fig. 2. Primary energy trends and renewable energy potentials in Japan (left), China (center), and India (right)

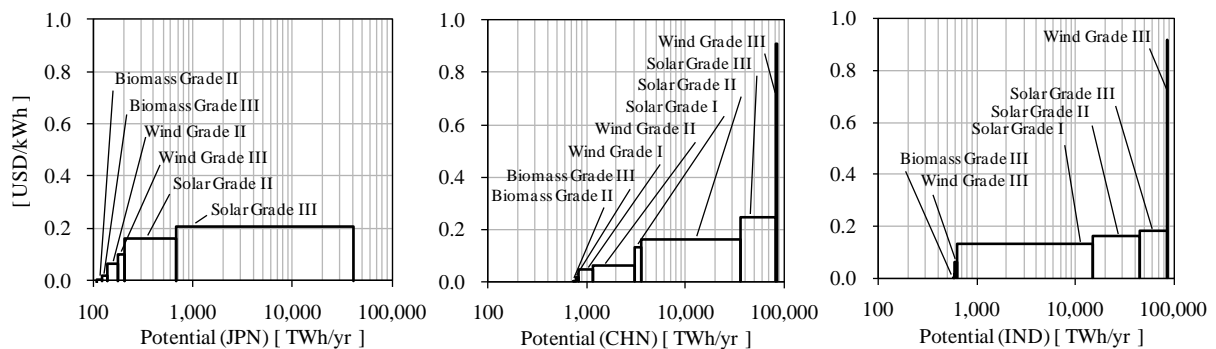


Fig. 3. Potential cost curves in Japan (left), China (center), and India (right)

#### 4. Conclusions

Diversified analysis of potential renewable energy contributions to energy supply in Asian regions was carried out. As a result, estimates of renewable energy potential were refined, the socio-economic mechanisms associated with the introduction of renewable energy were calculated, and the relevant characteristics of each Asian country were analyzed. The results suggest that almost all Asian countries will continue to develop and that the demand for energy will grow drastically and rapidly. The results indicate that almost all Asian countries will continue to develop and that the demand for energy will grow. With the aspect from potential amount, renewable energy supply is effective even though fossil fuels will continue to dominate totally energy mixes for the foreseeable future. In renewable energy supply, potential of solar is dominated and bears wide implication compared with that of wind and biomass. To ensure the best possible results, further research should be carried out on the optimal schedule for the multi-phased introduction of renewable energy in long-term policy.

## **References**

- [1] IPCC 2001a, Climate Change 2001 – IPCC Third Assessment Report, Working Group III: Mitigation, 2001
- [2] Hofman, Y., de Jager, D., Molenbroek, E., Schilig, F., Voogt, M., 2002. The Potential of Solar Electricity to Reduce CO<sub>2</sub> Emissions. Ecofys, Utrecht.
- [3] Grubb, M.J., Meyer, N.I., 1993. Wind energy: resources, systems, and regional strategies. In: Johansson, T.B., Kelly, H., Reddy, A.K.N., Williams, R.H. (Eds.), Renewable Energy: Sources for Fuels and Electricity. Island Press, Washington, DC.
- [4] Berndes, G., Hoogwijk, M., van den Broek, R., 2003. The contribution of biomass in the future global energy supply: a review of 17 studies. Biomass and Bioenergy 25 (1), 1–27.
- [5] MODIS/Terra Land Cover Type Yearly L3 Global 1km SIN Grid, 2005: Land Processes Distributed Active Archive Center (LPDAAC), U.S. Geological Survey (USGS).
- [6] GLOBE: The Global Land One-km Base Elevation 30-sec. DEM, National Geophysical Data Center (NGDC), NESDIS, NOAA, U.S. Department of Commerce.
- [7] Hastings, D. A. and Dunbar, P. K., 1999: Global Land One-km Base Elevation (GLOBE) Digital Elevation Model Documentation, Boulder, Colorado, NOAA National Geophysical Data Center, Publication KGRD 34.
- [8] GEBCO One Minute Grid - Version 1.02, 2006: General Bathymetric Chart of Oceans.
- [9] World Wilderness Areas, 1993: the Sierra Club and World Bank, as integrated by UNEP/GRID.
- [10] Insolation Incident On A Horizontal Surface (22-year Monthly & Annual Average for July 1983 - June 2005), 2008: Surface meteorology and Solar Energy (SSE) Release 6.0 Data Set, Atmospheric Science Data Center, NASA Langley Research Center (LaRC).
- [11] Wind Speed At 50m Above The Surface Of The Earth (10-year Monthly & Annual Average for July 1983 - June 1993), 2005: Surface meteorology and Solar Energy (SSE) Release 5 Data Set, Atmospheric Science Data Center, NASA Langley Research Center.
- [12] Bert J.M. de Vries, Detlef P. van Vuuren, and Monique M. Hoogwijk, Renewable energy sources: Their global potential for the first-half of the 21st century at a global level: An integrated approach, Energy Policy, 35, 2007, 2590-2610
- [13] FAO, FAOSTAT 2001 CD-ROM, Rome, 2001
- [14] IPCC 2001b, Special Report on Emissions Scenarios, 2001
- [15] IEA, World Energy Outlook, 2008
- [16] EUROPEAN COMMISSION, World Energy Technology Outlook 2050, 2006
- [17] ADB, Energy Outlook for Asia and the Pacific, 2009
- [18] Greenpeace, Energy Revolution Sustainable Energy Global Energy Outlook, 2008
- [19] Shell, Shell Energy Scenarios to 2050, 2008
- [20] OECD, OECD Environmental Outlook to 2030, 2008

## Scenario analysis of the potential for CO<sub>2</sub> emission reduction in the Iranian cement industry

Farideh Atabi<sup>1,\*</sup>, Mohammad Sadegh Ahadi<sup>2</sup>, Kiandokht Bahramian<sup>3</sup>

<sup>1\*</sup>Assistant Prof., Graduate School of Energy and the Environment, Science & Research Branch, Islamic Azad University, Tehran, Iran, P.O.Box: 14155/4933

<sup>2</sup>National Climate Change Office, Department of Environment, Tehran, Iran

<sup>3</sup>Environmental Engineer, Graduate School of Energy and the Environment, Science & Research Branch, Islamic Azad University, Tehran, Iran

\* Corresponding author. Tel: +989121341702, E-mail: far-atabi@jamejam.net

---

**Abstract:** This article investigates the impact of various policies on the reduction of CO<sub>2</sub> emissions from Iranian cement industry using a long range energy alternative planning (LEAP) model. A Business-as-Usual (BAU) scenario for the existing Iranian cement industry was applied. Moreover, the current and future demands for the cement industry were defined for 2005-2020. The current and future productivity of the cement industry was predicted in the BAU scenario. Then, three alternative scenarios were considered: replacement of heavy oil with natural gas, implementation of energy efficiency policies and integrated emission reduction, which includes all of the options over a 15-year period. The results indicated that in 2020, CO<sub>2</sub> equivalent emissions would reach 61 million tons in the baseline scenario and 53 million tons in the integrated emission reduction scenario. If fuel switching were employed, the emissions would reach 58 million tons (4.9 % reduction) and in the energy efficiency scenario, the emissions would reach 55 million tons (9.8% reduction) in 2020. Therefore, the integrated scenario reduces the total CO<sub>2</sub> equivalent emissions by 8 million tons (13% emission reduction).

**Keywords:** CO<sub>2</sub> emission, cement industry, scenario analysis, energy model

---

### 1. Introduction

Even though many countries have started to develop climate policies, scenario studies indicate that greenhouse gas emissions are likely to increase in the future in most regions around the world [1]. After the energy crisis of the 1970s, many researchers developed models to generate accurate predictions. Various models for prediction and the development of policies for mitigation can be divided into two groups: those used for mitigation in the energy sector, and those used to survey mitigation methods in the agriculture, forest and land use sectors [2]. One of the most important energy carriers in the industrial sector is natural gas, which plays a significant role in the reduction in the emission of environmental pollutants [3]. A study in Iran, evaluated the impacts of price reform and energy efficiency programs on the consumption of energy carriers and on GHG mitigation in the Iranian residential buildings sector using the LEAP model [4]. Research on substituting biomass with other energy carriers in Vietnam using the LEAP model, has shown that this fuel substitution leads to a 10.83 million-ton reduction in GHG emissions [5].

Another analysis of the environmental and economic impact of landfill gases (LFG) electricity generation in Korea using the LEAP model showed that LFG electricity generation would be an effective solution for CO<sub>2</sub> displacement over the medium term with additional energy profits and will reduce the global warming potential by a maximum of 75% when compared to spontaneous emissions of CH<sub>4</sub> [6]. Another study in Korea evaluated the environmental and economic aspects of chemical CO<sub>2</sub> absorption in power plants using this model; That study demonstrated that by applying various policies, the rate of CO<sub>2</sub> emissions will decrease by approximately 15% by 2014 [7]. Another study was also conducted to show the potential reduction in CO<sub>2</sub> emissions from oil refineries in Korea. Production analysis using the energy planning model showed that a 48% reduction in CO<sub>2</sub> emissions is feasible [8]. In this study, the energy demand of the Iranian cement industry is analysed with an

energy planning LEAP model. The effects of various policies on the baseline scenario and GHG mitigation scenario are also analysed and surveyed in the cement industry.

## 2. Methodology

Greenhouse gas emissions in the Iranian cement industry was surveyed in the format of a BAU scenario using the LEAP energy planning model. The results of employing different policies of energy efficiency and fuel switching on GHG mitigation in the format of mitigation scenario were then observed. Finally, the effectiveness of each policy applied in the cement industry over a 15-year period, from 2005 to 2020, was surveyed. In each scenario, the level of technological activity and energy intensity were specified, and in the activity data section, data relevant to consumption in the cement industry and the number of factories that use a specific resource, were defined in each scenario. Additionally, data describing the energy intensity of each type of fuel in each Factory were determined [9].

### 2.1. LEAP model

LEAP is an energy planning model that consists of an end-use structural model. Based on procedural analysis of the supply and demand network, the considered model describes technological energy carrier utilisation based on energy demand on one hand, and technological changes and therefore structural changes and efficiency of energy conversion systems as well as the rate and type of available primary energy resources on the other hand. This model consists of a hierarchical structure in which energy flows from the last point of usage (equipment and technology) toward higher levels. In fact, total energy demand is computed from each subcategory and category in a tree structure. In this model, the rate of total energy demand is computed according to Eq. 1.

$$\sum E_i = T_i \times I_i \quad (1)$$

where,  $E_i$  is the total energy demand (J),  $T_i$  is the data (i) activity level (ton), and  $I_i$  is energy intensity ( $\frac{J}{ton}$ ) [6].

### 2.2. BAU scenario

In the (BAU) scenario, it is assumed that the current status of the Iranian cement industry will be maintained in the future, and that greenhouse gas emission in Iran's cement industry will be predicted by the main variables of BAU, such as the growth rate of cement production from 2005 to 2020, the type and rate of fuel consumption, the rate of technological changes and energy intensity.

In this scenario, 2005 was selected as the base year and all relevant information was gathered from this year [10]. Then, a BAU scenario was developed according to current plans as well as future policies, changes in cement production capacity, energy intensity, the fuel contribution that supplies the energy demand and other factors in the cement industry from 2005 to 2020. The GHG emission rate was assessed, and analysed. It was predicted that in the BAU scenario, the natural gas share of the total energy carriers, will increase from 63.11% in 2005 to 80% in the 2020 in the cement industry [11]. The amount of energy intensity of the whole cement industry in the country can be calculated using Eq. 2:

$$I_t = \sum c_i I_i \quad (2)$$

where,  $I_t$  is total energy intensity (j),  $I_i$  is energy intensity of respected technology (J/ton), and  $c_i$  is the technology (i) share in the total cement production in the country (%).

Energy demand as shown in Eq. 3 is calculated by multiplying cement production (activity data) by energy intensity:

$$E = \sum_{i=1}^n A_i \times I_i \quad (3)$$

where,  $E$  is energy demand (million GJ),  $A_i$  is cement production (million tons), and  $I_i$  is energy consumption for each activity (million GJ/ton).

The LEAP model is used to calculate the equivalent emission of  $\text{CO}_2$  in the cement industry in three forms: (1) emission from direct consumption of energy carriers in cement industry, (2) emission from consumption of energy carriers in oil and gas refineries and power plants in order to supply the cement industry with both fuel and electricity (indirect), and (3) emissions from consumption of energy carriers in the industry, refineries and power plants to supply the energy demand to the cement industry (total emission).

### 2.3. Mitigation scenario

In the mitigation scenario, different policies to mitigate the energy demand are considered as input data for the LEAP model. Then, the model is compared with the BAU scenario by predicting the demands of energy carriers and the calculated mitigation in emissions. The policies surveyed here are fuel switching and more energy efficient technologies. In this scenario, it is assumed that all cement production units older than 20 years are replaced with new and efficient technologies and that energy efficient improvement plans are implemented on units that are 10 to 20 years old [12]. It is also assumed that the natural gas and biomass share in the mitigation scenario is 5% more than that in the BAU scenario in 2020. Energy carrier demand will increase 139% in this period.

## 3. Results and discussion

In Table 1, the average energy intensity for Iran's cement industry was calculated and presented separately based on the type of process. In the calculations, the average energy intensity weight was compared to the capacity of the entire cement industry in the country.

Table1. Energy intensity rate in the various cement industry technologies in Iran in 2005 [13]

| Technology                    | Proportion of Total Production (percent) | Production (ton/yr) | Capacity (ton/day) | Fuel Consumption Intensity (kcal/kg.clinker) | Electricity Consumption Intensity (kWh/ton) |
|-------------------------------|--|---------------------|--------------------|--|---|
| Dry high heater               | 5.14                                     | 1,600,500           | 4,850              | 1125   | 111   |
| Dry pre heater                | 40.51                                    | 12,606,000          | 38,200             | 950  | 108   |
| Dry pre heater & precalcinors | 51.70                                    | 16,087,500          | 48,750             | 890  | 114   |
| Mid dry pre calciners         | 0.64                                     | 198,000             | 600                | 1020   | 110   |
| Wet process                   | 2.01                                     | 627,000             | 1,900              | 2000   | 150   |
| Total / Weighted average      | 100                                      | 31,119,000          | 94,300             | 949.6  | 112.1                                       |

To evaluate the changes in energy intensity, in addition to recognizing current infrastructures in each of the subsectors of the industry, the theoretical potential for increasing the efficiency of equipment and energy intensity of industrial products in developed countries is also needed. In the BAU scenario, the annual increase in energy demand reaches 11.51% and the demand for all energy carriers shows an annual increase of 10.7%.

It is predicted that the share of natural gas in the BAU scenario among all energy carriers in this industry will increase from 63.11% in 2005 to 80% in 2020. Meanwhile, the mitigation scenario shows a 5% increase in 2020 compared to the BAU scenario in the same year. Results from LEAP in Fig. 1 show that in the BAU scenario, emissions of CH<sub>4</sub>, CO<sub>2</sub> and NO<sub>x</sub> have also increased during this period; CO<sub>2</sub> has the highest increase.

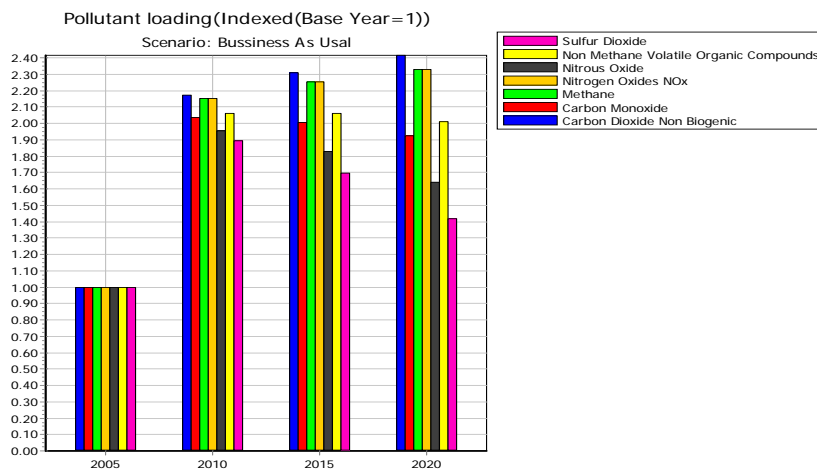


Fig.1. Prediction of the trends of the emission of pollutants and GHG (dimensionless) in the Iranian cement industry in the baseline scenario.

Meanwhile, the thermal energy demand in the mitigation scenario in 2020 shows a 33% reduction in the thermal energy demand compared to that of the BAU scenario. The emissions of all pollutants increase until 2010 and then decline because of the replacement of units that are older than 20 years with new and more efficient technologies. It should be noted that the emission of SO<sub>2</sub> and NO<sub>x</sub> in 2020 are 40% and 10% less than the emission of these pollutants in the first year (2005) respectively, whereas, the emission of NO<sub>x</sub> and SO<sub>2</sub> in the baseline scenario has increased by 40% and 65% , respectively. Therefore, after applying the

emission reduction policies (mitigation scenario), the emissions of SO<sub>2</sub> and NO<sub>x</sub> show 80% and 75% reduction in 2020 respectively, compare to those of the BAU scenario. Table 2. shows the energy carriers in the BAU scenario and the mitigation scenarios.

Table 2. Comparison among the different energy carriers, that are needed in the Iranian cement industry in the year 2020 in the BAU and mitigation scenarios

| Fuel        | Share of the total demand (%) 2005 | Share of the total demand (%) 2020 |              |
|-------------|------------------------------------|------------------------------------|--------------|
|             |                                    | Mitigation scenario                | BAU Scenario |
| Fuel oil    | 36.1                               | 9.21                               | 19.3         |
| Natural gas | 63.11                              | 85                                 | 80           |
| Diesel fuel | 0.79                               | 0.79                               | 0.79         |
| Biomass     | 0                                  | 5                                  | 0            |

As shown in Fig. 2, by implementing the policy of changing the process on one hand and the energy efficiency on the other hand, the amount of required energy carriers decreased from 340 million GJ in 2020 to 310 million GJ, and consequently, energy demand decreased by 11.5 percent.

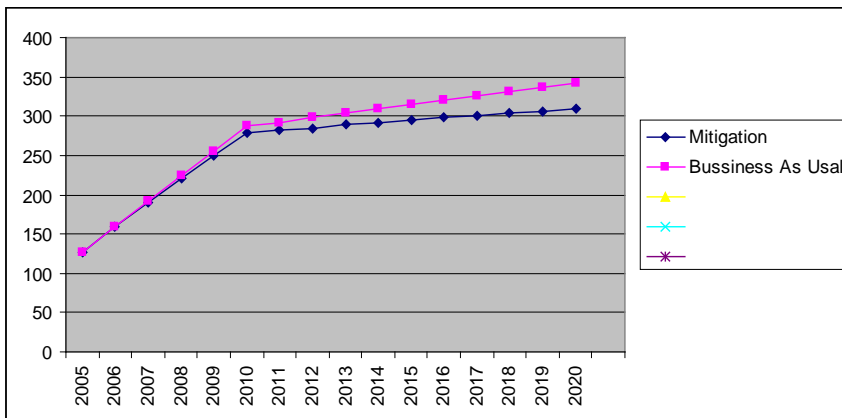


Fig. 2. Comparison of energy carriers demand in the baseline and mitigation scenarios in the Iranian cement industry (million GJ)

Results show that employing different policies regarding CO<sub>2</sub> emissions reduces these emissions from 16 million tons to 11 million tons in 2020. Fig. 3 shows a comparison of the CO<sub>2</sub> emissions in the BAU and mitigation scenarios in the Iranian cement industry.

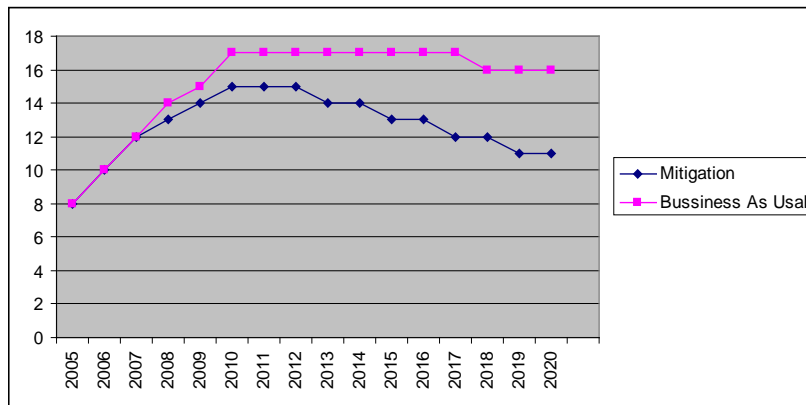


Fig.3. A comparison of CO<sub>2</sub> emission in the BAU and mitigation scenarios in the Iranian cement industry (million tons).

As shown in Fig. 4, GHG emission (CO<sub>2</sub> equivalent) is reduced as a result of the efficiency policy and the fuel switching policy by 9.8% and 4.9%, respectively. However, emission reduction will be up to 13% by employing both policies.

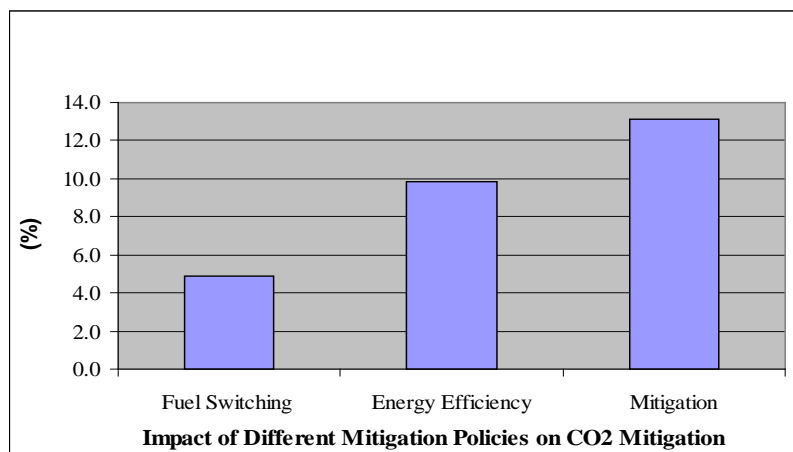


Fig. 4. Comparison of exerting different policies for GHGs (CO<sub>2</sub> equivalent) reduction and integration of different scenarios in the Iranian cement industry

#### 4. Conclusion

In this study, the process of technological changes that have improved the energy intensity in the Iranian cement industry specifically are used to predict the energy intensity in the BAU scenario and the mitigation scenario using LEAP software. To predict the greenhouse gas emissions rate in the different scenarios, the effects of the application of these actions on energy demand and fuel make-up are specified. A comparison of the effectiveness of different policies shows that the energy efficiency is more important than fuel switching in reducing CO<sub>2</sub> emissions.

#### Acknowledgement

The authors are especially grateful to Iran Fuel Conservation Company (IFCO) for its financial support.

## **References**

- [1] IPCC, 2000, Special Report on Emission Scenarios, A special report of working group III of Intergovernmental Panel on Climate Change, Cambridge University Press, Cambridge, UK
- [2] IPCC, 1997, Technical Paper 2 , Second assessment report
- [3] Ministry of energy, 2007, Energy balance, Energy Department, I.R.I
- [4] Ahadi, M.S. et al., 2005, Policy making of energy resources in industry, National Climate Change Office, Department of Environment, Tehran, Iran
- [5] Kumar Amit, et al., 2003, Greenhouse gas mitigation potential of biomass energy technologies in Vietnam using the long range energy alternative planning system model, Energy Policy Journal, No. 28, pp. 627-654
- [6] Shin, H.C., Park J.W., Kim, H.S., Shin, E.S., Environmental and economic assessment of landfill in Korea using LEAP model, Energy Policy Journal, No. 33, 2005 , pp.1261-1270
- [7] Song, HO-JUN, et al., 2007, Environmental and economic assessment of the chemical absorption, Energy Policy Journal, No. 35, pp. 5109-5116
- [8] Sangwon Park, et al., 2007, Assessment of CO<sub>2</sub> and reduction potential in Korea petroleum using energy models, Energy Journal, No. 35,pp. 2419-2420
- [9] Ministry of Industry, 2006, Cement production in 2020, Energy department, I.R.I
- [10] Energy Efficiency Office, 2005, Report on energy efficiency in the cement industry, Ministry of Energy, I.R.I
- [11] Institute for International Studies, 2004, Prediction of energy demand for in various energy sectors, Ministry of Oil, I.R.I
- [12] Hoseini, S.A., 2009, Assessment of energy efficiency potential in cement industry, Cement Research Center, I.R.I
- [13] Ministry of Energy, 2005, Report on energy intensity in the cement industry, Energy Department, I.R.I

Volume 3

Energy End-Use Efficiency Issues

## Review on graphite foam as thermal material for heat exchangers

Wamei Lin, Jinliang Yuan, Bengt Sundén\*

*Department of Energy Sciences, Lund University, P.O.Box 118, SE-22100, Lund, Sweden*

*\* Corresponding author. Tel: +46 46 2228605, Fax: +46 46 2224717, E-mail: bengt.sunden@energy.lth.se*

---

**Abstract:** Due to the increased power consumptions in equipment, the demand of effective cooling methods becomes crucial. Because of the small scale spherical pores, graphite foam has huge specific surface area. Furthermore, the thermal conductivity of graphite foam is four times that of copper. The density of graphite foam is only 20 % of that of aluminum. Thus, the graphite foam is considered as a novel highly - conductive porous material for high power equipment cooling applications. However, in the commercial market, aluminum and copper are still the preferred materials for thermal management nowadays. In order to promote the graphite foam as a thermal material for heat exchangers, an overall understanding of the graphite foam is needed. This paper describes the structure of the graphite foam. Based on the special structure, the thermal properties and the flowing characteristics of graphite foam are outlined and discussed. Furthermore, the application of graphite foam as a thermal material for heat exchangers is highlighted for electronic packages and vehicle cooling systems. The physical problems and other aspects, which might block the development of graphite foam heat exchangers, are pointed out. Finally, several useful conclusions and suggestions are given to promote the development of graphite foam heat exchangers.

**Keywords:** *Graphite foam, heat exchanger, thermal management*

---

### 1. Introduction

Nowadays the power of equipment is increased. For instance, the power of computer chips is increased, and the power of vehicle engines is also increased. This increased power leads to a requirement of an effective cooling method. Currently the thermal management has focused on aluminum and copper heat exchangers, because of high thermal conductivity (180 W/(m.K) for aluminum 6061 and 400 W/(m.K) for copper). However, when the density is considered, the specific thermal conductivity of aluminum or copper (thermal conductivity divided by specific gravity) is only 54 and 45 W/(m.K), respectively. Thus, when the weight is a significant factor, it is necessary to introduce a thermal material with low density, high thermal conductivity and large specific surface area.

An efficient thermal management method is the utilization of microcellular foam materials such as metal or graphite foams, based on the enhancement of heat transfer by huge fluid-solid contact surface area and the fluid mixing. An example of graphite foam application was developed at Oak Ridge National Laboratory (ORNL) in 1997. Klett et al. [1] found that the thermal conductivity of the solid component of graphite was as high as 1700 W/(m.K), which was around four times that of copper. The effective thermal conductivity of graphite foam was more than 150 W/(m.K), which was higher than the value of aluminum foam (2 - 26 W/(m.K)). On the other hand, the density of graphite foam was 0.2 - 0.6 g/cm<sup>3</sup>, which was only 1/5 of that of aluminum. The specific surface area was between 5000 and 50000 m<sup>2</sup>/m<sup>3</sup>.

Because of the high thermal conductivity, low density and large specific surface area, the graphite foam is recognized as an appropriate material for the thermal management. It is primarily focused on the electronic power heat sinks. A large number of studies have been carried out to analyze graphite foam heat exchangers. However, in the commercial market of heat exchangers, aluminum and copper are still the preferred thermal material. Thus, there are several problems blocking the development of graphite foam heat exchangers. Otherwise the graphite foam heat exchangers would be easily found in the market.

In order to promote the development of graphite foam as a thermal material for heat exchangers, this paper will present an overall view or conception about graphite foam heat exchangers. Firstly, the structure of graphite foam is introduced in Section 2. Based on the structure of graphite foam, the thermal properties and flow characteristics of graphite foam are explained in Section 2 as well. After that, the application of graphite foam heat exchangers is outlined in Section 3. In Section 4, potential problems blocking the development of graphite foam heat exchangers are pointed out. Based on the review and analysis, several useful conclusions and suggestions are highlighted in Section 5.

## 2. Structures and properties of graphite foam

### 2.1. Structures

Carbon foams were first developed in the late 1960s as reticulated vitreous (glassy) foam [2]. The initial carbon foams were made by pyrolysis of a thermosetting polymer foam to obtain a carbonaceous skeleton or reticulated vitreous carbon (RVC) foam. A blowing technique or pressure release is utilized to produce foam of the pitch precursor. Then the pitch foam is stabilized by heating in air or oxygen for many hours to cross-link the structure, and 'set' the pitch. In this case, the foam does not melt during the further heat treatment. However, stabilization can be a very time consuming and expensive process depending on the pore size. So ORNL [3] developed a new, little time consuming process to fabricate pitch - based graphitic foams without the traditional blowing and stabilization steps. This new foam is believed to be less expensive and easier to fabricate than the traditional foams.

Klett et al. [1] gave an overall view of the structure of the new graphite foam. The average pore diameter is from 275 to 350  $\mu\text{m}$  in the ARA24 - derived foams. The scanning electron micrographs of fracture surfaces, which reveals the pore structure of the ARA24 - derived foams heat - treated at 1000  $^{\circ}\text{C}$ , are shown in Fig. 1. Inside the foam, there are many spherical pores with small openings. These pores are three - dimensionally interconnected.

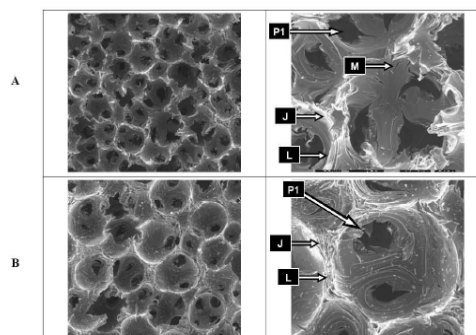


Fig. 1. Photomicrographs of the foams produced from Mitsubishi ARA 24 pitch at different densities  $A < B$  (PI: opening pore; M: microcrack; J: junction; L: ligament)[1].

### 2.2. Thermal properties of graphite foam

Because of the special structure of graphite foam, there are several prominent thermal properties in the graphite foam. The graphite foam made by the ORNL process exhibits high effective thermal conductivity (up to 182 W/(m.K)) and low density (0.2 -0.6  $\text{g}/\text{cm}^3$ ). The data in Table 1 show that the thermal conductivity in the z - plane is much larger than the one in the x - y plane. It implies that the high thermal conductivity of the graphite foam only exists in a certain direction. This is a disadvantage of the graphite foam. Klett et al. [4] found out that the heat inside the graphite lattice was transferred down the graphite lattice fast, because of the very stiff nature of the covalent bonds (as shown in Fig. 2). Moreover, the position and

vibration of atoms in the neighboring planes may impede the vibration of atoms in the plane of interest. The crystal perfection controls the thermal performance. In order to achieve high thermal conductivity in the graphite crystal, the structure must be comprised of aligned, straight grapheme planes, and so on.

Table 1. Properties of various graphite foams made by the ORNL method compared to Poco Foam[4].

|                        | Graphitization rate (°C/min) | Average bulk density (g/cm <sup>3</sup> ) | z -Plane thermal conductivity k <sub>z</sub> (W/(m.K)) | x-y Plane thermal conductivity k <sub>xy</sub> (W/(m.K)) |
|------------------------|------------------------------|---|--|--|
| ORNL graphite foam (A) | 10                           | 0.45                                      | 125  | 41   |
| ORNL graphite foam (B) | 1                            | 0.59                                      | 181  | 60   |
| PocoFoam <sup>TM</sup> | -                            | 0.61                                      | 182  | 65   |

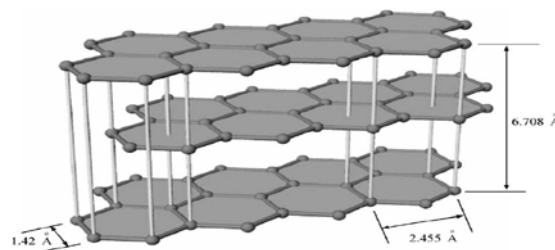


Fig. 2. Planar structure of hexagonal graphite [4].

On the other hand, Yu et al. [5] presented a model which was based on sphere - centered and interconnected unit cubes. The effective thermal conductivity was proved to be a function of the porosity of the graphite foam. Tee et al. [6] used a tapered, anisotropic strut model to predict the overall thermal conductivity of the porous graphite foam. When the size of the foam pores was increased, the convective heat transfer coefficient of the foam was reduced. By using graphite foams as the heat sinks, the enhancement of the convective heat transfer was not only because of its open and inter-connected pores, but also due to its high thermal conductivity and the extremely large surface areas. Furthermore, Straatman et al. [7] validated that the optimal thickness of graphite foam was 3 mm based on the thermal performance. Meanwhile the heat transfer increase was 28 % at low Reynolds numbers (150000). However, at high Reynolds number, the increase of the heat transfer was only 10 %.

### 2.3. Pressure drop of graphite foam

Graphite foam has a very high thermal conductivity, but it also has very high pressure drop, due to the large hydrodynamic loss associated with the open pores in the graphite foam [8]. Leong et al. [9] investigated pressure drop of four different configurations of graphite foams (as shown in Fig. 3). The pressure drops of these four configurations of graphite heat sinks are shown in Fig. 4. For the same inlet flow velocity, the block and baffle foams present the highest and the lowest pressure drop, respectively. On the other hand, Lin et al. [10] approved that the pressure drop through the corrugated passages could be reduced significantly while maintaining a high heat transfer coefficient. As shown in Fig. 5, for forced convection, the air is forced to go through a thin porous wall of graphite foam. Due to the short flow length inside the graphite foam, the pressure drop could be reduced greatly.

### 2.4. Advantages and disadvantages

Based on the special microscopic structures in graphite foams, the advantages of these materials can be summarized:

- (1) High thermal conductivity (thermal conductivity of solid graphite is 1700 W/(m.K), and the effective thermal conductivity of graphite foam is more than 150 W/(m.K));
- (2) Low density (0.2 to 0.6 g/cm<sup>3</sup>);
- (3) High specific surface area (5000 to 50000 m<sup>2</sup>/m<sup>3</sup>);

On the other hand, there are some disadvantages for the graphite foam materials:

- (1) High thermal conductivity only exists in a certain direction;
- (2) Due to the small scale pores and complex structures of the foam, the pressure drop through graphite foam is very high.

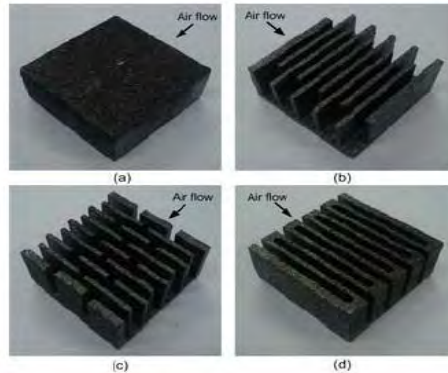


Fig. 3. Tested graphite foam heat sinks of (a) block, (b) staggered, (c) baffle and (d) corrugated configurations [9].

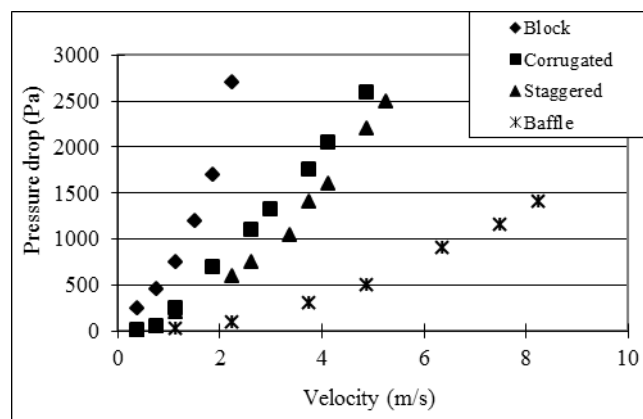


Fig. 4. Pressure drop versus inlet flow velocity of air flow through tested configuration [9].

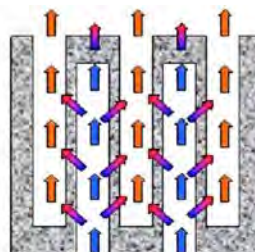


Fig. 5. Flow path inside the corrugated foam [10].

### 3. Applications of graphite foams

Due to the high thermal conductivity, low density and large specific surface area, the graphite foam is a good thermal material for heat exchangers or heat sinks. The major applications of graphite foam as materials for heat exchangers are: electronic package cooling, vehicle cooling systems, energy storage systems, and others.

### **3.1. Electronic package cooling**

Because of the large internal interfaces and the high thermal conductivity, the usage of graphite foam is considered as an effective cooling method to dissipate the high heat flux in electronic equipment. Furthermore, the coolant of electronic equipment can be air instead of water, due to the high thermal conductivity of graphite foam. The removal of water can avoid shorting the circuitry of electronic equipment by water leakage.

Gallego et al. [11] demonstrated that the foam-based heat sink can be used to reduce the volume of the required cooling fluid or eliminate the water cooling system altogether. In terms of thermal performance, the graphite foam is much better than the aluminum. Meanwhile, the graphite foam heat sinks respond to transient loads faster than the traditional aluminum heat sinks. This response time may be crucial for the power electronics. Williams et al. [12] investigated several different channel - insert configurations as mini - heat exchangers by using both copper fins and graphite foams. The graphite foam was proved to have strong potential as a mini - heat exchanger.

On the other hand, the usage of thermosyphons in the thermal management of electronics is established and the methods for evaporator enhancement are of interest. Gandikota et al. [13] investigated the cooling performance of graphite foams for evaporator enhancement in thermosyphons and in pool boiling with FC-72 as the operating fluid. The exhibited thermal resistance was very low, averaging at about 0.024 K/W at low heat flux. The thermal resistance rose with increasing heat flux, but still remained very low. Lu et al. [14] used the graphite foam as a wick in a vapor chamber. With ethanol as the coolant, the vapor chamber (25 mm x 25 mm x 6 mm) had been demonstrated at a heat flux of 80 W/cm<sup>2</sup>. The results showed that the performance of a vapor chamber using graphite foam was about twice that of one using a copper wick structure. Furthermore, Coursey et al. [15] found that 149 W heat load could be dissipated from a 1 cm<sup>2</sup> heated base at the operating temperature of 52 °C, by usage of a graphite foam thermosyphon evaporator.

### **3.2. Vehicle cooling systems**

Another important utilization of the graphite foam heat exchangers is in vehicle cooling systems. Because of the low density and large specific surface area, it might lead to a light and compact heat exchanger in vehicles. Meanwhile, graphite foam is considered as a potential material to solve critical heat rejection problems that must be solved before fuel cell and advanced power electronics technologies are introduced into automobiles.

The graphite foam could be utilized to produce a light and compact radiator in vehicles. In this case, the radiator might be placed away from the front of vehicles. If the size of the front of vehicles can be reduced, the vehicle does not push so much air in its forward motion. This implies less aerodynamic drag and increase of the fuel efficiency in vehicles. Kett et al. [16] designed a radiator (as shown in Fig. 6) with the carbon foam. Due to the increase of heat transfer coefficients, the number of coolant tubes in the radiator was reduced significantly. A typical automotive radiator with cross section of 48 cm x 69 cm might be reduced to 20 cm x 20 cm at the same heat removal rate. The reduced size will cut down the overall weight, cost, and volume of the cooling system. Thereby the fuel efficiency can be improved. Moreover, Yu et al. [17] compared a carbon foam fin - tube radiator with a conventional aluminum fin - tube radiator. The thermal performance of the carbon foam radiator was increased around 15 % without changing the frontal area or the air flow rate and pressure drop.

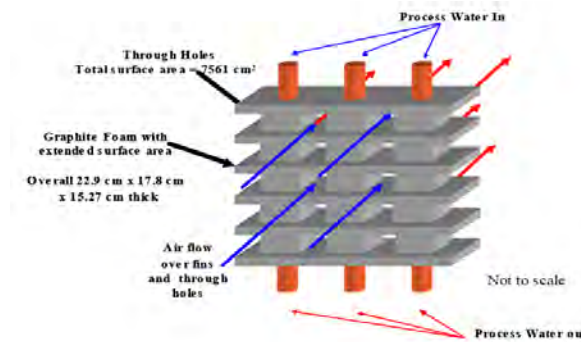


Fig. 6. Configuration of graphite foam radiator [16].

### 3.3. Energy storage system

Because of the high thermal conductivities in the graphite foam, the time used for heat transfer inside the material will be very short. This is a big advantage for energy storage applications. Lafdi et al. [18] investigated the thermal performance of graphite foams infiltrated with phase change materials for space and terrestrial energy storage systems. Because of the high thermal conductivity of graphite foams, the thermal performance of phase change material and foam system was improved significantly. In the phase change material related energy storage process, the higher thermal conductivity leads to a shorter time to charge or discharge, which implies better system performance.

## 4. Problems

Even though the graphite foam is an excellent thermal material, it is still very hard to find graphite foam heat exchangers in the commercial market. Thus, there are some problems blocking the development of graphite foam heat exchangers.

The most important problem facing the graphite foam heat exchanger is the high pressure drop. Because of the complex internal structure of the foam, the flow resistance inside the graphite foam is very high. This causes a high pressure drop through the graphite foam. Due to the high flow resistance, it is difficult for the cooling air to reach all the inter - faces and transfer the heat. Thus, the effective area of heat transfer is reduced greatly, which will result in a low thermal performance. Furthermore, the high pressure drop requires large input of pumping power to push the air through the graphite foam heat exchangers, which will cause a low coefficient of performance (COP, the ratio of the removed heat to the input pumping power). Garrity et al. [19] proved that the graphite foam heat exchanger had lower COP than the aluminum multilouvered fin. In order to reduce the high pressure drop, it is important to adopt an appropriate configuration of the graphite foams, as discussed in [9-10].

The second problem is that the mechanical properties of the graphite foam are not as good as those of the metal foam. The tensile strength of graphite foam with porosity of 75 % is only 0.69 MPa [20]. However, the tensile strength of nickel foam with the same porosity is 18.44 MPa, which is much higher than the one of graphite foam [21]. In order to reinforce the mechanical properties of graphite foam, it might be useful to introduce some other material to the graphite foam. For instance, the compressive strength can increase ten times after the graphite foam has been mixed with epoxy resin. However, by changing the fabrication process to improve the foam's mechanical properties, the high thermal conductivity might sacrifice [22].

The third problem is the dust block. Most research of the graphite foam focus on the electronic equipment heat sinks. Little attention was put to the vehicle radiator applications. The major reason is the dust blocking problem. When the open pores in graphite foams are blocked by dust, the cold air can not reach all inter - faces and bring away the heat. Thus, the effective heat transfer area is reduced greatly and the thermal performance will decrease too. Due to the operating conditions, the dust block problem is more serious in vehicle radiators than in the electronic equipment heat sinks.

Due to these problems, the development of graphite foams is relatively slow and difficult. Much work has to be done before a mature graphite foam heat exchanger appears in the commercial market.

## **5. Conclusions and suggestions**

The graphite foam has very high thermal conductivity, low density and large specific surface area. Because of these properties, the graphite foam is considered as a potential thermal material for heat exchangers. The graphite foam can be used as heat sinks to cool electronic packages. Also the graphite foam can be used as a radiator to cool the vehicle engines. Sometimes, the graphite foam can be used in energy storage applications.

However, due to the complex internal structure of the graphite foam, there is a very high pressure drop when the air flows through the graphite foams. There are also some other problems blocking the development of graphite foam, such as the low tensile strength, and the dust block. In order to promote the development of graphite foams as thermal material for heat exchangers, adopting an appropriate configuration might be useful to reduce the pressure drop through the graphite foam. On the other hand, mixing some other material with graphite foam might be helpful to reinforce the mechanical properties of graphite foam. Thus, much work has to be conducted before the graphite foam is accepted as a thermal material of heat exchangers.

## **Acknowledgments**

The authors acknowledge the financial support from the Swedish Energy Agency and industries.

## **References**

- [1] J. Klett, R. Hardy, E. Romine, C. Walls, and T. Burchell, High-thermal-conductivity, mesophase-pitch-derived carbon foams: effect of precursor on structure and properties, *Carbon* 38, 2000, pp. 953-973.
- [2] W. Ford, Method of making cellular refractory thermal insulating material, 1964, US Patent 3121050.
- [3] J. W. Klett, Process for making carbon foam, 2000, US Patent 6033506.
- [4] J. W. Klett, A. D. Mcmillan, N. C. Gallego, and C. A. Walls, The role of structure on the thermal properties of graphite foams, *Journal of Materials Science* 39, 2004, pp. 3659-3676.
- [5] Q. Yu, B. E. Thompson, A. G. Straatman, A unit cube-based model for heat transfer and fluid flow in porous carbon foam, *Journal of Heat Transfer* 128, 2006, pp. 354-360.

- [6] C. C. Tee, N. Yu, and H. Li, Modeling the overall heat conductive and convective properties of open-cell graphite foam, *Modelling Simulation Material Science Engineering* 16, 2008, 075006.
- [7] A. G. Straatman, N. C. Gallego, B. E. Thompson, H. Hangan, Thermal characterization of porous carbon foam - convection in parallel flow, *International Journal of Heat and Mass Transfer* 49, 2006, pp. 1991-1998.
- [8] A. G. Straatman, N. G. Gallego, Q. Yu, and B. E. Thompson, Characterization of porous carbon foam as a material for compact recuperators, *Journal of Engineering for Gas Turbines and Power* 129, 2007, pp. 326-330.
- [9] K. C. Leong, L. W. Jin, H. Y. Li, and J. C. Chai, Forced convection air cooling in porous graphite foam for thermal management application, 11th Intersociety Conference on Thermal and Thermomechanical Phenomena in Electronic Systems, 2008, pp. 57-64.
- [10] Y. R. Lin, J. H. Du, W. Wu, L. C. Chow, W. Notardonato, Experimental study on heat transfer and pressure drop of recuperative heat exchangers using carbon foam, *Journal of Heat Transfer* 132, 2010, 091902-1.
- [11] N. C. Gallego, and J. W. Klett, Carbon foams for thermal management, *Carbon* 41, 2003, pp. 1461-1466.
- [12] Z. A. Williams, and J. A. Roux, Graphite foam thermal management of a high packing density array of power amplifiers, *Journal of Electronic Packaging* 128, 2006, pp. 456-465.
- [13] V. Gandikota, and A. S. Fleischer, Experimental investigation of the thermal performance of graphite foam for evaporator enhancement in both boiling and an FC-72 thermosyphon, *Heat Transfer Engineering* 30(8), 2009, pp. 643-648.
- [14] M. H. Lu, L. Mok, and R. J. Bezama, A graphite foams based vapor chamber for chip heat spreading, *Journal of Electronic Packaging* 128, 2006, pp. 427-431.
- [15] J. S. Coursey, J. Kim, and P. J. Boudreaux, Performance of graphite foam evaporator for use in thermal management, *Journal of Electronic Packaging* 127, 2005, pp. 127-134.
- [16] J. Klett, R. Ott, and A. McMillan, Heat exchangers for heavy vehicles utilizing high thermal conductivity graphite foams, *SAE Technical Paper 2000-01-2207*, 2000.
- [17] Q. Yu, A. G. Straatman, B. E. Thompson, Carbon - foam finned tubes in air - water heat exchangers, *Applied Thermal Engineering* 26, 2006, pp. 131-143.
- [18] K. Lafdi, O. Mesalhy, and A. Elgafy, Graphite foams infiltrated with phase change materials as alternative materials for space and terrestrial thermal energy storage applications, *Carbon* 46, 2008, pp. 15-168.
- [19] P. T. Garrity, J. F. Klausner, R. Mei, Performance of aluminum and carbon foams for air side heat transfer augmentation, *Journal of Heat Transfer* 132, 2010, 121901-1.
- [20] M. D. Haskell, Thermal resistance comparison of graphite foam, aluminum, and copper heat sinks, <http://www.electronics-cooling.com/2006/02/thermal-resistance-comparison-of-graphite-foam-aluminum-and-copper-heat-sinks/>.
- [21] S. B. Zhao, Thought about the exponential item in formulas calculating tensile strength for high - porosity materials, *Materials and Design* 23, 2002, pp. 497-499.
- [22] ORNL's graphite foam may aid transportation, [http://www.ornl.gov/info/ornlreview/v33\\_3\\_00/foam.htm](http://www.ornl.gov/info/ornlreview/v33_3_00/foam.htm).

## The thermal response of heat storage system with paraffin and paraffin/expanded graphite composite for hot water supply

P. Zhang\*, L. Xia, R.Z. Wang

*Institute of Refrigeration and Cryogenics, Shanghai Jiao Tong University, Shanghai 200240, China*

\* Corresponding author. Tel.: +86-21-34205505; fax: +86-21-34206814 E-mail: zhangp@sjtu.edu.cn (P. Zhang)

**Abstract:** The low thermal conductivity of phase change material (PCM) leads to low heat storage/retrieval rates. The expanded graphite (EG) was used to enhance the thermal conductivity. EG/paraffin composite with the 7% mass fraction of EG was prepared as a good candidate for the latent thermal energy storage (LTES) system. A shell and tube LTES system built for room heating and hot water supply in a family was experimentally investigated. The paraffin and paraffin/EG composite were used as the heat storage material, respectively. The experimental results indicated: The utilization of EG/paraffin composite PCM greatly improved the heat storage/retrieval rates of the LTES system. The LTES system with paraffin/EG composite showed a 44% reduction in heat storage duration and a nearly 69% reduction in the retrieval duration, respectively, compared to those for the system using pure paraffin. The most outstanding advantage, for the LTES system filled with paraffin/EG composite, was that the outlet temperature of water can be maintained at a higher level for a longer term than that with paraffin. However, the LTES system filled with EG/paraffin composite did not show an obvious advantage in the step-by-step heat retrieval mode, compared with paraffin.

**Keywords:** Latent thermal energy storage, Paraffin/expanded graphite composite, Heat storage/retrieval rate

### 1. Introduction

In a latent thermal energy storage (LTES) system by solid-liquid phase change, energy is stored during melting while it is retrieved during solidification of a phase change material (PCM), thus a LTES system with a good performance requires that the PCM possesses the appropriate phase change temperature, high heat storage density and high thermal conductivity. Besides, a good LTES system also lies on a rational structure design of the system which will decide the filling capacity of PCM and the heat exchange surface.

Based on an extensive study by Lane et al. [1] there are about 20,000 substances with the melting point in the range 10-90 °C. Majority of them was abandoned for application due to improper melting point, melting with decomposition or lack of essential reference data [2]. Among these PCMs, normal paraffin of type  $C_nH_{2n+2}$  has shown outstanding performance for application in LTES systems for solar heating and cooling [3-4]. This is because of its appropriate melting point, large latent heat, low cost, high stability and compatibility, and a low negative environmental impact. Despite the many desirable properties of paraffin, its low thermal conductivity, generally below 0.4 W/(m·K), is one of the major drawback.

The PCM containers with different geometries have their own advantages and disadvantages. Various LTES techniques have been developed and various encapsulations have been used in LTES systems. Two geometries commonly employed as PCM containers are the rectangular and cylindrical containers [5]. In particular, cylindrical containers accounts for more than 70% in all the used LTES system which commonly involves the three modes. The first is the heat storage unit in which the PCM fills the shell and the heat transfer fluid (HTF) flows through the central tube [6-8]. In the second mode, the PCM fills the tube and the HTF flows parallel to the tube [9]. The third cylinder mode is the shell and tube system [10, 11].

In the present work, expanded graphite (EG), with high thermal conductivity, was added into PCM to form a kind of composite phase change material and to enhance the heat transfer of the inner PCM. EG/paraffin composite PCM with 7% mass fraction of EG was prepared. This ratio was considered as the balance by compromising the heat transfer enhancement and latent heat storage capacity [12]. The EG/paraffin composite PCM was filled in the stainless steel tubes, and then these LTES tubes were compactly arranged in a tank. As a comparison, the paraffin was also used in this system as the heat storage material. The heat storage and retrieval performance of this LTES system, filled with EG/paraffin composite and paraffin, were experimentally tested, respectively. The influence of the HTF flow rate on the performance of the LTES system was also investigated. Moreover, two heat retrieval modes viz.: continuous and step-by-step heat retrieval, which were commonly used in the utilization of LTES system, were executed respectively for testing the heat retrieval performance of the LTES system with two PCMs.

## 2. Experimental setup and procedure

The PCM used in this study was technical grade paraffin with the purity of 99% and a melting temperature of 62 °C. The EG was prepared by making the raw expandable graphite (mesh 80, type KP80, from Qingdao Tianhe Graphite Co. Ltd, China) subjected to heat treatment in a furnace at 700 °C for a duration of 15 minutes. These paraffin and EG were used to prepare EG/paraffin composite. The paraffin was heated to a temperature of 85 °C, in order to be liquefied, after which the liquid paraffin was impregnated into EG and was stirred using a roll mixer. Then, the EG/paraffin composite with 7% mass fraction of EG was obtained.

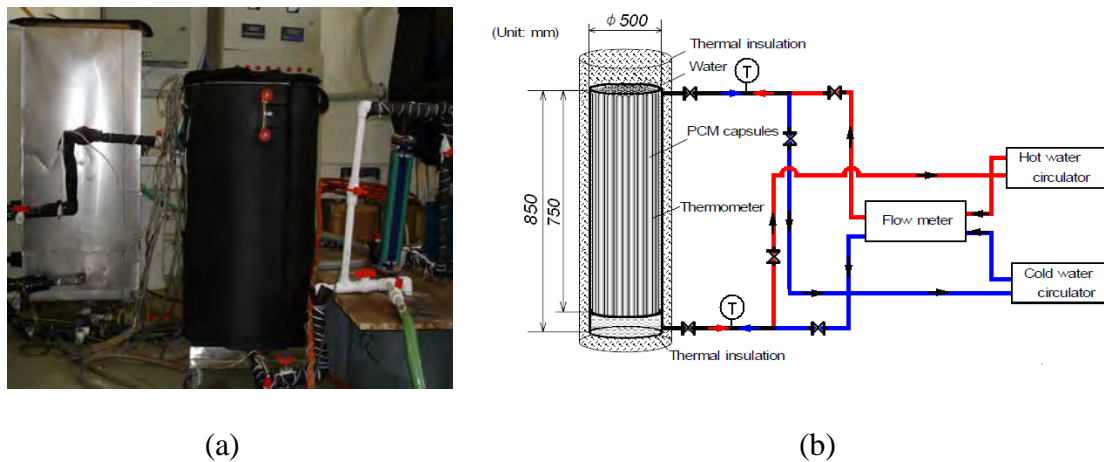


Fig. 1 Experimental setup (a) Photographic view (b) Schematic of LTES system

The schematic diagram of the experimental apparatus is shown in Fig. 1. The stainless-steel LTES tank, insulated with thermal insulation material of 50 mm in thickness, had a capacity of 166 L (500 mm diameter and 850 mm height), in which 27 heat storage tubes with the 76 mm in inner diameter and 750 mm in height were uniformly packed and supported by a wire mesh. The paraffin and EG/paraffin composite PCM were used as PCMs and water was used as the HTF. A hot water tank was used for heating during the heat storage and cold water from a cold water tank was used for cooling during the heat retrieval. During heat storage, the hot water was supplied from the top of LTES tank and was drained from the bottom, whereas, during heat retrieval, the flowing direct for the cooling water was just reversed. The temperatures of HTF at the inlet and the outlet were measured by two PT1000 platinum resistance temperature sensors.

The schematic of the cylindrical heat storage unit, as shown in Fig. 2, was a vertical tube (stainless steel, outer diameter of 78 mm and wall thickness of 1 mm) in which the PCM was impregnated. Four thermocouples (K-type) were used to measure the temperature of the PCM and were fixed near the centre axis of the tube, as shown in Fig. 2 (b). The heat storage unit which was equipped with thermocouples was set at the center of the LTES tank. The temperature variations of PCM during heat storage and retrieval were monitored and collected using a data logger.

Initially, 80% of the tube volume was filled with the solid PCM at a room temperature of 28 °C. The remaining 20% of the volume was left to accommodate the volume increase of the PCM during melting. Water was used as HTF, whose temperature at the inlet of the heat storage unit was kept at 85 °C during heat storage and was kept at 28 °C during heat retrieval. There were three different flow rates of the hot water (100, 150, 200 L/h) during heat storage and three different flow rates of the cooling water (150, 200, 250 L/h) during heat retrieval.

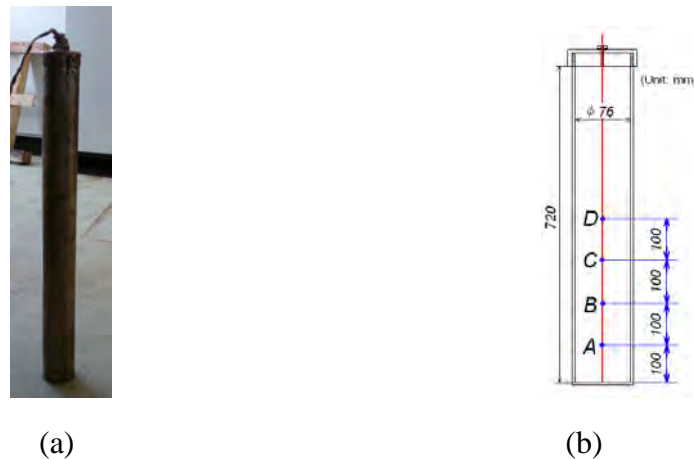


Fig. 2. LTES unit (a) and locations of the thermocouples (b)

After heat storage of the LTES tank, the heat retrieval experiments were carried out in both continuous and step-by-step heat retrieval modes. In the continuous mode, the cold water of 28 °C continuously flow through the storage tank until the temperature of the water at the outlet reached 28 °C; while in the step-by-step heat retrieval mode, the cold water at 28 °C was impregnated in the LTES tank and had been kept there for one hour. Then, the heated HTF was withdrawn and at the same time the temperature was recorded. The above process was repeated until the temperature of the withdrawn HTF is below 35 °C. Nearly five batches of hot water could be withdrawn from the LTES tank in the step-by-step heat retrieval mode.

### 3. Results and discussion

#### 3.1. Heat storage and retrieval performance

In the experiment for investigating the heat storage and retrieval performance of the LTES system, flow rate of the water was kept constantly at 150 L/h and the inlet HTF temperature during the heat storage and retrieval was 85 °C and 28 °C, respectively. The heat retrieval is in the continuous mode.

Figure 3 shows the temperature evolutions at the tested point C (as shown in Fig. 2) of pure paraffin and EG/paraffin composite during heat storage and retrieval circle. It can be found in

Fig. 3 that the tested point in both pure paraffin and EG/paraffin composite experienced three steps during melting, viz.: the sensible heat storage where the temperature rose rapidly, the latent heat storage (phase change) with the isothermal behavior and the following sensible heat storage where the temperature rose rapidly again until it reached the thermal equilibrium. The similar analysis was also effective during freezing. However, a discrepancy between the measured results of pure paraffin and those of the EG/paraffin composite was observed. The heat storage and retrieval durations of the LTES tank with EG/paraffin composite was much shorter than those with pure paraffin, i.e., the addition of EG drastically enhanced the heat transfer of inner PCM.

It took about 8000 s for pure paraffin to finish the heat storage, whereas, it took only 4500 s for EG/paraffin composite to reach the temperature equilibrium with the heating source, showing a 44% time reduction compared with that for pure paraffin. It was obvious that the heat storage rate of the composite PCM was higher than that of pure paraffin. It can also be seen from Fig. 3 that it took about 18000 s for the temperature of pure paraffin to drop from 85 °C to 30 °C, whereas, it took only 5500 s for EG/paraffin composite to complete the heat retrieval, indicating a 69% reduction in the heat retrieval duration.

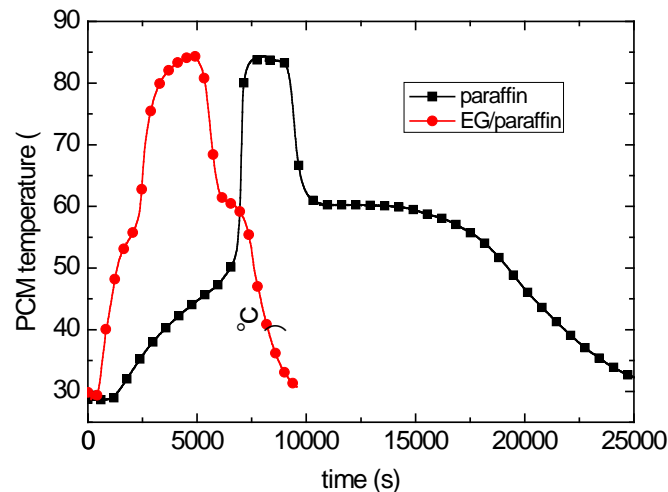


Fig. 3. Temperature evolutions of the LTES unit with pure paraffin and EG/paraffin composite during heat storage and retrieval circle

The heat storage and retrieval durations were both considerably reduced for EG/paraffin composite which was attributed to the addition of EG. However, it can also be seen that the effect of EG was more significant in heat retrieval than in heat storage. These phenomena can be attributed to the melting/freezing characteristic of each PCM: the melting of pure paraffin was accelerated during heat storage (melting) because of the intensive natural convection in the melted paraffin, whereas the natural convection did not play significant role in the heat transfer during heat retrieval (freezing); as for EG/paraffin composite, the natural convection could be neglected during both melting and freezing because of the existence of EG.

The outlet temperature evolutions of HTF during heat storage and retrieval are shown in Fig. 4(a) and (b), respectively. During heat storage, the outlet temperature of the HTF in the LTES system filled with EG/paraffin composite was more rapidly raised to the inlet temperature (85 °C) than in the system filled with paraffin, as shown in Fig. 4(a). Moreover, in the earlier stage of the heat storage the outlet temperature of the HTF for the LTES system filled with EG/paraffin composite was higher than that with paraffin. These phenomena both indicated

the system filled with EG/paraffin composite had a better heat transfer performance than the system with paraffin.

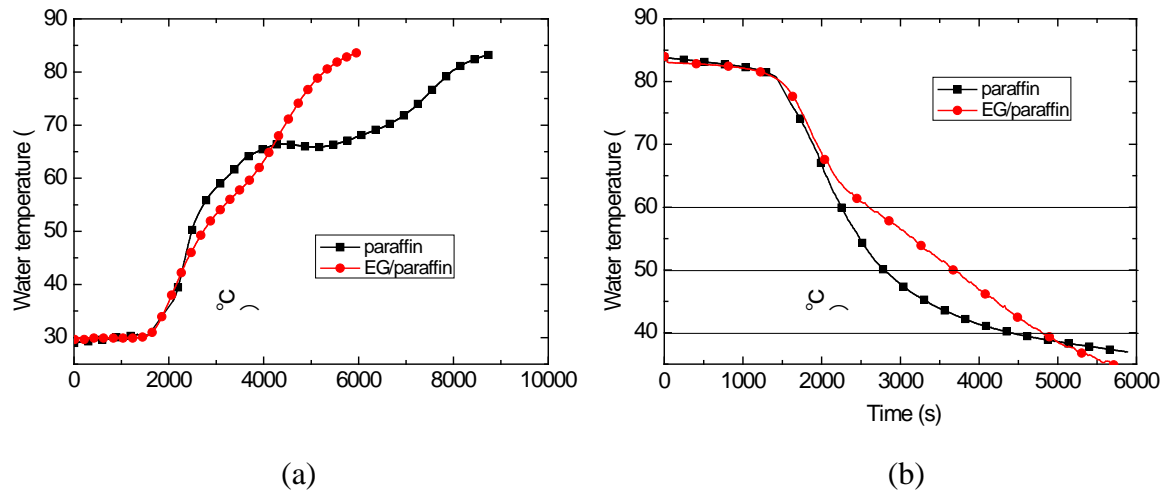


Fig. 4. Outlet temperature evolutions of the HTF during (a) heat storage and (b) heat retrieval

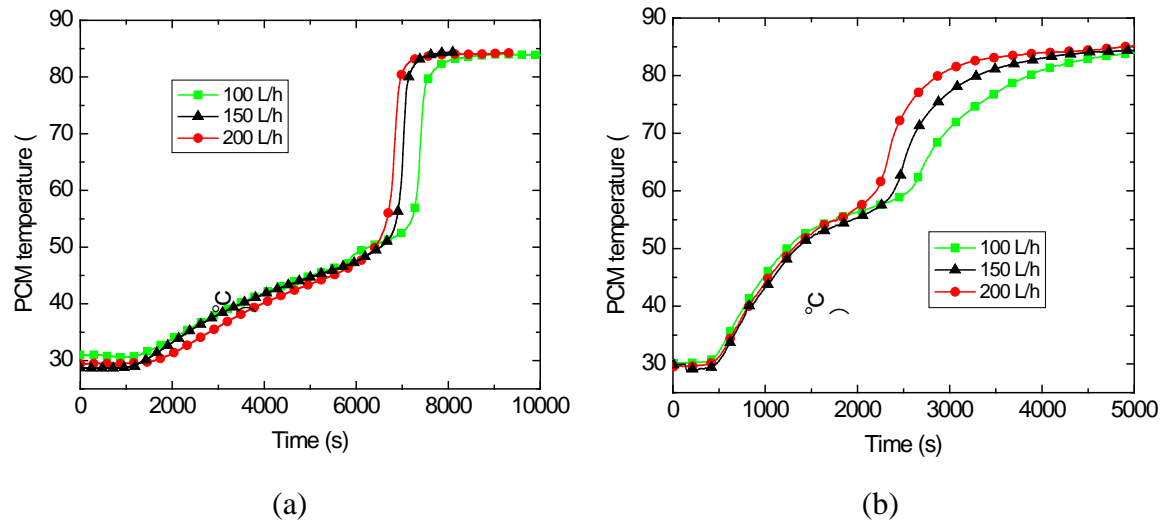


Fig. 5. Temperature evolutions of the pure paraffin (a) and EG/paraffin composite (b) with the varying flow rate of the HTF during heat storage

As well known, for a LTES system, it is important to have a large heat storage capacity; however, the most important performance is whether it can supply a high heat retrieval power. In an excellent LTES system, the HTF should be heated up rapidly and the temperature of the HTF can be raised to a higher value so as to meet the requirement of the user as the HTF flows through it during heat retrieval. As can be seen from Fig. 4 (b) for the LTES system filled with paraffin/EG composite, the outlet temperature of the HTF could maintain a high level in a longer term than that with paraffin, such as the outlet temperature of HTF of the LTES system filled with paraffin/EG composite could be maintained above 50 °C for another more 1000 s than that with paraffin. Thus, it is indicated the stored thermal energy can be rapidly and intensively released in the system filled with paraffin/EG composite, which was significant for the utilization of the LTES system.

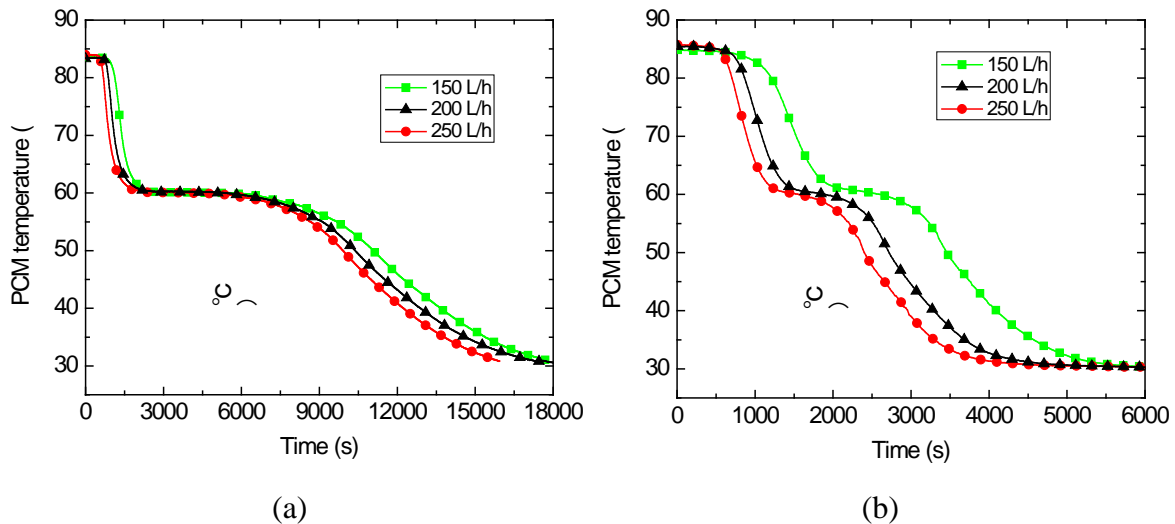


Fig. 6. Temperature evolutions of the pure paraffin (a) and EG/paraffin composite (b) with the varying flow rate of the HTF during heat retrieval

### 3.2. Influence of the flow rate of the HTF on the heat storage and retrieval performance

Figure 5 shows the temperature evolutions of PCM when varying flow rate of the HTF during heat storage, where Fig. 5(a) is temperature evolutions of the paraffin and Fig. 5(b) is temperature evolutions of the paraffin/EG composite. Figure 6 shows the temperature evolutions of PCM when varying flow rate of the HTF during heat retrieval.

From Fig. 5 and 6, it can be obviously seen that a higher flow rate of the HTF led to a better heat transfer performance and consequently a more rapid heat storage and retrieval. To increase the flow rate is always an effective and positive means during heat storage, whereas higher flow rate of the HTF may cause lower outlet temperature of the HTF during heat retrieval though it can enhance the heat retrieval power.

### 3.3. Test for the step-by-step heat retrieval mode

For the utilizations of the LTES system, the heat retrieval mode is not only continuous but also discontinuous, for example, the requirement of the hot water is intermittent in the domestic hot water system. Thus, the information about the step-by-step heat retrieval mode of the LTES system was also necessary and the retrieval performance of the LTES system was investigated in such case. Figure 7(a) shows the temperature evolutions of PCM and Fig. 7(b) shows the temperature evolutions of the outlet HTF during step-by-step heat retrieval. In each figure, the performance of the LTES system with paraffin was compared with that with EG/paraffin composite. The experimental result indicated: 1. There is a large difference between the temperature evolutions of the pure paraffin and EG/paraffin composite. This is because the EG/paraffin composite with high thermal conductivity is more sensitive to the varying of the HTF temperature and can quickly response this varying; 2. The temperature evolutions of the outlet HTF in the two LTES systems are almost the same with each other. This is because the waiting duration of one hour in each step is an enough time period to allow new temperature equilibrium is reached and maintained between PCM and HTF for both two LTES systems.

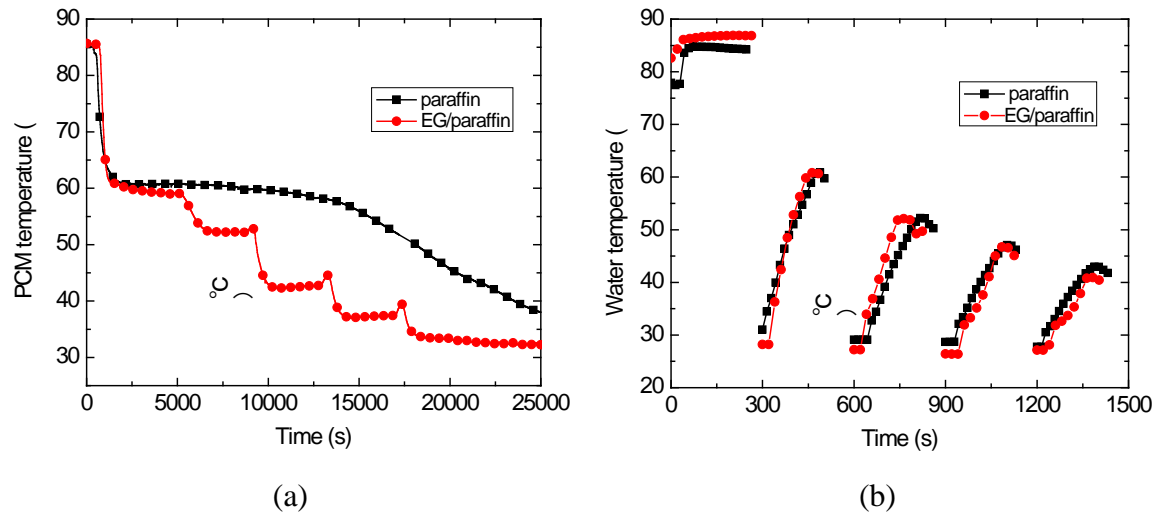


Fig. 7. Temperature evolutions of PCM (a) and the outlet HTF (b) during step-by-step heat retrieval

#### 4. Conclusions

Paraffin/EG composite PCM with 7% mass fraction of EG was prepared for enhancing the heat transfer of paraffin. The paraffin/EG composite PCM and the paraffin were used in a shell and tube heat storage system and the performance of the LTES system was experimentally investigated. The following conclusions were drawn:

1. The utilization of paraffin/EG composite PCM greatly enhanced the heat storage/retrieval rates of the LTES system. The LTES system with paraffin/EG composite PCM, under the operation condition (flow rates: 150 L/h during both heat storage and heat retrieval; the inlet temperature of HTF: 28 °C during heat retrieval and 85 °C during heat storage), showed a 44% reduction in heat storage duration and a nearly 69% reduction in the retrieval duration, respectively, compared to those for pure paraffin.
2. The most outstanding advantage, for the LTES system filled with paraffin/EG composite, was that the outlet temperature of HTF can be maintained at a higher level in a longer term than that with paraffin, which was significant for the utilization of the LTES system.
3. A higher flow rate of the HTF led to a better heat transfer performance and consequently more rapid heat storage and retrieval. It is positive for heat storage, whereas higher flow rate of the HTF may cause lower outlet temperature of the HTF during heat retrieval though it can enhance the heat retrieval power.
4. There was a large difference between the temperature evolutions of the pure paraffin and paraffin/EG composite PCM in the step-by-step heat retrieval mode, whereas the temperature evolutions of the outlet HTF in the two LTES systems were almost the same with each other.

#### References

- [1] G.A. Lane, Solar heat storage: latent heat materials, background and scientific principles vol. I. Florida: CRC Press Inc, 1983.

- [2] A. Felix Regin, S.C. Solanki, J.S. Saini, Heat transfer characteristics of thermal energy storage system using PCM capsules: A review, *Renewable and Sustainable Energy Reviews* 12, 2008, pp. 2438–2458.
- [3] C. Arkar, B. Vidrihb, S. Medveda, Efficiency of free cooling using latent heat storage integrated into the ventilation system of a low energy building, *International Journal of Refrigeration* 30, 2007, pp. 134–143.
- [4] A. Benmansour, M.A. Hamdan, A. Bengeuddach, Experimental and numerical investigation of solid particles thermal energy storage unit, *Applied Thermal Energy* 26, 2006, pp. 513–518.
- [5] F. Agyenim, N. Hewitt, P. Eames, M. Smyth, A review of materials, heat transfer and phase change problem formulation for latent heat thermal energy storage systems (LHTESS), *Renewable and Sustainable Energy Reviews* 14, 2010, pp. 615–628.
- [6] A. Trp, An experimental and numerical investigation of heat transfer during technical grade paraffin melting and solidification in a shell-and-tube latent thermal energy storage unit, *Solar Energy* 79, 2005, pp. 648–660.
- [7] H.A. Adine, H.E. Qarnia, Numerical analysis of the thermal behaviour of a shell-and-tube heat storage unit using phase change materials, *Applied Mathematical Modelling* 33, 2009, pp. 2132–2144
- [8] F. Agyenim, P. Eames, M. Smyth, A comparison of heat transfer enhancement in a medium temperature thermal energy storage heat exchanger using fins, *Solar Energy* 83, 2009, pp. 1509–1520.
- [9] M. Esen, A. Durmus, Geometric design of solar-aided latent heat store depending on various parameters and phase change materials. *Solar Energy* 62, 1998, pp. 19–28.
- [10] F. Agyenim, P. Eames, M. Smyth, Heat transfer enhancement in medium temperature thermal energy storage system using a multitube heat transfer array. *Renewable Energy* 35, 2010, pp. 198–207.
- [11] A.A. Ghoneim, Comparison of theoretical models of phase-change and sensible heat storage for air and water-based solar heating systems, *Solar Energy* 42, 1989, pp. 209–220.
- [12] L. Xia, P. Zhang, R.Z. Wang, Preparation and thermal characterization of expanded graphite/paraffin composite phase change material, *Carbon* 48, 2010, pp. 2538-2548

## Effect of different working fluids on shell and tube heat exchanger to recover heat from exhaust of an automotive diesel engine

S. N. Hossain<sup>\*</sup>, S Bari

*Sustainable Energy Centre, School of Advanced Manufacturing and Mechanical Engineering, University of South Australia, SA 5095, Australia*

*\* Corresponding author. Tel: +61430854206, Fax: +61 8302 3380, E-mail: shekh.rubaiyat@unisa.edu.au*

---

**Abstract:** In this research, experiments were conducted to measure the exhaust waste heat available from a 60 kW automobile engine. The performance of an available shell and tube heat exchanger using water as the working fluid was conducted. With the available data, computer simulation was carried out to improve the design of the heat exchanger. Two heat exchangers were used: one to generate saturated and the other to generate super heated vapours. These two heat exchangers can be arranged in parallel or series. In series arrangement, the exhaust gas was first passed through superheated heat exchanger and then through the saturated heat exchanger. Whereas, in parallel arrangement, the exhaust gas was divided to pass through saturated and superheated heat exchangers. In both cases, working fluid was passed first through saturated heat exchanger and then through superheated heat exchanger. Computer simulation was carried out to investigate the effectiveness of the proposed heat exchanger for different working fluid like water, ammonia, and HFC-134a. It is found that with the exhaust heat available from the diesel engine additional 15%, 13% and 8% power can be achieved by using water, HFC-134a and ammonia as working fluid respectively.

**Keywords:** *Waste heat recovery, Organic Rankine Cycle, Diesel engine*

---

### 1. Introduction

Diesel engines represent a major kind of Internal Combustion Engine (ICE). These diesel engines have a wide field of applications and as energy converters they are characterized by their high efficiency. Trucks and road engines usually use high speed diesel engines with 220 kW output or more. Earth moving machineries use engines with an output of up to 520 kW or even higher up to 740 kW. Diesel engines are also used in small electrical generating units or as standby units for medium capacity power stations. However, Small air-cooled diesel engines of up to 35 kW output are used for irrigational purposes, small agricultural tractors and construction machines whereas large farms employ tractors of up to 150 kW output.

In general, diesel engines have an efficiency of about 35% and thus the rest of the input energy is wasted. Despite recent improvements of diesel engine efficiency, a considerable amount of energy is still expelled to the ambient with the exhaust gas. In a water-cooled engine about 35 and 30-40% [1] of the input energy is wasted in the coolant and exhaust gases respectively. The amount of such loss, recoverable at least partly, greatly depends on the engine load. Johnson [2] found that for a typical 3.0 l engine with a maximum output power of 115 kW, the total waste heat dissipated can vary from 20 kW to as much as 40 kW across the range of usual engine operation. It is suggested that for a typical and representative driving cycle, the average heating power available from waste heat is about 23 kW.

Since the wasted energy represents about two-thirds of the input energy and for the sake of a better fuel economy, exhaust gas from diesel engines can provide an important heat source that may be used in a number of ways to provide additional power and improve overall engine efficiency. These technical possibilities are currently under investigation by research institutes and engine manufacturers. For the heavy duty automotive diesel engines, one of the most promising technical solutions for exhaust gas waste heat utilization appears to be the use of a “Bottoming Rankine Cycle”. A Rankine cycle using water as working fluid is not enough

efficient to recover waste heat below 640 K [3]. The Organic Rankine Cycle (ORC) is a promising process to recover the heat from the exhaust of an engine and generate electricity from it [4, 5]. The ORC works like a simple Rankine steam power cycle but uses an organic working fluid instead of water. A certain challenge is to choose a suitable organic working fluid for the ORC. The working fluid should fulfil safety criteria; it should be environmentally friendly, and inexpensive. Another important aspect for the choice of the working fluid is the temperature of the available heat source. A question, which also has to be considered for using ORC, is whether an organic substance is really better than water as working fluid for a given task.

A systematic approach towards using an installation based on the Rankine Cycle in truck applications dates back to the early 1970s where a research program funded by the US Department of Energy (DOE) was conducted by Mack Trucks and Thermo Electron Corporation [6-8]. Under this program, an ORC system was installed on a Mack Truck diesel engine and the lab test results revealed an improvement of bsfc of 10–12%, which was verified by highway tests. During the following years similar research programs were performed by other research institutes and vehicle manufacturers. Aly [9] was able to produce 16% additional power from the exhaust of a Mercedes-Benz OM422A diesel engine by using R-12 as working fluid for the ORC. ORC systems with capacities from 750 to 1500 kW were examined by Koebelman [10]. Recently, the solution of Rankine Cycle Systems has increased its potential competitiveness in the market even more [11, 12]. This is a result of technical advancements in a series of critical components for the operation of such an installation (heat exchanger, condenser and expander) but also stems from the highly increased fuel prices. Nowadays, the installation of a Rankine Cycle is not only considered as a feasible solution for efficiency improvement in heavy duty diesel engines for trucks [13, 14] but also for smaller application such as passenger cars [15].

In this project, experiments were conducted to measure the exhaust heat available from a 60 kW automobile engine at different speeds and loads. A shell and tube heat exchanger was purchased and installed into the engine. The performance of the heat exchanger using water as the working fluid was then conducted. With the available data, computer simulation was carried out to improve the design of the heat exchanger. The optimized model of the heat exchanger was then simulated to generate super heated vapour. Ammonia and HFC-134a is used as working fluids. Water is used as reference for comparison. The thermo physical properties of working fluids are compared and presented in Table 1. It is apparent that dry and isentropic organic fluids generally have much lower relative enthalpy drops during expansion than the water-steam mixture. Unlike water, most organic fluids suffer chemical decomposition and deterioration at high temperature and pressure. Therefore, an ORC system must be operated well below the temperature and pressure at which the fluids are chemically unstable. Most organic fluids have relatively low critical pressures and are therefore usually operated under low pressures and with much smaller heat capacities than water-vapour cycles. A suitable organic fluid must have a relatively high boiling point. Based on these features ammonia and HFC-134a are selected for the current study. Finally, power output from the turbine is calculated considering isentropic efficiency of real turbine [16, 17].

Table 1. Thermophysical properties of working fluids.

| Parameter                                | H <sub>2</sub> O | NH <sub>3</sub> | HFC-134a   |
|--|------------------|-----------------|------------|
| Molecular weight                         | 18               | 17              | 102        |
| Slope of the saturation vapour line      | Negative         | Negative        | Isentropic |
| Enthalpy drop across the turbine (kJ/kg) | 1570~900         | 725~70          | 55~22      |
| Max. Stability Temperature (K)           | None             | 750             | 450        |
| Critical point (K)                       | 647              | 405.3           | 374.15     |
| Boiling point at 1 atm (K)               | 373              | 239.7           | 248        |
| Latent heat at 1 atm (kJ/kg)             | 2256.6           | 1347            | 215.52     |

## 2. Experimental setup

The engine used in the current study is a four cylinder Toyota 13B diesel engine which is coupled with a water dynamometer. The specification of the engine is given in the Table 2. The schematic of the experimental setup is shown in Fig. 1. The engine run at different loads with variable speeds and exhaust temperatures were recorded to calculate available heat energy from the exhaust. Then the exhaust of the engine was connected to a shell and tube heat exchanger to study the performance of the heat exchanger and those data were used to improve the design of the heat exchanger by computer simulation.

Table 2. Engine specification.

|                   |   |
|-------------------|---|
| Engine model      | 13B   |
| Make              | Toyota  |
| Type of engine    | 4 cylinder charged water cooled diesel engine |
| Bore              | 102 mm  |
| Stroke            | 105 mm  |
| Compression ratio | 17.6:1  |
| Torque            | 217 N.m @ 2200 rpm                            |

## 3. Heat Exchanger design

The data found from the experiment are used to optimize the design of shell and tube heat exchanger by computer simulation. Effect of important parameter of heat exchanger like radius of the shell, no of tubes, length of the heat exchanger, pressure drop is investigated and final model of the heat exchanger is proposed. The specification of the model of the proposed shell and tube heat exchanger is shown in the Table 3. Two heat exchangers are used: one heat exchanger is used to generate saturated vapor from the liquid working fluid and the second heat exchanger is used to generate super heated vapor from that saturated vapor. These two heat exchangers can be arranged into two configurations, parallel and series as shown in the Fig. 2.

Table 3. Heat exchanger specification.

|                              |   |
|------------------------------|---|
| Heat exchanger type          | Shell and tube counter flow, hot fluid in tubes and cold fluid in the shell |
| Shell inside radius          | 35.4 mm   |
| No of tube                   | 18  |
| Tube inside diameter         | 10 mm   |
| Length of the heat exchanger | 2 m   |

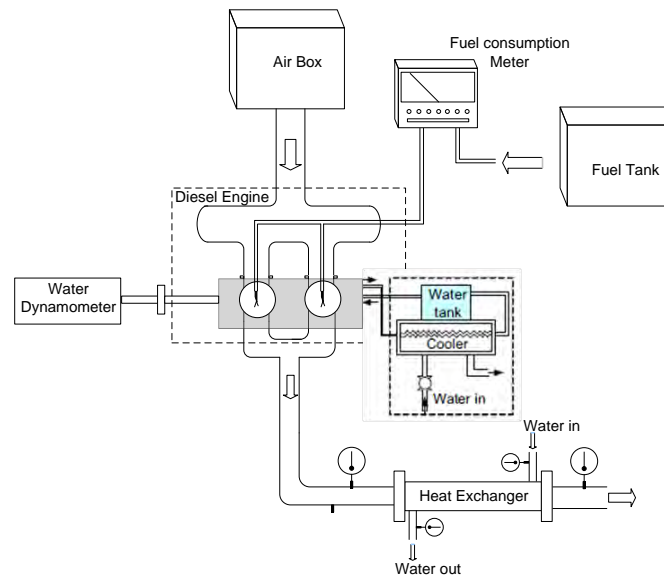


Fig. 1: Schematic diagram of experimental setup.

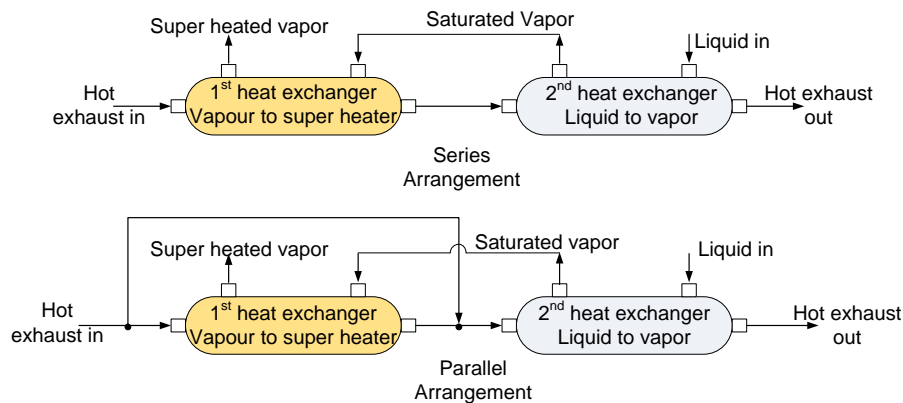


Fig. 2: Heat exchanger arrangement.

#### 4. CFD Model

The optimized design of the shell and tube heat exchanger is modeled for heat transfer between hot and cold fluid in Flow Simulation which is CFD simulation module of Solidworks 2009. The computational mesh used to solve the model heat exchanger contained 109,992 cells. The cold fluid was considered to be liquid phase at 323K with corresponding saturation pressure for the second heat exchanger (Fig. 2) and saturated vapor at working pressure for the first heat exchanger (Fig. 2). The hot fluid considered as air with mass flow rate of  $0.10215 \text{ kgs}^{-1}$  and temperature of 938 K. The operating pressure of hot fluid is set to 101.325 kPa and the cold fluid supply pressure and mass flow rate are varied. Steady and incompressible flow was assumed in all models. The Standard  $k-\epsilon$ , a two-equation Reynolds-Averaged Navier-Stokes (RANS) model that is currently the most widely used for calculating flow problems has been used in this model.

#### 5. Results

To design an effective heat exchanger for heat recovery from the exhaust of an engine, it is required to know how much energy is available in the exhaust. So some base line tests are performed. The exhaust gas temperature at various speed and engine power is presented in the Fig. 3. It is found from the figure that engine power and the temperature of the exhaust gases

for all three engine speeds show an approximately linear relationship. Exhaust gas temperature increases with increase of power output and speed of the engine. This indicates that heat recovery will be more viable for higher powers.

In the relationship between power and temperature there is a definite relationship between engine power and the amount of recoverable energy present in the exhaust gases. The relationship this time is not linear but there is still a general upward trend, revealing that, as the engine power increases, so does the amount of recoverable energy. This is clearly seen in Fig. 4. This finding is highly significant section in terms of the focus of this research project.

In particular, the potential applications which formed the original thinking behind this project are given credibility, in that the amount of energy which may be tapped is of an order that

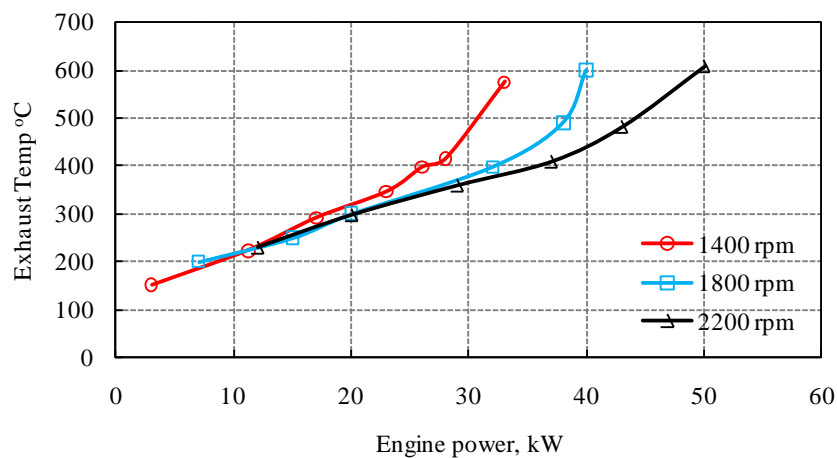


Fig. 3: Exhaust gas temperature variation with engine power from experiment.

justifies the attempt to capture and exploit it. For example, even if the results of just the lowest speed (1400 rpm) are considered, the potential to capture and use what is currently wasted energy, is extremely significant - the maximum recoverable energy for this speed is approximately 17 kW from the exhaust gas with the engine running at 33 kW (which is half the engine's power). Similarly, at 1800 rpm, a maximum value of approximately 21 kW was obtained from the exhaust gases, with the engine running at approximately 39 kW. At 2200 rpm the results show a maximum recoverable potential of approximately 23 kW when running at 45 kW. These results indicate that some 50% of the engine's running load is currently wasted but could be recoverable and converted to a usable form. All the above calculations were based on the abilities of a heat exchanger to be able to reduce the initial exhaust temperature at any particular speed and load to 50°C.

Based on the available data from the experiment, the heat exchanger design was optimized by computer simulation. Fig. 5 shows that the effectiveness of the heat exchanger decreases with the larger shell diameter for all three working fluids. Rubaiyat and Bari [18] found that there is no significant effect of working pressure on heat exchanger effectiveness. They also found that average pressure drop for different parameter of heat exchanger was about 250 Pa[18]. Effectiveness is higher for smaller diameter of the shell because of turbulent flow which facilitates the heat transfer. Heat exchanger effectiveness increases with the length of the heat exchanger as presented in the Fig. 6. It is found from the figure that after 1.6 m length the effectiveness increase is not very significant.

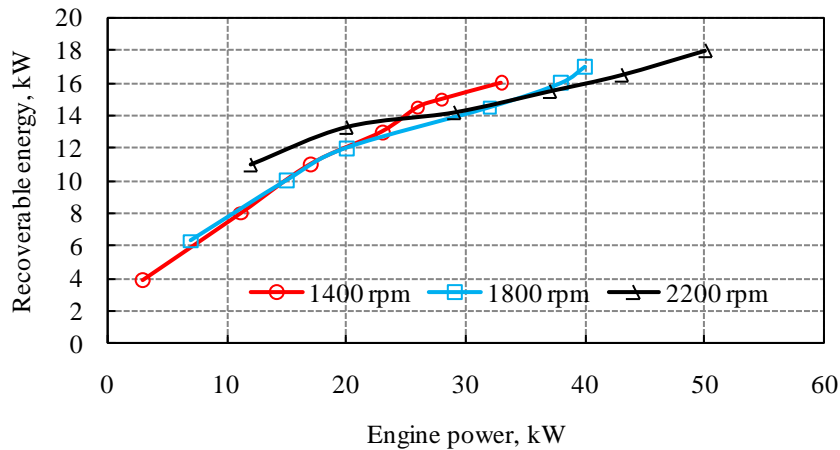


Fig. 4: Recoverable energy variation with engine power from experiment.

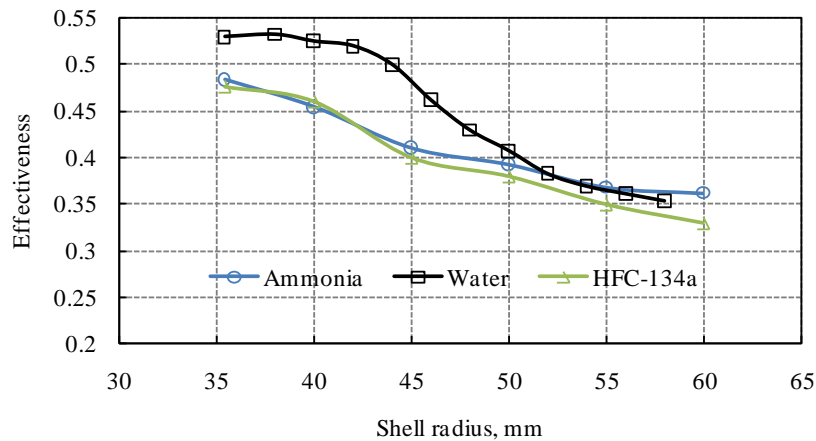


Fig. 5: Heat exchanger effectiveness vs. shell radius from CFD simulation.

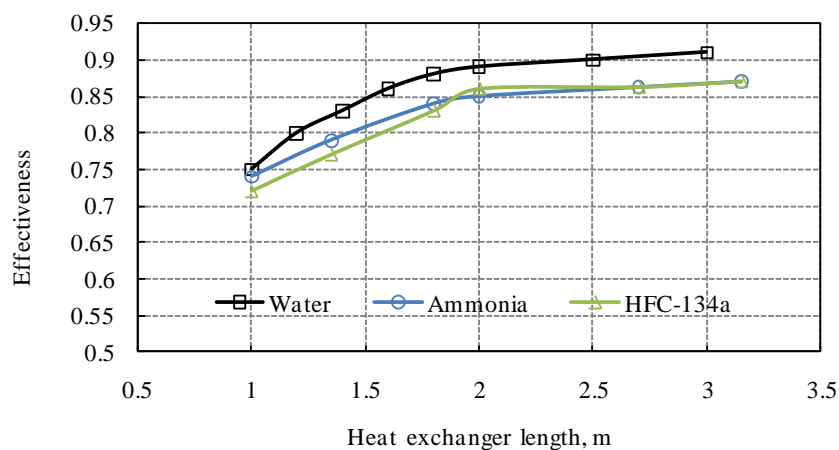


Fig. 6: Heat exchanger effectiveness vs. heat exchanger length from CFD simulation.

Extra power that can be recovered from the exhaust of the diesel engine with the proposed shell and tube heat exchanger model is presented in the Fig. 7. It is found that additional output power increases as the working pressure increases for both the parallel and series

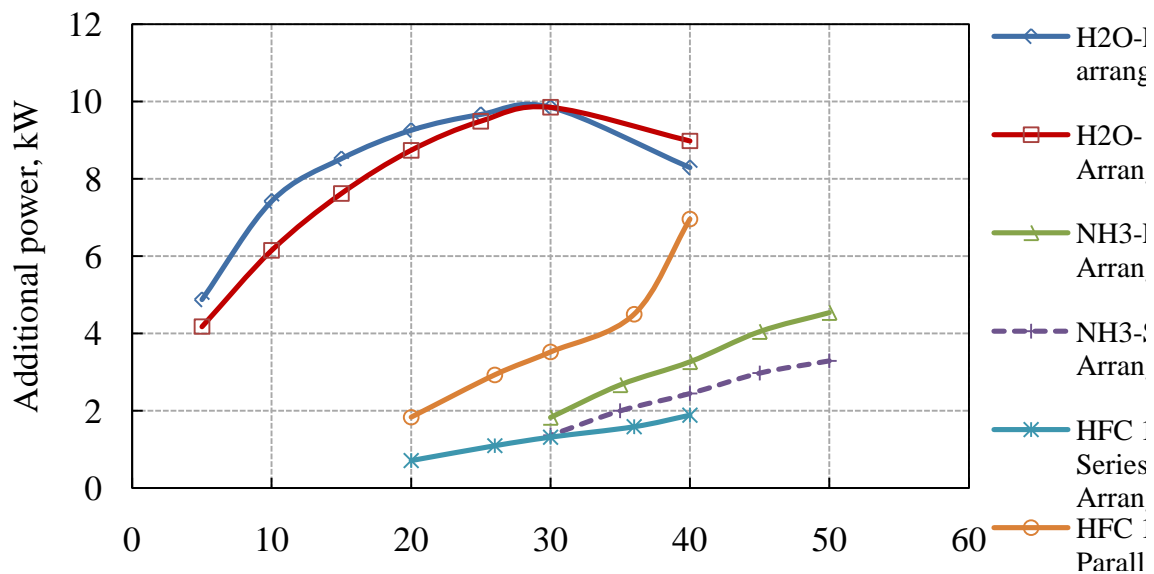


Fig. 7: Additional power output variation for different working fluids with working pressure from CFD simulation.

arrangement (Fig.2) of the heat exchangers for all three working fluids. This is because the condensing pressure was kept constant and as the working pressure increases the enthalpy drop across the turbine also increases. From the figure it is clear that water can recover heat most efficiently from the exhaust of the engine than the other organic fluids. This is because water has very high enthalpy drop across the turbine (Table 1) compared to other two organic fluids. Interestingly, it is found for water that higher power output can be achieved for parallel arrangement below 30 bar working pressure than the series arrangement whereas series arrangement can achieve higher power output above 30 bar working pressure than parallel arrangement. Maximum power output also achieved at the 30 bar working pressure. But other working fluids, ammonia and HFC-134a do not show any trend like that. For both ammonia and HFC-134a working fluid, parallel arrangement of the heat exchangers gives more additional power output. The proposed shell and tube heat exchanger can recover maximum 15%, 13% and 8% additional power from the exhaust of the diesel engine using water, HFC-134a and ammonia as working fluid respectively considering 70% isentropic efficiency of the turbine [16, 17].

## 6. Conclusion

The experimental and simulation results of the current project proved the concept of heat recovery from waste heat from the exhaust of diesel engines by using different working fluids. This research work shows that ORC can be a good option for waste recovery from diesel engines. This technique can increase the overall efficiency of diesel engine. Hence, this technology will reduce the fuel consumption and thereby will also reduce Green House Gases (GHG) and toxic emissions per kW of power produced. Additional 15%, 13% and 8% more power can be achieved with the proposed shell and tube heat exchanger by using water, HFC-134a and ammonia respectively.

## References

- [1] M. Hatazawa, H., Sugita, T., Ogawa, Y., Seo, "Performance of a thermoacoustic sound wave generator driven with waste heat of automobile gasoline engine," Transactions of the Japan Society of Mechanical Engineers (Part B, vol. 70, pp. 292–299, 2004.
- [2] V. Johnson, "Heat-generated cooling opportunities in vehicles," SAE Technical Papers 2002.
- [3] T. C. Hung, et al., "A review of organic rankine cycles (ORCs) for the recovery of low-grade waste heat," Energy, vol. 22, pp. 661-667, 1997.
- [4] J. E. Boretz, in 5th Proceedings of the International Offshore Mechanics and Arctic Engineering Symposium (4th ed.), 1986, p. 279.
- [5] P. De Marchi Desenzani and M. Gaia, Performance analysis of innovative collector fields for solar-electric plants, using air as heat transfer medium, 1984.
- [6] F. DiBella, et al., "Laboratory and on-highway testing of diesel organic Rankine compound long-haul vehicle engine," SAE Technical Papers 1983.
- [7] E. Doyle, DiNanno, L, Kramer, S, "Installation of a Diesel-Organic Rankine Compound Engine in a Class 8 Truck for a Single-Vehicle Test," SAE Technical Papers 1979.
- [8] P. Patel, Doyle, EF, "Compounding the Truck Diesel Engine With An Organic Rankine-Cycle System," SAE Technical Papers 1976.
- [9] S. E. Aly, "Diesel engine waste-heat power cycle," Applied Energy, vol. 29, pp. 179-189, 1988.
- [10] W. Koebbeman, "Geothermal wellhead application of a 1-MW industrial ORC power system," 1985, pp. 2712-2717.
- [11] S. Hounsham, Stobart, R, Cooke, A, Childs, P, "2008-01-0309 Energy Recovery Systems for Engines," SAE SP, vol. 2153, p. 79, 2008.
- [12] M. Kadota and K. Yamamoto, "Advanced transient simulation on hybrid vehicle using Rankine cycle system," SAE International Journal of Engines, vol. 1, p. 240, 2009.
- [13] C. Nelson, "Exhaust Energy Recovery," presented at the Diesel Engine-Efficiency and Emissions Research (DEER) Conference, Dearborn, Michigan, 2008.
- [14] R. W. Kruiswyk, "An Engine System Approach to Exhaust Waste Heat Recovery," presented at the Diesel Engine-Efficiency and Emissions Research (DEER) Conference, Dearborn, Michigan, 2008.
- [15] J. Ringler, et al., "Rankine cycle for waste heat recovery of IC engines," SAE International Journal of Engines, vol. 2, p. 67, 2009.
- [16] M. J. Moran and H. N. Shapiro, Fundamentals of Engineering Thermodynamics, USA: John Wiley & Sons, 4th ed., 2000, pp. 281-283.
- [17] Y. A. Cengel, et al., Fundamentals of Thermal-Fluid Sciences, McGrawHill, 3rd ed., 2008, pp. 337-339.
- [18] S. N. H. Rubaiyat and S. Bari, "Waste heat recovery using shell and tube heat exchanger from the exhaust of an automotive engine," in 13th Asian Congress of Fluid Mechanics, Gazipu, Bangladesh 2010.

## Working fluid selection for Organic Rankine Cycle applied to heat recovery systems

D. C. Bândean<sup>1</sup>, S. Smolen<sup>2\*</sup>, J. T. Cieslinski<sup>3</sup>,

<sup>1</sup>Technical University of Cluj-Napoca, Cluj-Napoca, Romania

<sup>2</sup>University of Applied Sciences, Bremen, Germany

<sup>3</sup>Gdansk University of Technology, Gdansk, Poland

\* Corresponding author. Tel: 0049-(0)421-5905-3579, Fax: 0049-(0)421-5905-3505, E-mail: smolen@fbm.hs-bremen.de

**Abstract:** The selection of suitable organic fluids for use in Organic Rankine Cycle (ORC) for waste energy recovery from many potential sources of low-medium temperature (up to 350 °C) is a crucial step to achieve high thermal efficiency. In order to identify the most suitable organic fluids, several general criteria have to be taken into consideration, from the thermophysical properties of the fluids leading to the environmental impact and cost related issues. The aim of the study is to elaborate a tool for the comparison of the influence of different working fluids on performance of an ORC heat recovery power plant installation. A database of a number of organic fluids as well as a software (code) which allows the user to select the proper organic fluid for particular application have been developed. Calculations have been conducted for the same heat source and installation component parameters. The elaborated tool should create a support by choosing an optimal working fluid for special applications and become a part of a bigger optimization procedure by different frame conditions.

**Keywords:** Organic Rankine Cycle, Database, Heat Recovery

### Nomenclature

|   |   |
|---|---|
| $\dot{Q}_{in}$ heat flux input ..... kW                           | $p_{low}$ low system pressure ..... MPa                     |
| $\dot{m}$ mass flow rate ..... kg·s <sup>-1</sup>                 | $\eta_{turbine}$ internal efficiency of the turbine ..... % |
| $\pi$ pressure ratio  | $\eta_{pump}$ internal efficiency of the pump ..... %       |
| $h_i$ specific enthalpy for process point i...kJ·kg <sup>-1</sup> | $\eta_{system}$ system efficiency ..... %                   |
| $T_{high}$ high system temperature ..... °C                       | $P_{pump}$ power used by the pump ..... kW                  |
| $T_{low}$ low system temperature ..... °C                         | $P_{turbine}$ output power of the turbine ..... kW          |
| $p_{high}$ high system pressure ..... MPa                         | $\dot{Q}_{out}$ heat flux output in the condenser ..... kW  |

### 1. Introduction

Nowadays, with energy demand rising at an ever increasing rate, efficient use of energy has become a major issue. One candidate suitable for improving efficiencies of existing applications and allowing the extraction of energy from previously unsuitable sources is the Organic Rankine Cycle. Applications based on this cycle allow the use of low temperature energy sources such as waste heat from industrial applications, geothermal sources, biomass fired power plants and micro combined heat and power systems.

Waste heat represents the heat produced by machines, electrical equipment and industrial processes which has no practical use. Usually it's generated by fuel combustion or by chemical reaction. The difficulty of capturing, distribution or transformation into other forms of energy comes from the characteristics of the heat source and the high costs connected to the equipment needed to transform the heat into useful energy. Statistical investigations indicate that low-grade waste heat accounts for 50% or more of the total heat generated in industry [1]. There are several types of industrial waste heat sources, some of which are presented in Table 1.

Table 1. Waste heat sources and their quality. [2]

| Waste heat source  | Quality of waste heat and possible use   |
|--|--|
| Heat in flue gases   | The higher the temperature, the greater the potential value for heat recovery  |
| Heat in vapor streams  | As for heat in flue gases, but when condensed, latent heat is also recoverable   |
| Convective and radiant heat loss from the exterior of equipment            | Low grade – if collected, may be used for space heating or air preheating  |
| Heat losses in cooling water   | Low grade – useful gains if heat is exchanged with incoming fresh water  |
| Heat losses in providing chilled water or in the disposal of chilled water | 1. High grade if it can be utilized to reduce demand for refrigeration<br>2. Low grade if refrigeration unit used as a form of heat pump |
| Heat stored in products leaving the process                                | Quality depends upon temperature   |
| Heat in gaseous and liquid effluents leaving process                       | Poor, if heavily contaminated & thus require alloy heat exchanger  |

Organic Rankine cycle is a Clausius – Rankine cycle which uses an organic fluid instead of water. The replacement of water with organic fluids brings a number of advantages over the classical steam process. Due to their thermophysical characteristics, such as low critical point, low boiling temperature and high molecular mass, the transformation of low temperature heat into useful electrical energy is possible and can be effective (higher efficiency than other possibilities).

Because of the low critical point relative to water and because the temperature level of the heat input is much lower than in the case of steam processes, the working pressures are lower and thus, they lead to a small-scale, low-cost installation which in most cases does not require permanent supervision [6].

Fluid selection for any type of ORC application is a very important step in designing an efficient working system. There are many important aspects that need to be taken into consideration before choosing an organic fluid. In this context a special fluid database with an implemented selection algorithm has been created with the possibility of continuous development.

## 2. Database

The database has been assembled in MS Excel due to the wide spread of the program and the fact that it facilitates the structuring and organization of data sets in an easy and intuitive way. Another major advantage of MS Excel is the relative ease with which one can import data either from other databases or from experimental data. The characteristics of the fluids have been sorted in two major groups, each containing multiple parameters: thermophysical characteristics and environmental characteristics.

### 2.1. Thermophysical characteristics

One of the thermophysical characteristics of the organic fluids is the slope of the saturation curve in the temperature-entropy diagram. It can be negative, isentropic or positive, as shown in Fig. 1.

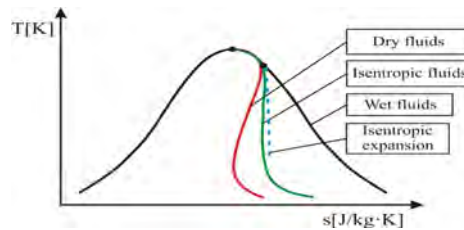


Fig. 1. Typical  $T$ - $s$  diagram for dry, isentropic and wet fluids

In the case of dry and isentropic fluids there is no need for overheating. Because of the theoretical isentropic expansion in the turbine, in the case of wet fluids, overheating must be applied in order to avoid the creation of liquid droplets during the expansion in the turbine which would damage the turbine blades. Due to this characteristic the database contains information about the type of saturation curve for each contained fluid.

For practical reasons the low pressure value has been set to just above the atmospheric pressure (0.15 MPa). This limit must be imposed in order to avoid infiltration of air in the installation which would lead to the damaging of components. Also, for the moment, the low temperature value has been set to the value of normal ambient temperature (20 °C). Of course the real frame conditions of a real process, especially the temperature of the cooling medium, determine these values, which can be varied.

Another important characteristic is the boiling temperature at the low pressure value of the fluid. If it's lower than the ambient temperature then the minimal pressure value at which the fluid is in a liquid state at room temperature must be identified and set as the new low pressure value. This has to be done in order to maintain the highest possible value for the pressure ratio  $\pi$  of the expander, as a higher pressure drop yields a higher efficiency and it has been done for each fluid in the database.

There are other thermophysical parameters that must be taken into consideration when choosing a working fluid. Some of these are:

- low freezing point, so that the fluid will not solidify when it's in the low-temperature area of the process;
- the critical pressure and temperature should be above the highest values of these parameters in the process;
- the vaporization heat and the density of the fluid should be high, as a fluid with these characteristics will absorb more energy from the source in the evaporator and thus reduce the required flow rate, the size of the facility, and the pump consumption.

## 2.2. Environmental characteristics

Although high system efficiency is the main goal when designing heat recovery systems, one has to take into account the environmental characteristics for safety and practical considerations. For example, as the HCFCs still contain chlorine and have an associated Ozone Depletion Potential, they will be phased out in the EU Community from the 1<sup>st</sup> of January 2010 [3]. So, the availability of HCFCs for equipment servicing following the phase-out may not allow for predictable economical use.

Two main environmental characteristics are the ODP (Ozone Depletion Potential) and the GWP (Global Warming Potential). ODP represents the relative amount of degradation that a fluid can cause to the ozone layer. The standard of reference has been set for trichlorofluoromethane (R11). It has the value of 1 and the maximum potential of ozone depletion among chlorocarbons because of the three chlorine atoms in its composition. [4]

GWP represents a parameter that quantifies the contribution of a given mass of greenhouse gas to global warming. The standard of reference in this case is set for carbon dioxide with a given value of 1. Another important characteristic is the safety classification. After a careful analysis the ASHRAE (American Society of Heating, Refrigerating and Air-Conditioning Engineers) classification has been chosen because of the high number of organic fluids covered and the relative simplicity of the annotations of the safety classes. These are as follows in Table 2:

Table 2. ASHRAE safety classification. [5]

| Flammability  | Low toxicity | High toxicity |
|---------------|--------------|---------------|
| High          | A3           | B3            |
| Low           | A2           | B2            |
| Non-flammable | A1           | B1            |

### 2.2.1. Toxicity classification [5]

Refrigerants are divided into two groups according to toxicity:

- Class A signifies refrigerants for which toxicity has not been identified at concentrations less than or equal to 400 ppm;
- Class B signifies refrigerants for which there is evidence of toxicity at concentrations below 400 ppm.

### 2.2.2. Flammability classification [5]

Refrigerants are divided into three groups according to flammability:

- Class 1 indicates refrigerants that do not show flame propagation when tested in air at 21°C and 101 kPa;
- Class 2 indicates refrigerants having a lower flammability limit of more than 0.10 kg/m<sup>3</sup> at 21°C and 101 kPa and a heat of combustion of less than 19 kJ/kg;
- Class 3 indicates refrigerants that are highly flammable as defined by a lower flammability limit of less than or equal to 0.10 kg/m<sup>3</sup> at 21°C and 101 kPa or a heat of combustion greater than or equal to 19 kJ/kg.

The database interface allows the user to select the type of installation for which the fluid data will be analyzed. Momentarily the installation layouts that are available are:

- Undercritical single stage;
- Undercritical single stage with recovery;
- Undercritical two-stage;
- Supercritical single stage.

The major fluid parameters are introduced for each existing fluid in the database, with the possibility of adding either other fluids and/or other parameters of interest. The general layout of the existing list with some of the parameters present in the developed program can be seen in Fig. 2:

| Working fluid                    | Boiling point at p=0.1 MPa [°C] | CRITICAL POINT   |                | Molar mass [g/mol] | Slope      | Toxicity group | L50 [°C] |
|----------------------------------|---------------------------------|------------------|----------------|--------------------|------------|----------------|----------|
|                                  |                                 | Temperature [°C] | Pressure [MPa] |                    |            |                |          |
| R11 (Trichlorofluoromethane)     | 23,77                           | 471              | 4,41           | 137,37             | Isentropic | A1             | 1        |
| R113 (Trichlorotrifluoroethane)  | 47,6                            | 487,26           | 3,39           | 187,37             | Positive   | A1             | 0,9      |
| R114 (Dichlorotetrafluoroethane) | 5,5                             | 419,1            | 3,25           | 170,9              | Positive   | A1             | 0,85     |
| R115 (Chloropentafluoroethane)   | -39,1                           | 353,1            | 3,15           | 154,5              | -          | A1             | 0,4      |
| R115b (Chloropentafluoroethane)  | -78,2                           | 293,1            | 3,04           | 138                | -          | A1             | 0        |
| R12 (Dichlorodifluoromethane)    | -29,8                           | 385              | 4,41           | 120,91             | Negative   | A1             | 0,82     |
| R123 (Dichlorotrifluoroethane)   | -27,6                           | 456,9            | 3,7            | 152,93             | Positive   | B1             | 0,02     |
| R124 (Chlorotetrafluoroethane)   | -11                             | 395,5            | 3,62           | 136,5              | Isentropic | A1             | 0,022    |
| R125 (Pentafluoroethane)         | -48,5                           | 359,4            | 3,63           | 120                | Isentropic | A1             | 0        |
| R13 (Chlorotrifluoromethane)     | -81,3                           | 302              | 3,97           | 104,5              | Negative   | A1             | 1        |
| R13B1 (Bromotrifluoroethane)     | -57,75                          | 340,08           | 3,95           | 148,91             | -          | A1             | 13       |
| R134a (Tetrafluoroethane)        | -26,1                           | 374,2            | 4,06           | 102                | Isentropic | A1             | 0        |
| R14 (Tetrafluoroethane)          | -127,8                          | 227,5            | 3,75           | 88                 | Negative   | A1             | 0        |
| R141b (dichlorodifluoroethane)   | 32,05                           | 477,6            | 4,25           | 117                | -          | -              | 0,1      |
| R142b (chlorodifluoroethane)     | -9,8                            | 410,4            | 4,12           | 100,5              | -          | A2             | 0,07     |
| R143a (Trifluoroethane)          | -47,6                           | 346,1            | 3,78           | 84                 | -          | A2             | 0        |
| R152a (Difluoroethane)           | -25                             | 386,5            | 4,52           | 66,1               | Negative   | A2             | 0        |
| R21 (Dichlorofluoromethane)      | 8,92                            | 451,7            | 5,71           | 102,9              | Negative   | -              | 0,04     |
| R218 (Octafluoropropane)         | -36,7                           | 345,1            | 2,68           | 168                | -          | A1             | 0        |
| R22 (chlorodifluoroethane)       | -40,8                           | 363,3            | 4,99           | 86,5               | Negative   | A1             | 0,05     |

Fig. 2. Fluid list with selected available fluids and parameters

Each fluid has a series of static parameters, such as ODP, GWP, molar mass, boiling point at atmospheric pressure and others, which are introduced when the fluid is added to the database and which never change. The dynamic parameters such as the cycle efficiency, the mass flow rate and the pressure ratio are calculated and are modified with the alteration of the input parameters which will be described in the following section.

Because the program is developed in MS Excel the interface and the fluid data are stored in the same document on different worksheets. Fig. 3 presents captions from both the interface and the database and the flow of data through them:



Fig. 3. Flow of data through the program

For each fluid from the database there are three worksheets. One contains the liquid and vapor enthalpy and entropy and other parameter values for the fluid along the saturation curve, one contains temperature, enthalpy and entropy values for the different process points and the third worksheet contains the calculation interface for the fluid and all the functions needed to implement the calculation procedure in the program. The user introduces the values for the input parameters, marked by the red rectangles, and the program returns the output parameters, marked with the green rectangles. For example, the program reads the temperature value introduced by the user and, by using the "MATCH" function from Excel, it extracts the values for the enthalpy, entropy and pressure from the first data worksheet (saturation property curve) for each fluid. With these values, the program calculates and extracts values for the parameters for each process point and, finally, it returns the cycle efficiency. This value is introduced in the fluid list and it is updated whenever the input parameters are modified. From here the program returns a list of the fluids which yield the highest efficiencies (the top 4 in example from Fig. 3) for this set of input parameters.

### 3. Calculation procedure

As mentioned above, beside the general and environmental properties, the program returns the cycle efficiency for each fluid. This is done by employing a set of functions embedded in Excel which interrogate, search, match and return the desired data.

For the moment, the program executes calculations for a standard single stage cycle without recovery. The general layout of the installation, the process points and the T-s diagram (in this case for R114) can be seen in Fig. 4.

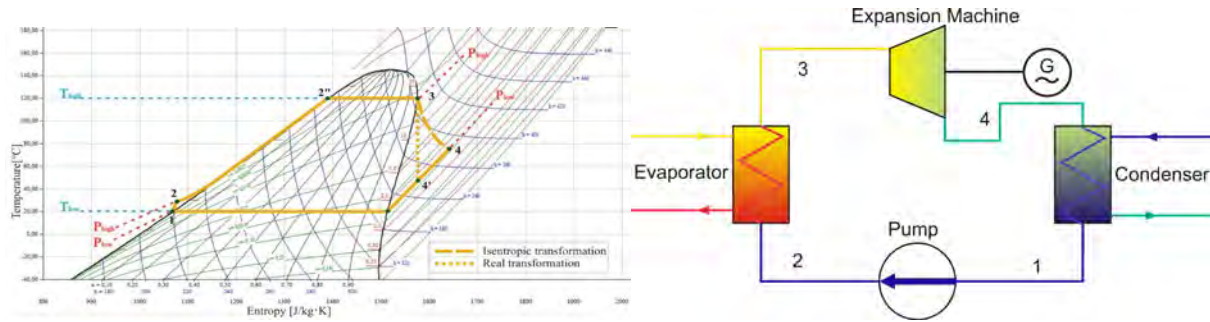


Fig. 4. *T-s diagram and installation layout for a simple one-stage process*

At the current state, the major input parameters for the program are the heat flux transferred to the system and the temperature at the inlet of the turbine (process point 3 in this case). The program calculates the efficiency of the cycle without overheating. So after introducing the heat flux and the turbine inlet temperature, the program chooses the corresponding pressure from the saturation curve for each fluid. The low pressure value is set to just above the atmospheric pressure (at 0.15 MPa) and the low temperature is set to the standard ambient temperature (20 °C).

With the value of the heat flux, the program calculates the mass flow rate:

$$\dot{m} = \frac{\dot{Q}_{in}}{h_3 - h_2} \quad (1)$$

where  $h_2$  and  $h_3$  represent the enthalpy values for process points 2 and 3.

By obtaining the high pressure value from the saturation curve, the program calculates the pressure ratio which is a good indicator for the system efficiency.

$$\pi = \frac{P_{high}}{P_{low}} \quad (2)$$

The internal efficiencies of the turbine and the pump are also input values. They can be selected from a drop-down list within the range of 0% to 100%, leading to a number of four input parameters. The expansion in the turbine is theoretically isentropic. The values for the irreversible process are obtained from the internal efficiency of the turbine.

$$\eta_{turbine} = \frac{h_3 - h_4}{h_3 - h_4'} \quad (3)$$

where the enthalpy values are obtained from the database for each fluid by matching the temperature and entropy values. By obtaining the value for the enthalpy in process point 4 the other parameters are extracted from the database. The power required for the pump is calculated with the following formula:

$$P_{pump} = \frac{v \cdot (P_{high} - P_{low})}{\eta_{pump}} \cdot \dot{m} \quad (4)$$

The output power of the turbine is calculated with the help of the internal efficiency of the turbine and by extracting the enthalpy values for process points 3 and 4 from the database:

$$P_{turbine} = \dot{m} \cdot \eta_{turbine} \cdot (h_3 - h_4) \quad (5)$$

The heat flux extracted in the condenser is calculated with the following formula:

$$\dot{Q}_{out} = \dot{m} \cdot (h_4 - h_1) \quad (6)$$

After obtaining the values for each of these parameters, the program calculates the system efficiency as follows:

$$\eta_{system} = \frac{P_{turbine} - P_{pump}}{\dot{Q}_{in}} \cdot 100 \quad (7)$$

The program returns the value for the system efficiency for each fluid in the database. If the input parameters lead to data that is outside the set conditions it will return “N/A” which signifies that the fluid is not suitable for the given input parameters.

In the current version the program returns a list of fluids which allow the highest system efficiencies for the input data set. In the following months more data and calculation procedures will be introduced so the program can calculate efficiencies of other types of installations, as shown in Figures 5, 6 and 7.

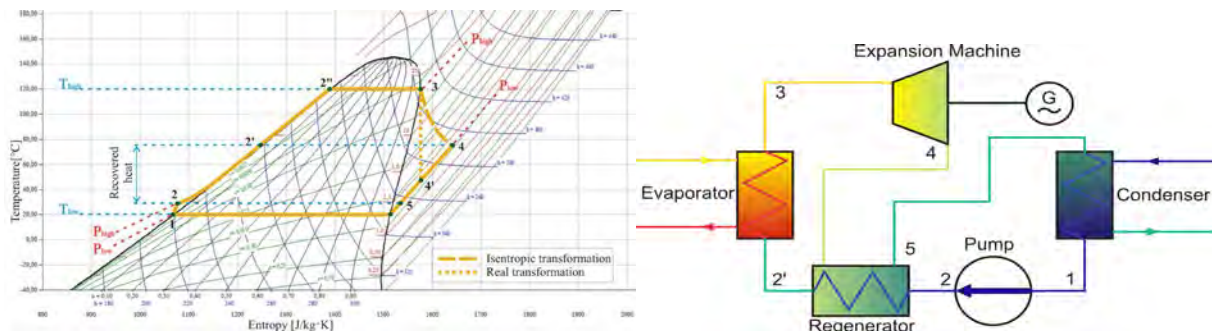


Fig. 5. T-s diagram and installation layout for a one-stage with recovery process

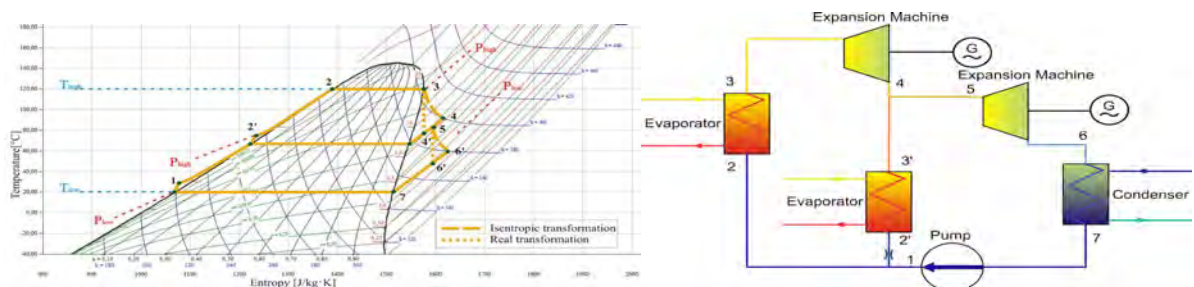


Fig. 6. T-s diagram and installation layout for a two-stage process

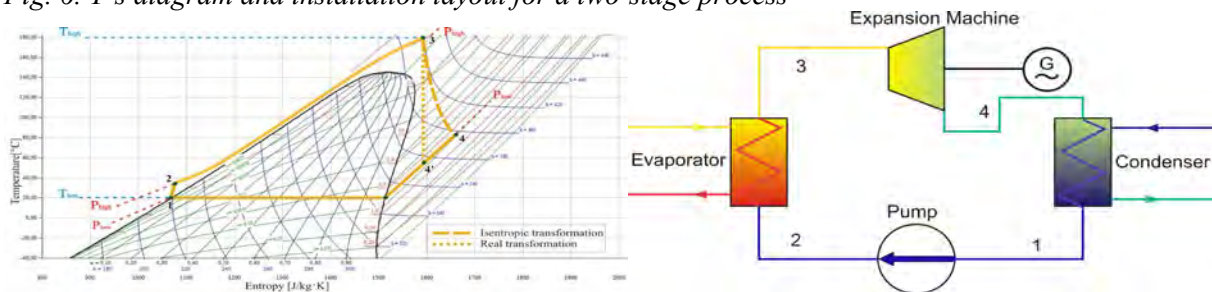


Fig. 7. T-s diagram and installation layout for a supercritical one-stage process

Further steps will consist of introducing the possibility of overheating and thus moving away from the saturation curve, the possibility of modifying the set values for the low pressure and

temperature as well as different sorting criteria such as cost, environmental aspects, availability and others.

#### 4. Conclusions

Fluid selection is a major step in designing heat recovery systems based on the organic Rankine cycle. Although at this moment the sorting criterion for the fluids is the system efficiency, further development of the proposed program will create the possibility for different sorting criteria.

Developing this application has revealed that a program dedicated to fluid selection for heat recovery systems has a high degree of complexity. Although this application can give an idea to the user about the performance of different fluids applied to the same type of installation, one has to remember that the data still has to be compared to experimental data.

While the program is a good indicator for the influence on the system performance of different organic fluids, returning other fluid parameters in the process, the final decision of selection of an organic fluid for a given set of frame conditions remains to be made by the engineer designing the system. Costs related to fluid purchase, lifetime costs, taxes and availability may lead the designer to choose a lower efficiency yielding fluid.

To increase the level of complexity of the program and to bring the results, from theoretical, closer to real, measurable values, the interface from the heat source and the system will be investigated.

Another task that needs to be considered within the next steps is the investigation of energy and exergy losses in the expansion machine and exergy losses in the heat exchangers.

#### References

- [1] T. C. Hung, T. Y. Shai, S. K. Wang, A review of organic Rankine cycles (ORCs) for the recovery of low-grade waste heat, *Energy*, Vol. 22, No. 7, 1997, pp. 661 – 667.
- [2] United Nations Environment Programme, 2006, [www.energyefficiencyasia.org](http://www.energyefficiencyasia.org).
- [3] Europa, Summaries of EU legislation, <[http://europa.eu/legislation\\_summaries/environment/air\\_pollution/ev0021\\_en.htm](http://europa.eu/legislation_summaries/environment/air_pollution/ev0021_en.htm)>.
- [4] Ozone Depletion and Chlorine Loading Potential of Chlorofluorocarbon Alternatives, CIESIN Thematic Guides, <<http://www.ciesin.org/TG/OZ/odp.html>>.
- [5] Classification of refrigerants, International Institute of Refrigeration, <<http://www.iifir.org/en/doc/1034.pdf>>.
- [6] A. Pislă, D.C. Bândeian, Investigations on a Two Stage ORC Installation, 2010 IEEE International Conference on Automation, Quality and Testing, Robotics, AQTR 2010 - THETA, Cluj-Napoca, Romania.

---

## Examining the effect of heat storage in a cogeneration system

G.R. Salehi<sup>1\*</sup>, E. Taghdiri<sup>2</sup>, D. Deldadeh<sup>2</sup>

<sup>1</sup>Islamic Azad University Noshahr Branch, Noshahr, Iran

<sup>2</sup>KNToosi University of Technology, Tehran, Iran

\* Corresponding author. Tel: +989122031671, E-mail: rezasalehi20@gmail.com

---

**Abstract:** Small power plants of cogeneration of power, heat and cooling are good solutions of increasing the efficiency of energy consumption for fossil fuels in order to protect natural resources and the environment. However, at moments when heat demand is lower than the heat production of the CHP module, the excess heat has to be rejected to the environment and this fact results in waste of energy. Also, since CHP modules are basically heat driven, when heat demand is lower than a certain value, the module will be switched off just to be switched on later when heat demand increases. This cycle of switching on and off is harmful for the CHP module if it happens repeatedly. A solution is to use heat storage and an alternative control method. In this paper, a CHP system is chosen for an educational building and the design is carried out in two forms, with and without heat storage and the results are compared and judgment is made about the optimal system.

**Keywords:** CHP, optimization, environment, heat storage

---

### 1. Introduction

When power is produced traditionally, a large portion of original energy of the fuel is wasted as heat and hardly more than 40 percent of this energy is transformed into electricity. Moreover, usually consumers are located far away from the power plant and this distance causes more waste of energy in distribution of electricity. One way to tackle these problems is using local cogeneration. In this modern method of power generation, power is produced at the location of consumption and the majority of lost heat is recovered to supply heat demands of the user. This results in a considerable improvement in efficiency. Furthermore, since power is generated at the same location where it is consumed, distribution losses will be avoided. The total efficiency of cogeneration power plants amounts up to 90%, while the electrical efficiency of a traditional power plant hardly reaches 40%.

Among different options of power generation in the form of cogeneration, reciprocating engines seem to be the most suitable for buildings which essentially have small demands. They have high power to heat ratios compared to gas turbines and due to advances made in automotive industry, enjoy a higher degree of modernization [9]. Although stationary reciprocating engines have traditionally been diesel engines but some issues like environmental issues and good access, have been promoting the users in recent years to use natural gas as the fuel instead. In Iran, a Persian gulf country with the second largest resource of natural gas in the world, even automobiles are increasingly using gas burning and dual fuel engines.

X Q Kong et al (2004) optimized a trigeneration system (cogeneration of heat, power and cooling) based on gas turbine. In their research a trigeneration system was modeled and then, after specifying constraints and an objective function, the solution was optimized using a linear modeling program [2]. In another work, they examined a cogeneration system and presented the results as graphs and tables [3]. In 2005 P. Arcuri et al designed optimally a trigeneration system using a mixed integer model. They optimized a trigeneration system for a hospital employing a reciprocal engine as its prime mover [4]. In 2006 E. Cardona and A. Piacentino designed and optimized a trigeneration system for a hospital application from the thermoeconomic point of view [5]. The same researchers carried out another analysis for an apartment building using the thermoeconomic method [6]. In 2008, Behbahani Nia et al. [7]

optimized a cogeneration system based on gas turbine with the aim of minimizing the capital cost in which they considered electricity, heat and cooling demands for each month.

In this paper, a cogeneration system is designed and optimized for the building of mechanical engineering faculty of K.N. Toosi University of technology in Tehran, Iran, using two different strategies, with heat storage and without heat storage. First, energy simulation is carried out using the software Carrier HAP 4.2 resulting in values of electricity and heating demands in all 8760 hours of the year. Later, based on these demands, the main components of the CHP system are designed based on products of the Austrian manufacturer, Jenbacher®. Products of this company are cogeneration modules including the reciprocating engine, heat recovery system and electrical generator all in one, covering a range of capacities from 400kWth to 3MWth.

## 2. A description of the building

The building of mechanical engineering faculty of K.N. Toosi University of technology is a ten-floor building, including 3 underground floors and covering about 20 thousand square meters of area. The second and third floors contain classes, fourth and fifth floors contain administrative rooms, almost all of which benefit from natural light during daytime. The sixth floor is dedicated to professors' rooms about half of which have access to natural light. The library and some laboratories are placed on the first floor. Ground floor primarily contains public places like the big lobby, the pray place, computer services hall and so forth. The floor -1 contains laboratories, cafeteria, the big restaurant and the amphitheatre. The floors -2 and -3 are for workshops and labs and also sport activity salons. Table 1 shows a list of areas of these floors.

Table 1. Area of each floor of the building

| Floor        | Area (m <sup>2</sup> ) | Floor | Area (m <sup>2</sup> ) |
|--------------|------------------------|-------|------------------------|
| Ground floor | 2561.6                 | Fifth | 1005                   |
| First        | 2500                   | Sixth | 1007                   |
| Second       | 1006.9                 | -1    | 3100                   |
| Third        | 1005.99                | -2    | 3100                   |
| Fourth       | 1004.36                | -3    | 3100                   |

## 3. Calculation of loads

Thermal and electrical loads have been calculated using the energy simulation function of the software Carrier HAP 4.2. All parts of the building were modeled and wattages of lights, electrical equipments, geometrical and heat transfer features of rooms were entered in the software. A total of 270 spaces were defined in the process. Another important issue in determining loads is the presence of people in different spaces. Schedules were defined for presence of people in different types of spaces including classes, amphitheatre, computer services salon, corridors, administrative rooms, pray place, restaurant and security compartments, and also for lighting for each of these types of places, based on percentages of full presence or full lighting in different hours of the day and different days of the year. National holidays and weekends were considered based on the year 2009 which covers portions of Persian years 1387 and 1388. The difference of intensity of natural light in summer and winter days and different levels of presence of students and employees in different months of the year and different hours of the day were all considered based on personal observation of the second author who has been a studying in the same building for two years. The monthly distribution of heating and cooling loads resulting from this energy simulation is as shown in figure 1.

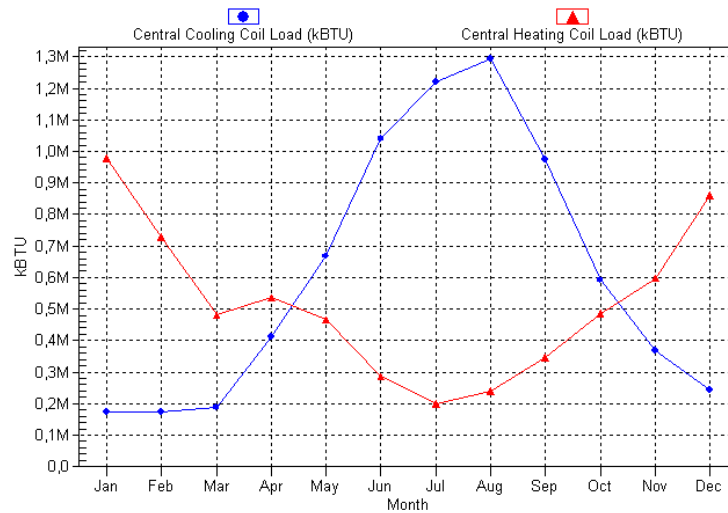


Fig. 1. Heating and cooling loads throughout the year.

The weather conditions were defined based on simulation information of [www.Carrier.com](http://www.Carrier.com) of Tehran including hot and cold bulb temperatures and sunlight situation throughout the year.

#### 4. Selection of cogeneration modules

Selection was carried out based on products of Jenbacher, including 13 models of CHP modules. The manufacturer did not reply requests of price quotation and purchase equipment costs and O&M charges were estimated using the information in [9] and by curve fitting. The cost of natural gas and electricity were taken 690 Rials per m<sup>3</sup> and 773 Rials per kWh, equal to Iranian unsubsidized rates.

Another issue which was considered in this optimization was the environmental issue. According to [9], emission of pollutants imposes costs which are in fact costs of reduced performance of human beings caused by these pollutants. This fact is considered as costs assigned to pollutants CO, CO<sub>2</sub> and NO<sub>x</sub>. According to catalogs of the manufacturer, using the lean combustion system and SCR catalysts, emissions of CO and NO<sub>x</sub> caused by their products are limited to 100 mg/Nm<sup>3</sup> for No<sub>x</sub> and 300 mg/Nm<sup>3</sup> for CO. CO<sub>2</sub> emission from natural gas combustion is equal to 1.15m<sup>3</sup>/1m<sup>3</sup> Natural Gas according to [11] which by considering the density of carbon dioxide in normal conditions equals to 20420mg/Nm<sup>3</sup>. Values of emissions of CO and NO<sub>x</sub> for small boilers are 641mg/Nm<sup>3</sup> and 1506 mg/Nm<sup>3</sup> respectively, according to [12]. As calculated in [9], the social cost associated with these emissions is 81750 Rials/kg for carbon monoxide, 240 Rials/kg for carbon dioxide and 64240 Rials/kg for Nitrogen oxides. Therefore, the social costs for burning of each cubic meter of natural gas for Jenbacher® reciprocating engines and the boiler are as shown in tables 2 and 3.

Table 2 Emissions and their costs for natural gas-burning boiler

|                             | (mg/m <sup>3</sup> ) | kg/kWh      | Unit cost(\$/kg) | Unit cost (\$/kWh) |
|-----------------------------|----------------------|-------------|------------------|--------------------|
| NO <sub>x</sub>             | 1506                 | 0.014843136 | 6.424            | 0.095352306        |
| CO                          | 641                  | 0.006317696 | 8.175            | 0.051647165        |
| CO <sub>2</sub>             | 20420                | 0.20125952  | 0.024            | 0.004830228        |
| Total emission cost(\$/kWh) |                      |             |                  | 0.151829699        |

Table 3 Emissions and their costs for natural gas-burning engine

|                             | (mg/m <sup>3</sup> ) | kg/ kWh    | Unit cost(\$/kg) | Unit cost(\$/kWh) |
|-----------------------------|----------------------|------------|------------------|-------------------|
| No <sub>x</sub>             | 100                  | 0.0009856  | 6.424            | 0.006331494       |
| CO                          | 300                  | 0.0029568  | 8.175            | 0.02417184        |
| CO <sub>2</sub>             | 20420                | 0.20125952 | 0.024            | 0.004830228       |
| Total emission cost(\$/kWh) |                      |            |                  | 0.035333563       |

## 5. Choosing capacities of components and optimization

### 5.1. The case without heat storage

In this section, sizing is carried out in two different strategies, one is the absence of heat storage and the other is its presence. In both strategies, modules of cogeneration and their annual working durations are determined so that the total annual cost is minimized.

For the case where there is no heat storage system, the CHP system is designed based on load-duration curves. These curves are constructed using the hourly load data taken from energy simulation, i.e. first values of heating and electrical loads for all 8760 hours of the year are taken from outputs of Carrier HAP and then, those numbers are put in descending order and plotted against duration, from 1 hour to 8760 hours. According to [13], the largest rectangle which can be circumscribed in that curve represents the optimal choice of the CHP system, in terms of capacity (on the vertical axis) and number of total working hours throughout the year, on the horizontal axis. Here, the basic idea is quiet similar. However, this curve is used here to determine the capacity of the supplementary boiler which is the difference of maximum load with the heat production of the CHP module and its total heat production throughout the year being equal to all heat demand not satisfied by the module.

Electricity is considered as a bi-product of the system that can be used locally or sold to the network. The rates of buying and selling power to the network are very close to each other in Iran [20] and both are assumed to be 773 Rials. If a CHP system is independent from the grid, it can employ batteries to store excess electricity to be used later but when selling power to the grid is possible, using storage of electrical energy is not economical [9].

The control strategy used for the case where there is no heat storage system is as follows: When the number of working hours of the CHP module determined from optimization is plot with load-duration curve, the point where it intersects that curve shows the value of minimum load for operation of the module, i.e. when the thermal load is lower than that value, the module will be switched off and when the load exceeds that value, the module will be switched back on.

In manufacturer's catalogs, two heuristics are suggested:

- The thermal power of the cogeneration power should be between 30 to 50 percent of the peak value of thermal power demand.
- The module of cogeneration should work at least 4000 hours during a year.

Figure 2 shows an example of load-duration curve.

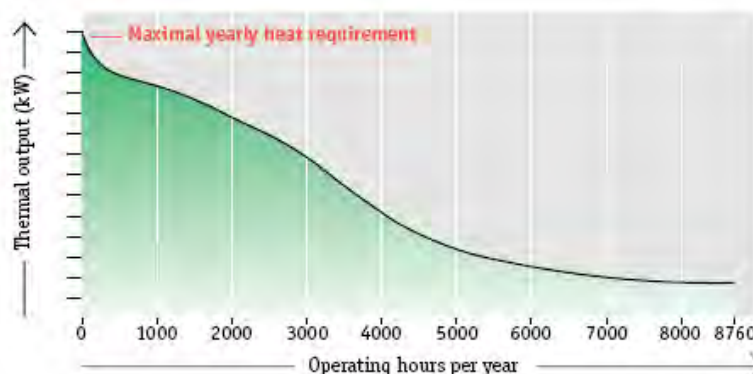


Figure 2. Load duration curve for heating load

Naturally there will be times when the heat demand is higher than the production of modules and at these times this heat shortage is covered by the auxiliary boiler.

Load-duration curves for heating, and electrical loads of our building are shown in figures 3 and 4.

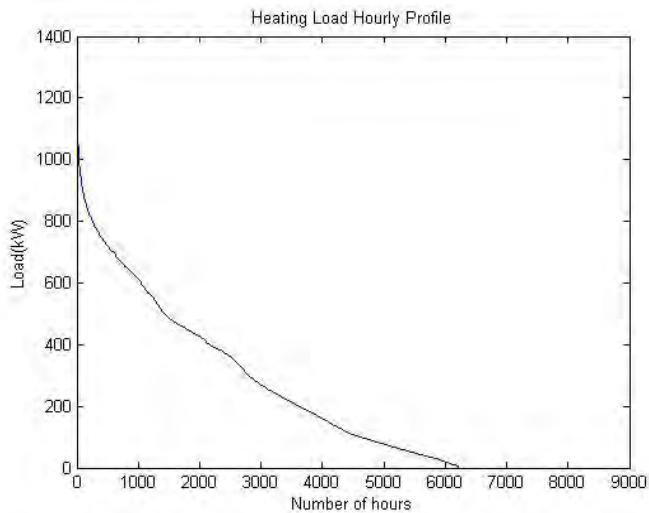


Figure 3. Load-duration curve for heating load

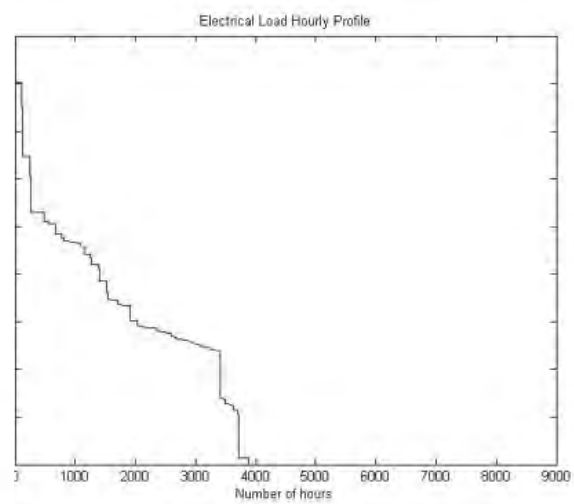


Figure 4. Load-duration curves for electrical load

Now, the objective function for the optimization is defined as the total annual cost of the system. To calculate the total annual cost, first we should annualize capital investments using the capital recovery factor (CRF).

Where  $i_r$ , the interest rate, according to [14] is taken 12 percent, and  $n$  is the number of years of life time of the system, here taken 20 years. Thus, the objective function is:

$$C_{Ann} = CRF \times (C_{TCM} + C_{TCAB} + C_{TCST}) + C_{O\&M\ Module} + C_{O\&M\ AB} + C_{Emi} - C_{el} \quad (1)$$

Where  $C_{Ann}$  is the total annual cost,  $C_{TCM}$  is the total capital investment for the CHP module,  $C_{TCAB}$  is the total capital cost for the auxiliary boiler,  $C_{TCST}$  is the total capital cost for the storage tank (if included),  $C_{O\&M\ Module}$  is yearly O&M plus fuel costs for the cogeneration modules,  $C_{O\&M\ AB}$  is the yearly O&M plus fuel costs for the auxiliary boiler,  $C_{Emi}$  is the yearly emission cost and  $C_{el}$  is yearly cost of electricity production which is the profit of the system and therefore appears with a negative sign in the total annual cost. The optimization is carried out using the direct search method. For this optimization, decision variables are taken to be capacities of CHP modules and their durations of operation throughout the year. Constraints are defined based on heuristics provided by the manufacturer, namely each module should not operate less than 4000 hours in the year, and the values of capacities of modules and the boiler, naturally may not be negative and the values of working hours of each of modules cannot be more than 8760 hours. Results are as presented in the next section.

### 5.2. The case with heat storage

If we decide to employ heat storage in our system for more smooth operation and less waste of energy, a different design and operation strategy has to be used. Heat is stored as hot water (90°C) in a well insulated storage tank. Its cost data is taken from [14] and (1) is also used for cost estimation, using two different values of the exponent  $\alpha$  (0.3 and 0.65) based on the calculated volume. The cost data is available in terms of volume of the storage tank while in the optimization, the capacity in terms of energy storage is considered. As mentioned in [15], the CHP module receives cooling water at 40°C and sends it out at 90°C. Thus, in order to determine the volume of the storage tank conservatively, we take the unit volume energy of the water stored in this tank as the difference of enthalpy of water in those input and output states.

Thus, by storing each cubic meter of water in the storage tank, we have stored 58.167kWh thermal energy.

After calculating the Purchased Equipment Cost (PEC) in terms of energy storage capacity, we calculate the Total Capital Investment (TCI) based on the Fixed Capital Investment (FCI) and the PEC using the factors listed in table 4. The data in this table are based on results reported in [14]. For costs having upper and lower bounds of the range of value, in absence of other data, the average of the two bounds mentioned in table 4 is used in calculations.

Table 4. Components of total capital investment

|  |
|--|
| I - Fixed Capital Investment (FCI)   |
| A- Direct costs  |
| 1- Costs associated with the site  |
| • Purchased Equipment Cost (15-40% FCI)  |
| • Installation cost (20-90% PEC)   |
| • Piping (10-70% PEC)  |
| • Instrumentation and control equipments (6-40% PEC)                             |
| • Electrical Equipments (10-15% PEC)   |
| 2- Off-site costs  |
| • Land (0-10% PEC)   |
| • Civil, architectural and structural costs (15-90% PEC)                         |
| • Service facilities (30-100% PEC)   |
| B- Indirect costs  |
| 1- Engineering and supervision (25-70% PEC)                                      |
| 2- Construction cost including the profit of the contractor (15% of direct cost) |
| 3- Contingencies (8-25 % the sum of the above costs)                             |
| II- Other costs  |
| A- Start up cost (5-12% FCI)   |
| B- Working capital (10-20% TCI)  |
| C- Research and development (not considered in this paper)                       |

When designing the cogeneration system with heat storage, we need to use load-time curves instead of load-duration curves. These curves show the value of thermal/electrical load at every hour for all 8760 hours of the year. Load-time curves for thermal and electrical loads are shown in figures 5 and 6.

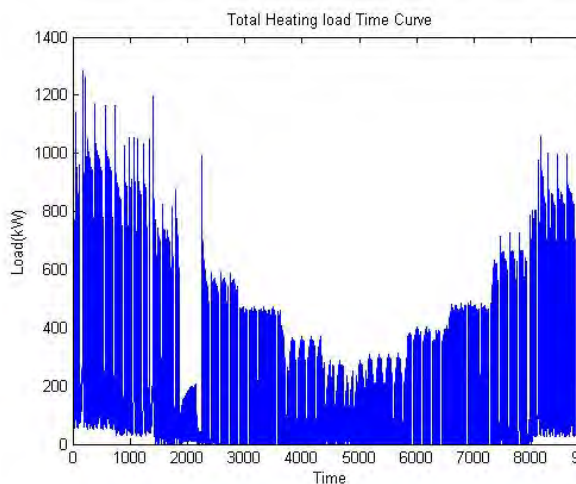


Figure 5. Load-time curve for heating load

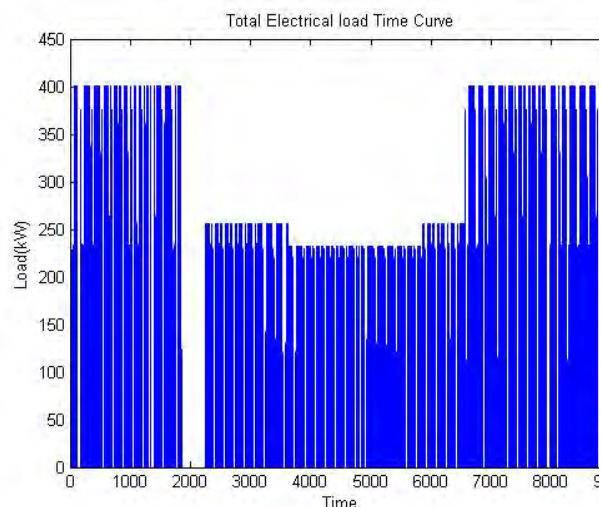


Figure 6. Load-time curve for electrical load

As a result of the above mentioned strategy, there will be fewer start-stop cycles and probably, less heat rejection to the surroundings. When optimizing the system in this case, working duration of the module will no longer be a decision variable but instead, the volume of the storage tank will be searched for its optimal value and working duration of the module will be determined from the volume of the storage tank and load-time curve. The other decision variable will be the size of the CHP module, as before. The results of optimization of this case are presented in the following section.

## 6. Results

Table 5. Optimization results for a CHP module without heat storage

|  | Capacity        | Duration/amount of yearly operation | Capital investment cost (Rials) | O and M +Fuel costs (Rials per year) | Emission cost (Rials per year) |
|--|-----------------|-------------------------------------|---------------------------------|--------------------------------------|--------------------------------|
| CHP Module   | 497kWh (J 312L) | 4011h                               | 8.63E+09                        | 5.79E+08                             | 1.55E+09                       |
| Boiler   | 786.6kW         | 439843kWh                           | 3.44E+09                        | 4.25E+07                             | 9.21E+08                       |
| Value of yearly electricity production of the CHP module (Rials)   |                 |                                     |                                 | 1.35E+09                             |                                |
| Maximum load (kW)  |                 |                                     |                                 | 1284                                 |                                |
| Total annual cost (Rials)  |                 |                                     |                                 | 3.36E+09                             |                                |
| Yearly heat dissipation to surroundings(thermal energy waste)(kWh) |                 |                                     |                                 | 450306                               |                                |

Table 6. Optimization results for a CHP module with heat storage

|   | Capacity            | Duration/amount of yearly operation | Capital investment cost (Rials) | O and M +Fuel costs (Rials per year) | Emission cost (Rials per year) |
|---|---------------------|-------------------------------------|---------------------------------|--------------------------------------|--------------------------------|
| CHP Module  | 497kW(312L)         | 8550h                               | 8.63E+09                        | 1.24E+09                             | 3.31E+09                       |
| Boiler  | 994.1kW             | 292966 kWh                          | 3.44E+09                        | 2.83E+07                             | 6.14E+08                       |
| Storage Tank  | 3.474m <sup>3</sup> | 202.1kWh                            | 3.36E+08                        | -                                    | -                              |
|   |                     | (Max storage)                       |                                 |                                      |                                |
| Value of yearly electricity production of the CHP module (Rials)    |                     |                                     |                                 | 2.88E+09                             |                                |
| Maximum load (kW)   |                     |                                     |                                 | 1284                                 |                                |
| Total annual cost (Rials)   |                     |                                     |                                 | 4.06E+09                             |                                |
| Yearly heat dissipation to surroundings(thermal energy waste) (kWh) |                     |                                     |                                 | 1.95E+06                             |                                |

As it is evident from tables 5 and 6, heat dissipation to surroundings and total annual cost are both higher for the case with heat storage than the simple case. Moreover, as illustrated in results, curves of electrical and thermal loads have more consistency with curves of energy production of the module in the simple case. However, in the case with the possibility of heat storage, more electricity is produced and the module works for a longer total duration, representing a smaller number of switching off and on cycles which is better for durability of the reciprocal engine and the whole module.

## 7. Conclusion

Heating and electrical loads were calculated for a 10-floor educational building using energy simulation of Carrier HAP®, and based on those loads, cogeneration systems were designed

to provide electricity and heating needs of the building. The CHP module was selected among 13 models of a globally renowned manufacturer.

Firstly, a simple CHP system was designed containing a CHP module and an auxiliary boiler. Secondly, the possibility of heat storage was taken into account using a storage tank as heat accumulator. Two different control strategies were considered for these two cases and consequently, design and optimization were also carried out differently.

Comparison of results showed that the simple system excluding heat storage had a lower total annual cost and heat dissipation to surroundings. On the other hand, it had a lower work duration for the CHP module and consequently, a larger number of switching on and off cycles representing its disadvantage to the system with heat storage.

## References

- [1] X. Q. Kong, R. Z. Wong, X. H. Huang, Energy optimization model for a CCHP system with available gas turbines, *Applied Thermal Engineering* 25 (2005) 377–391.
- [2] D. W. Wu, R. Z. Wang, Combined cooling, heating and power: A review, *Progress in Energy and Combustion Science* 32 (2006) 459–495.
- [3] P. Arcuri, G. Florio, P. Fragiaco, 2007, A mixed integer programming model for optimal design of trigeneration in a hospital complex, *Energy* 32, 1430–1447.
- [4] E. Cardona, A. Piacentino, A new approach to exergoeconomic analysis and design of variable demand energy systems, *Energy* 31 (2006) 490–515.
- [5] E. Cardona, A. Piacentino, Optimal design of CHCP plants in the civil sector by thermoeconomics, *Applied Energy* 84 (2007) 729–748.
- [6] Karimi Alavijeh, Saeed. Behbahaninia, Ali. Amidpour, Majid, Modeling and optimization of energy in a CHCP system with gas turbine prime mover, *International Conference of Nonlinear Problems (ICNPAA 2008)*, 24–26 June 2008, Italy.
- [7] Feasibility study of private sector's investment in development of local cogeneration systems in Iran, The department of power and energy of Iranian ministry of power, 2008, Tehran, Iran, 24–26
- [8] Technology characterization, reciprocating engines, *Energy and Environmental analysis*, Arlington, Virginia, December 2008, 12–16
- [9] Mahdi Ali Ahyayi, Sharif University of technology, Tehran, Iran, Design and optimization of cogeneration of power, heating and cooling in different climate conditions of Iran, 2007, 41–45
- [10] S.K. Sadr Nezhad, A. Kermanpour, *Fuel and Energy*, 2001, Tehran, Iran
- [11] [www.epa.gov/ttnchie1/ap42/ch01/final/c01s04.pdf](http://www.epa.gov/ttnchie1/ap42/ch01/final/c01s04.pdf)
- [12] S.S Bernow, D.B. Marron “Valuation of Environmental Externalities for Energy planning and Operations”, May 1990, Tellus Institute, Boston, Mass., 1990
- [13] Dries Haeseldonckx, Leen Peeters, Lieve Helsen, William D'haeseleer, The impact of thermal storage on the operational behaviour of residential CHP facilities and the overall CO<sub>2</sub> emissions, 26 September 2005
- [14] Adrian Bejan et al, *Thermal design and optimization*, 1996
- [15] A.D. Hawkes a, P. Aguiar b, B. Croxford c, M.A. Leach a, C.S. Adjiman b,d, N.P. Brandon Solid oxide fuel cell micro combined heat and power system operating strategy: Options for provision of residential space and water heating, 28 November 2006

## Low exergy heat recovery for sustainable indoor agriculture

Anthony Goncalves<sup>1</sup>, Daniel Rouse<sup>1,\*</sup>, Julien Milot<sup>2</sup>

<sup>1</sup> t3e Industrial research chair, École de technologie supérieure, Montréal, Canada

<sup>2</sup> Energy Solutions Associates, Lévis, Canada

\* Corresponding author. Tel: +1 (418) 833-2110, Fax: +1 (418) 396-8950, E-mail: daniel@t3e.info

**Abstract:** With improved greenhouses, farmers have to ventilate. An air-to-air multi-tube counter flow heat exchanger unit was installed in a greenhouse used for the experimental cultivation of hydroponic tomatoes and cucumbers. This 24m long unit involves a 12" O.D. external shell used to exhaust moist air and five inner tubes to bring fresh air inside. The tests, carried out between March and May in a 576 m<sup>3</sup> enclosure, demonstrated that average efficiencies of  $\eta=84\%$  and  $\eta=78\%$  were obtainable with air volumetric exchanges rates of 0.5 and 0.9 change per hour, respectively. Latent heat was found to play a major role in the overall heat transfer, contributing about 40% of the total energy exchanged in some situations. The exchanger could be buried underneath the ground or suspended above the crops. The unit made of plastic is durable, rot and rust resistant, affordable, and is ice and frost compliant. A pre commercial implementation with an improved design is now considered in collaboration with Gaz Metro. This paper presents the original prototype that help in reducing the consumption of natural gas, fuel, bunker, or propane.

**Keywords:** Heat exchanger, Latent heat recover, Sensible heat recovery, Plastic.

### Nomenclature

|           |                                   |                 |           |                              |             |
|-----------|-----------------------------------|-----------------|-----------|------------------------------|-------------|
| <i>A</i>  | Surface area.....                 | $m^2$           | <i>l</i>  | length of the tubes .....    | $m$         |
| <i>cp</i> | specific heat .....               | $J.kg^{-1}$     | <i>m</i>  | mass flow rate.....          | $kg.s^{-1}$ |
| <i>f</i>  | friction factor.....              | $m^2$           | <i>Nu</i> | Nusselt number, $hD/k$ ..... | -           |
| <i>D</i>  | diameter of the tubes.....        | $m$             | <i>Re</i> | Reynolds number .....        | -           |
| <i>h</i>  | heat transfer coefficient .....   | $W.m^{-2}$      | <i>T</i>  | temperature .....            | $K$         |
| <i>k</i>  | thermal conductivity .....        | $Wm^{-1}K^{-1}$ | <i>i</i>  | specific enthalpy.....       | $J.kg^{-1}$ |
| <i>L</i>  | contribution of latent heat ..... | %               |           |                              |             |

## 1. Introduction

### 1.1. Context

In recent years, passive infiltration of air into greenhouses has been reduced from three or more air changes per hour to less than one half [1]. The reduction of air infiltration into greenhouses leads to significant reductions in heating costs. However, this may be achieved to the detriment of the crops being grown. Very low air exchange rates can lead to abnormally high levels of humidity both during the daytime and at night.

The characterization of the influences of humidity on plant response has not yet been thoroughly investigated unlike those of light, temperature, and carbon dioxide [2]. This may be, in part, due to the difficulty in measuring and controlling humidity in large enclosures and to relate the humidity measurements to the transpiration rates of the crops [3]. Nevertheless, an afternoon above 95% RH may kill or damage a whole harvest. Furthermore, even when the crops are producing at high levels of humidity without any damage, their production rate is much lower than in a controlled environment.

To avoid excessively high humidity levels, venting and heating often remains the only solution to the farmer and this may annihilate the gains achieved by the reduction of infiltration. Traditional heating and ventilation systems result in an inefficient and expensive use of energy, especially during winter in cold regions of the world. To keep sustainable

development strategies, this exchanger should be low cost, user friendly, rot and corrosion resistance, efficient even when ice and frost are present, and, obviously, save energy. The purpose of this study is to design, build, and test such an exchanger to be used in greenhouses located in Northern countries.

## 1.2. Economics in cold regions

The *Syndicat des Producteurs en Serres du Québec* (SPSQ) [4] lists the problem of humidity control in greenhouses as a top priority for this industry. Table 1 [5] indicates the average annual energy requirement per unit area and its corresponding unit cost of operation, for a greenhouse located in Quebec (Canada), as a function of its dehumidification strategy. The data for unit costs are updated for 2011.

Table 1. Energy requirements and costs as a function of the ventilation strategy in greenhouses.

| Dehumidification Strategy | Energy Requirement (MJ/m <sup>2</sup> ) | Cost* (\$/m <sup>2</sup> ) |       |             | Difference with/without (\$/m <sup>2</sup> ) |      |             |
|---------------------------|---|----------------------------|-------|-------------|--|------|-------------|
|                           |   | Gas                        | Oil   | Electricity | Gas  | Oil  | Electricity |
| None                      | 1672                                    | 29,14                      | 44,13 | 35,76       | -  | -    | -           |
| 1 vol/h                   | 1883                                    | 32,81                      | 49,70 | 40,28       | 3,68   | 5,57 | 4,51        |
| Proportional              | 1980                                    | 34,50                      | 52,26 | 42,35       | 5,37   | 8,13 | 6,59        |

Cost estimates based on:  
 37.3MJ/m<sup>3</sup>@0.48\$/m<sup>3</sup> and 80% efficiency for natural gas  
 38.9MJ/L@0.54\$/L and 75% efficiency for oil no.2  
 3.6MJ/kW-h@0.077\$/kW-h for electricity

In Table 1, the first row corresponds to unit heating costs when dehumidification is due to exfiltration of moist air only (balanced by infiltration of cold air), while most of the vapour condenses on the roof and the walls of the greenhouse. This situation is mostly found in old installations where passive infiltration is important. The second row shows figures for a situation where a whole change of air is made in the greenhouse in an hour. The last results presented in the third row of Table 1 pertain to the situation where the farmer ventilates to maintain an adequate level of humidity all the time. Table 1 shows that in cold climates: (1) about 13% to 18% of the heating costs of a standard greenhouse are due to humidity management; (2) proportional ventilation is about 5.4 (for natural gas) to 8.1 CDN\$/m<sup>2</sup> (for Oil, indeed electricity is cheaper than oil in Québec) per year more expensive than no ventilation. This is twice as much as in the 1990s for which this cost varied from about 2.5 (for natural gas) to 4.7 CDN\$/m<sup>2</sup> (for electricity). This represents a minimum extra cost of about 800\$/y for a small 144 m<sup>2</sup> unit which results in millions of dollars for the 110 hectares of crops and 134 hectares of ornamental plants being grown in Quebec only. Hence, one of the objectives of the work is to provide an equipment with a low payback period to be used by most farmers. At last, it should be stated that the critical periods for ventilation are fall and spring for which crops are growing and a fast rate and condensation on the walls is not as important as in winter.

## 2. Methodology

### 2.1. Description of the prototype

After a feasibility study, it was decided to build a multi-tube counter-flow heat exchanger. In view of the restrictions formulated in the introduction, corrugated and flexible thermoplastic drainage tubing [6] was selected to serve as the core of the multi-tube exchanger, four thermoplastic tubes 76 mm I.D. wrapped around a central 101 mm I.D. tube were used. The external kernel or shell of the exchanger that carries the warm and moist air was a tube 305

mm I.D. with a corrugated outer surface (361 mm O.D.) and a smooth inside surface to permit ease of assembly [7], see Fig. 1.

Due to the unlimited amount of space available within greenhouses and because the major part of the exchanger could be buried or suspended, compactness [8] was not a critical parameter here. As a result the heat transfer area density of the first prototype was about  $27 \text{ m}^2/\text{m}^3$ . The first exchanger prototype was 24.3 m long and involved about  $66.9 \text{ m}^2$  of direct exchange area. In the calculation of the exchange area, the effects of the corrugations have been taken into account. This yields about 100% increase over smooth tubes. The surface increase for the 76 mm tube is the same. Fig. 2(a) shows the warm end of the unit: the four gray tubes are carrying the warm moist air which is injected in the external shell. Fig. 2(b) shows the cold end of the prototype.

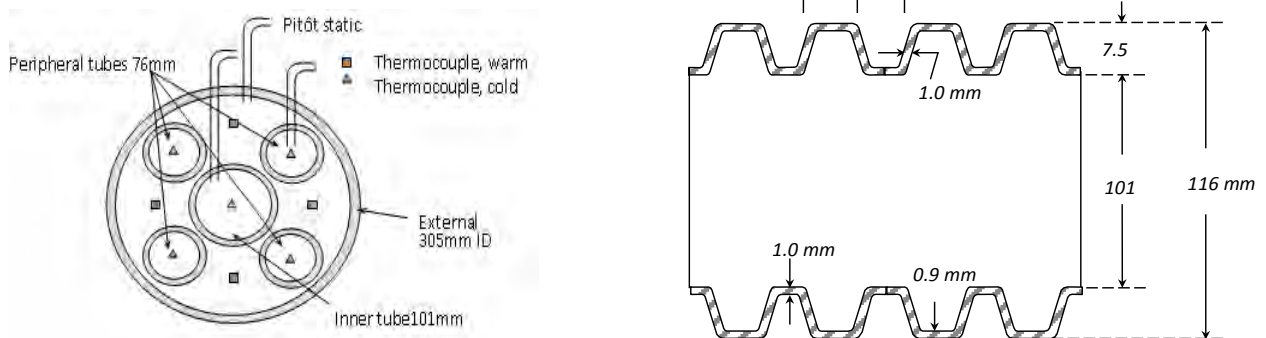


Figure 1: Schematic of the prototype: (left) cross-section; (right) longitudinal cross-section and geometrical details of the 101mm I.D. tube

It can be seen in Fig. 2b that the ventilator is built into the plenum and that the tubes are isolated to prevent condensation in the greenhouse. The overall cost of this prototype, excluding the fans, is much below 2000 CDN\$.

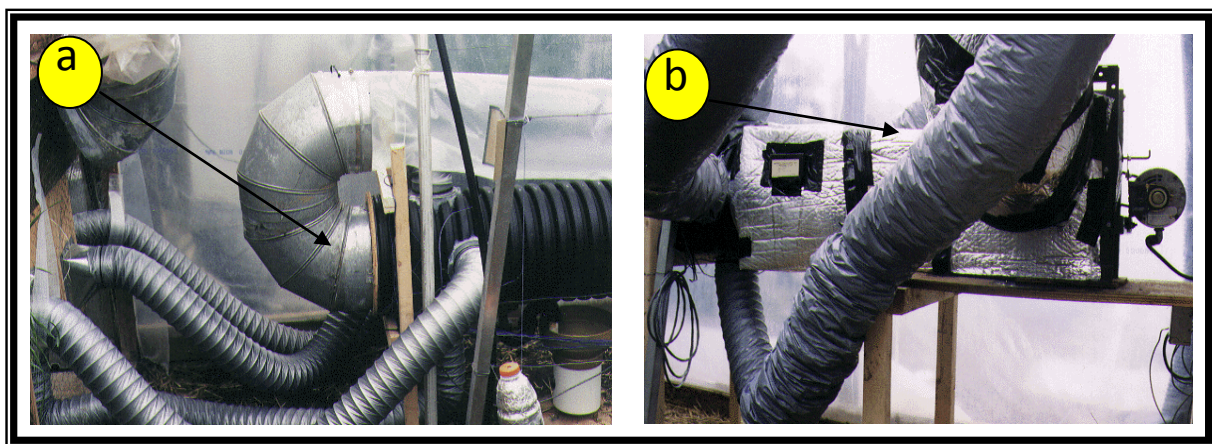


Figure 2: (a) The warm end of the unit; (b) The cold end of the unit

The size of the prototype is justified by the requirement to operate at subzero temperatures for which accumulation of ice should not significantly increase the pressure drop and decrease the overall efficiency. In addition to having a low area density, the original unit has been designed to permit a maximum volumetric exchange rate of one volume per hour in a  $576 \text{ m}^3$  greenhouse located at the *Institut des Technologies Agro-alimentaires de St-Hyacinthe*,

Québec. The greenhouse is part of a larger complex involving several units. It is entirely covered by polyethylene films on the top and on its sides.

## 2.2. Numerical design tool

Brundrett et al. [1] proposed a simple model to design heat exchangers to be used as dehumidifiers in greenhouses. In [1], the authors proposed to carry out energy balances along the axis of the exchanger from one volume to the next. In dry and wet zones, the overall heat transfer coefficient is calculated differently while the external kernel is assumed to be adiabatic. These researchers validated their model with respect to results obtained from two prototypes. The prototypes involved two air streams separated by a polyethylene film on which condensation occurred as the warm and moist stream reached its dew point. In [1], the comparison between experimental and predicted performance is reported to be excellent. In that study [1], the discrepancies are believed to be due to heat transfer to the outer shell of the exchanger which is neglected in the model. Nevertheless, based on the model of Brundrett *et al.* [1], a one-dimensional basic numerical design tool was developed and implemented to allow for the design of the above-described prototype. The correlation that was used for the internal and external surfaces of the five tubes that constitute the core of the unit is the acknowledged relation proposed by Gnielinski [9,10] with the entrance correction factor derived by Hausen [11,12]. For the internal Nusselt number this yields:

$$Nu_i = \frac{(f/8)(Re_{Di} - 1000)Pr}{1 + 12.7\sqrt{f/8}(Pr^{2/3} - 1)} \left[ 1 + \left( \frac{D_i}{l} \right)^{2/3} \right] \quad (1)$$

where  $Re_{Di}$  is the Reynolds number, based upon the tube diameter  $D_i$ ,  $Pr$  is the Prandtl number, and  $f$  is the friction factor [8]. For corrugated drainage tubes, there are no data available to quantify the relative roughness,  $\varepsilon/D$ . Hence, after a series of pressure drop measurements,  $\varepsilon$  was approximated to an average of 0.001m.

The outer shell was assumed to be adiabatic. The predictions then have to include the specifications of the psychrometric properties of the hot air, with wet and dry bulb air temperatures and absolute pressure being required. The prediction model thus determines where the warm fluid will experience condensation of moisture by dropping below its dew point temperature. The calculation of the overall exchanger is then divided into two sections: the first where heat transfer occurs exclusively by sensible transfer and the second where heat transfer involves latent as well as sensible heat. The overall heat transfer between the hot and cold fluids is given by:

$$q = \dot{m}_o (i_{o,inlet} - i_{o,outlet}) = \dot{m}_i (i_{i,outlet} - i_{i,inlet}) \quad (2)$$

An iterative procedure is employed in the two sections until a balance is obtained in the calculation of the heat transfer with Eq.(2) and that with UA LMTD [8]. The contribution of latent heat to the total heat transfer was estimated with:

$$L = \left[ 1 - \frac{c_p (T_{o,inlet} - T_{o,outlet})}{i_{o,inlet} - i_{i,inlet}} \right] * 100 \quad (3)$$

where subscript  $i$  refers to the stream inside the tubes and subscript  $o$  refers to that outside the tubes or into the kernel. The efficiency is defined as:

$$\eta = \frac{T_{o,inlet} - T_{i,inlet}}{T_{i,outlet} - T_{i,inlet}}$$

### 3. Results

#### 3.1. Global results

In this section overall results are provided for the period extending from March 21<sup>st</sup> to May 21<sup>st</sup>. Spring is selected as it corresponds to a critical period as the plants are active and condensation rates on the walls very low due to higher temperatures than those found in the winter. At a rate of  $\dot{Q}=0.5$  air change per hour, the average efficiency based on temperature for the whole period of investigation was about :  $\eta=84\%$  with a 5% standard deviation. For the results obtained with  $\dot{Q}=0.9$  air change per hour, the average efficiency decreased to  $\eta=78\%$  with a 3.5% standard deviation.

The experimental results carried out over the two months period indicate that for  $T_{i,inlet}$  varying between 1 and 3°C with RH varying between 63% and 70%, the contribution of the latent heat to the overall heat transfer fell within a 39 to 43% range. To obtain such results, the amount of condensation recovered is measured (to estimate latent heat recovery) as well as the overall temperature differences.

The amount of water that condenses on the walls is calculated based on the variation of the absolute water content of the warm moist fluid along the exchanger. A typical rate of condensation is about 1680 mL/h. The maximum condensation rate was found to reach 3200 mL/h when the external temperature was -10°C and the internal temperature 20°C with 85% RH. The maximum power used by the Delhi fans was 637 W, and the rate of heat gained by the cold fluid varied from 874 W at  $T_{i,inlet} = 14^\circ\text{C}$  to 3 089 W at  $T_{i,inlet} = -10^\circ\text{C}$ . This indicates a variation in the COP such that:  $1.4 < \text{COP} < 4.8$ .

The first day was March 26th, when the volumetric flow rate of warm fluid,  $\dot{v}_h$ , was 0.099 m<sup>3</sup>/s and that of the cold fluid,  $\dot{v}_c$ , was 0.079 m<sup>3</sup>/s. The profile presented in Fig. 3 (a) is typical of what was observed when the prototype operated at 0.5 air change per hour.

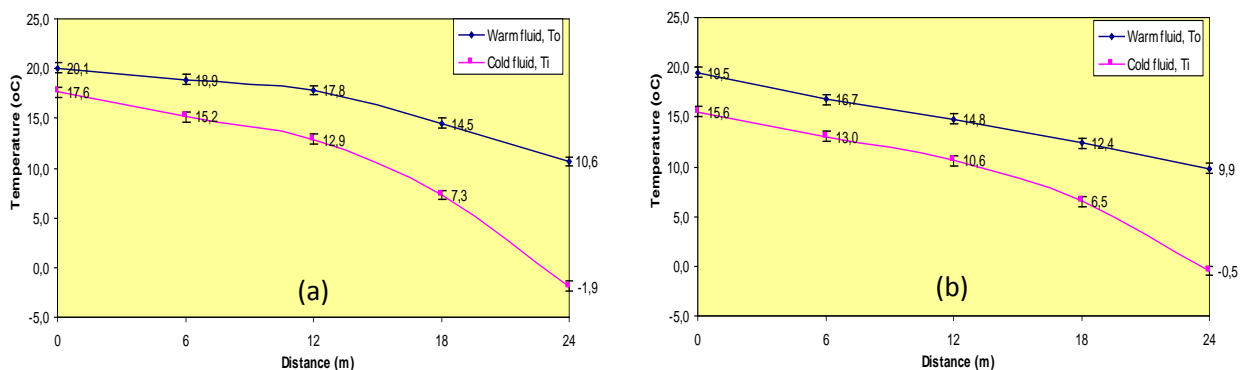


Fig. 3: Temperature distribution. (a) March 26th: 8h10, 0.5 air chg / h; (b) April 5th: 4h50, 0.9 air chg / h

For this case, the relative humidity at the warm exit of the cold stream was 15.7% while it was almost completely saturated at 93.5% at the cold exit of the warm stream. The efficiency was 89%. The heat recovery was excellent: 1948W. And at that time of the day, provided that the fans needed 355W, the COP was 5.51.

Fig. 3(b) shows results for April 5th, when  $\dot{v}_h$  was  $0.148 \text{ m}^3/\text{s}$  and  $\dot{v}_c$  was  $0.141 \text{ m}^3/\text{s}$ . Similar trends can be observed. For this second case, the relative humidity at the warm exit of the cold stream was 18.9% and the efficiency was 81%. 2856W were recovered while 637W were used: the COP was 4.48.

### 3.2. Psychometrics results

The relative humidity was also monitored to assess the ability of the unit to fulfil the needs of the plants. It is worth noting that  $0.9 \text{ air chg/h}$  is not enough to maintain an adequate level of humidity in the complex all year long: it should be adequate about 80% of the time. But for this design, only general characteristics were to be obtained. The test was carried out in the critical period of growth for a greenhouse in Québec. As a result, it was expected that the humidity level would be very high in this period even under operation: traditional ventilation had to be used as a complement. Fig. 4 shows the relative humidity distribution for March 26th.

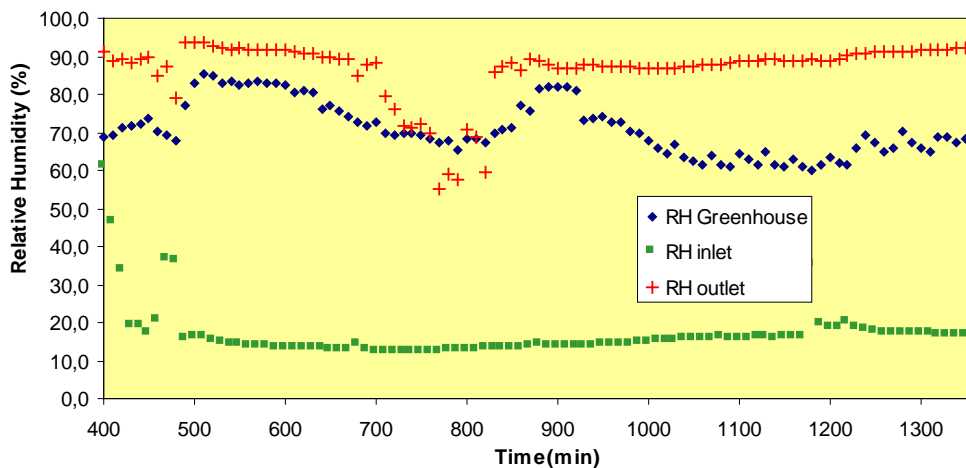


Fig. 4: Relative humidity distribution in the greenhouse on March 26<sup>th</sup>

The results for the humidity in the greenhouse (diamonds) show a first peak early in the morning: March 26th was sunny and the plants were active early. The humidity had to be lowered with standard ventilation as the unit was not able to deliver a sufficient flow rate to evacuate a sufficient amount of moisture. A second peak appears at about  $t = 900 \text{ min}$ , that is when the sun sets. At that time, the greenhouse had to be closed as the external temperature became too low to maintain an adequate temperature level inside. The interesting part of the curve is that the unit was able to lower the humidity level rapidly after sunset. In brief, a bigger unit would have been needed only in the morning for that day. The inlet stream humidity results (squares) show the period in the day when it stopped: the unit operated almost continuously. The last results (crosses) show that air was saturated in the warm stream except when additional ventilation was used. In these conditions, the humidity level in the greenhouse was below 75%.

Fig. 5 presents typical results obtained for a period ranging from April 5th to April 9th. This sequence demonstrates the performance of the prototype as a dehumidifier over an extended period. At that time, about 300 mature plants of tomato and cucumber were growing. During this period, the exchanger was operated continuously with a RH threshold of 75%. The transpiration cycle of the plants can be interpreted as follows. The photosynthesis activities diminish after sunset. As shown in the figure, the relative humidity then reaches peak lows of

about 79 to 82%. The high peaks occur at about noon with maximum relative humidity of about 90 to 91%. On an average, the relative humidity was about 85% in the greenhouse.

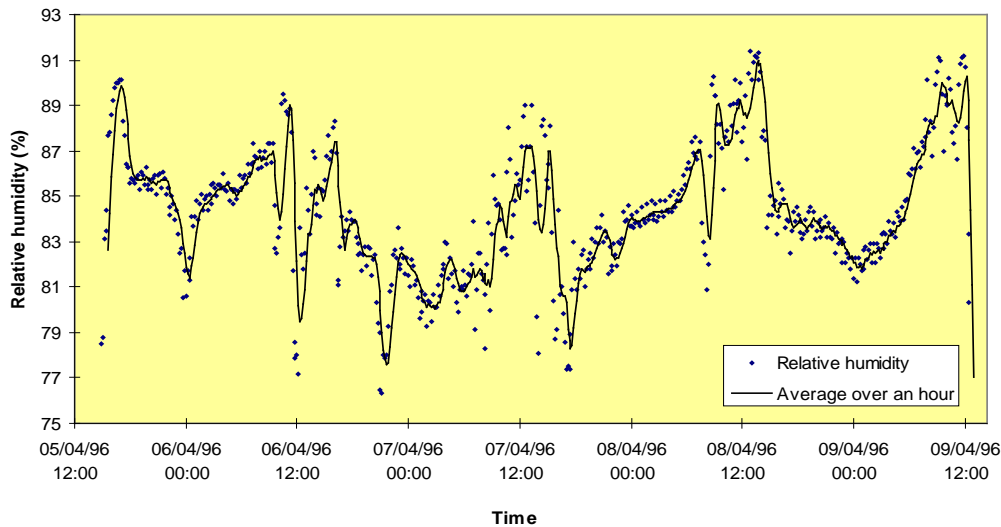


Figure 5: Relative humidity distribution in the greenhouse between April 5<sup>th</sup> and 9<sup>th</sup>

Again, it is shown in Fig.5 that the prototype is too small to permit a total compensation for the needs of the plants: the threshold of 75%RH is never reached. This was predicted as the capacity of the exchanger is about 5 times lower than the maximum greenhouse requirement. However, these results are interesting as they permit one to compare the humidity management using the undersized unit with traditional ventilation techniques. Here, the cycles never reach 100% relative humidity which would sometimes be nearly the case with manual ventilation. This indicates that although two to five air changes/h may be needed in critical periods, the smaller unit of about one air change/h can nevertheless permit preventing relative humidity to shoot above 91%. Results from Fig.4 and 5 were used in the design of a second generation of pre-commercial units that are now undergoing a more thorough experimental testing procedure. Knowing both incoming and outgoing volumetric flow rates in conjunction with their relative humidities and temperatures, a mass balance can be performed for water vapor in the greenhouse.

### 3.3. Payback period

Here the payback period is estimated with no account for the improvement of the crops growth with adequate level of humidity: the “real” performance of the exchanger should be better. The integrated heat recovery is used to estimate the payback with no account of the fan power as if they were used anyway to extract the moisture from the greenhouse. It has been found that the units were able to recover 9840 kW-h over the whole year which corresponds to a cost of 617\$ for gas heating and 935\$ for oil heating. As the experimental unit costs 1140\$ (calculations carried out for a production and installation of 100 per year), the simple payback period is about 1,5 year (from 1,2 to 1,9 years, without subsidy).

## 4. Conclusion

A prototype air-air counter-flow multi-tube heat exchanger has been designed and built to meet the specific greenhouse requirements of operating in a cold climate. The uncompact design involving plastic components was retained so as to meet the following requirements: (1) low cost, CDN\$ < 2000 (1,5 year pay-back period); (2) ease of assembly, maintenance,

repair, and operation; (3) corrosion and rotteness resistance; (4) satisfactory operating efficiency when frost present.

The prototype was designed using a basic numerical tool. Drainages tubing were retained as they readily permitted one to meet the design requirements. One of the goals was to convince producers that such a simple design could spare them a substantial part of their yearly heating costs. The unit was assembled and calibrated in a greenhouse used for the experimental cultivation of hydroponic tomatoes and cucumbers during winter. The first series of tests, carried out between March to May, demonstrated that average efficiencies of  $\eta=84\%$  and  $\eta=78\%$  were obtainable with air volumetric exchanges rates of 0.5 and 0.9 change per hour, respectively, in a 576m<sup>3</sup> greenhouse. Latent heat was found to play a major role in the overall heat transfer, contributing about 40% of the total energy exchanged in some situations.

In conclusion, with sufficient exchange area, simple heat exchangers can be economically used as dehumidifiers in several applications. The encouraging results presented and mentioned here demonstrate that yet other applications could be found for heat exchangers in sustainable development strategies.

## References

- [1] E. Brundrett, T.J. Jewett, and R. Quist, Evaluation of polytube heat exchangers for greenhouse ventilation". *Acta-horticulturae*, 148, 1984, pp.49-55.
- [2] J.N. Walker and D.J. Cotter, Condensation and resultant humidity in greenhouses during cold weather, *Trans. ASEA*, 11(2), 1968, pp.263-266.
- [3] D.J.Cotter and R.T. Seay, The effect of circulating air on the environment and tomato growth response in a plastic greenhouse, *Roc. ASHS*, 77, 1961, pp.345-342.
- [4] SPSQ., Ékiloerre; Projet d'amélioration de la situation énergétique de l'industrie serricole québécoise, Rapport Final, Syndicat des Producteurs en Serre du Québec, St-Hyacinthe, 1995.
- [5] D. DeHalleux, and L. Gauthier, Consommation énergétique due à la déshumidification des serres au Québec, Université Laval, Québec, 1995.
- [6] BNQ., Norme 3624-115 (91-08-01); Tubes annelés flexibles et raccords en thermoplastique pour le drainage des sols, Bureau de Normalisation du Québec, Québec, 1991.
- [7] BNQ., Norme 3624-120 (90-02-20); Tuyaux annelés à l'intérieur lisse et raccords en plastiques Pe ou PP pour l'évacuation des eaux pluviales, Bureau de Normalisation du Québec, Québec, 1990.
- [8] A. Bejan, *Convection Heat Transfer*, 2nd ed., Wiley, New-York, 1993
- [9] V. Gnielinski, New Equations for Heat and Mass Transfer in Turbulent Pipe and Channel Flow, *Int. Chem. Eng.*, vol.16, 1976, pp.359-368.
- [10] V. Gnielinski, Forced Convection in Ducts, in G.F.Hewitt (ed.), *Handbook of Heat Exchanger Design*, Begell House, NY, 1952, section 2.5.1-5.
- [11] H. Hausen, Darstellung des Wärmeüberganges in Rohren durch verallgemeinerte Potenzbeziehungen, *Z. Ver. Dtsch. Ing. Beiheft Verfahrenstech.*, vol.4, 1943, pp.91-134.
- [12] H. Hausen, *Heat Transfer in Counterflow, Parallel Flow and Cross Flow*, McGraw-Hill, USA, 1983.

## Environmental analysis of various systems for the cogeneration of biogas produced by an urban wastewater treatment plant (UWTP). (III).

J.J. Coble<sup>1</sup> and A. Contreras<sup>2\*</sup>

<sup>1</sup> Department of Industrial Engineering. Nebrija Universidad. Madrid, Spain

<sup>2</sup> Department of Chemistry. ETSII. UNED. Madrid. Spain.

\* Corresponding author. Tel: 34 91 3986496, Fax: 34 91 3986043. Email: [acontreras@ind.uned.es](mailto:acontreras@ind.uned.es)

---

**Abstract:** To complete the study on harnessing the biogas produced by a UWTP as an energy source, using cogeneration with motor-generators and phosphoric acid fuel cells, in this paper we present the results of the environmental study. This completes the study made of both systems, enabling us to conclude which of the two methods is best in terms of obtaining the largest amount of energy, at the lowest cost, and with minimum impact on the environment.

For the environmental analysis we compared, amongst other parameters, the contaminating gas emissions produced by each cogeneration device, and assessed the financial cost of the environmental damage caused by these emissions. We also bore in mind the emission levels created by the emissions from each system, both immediately around the plant and in the surrounding areas affected by prevailing wind directions. Finally, we compared the noise levels of the two devices and determined the financial cost of applying corrective acoustic insulation where necessary.

The overall study of both systems has made it clear that to evaluate them correctly, it is necessary to internalize all the costs that are currently externalized. This is the only way to find the true cost of each system.

**Keywords:** Cogeneration, UWTP, Motor-generators, Phosphoric acid fuel cell, Environmental analysis, Emissions.

---

### 1. Introduction

In the first part of this study [1], it was found that both systems showed substantial differences in terms of their energetic, exergetic and thermo-economic performance. The irreversible factors of both systems are shared out among their components in different ways but, overall, there are fewer of these factors in the phosphoric acid fuel cell system. However, if we take the energy analysis alone into account, the total year-on-year costs are lower for the motor-generation system, and this is the option that would normally be chosen.

In this second part of the study it becomes apparent that if we add up the costs of both thermo-economic analysis and environmental analysis, i.e.: by internalizing all the costs of both systems, cogeneration with phosphoric acid fuel cells is an investment that can be eventually be recovered. However, this is not the case with cogeneration using motor-generators.

### 2. Methodology

The environmental analysis compares the two cogeneration systems on the basis of the following features:

Emission levels of atmospheric pollutants and greenhouse gases, along with their financial cost.

Emission levels in surrounding and sensitive areas, and their environmental impact.

Noise levels and their financial cost.

Once the environmental impacts have been assessed, they must be assigned a financial cost and this must be internalized with the rest of the system's costs. The cost of externalities has

been evaluated by various international organizations. Two studies are fundamental if we wish to make an assessment of the costs of the externalities of the systems studied in this paper: one is European [2], and was subsequently developed in [4, 5], and the other is American [3]. The American model basically uses resolution algorithms, which are in turn based on the same concept: the cost of environmental damage attributable to each unit of mass or volume of pollutant.

However, we decided to use the European model [2, 4, 5], because its conclusions are better suited to the environment in which this study took place, but mainly because it is a more conservative model insofar as the numeric values that are obtained are always higher than the real ones. This provides us with a safety margin that is always appreciated by technicians.

In order to assign costs to the externalities, it is first necessary to decide which of these should be taken into account. In this study, we considered those that are due to the emission and noise levels produced by the systems.

We also calculated the levels of emission of chemical pollutants (gaseous compounds and particles), depending on the location's various climatic conditions, so as to compare the final environmental impact of the emissions from each system. No cost was assigned to them, however, because taking into account the costs of the irreversible energy factors and the emissions alone was sufficient proof of the financial difference between the two systems.

From the results obtained in the studies mentioned [2, 4, 5], the emission costs for various scenarios can be inferred, as shown in Table 1. These differ depending on the financial valuation of the emissions.

Table 1. Costs of the emissions of pollutants in various scenarios (euros/ton)

| ATMOSPHERIC POLLUTANT | LOW LEVEL (€/t) | MEDIUM LEVEL (€/t) | HIGH LEVEL (€/t) |
|-----------------------|-----------------|--------------------|------------------|
| CO <sub>2</sub>       | 9.90            | 26.40              | 41.60            |
| CO                    | 506.23          | 1,055.87           | 2,494.26         |
| SO <sub>2</sub>       | 1,635.98        | 1,869.77           | 4,933.99         |
| NO <sub>x</sub>       | 1,049.27        | 7,919.03           | 10,030.77        |
| PM                    | 3,128.55        | 4,839.41           | 13,616.33        |
| VOC                   | 1,113.06        | 5,265.79           | 6,489.20         |

In this study, we have chosen the medium-level costs of emissions shown in Table 1, as we consider them to be the most representative. The nomenclature used for the financial costs that have been developed and used in this study (set-up and operation, energy inefficiency, emissions) is as follows:

**C<sub>1</sub> (€/year):** Set-up and operating costs during the first year. In subsequent years only operating costs will be taken into account.

**C<sub>2</sub> (€/year):** Costs of energy inefficiency derived from the thermo-economic analysis.

**C<sub>3</sub> (€/year):** Costs of noise emissions and atmospheric pollutants.

### 3. Results

The results of the emission and noise levels for each of the two cogeneration systems studied are shown below.

#### 3.1. Level of emissions from the cogeneration system using motor-generators

The combustion reactions of the motor-generators were modelled on the basis of the excess of air  $n = 1.5$  that was considered. Using the formula created with the EES programme [10], we obtained the motor-generator emission results shown in Table 2, and these were compared with those of the phosphoric acid fuel cells.

Table 2. Comparison of gases emitted by biogas cogeneration by motor-generators and in fuel cells, in grams per second.

| NO <sub>x</sub> EMISSIONS(g/s) |         | SO <sub>2</sub> EMISSIONS (g/s) |      | CO <sub>2</sub> EMISSIONS(g/s) |           | CO EMISSIONS(g/s) |         |
|--------------------------------|---------|---------------------------------|------|--------------------------------|-----------|-------------------|---------|
| Motor-generator                | PAFC    | Motor-generator                 | PAFC | Motor-generator                | PAFC      | Motor-generator   | PAFC    |
| 4.51364                        | 0.00214 | 0.03482                         | 0    | 731.13516                      | 244.66268 | 24.48778          | 0.00497 |

#### 3.2. Level of emissions from the cogeneration system using phosphoric acid fuel cells.

Using the available data [7, 8], the emissions from fuel cells were modelled on the basis of the level of working power. With the formula created by the EES programme [6], we obtained the emission results that are also shown in Table 2, above.

The SO<sub>2</sub> emissions for fuel cells are negligible and have not been taken into account. To make a financial assessment of the emissions, we used the average value of emission costs shown in Table 1. Using these values as a reference, we were able to determine the emission costs of all the compounds mentioned in the study.

Table 3 shows the costs resulting from the emissions from each cogeneration system and compound, whereas Table 4 shows the sum of all the costs for each case.

Table 3. Financial comparison of emission costs for NO<sub>x</sub>, SO<sub>2</sub>, CO<sub>2</sub> and CO emissions, from both cogeneration systems (€/year).

| COST OF NO <sub>x</sub> EMISSIONS (€/year) |        | COST OF SO <sub>2</sub> EMISSIONS (€/year) |      | COST OF CO <sub>2</sub> EMISSIONS (€/year) |           | COST OF CO EMISSIONS (€/year) |       |
|--|--------|--|------|--|-----------|-------------------------------|-------|
| Motor-generator                            | PAFC   | Motor-generator                            | PAFC | Motor-generator                            | PAFC      | Motor-generator               | PAFC  |
| 539,285.94                                 | 256.02 | 981.63                                     | 0.00 | 291,219.64                                 | 97,452.22 | 390,071.85                    | 79.25 |

Table 4. Financial comparison of total costs ( $C_3$ ) from emissions of  $NO_x$ ,  $SO_2$ ,  $CO_2$  and  $CO$ , from both cogeneration systems (€/year).

| TOTAL COST OF $C_3$ EMISSIONS (€/year) |           |
|--|-----------|
| Motor-generator                        | PAFC      |
| 1,221,559.06                           | 97,787.49 |

As can be seen from Table 4, the total costs of atmospheric emissions from the motor-generators are 5.64 times higher than those of fuel cells.

As shown by the figures in Table 1, the financial cost of emissions is considered to be included in the cost of emissions shown in the previous section. However, in this study, we took into account the dispersion of pollutants according to the atmospheric conditions of the location, and emission maps were subsequently made. This was because the way in which emissions are financially assessed - which currently includes the effects of immissions - needs to be improved. It should be requisite for a device's emission levels to be used simultaneously with emission maps calculated for the device's various weather scenarios. This study will make it possible to achieve a more accurate financial assessment of the environmental impact.

Level of emissions from the cogeneration system using motor-generators.

We show below a summary of the results of the emission level calculations for each pollutant and each cogeneration system. We used the DISPER 3.0 programme [9] and an Excel spreadsheet [10], introducing the emission data calculated in Table 2 into the programme's user interface (except for the  $CO_2$  figures). By also introducing the weather and other relevant location data, we obtained the  $CO$  results shown below, in Figure 1, as well as each kind of atmospheric stability for the profile on the XZ plane of the central line of the plume (X axis).

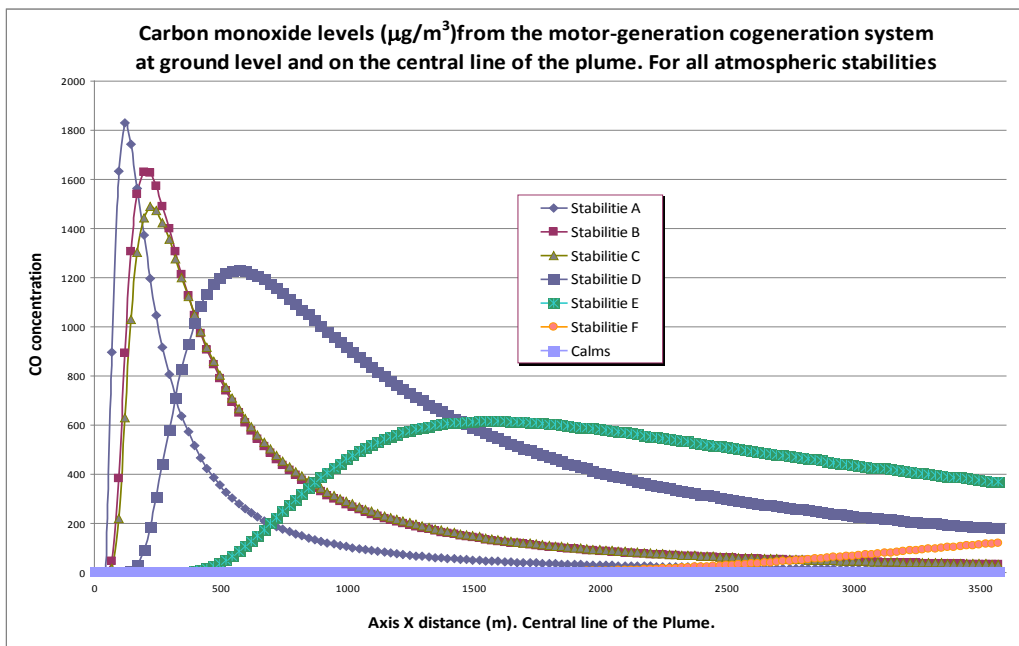


Figure 1. Carbon monoxide levels from the motor-generation cogeneration system at ground level and on the central line of the plume. For all atmospheric stabilities.

As can be seen in Figure 1, the maximum concentration of carbon monoxide immission for the most unfavourable atmospheric stability is:

$$1800 \mu\text{g}/\text{m}^3 = 1,8 \text{ mg}/\text{m}^3 < 6 \text{ mg}/\text{m}^3 \text{ (legal limit).}$$

This in no case exceeds the legal limits in force since January 1, 2005 [11].

Level of emissions from the cogeneration system using phosphoric acid fuel cells.

Carbon monoxide is mainly produced in the fuel cell during the process of reforming the biogas vapour to obtain hydrogen. This carbon monoxide has to be removed from the fuel flow into the cell to avoid poisoning the catalyst.

This CO has to be removed from the reformed gas flowing into the fuel cell, because carbon monoxide concentrations as low as 1% in the input flow of these cells can poison the platinum catalyst. Although the operating temperature of the cells is between 150-200°C, the effects of catalyst poisoning can be detected at concentrations of 10,000ppm of CO in the input flow. The main effect of such poisoning is either an increase in the input flow required to produce the same power, or a drop in the power output [12].

The results of the levels of carbon monoxide emission calculated in this case provide a maximum concentration figure for the most unfavourable atmospheric stability of:

$$2.5 \mu\text{g}/\text{m}^3 = 0.0025 \text{ mg}/\text{m}^3 \lll 6 \text{ mg}/\text{m}^3 \text{ (legal limit)}$$

If the above figure is compared to the concentration level of CO emissions from motor-generator emissions for the least favourable atmospheric stability, it can be seen that emissions from the motor-generators are around 720 times higher than those of the set of fuel cells.

Similar results were obtained for the rest of the polluting gases considered in this paper. As for emission and emission levels, the motor-generator cogeneration system is at a clear disadvantage when compared to the phosphoric acid fuel cell system.

The noise level of the motor-generator cogeneration system.

For the calculations in this section, we used the data provided by the manufacturers – which, in both cases, dealt with emissions into the indoor (rather than outdoor) atmosphere of 95 dBA for motor-generators, and 60 dBA for fuel cells [13, 14], as well as current regulations.

To check that the noise level limits set by the current legislation were not exceeded, we used the CUSTIC 1.0 application, by Canarina Software Ambiental [15], to calculate the noise emission levels. These were viewed on isophonic layout maps, for both the installation using motor-generators and the one using phosphoric acid fuel cells.

In the case of the motor-generators, the noise levels calculated in the simulation would exceed the 60dBA day-time limit, beyond the walls of the motor-generation building, unless appropriate corrective measures were put in place. In order to comply with the law, it would be necessary to take corrective measures amounting to 43,500 Euros. With fuel cells, no corrective measures are required

#### **4. Conclusions**

By considering environmental effects in our analysis of the two cogeneration systems, we were able to reach the following conclusions.

The most important aspect of this second part of the study is that the environmental cost of the phosphoric acid fuel cell cogeneration system has been valued at 97,787.487 €/year, whereas that of the motor-generator cogeneration system was 1,221,559.061 €/year. As you can see, the latter is far higher than the phosphoric acid fuel cell system.

Furthermore, in the case of motor-generators, acoustic insulation would need to be provided for the building in which they are installed, so as to comply with current legislation on noise emission levels. In the case of the fuel cell cogeneration system, however, no corrective measures are needed to comply with these regulations.

#### **References**

- [1] J.J. Coble, and A. Contreras. Energetic, Exergetic, Thermo-economic and Environmental Analysis of Various Systems for the Cogeneration of Biogas Produced by an UWTP (1). 18 World Hydrogen Energy Conference, 16-21 May 2010, Essen, Germany.
- [2] Scheleisner and Nielsen, (1997). ExternE National Implementation Project (CEC, 1995)
- [3] R. D. Rowe et al.,. The New York Electricity Externality Study. Oceana Publications, New York. 1995.
- [4] Carlson Annelie, Energy system analysis of the inclusion of monetary values of environmental damage, Biomass and Bioenergy (2002), 22,3,177-177
- [5] European Commission ExternE- Externalities of Energy, EUR 16520 EN-EUR 16525 EN, Directorate-General XII, Office for Official Publications of the European Communities, Luxembourg, 1995.
- [6] EES (Engineering Equation Solver). F-Chart Software. [www.fchart.com](http://www.fchart.com).
- [7] Greenhouse Gas Technology Center Southern Research Institute. EPA & New York State Energy Research and Development Authority (2004). "Environmental Technology Verification Report: Electric Power and Heat Generation Using UTC Fuel Cells' PC25C Power Plant and Anaerobic Digester Gas".
- [8] Ott G. Sanger D. Tooze D. Hydrogen Fuel Cells: A Solution for Utilizing Waste Methane at Columbia Boulevard Wastewater Treatment Plant. Final Technical Report. Climate Change Fuel Cell Program (2000). City of Portland. Oregon
- [9] Canarina environmental software, program DISPER 3.0 advanced version. [www.canarina.com](http://www.canarina.com)
- [10] Microsoft Excel software. <http://office.microsoft.com>
- [11] BOE num. 260, 30/10/2002. Ministry of the Presidency. Royal Decree 1073/2002, of 18 October, on the evaluation and management of air quality in relation to sulphur dioxide, nitrogen dioxide, nitrogen oxide, particles, lead, benzene and carbon monoxide.
- [12] Song Rak-Hyung, Shin D. R., Influence of CO concentration and reactant gas pressure on cell performance in PAFC, International Journal of Hydrogen Energy 26 (2001) 1259-1262.
- [13] PureCell™ Model 200 power solution. [www.utcpower.com](http://www.utcpower.com).

- [14] J. Larminie and A. Dicks. *Fuel Cell Systems Explained (Second Edition)*. J. Wiley and Sons.
- [15] Canarina environmental software, program CUSTIC 1.0 advanced version. [www.canarina.com](http://www.canarina.com).